HYDRAULICS OF CIRCULAR BOTTOM INTAKE ORIFICES

A THESIS SUBMITTED TO
THE GRADUATE SCHOOL OF NATURAL AND APPLIED SCIENCES
OF
MIDDLE EAST TECHNICAL UNIVERSITY

BY

MUHAMMED BULUT

IN PARTIAL FULFILLMENT OF THE REQUIREMENTS
FOR
THE DEGREE OF MASTER OF SCIENCE
IN
CIVIL ENGINEERING

AUGUST 2013

Approval of the thesis:

HYDRAULICS OF CIRCULAR BOTTOM INTAKE ORIFICES

Submitted by **MUHAMMED BULUT** in partial fulfillment of the requirements for the degree of **Master of Science in Civil Engineering Department, Middle East Technical University** by,

Prof. Dr. Canan Özgen
Dean, Graduate School of **Natural and Applied Sciences** _____________

Prof. Dr. Ahmet Cevdet Yalçıner
Head of Department, **Civil Engineering** _____________

Prof. Dr. Mustafa Göğüş
Supervisor, **Civil Engineering Dept., METU** _____________

Examining Committee Members

Assoc. Prof. Dr. Ayşe Burcu Altan Sakarya
Civil Engineering Dept., METU _____________

Prof. Dr. Mustafa Göğüş
Civil Engineering Dept., METU _____________

Assoc. Prof. Dr. Mehmet Ali Kökpınar
TAKK Dept., DSİ _____________

Assoc. Prof. Dr. Mete Köken
Civil Engineering Dept., METU _____________

Assist. Prof. Dr. Önder Koçyiğit
Civil Engineering Dept., Gazi University _____________

Date: _____________

I hereby declare that all information in this document has been obtained and presented in accordance with academic rules and ethical conduct. I also declare that, as required by these rules and ethical conduct, I have fully cited and referenced all material and results that are not original to this work.

Name, Last name: Muhammed BULUT

Signature :

ABSTRACT

HYDRAULICS OF CIRCULAR BOTTOM INTAKE ORIFICES

Bulut, Muhammed
M,Sc., Department of Civil Engineering
Supervisor: Prof. Dr. Mustafa Göğüş

August 2013, 159 pages

In this study, the hydraulics of circular bottom intake orifices was investigated experimentally in a hydraulic model constructed in the laboratory. For this reason, a series of circular orifices at various diameters were located at the bottom of a flume and tested under a wide range of different flow conditions. The discharge passing through the orifice of known diameter, location and slope were measured and recorded along with the corresponding flow rate of the main channel and its flow depth. One or some of the variables as diameters, locations and slopes of the orifices were changed in the experiments. From the data obtained, the discharge coefficients, C_D, of the orifices and their variations with the dimensions and locations of the orifices were determined. Similar experiments were repeated with orifices located on the inclined channel bottom and the effects of the bottom inclination on the variation of discharge coefficient, C_D and coefficient obtained from the dimensional analysis, K, were investigated. The relationship between these coefficients, C_D, and K, and some other dimensionless parameters were presented graphically. Using these graphs, one can determine the discharge coefficient, C_D, and other coefficient, K, necessary to find the amount of water diverted by a circular bottom intake orifice with known diameter, place and slope from a main channel of which the total discharge is known. The effects of multiple bottom intake orifices on the aforementioned coefficients were also investigated within the scope of this study.

Keywords: Bottom intake structures, hydraulics, intake racks, circular orifices, dimensional analysis.

ÖZ

DAİRESEL KESİTLİ TABANDAN SU ALMA ORİFİSLERİNİN HİDROLİĞİ

Bulut, Muhammed
Yüksek Lisans, İnşaat Mühendisliği Bölümü
Tez Yöneticisi: Prof. Dr. Mustafa Göğüş

Ağustos 2013, 159 sayfa

Bu çalışmada dairesel kesitli tabandan su alma orifislerinin hidroliği laboratuvarda inşa edilen bir hidrolik modelde deneysel olarak araştırılmıştır. Bunun için, farklı çapta dairesel orifisler bir su kanalının tabanına yerleştirilmiştir ve bu orifisler çok miktarda değişik akım şartlarında test edilmişlerdir. Çapı, kanal tabanındaki yeri ve eğimi bilinen bir orifisten geçen su debisi ölçülmüştür ve bunun değeri kanaldan geçen debi ve su derinliği ile birlikte kayıt edilmiştir. Orifislerin çap, yer ve eğim gibi değişkenlerinden bir veya birkaçı, deneylerde değiştirilmiştir. Elde edilen verilerden, orifislerin debi katsayıları, C_D, ve bunların, orifislerin çapları ve kanal tabanındaki yerleri ile değişimleri tespit edilmiştir. Benzer deneyler eğimli kanal tabanına yerleştirilen orifislerle de tekrarlanmış ve kanal taban eğiminin debi katsayısına, C_D, ve boyut analizinden elde edilen diğer katsayıya, K, etkisi araştırılmıştır. Katsayılar, C_D ve K, ve diğer boyutsuz değişkenler arasındaki ilişki grafiksel olarak sunulmuştur. Bu grafikler kullanılarak, toplam debisi bilinen ana kanaldan; çapı, yeri ve eğimi bilinen bir dairesel delikli su alma orifisiyle alınabilecek su miktarını bulmak için gerekli, debi katsayısı, C_D ve diğer katsayı, K belirlenebilir. Çok sayıdaki dairesel kesitli su alma orifislerinin yukarıda belirtilen debi katsayıları üzerindeki etkileri de bu çalışma kapsamında araştırılmıştır.

Anahtar kelimeler: Tabandan su alma yapıları, hidrolik, su alma ızgaraları, dairesel orifisler, boyut analizi.

To my family…

ACKNOWLEDGMENTS

Firstly, I want to express my sincere thankfulness to, Prof. Dr. Mustafa GÖĞÜŞ, for being my thesis supervisor, his insightfulness in every conditions, support, encouragement and confidence on me during this study.

Also, I would like to thank to my best friends, Ali Baykara, Aysim Damla Atalay, Hayati Arslan, Oğuz Barın, Remzi Başar Ataman, Utku Albostan, Yunus Avcıi Yusuf Eren Akın and to my cousin Serdar Sancak and Hülya Sancak for not leaving me alone and supports during this study.

I would like to thank to Middle East Technical University Civil Engineering Department Hydromechanics Laboratory Technicians for their helps to prepare my laboratory set-up and supports during the laboratory experiments.

Moreover, I want to show my appreciation to my workmates at Public Procurement Authority; especially Kadir Çağlar Çetintaş, Timur Dinçer, Işıl Şahbudak, Abdullah Cangir, Ali Osman Bulut, Doğukan Demirci, İsmail Altun and Mehmet Kadir Çakır for their supports during this study.

Finally, for their supports in all my life, and especially, during this study, thanks to my dear family: Kadriye Bulut, İrfan Bulut, Serpil Bulut, Mustafa Bulut, Özgür Torun, and my sweetie niece, Ada.

TABLE OF CONTENTS

LIST OF TABLES

TABLES

LIST OF FIGURES

LIST OF SYMBOLS

A	:	Location name of the orifice
A_0	:	Circular orifice area
A_T	:	Total flow area at the depth measurement section or section (1)
a	:	Center spacing
B	:	Location name of the orifice
C	:	Location name of the orifice
C_c	:	Coefficient of contraction
C_L	:	Center line
C_D	:	Discharge coefficient
$(C_D)_{calculated}$	:	Discharge coefficient calculated from empirical equations
$(C_D)_{measured}$	:	Discharge coefficient calculated from measured values in the experiments
C_{va}	:	Coefficient to account for exclusion of the approach velocity head from the equation
C_{vf}	:	Coefficient of velocity caused by friction loss
D	:	Orifice diameter, location name of the orifice
d	:	Diameter of the holes on the perforated plate
D/h	:	Dimensionless variable 1 obtained from dimensional analysis
E	:	Rack area opening rate, location name of the orifice
e	:	Net opening or clear distance between two rack bars
Fr	:	Froude number $=\frac{V_T}{\sqrt{gh}}$
g	:	Gravitational acceleration
h	:	Flow depth at the depth measurement section of the channel
h_1	:	Upstream head
h_2	:	Downstream head
H_c	:	Critical specific energy head of the flow over screen
K	:	Coefficient obtained from the dimensional analysis
$K_{calculated}$	:	K calculated from empirical equations
$K_{measured}$	:	K calculated from measured values in the experiments
k	:	Regression variable 1
L	:	Length of the Tyrolean screen
l	:	Regression variable 2
L_2	:	Total wetted rack length
m	:	Regression variable 3
n	:	Regression variable 4
Q_T	:	Total discharge at the channel
$(Q_0)_{cal.}$	:	Calculated discharge passing through the orifice
$(Q_0)_{mea.}$	:	Measured discharge passing from the orifice during the time period t in the experiment
$(Q_0)_{the.}$	:	Theoretical discharge passing through the orifice
$(q_w)_i$	:	Diverted unit discharge by the Tyrolean screen
$(q_w)_T$	:	Total unit discharge in the main channel

R^2	:	Correlation coefficient
Re	:	Reynolds number
t	:	Time to measure V
V	:	Measured volume passing from the orifice during time, t
V_0	:	Flow velocity at section (2)
V_T	:	Flow velocity at the depth measurement section of the channel
w	:	Width of the main channel
w/h	:	Dimensionless variable 3 obtained from dimensional analysis
x_i	:	Distance measured from the downstream end of the screen to the center of the circular orifice
x_1	:	Distance measured from the downstream end of the screen to the center of the circular orifice, A
x_2	:	Distance measured from the downstream end of the screen to the center of the circular orifice, B
x_3	:	Distance measured from the downstream end of the screen to the center of the circular orifice, C
x_4	:	Distance measured from the downstream end of the screen to the center of the circular orifice, D
x_5	:	Distance measured from the downstream end of the screen to the center of the circular orifice, E
x/h	:	Dimensionless variable 2 obtained from dimensional analysis
y_0	:	Normal flow depth in the main channel
Δh	:	Differential head
$(\Delta Q_0)_{CD}$	:	Difference between $(Q_0)_{mea.}$ and $(Q_0)_{cal.}$ for C_D values
$(\Delta Q_0)_K$	:	Difference between $(Q_0)_{mea.}$ and $(Q_0)_{cal.}$ for K values
μ	:	Viscosity of water
ρ	:	Density of water
π	:	Symbol of the dimensionless numbers
ω	:	Rack porosity
θ	:	Slope of the screen on which the orifice is located

CHAPTER 1

INTRODUCTION

1.1 General

Hydropower is the most popular and the cleanest renewable source to produce energy after wind and solar energy in the world conditions. Since the wind energy is expensive and is produced when the weather is windy, it is not preferred in the most countries in the world. Moreover, because the solar energy is dependent on the sunshine duration of the region and is not widespread between the public, it is not also rational for the countries. Therefore, if there were a lot of water sources and the hydropower potential in the country, the most sensible and the cleanest source for the energy is the hydropower. If the necessary precautions are not taken to prevent energy shortage, with the increased population and the development of the industrial production, the energy shortage is waiting for Turkey in the next years. According to this brief information, hydropower is very suitable for Turkey geography because Turkey generally consists of mountainous regions and steep river basins. The water resources have very much hydropower potential. In the last years, Turkey noticed the hydropower potential and; therefore, lots of runoff river power plants and huge dams were constructed and are being continued to be constructed; especially in Eastern Anatolia Region and Eastern Black Sea Region. Runoff river power plants are more preferable than the huge dams because they damage the nature and change the climate of the region less.

For runoff river power plants, the bottom intake orifices or racks are preferred to prevent the sediment flowing with the water on the river basin because sediment causes serious damages on the turbine blades. They are simple constructed structures consisting of a channel on the river bottom perpendicular to the river flow and a screen on the top of the channel. Therefore, Tyrolean weirs or bottom intake structures are known as the most suitable intake structures with minimum amount of sediment carried by the diverted flow. Moreover, the amount of the water diverted from the river by the bottom intake orifices is the most important factor affecting the amount of the produced energy by the turbines of the hydroelectric power plants because if the amount of the water diverted from the river by the orifices is less than the design discharge of the orifices, it might cause the economic damage for the investor of the project. Therefore, the efficiency of the orifice must be investigated, carefully. That is to say, the screen must be sized according to the sediment size on the riverbed not to enter the channel and large enough for diverting water needed by the turbines. A sketch of a typical Tyrolean weir is shown in Figure 1.1 with its parameters. In the figure, there are two types of screens for bottom intake structures. The first one is composed of steel racks with suitable rectangular holes. The other one is the perforated plate that has circular holes in definite places (Figure 1.1). In this study, the water capture efficiency of the second one that's the circular bottom intake orifices was investigated by means of some experiments conducted.

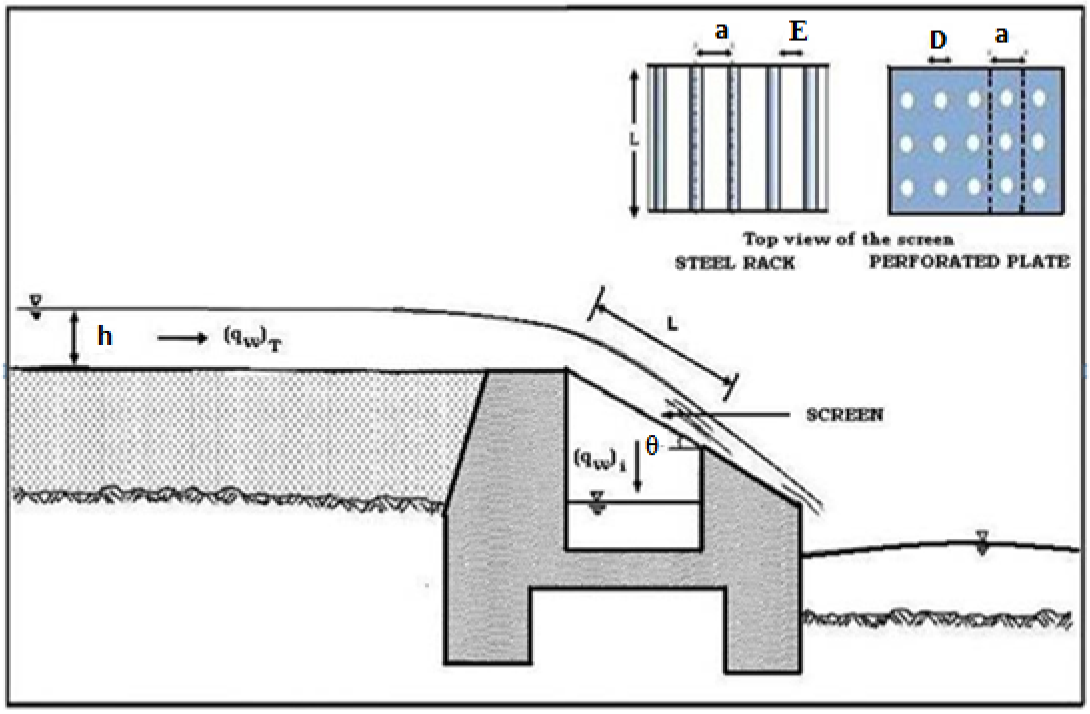

Figure 1.1: Typical Tyrolean weir and its screen types (Sahiner, H., 2012)

In Tyrolean weirs, water and sediment carried by the flow or river are diverted from the river by favor of a screen made of metal plates generally steel into a collection channel. The collection channel is usually a concrete-made structure. The water intake screens are located over the collection channel at a certain inclination and size. After the collection channel, water and sediment flow to the sediment tank by the help of gravity. The most important point for these structures is to have maximum water and minimum sediment diverted by the orifices to the collection channel bound to the turbines.

The basic design variables for circular bottom intake orifices are the diameter of the perforation and the center spacing between the openings "a" (Figure 1.1). These variables can be changed according to the material passing from the orifices.

It is the purpose of this thesis study to investigate the relationship between the discharge of the diverted flow and the properties of bottom intake orifices for instance, orifice diameter, D, distance from the free fall at the orifice to the center of the circular orifice, x, and angle of the orifice with respect to the plane of the channel, θ, moreover, flow properties such as flow or water depth at the channel, h. Therefore, a series of experiments were carried out in a hydraulic model of the flow channel with circular bottom intake orifices that are in different diameters, locations and slopes in the Hydromechanics Laboratory at METU since the model studies are usually needed for this type of researches.

The literature review is represented in the next section. After that, the theoretical study about the thesis topic is shared in Chapter II. In Chapter III, the experimental setup and the details about the experimental procedure are stated. Analysis of the experimental data and discussion of the results are considered in Chapter IV. Conclusions and the further recommendations are given in Chapter V. Finally, the measured and calculated parameters for the experiments performed with single and multiple circular bottom intake orifices are presented in Appendix A and B, respectively.

1.2 Literature Review

Brunella, et al. (2003) carried out a range of experiments in order to obtain useful information about the effect of the rack geometry, the rack porosity and the bottom slope on the hydraulic performance of the bottom rack intakes. They used a rectangular channel for the experiments which sized 0.5 m in width and 7.0 m in length. The elevation difference between the upstream and downstream beds was 0.493 m. Different geometries of circular bars comprising the bottom rack intake used in the experiments were 12 and 6 mm in diameter, 0.60 m and 0.45 m in length, had a clear spacing of 6 mm and 3 mm. The angle values of bottom rack intake were 0, 7, 19, 28, 35, 39, 44 and 51°. During the experiments, the water surface profiles and velocity distributions over the bottom rack were measured and it was showed that for small and large bottom inclinations, the free surface profiles are almost the same. Brunella et al. derived an equation for relative intake length using their own data and some other data from the literature obtained from the tests of circular racks and ovoid profiles practically 100% intake discharge $[(q_w)_i = (q_w)_T]$:

$C_D\, \omega\, (L_2/H_c)=0,83$ ………………………………………………………………………… (1.1)

where C_D is the discharge coefficient and was found varying between 0.87 and 1.10 as a function of ω, ω is rack porosity corresponding to the ratio of the total net spacing between the rack bars to the main channel width, L_2 is the wetted rack length and H_c is the critic energy head. It was also stated that the value of C_D could attain values higher than one as a consequence of the Coando effect arising when the bar clearance is small enough.

Kamanbedast and Bejestan (2008) did a scientific research about the effects of slope and area opening of the screen on the discharge ratio in bottom intake structures made of steel rectangular racks. They did not use circular orifices in their study, but the main objectives are the same. For their aims, a bottom intake model was constructed in a flume 60 cm wide, 8 m long and 60 cm high. The model was tested under five different flow discharges, four different screen slopes of 10, 20, 30 and 40% and three different rack area opening rates (E) of 30, 35 and 40% using two different sizes of bars, 6 and 8 mm diameter. Figure 1.2 shows that firstly, as the slope of rack increases, the discharge ratio increases, too. After the maximum value of the discharge ratio, it decreases towards the minimum value. Moreover, as the rack area opening rate increases, the discharge ratio also increases. As a result, the maximum discharge ratio, 0.8, was obtained when the rack area opening rate and the slope was 40% and 30%, respectively.

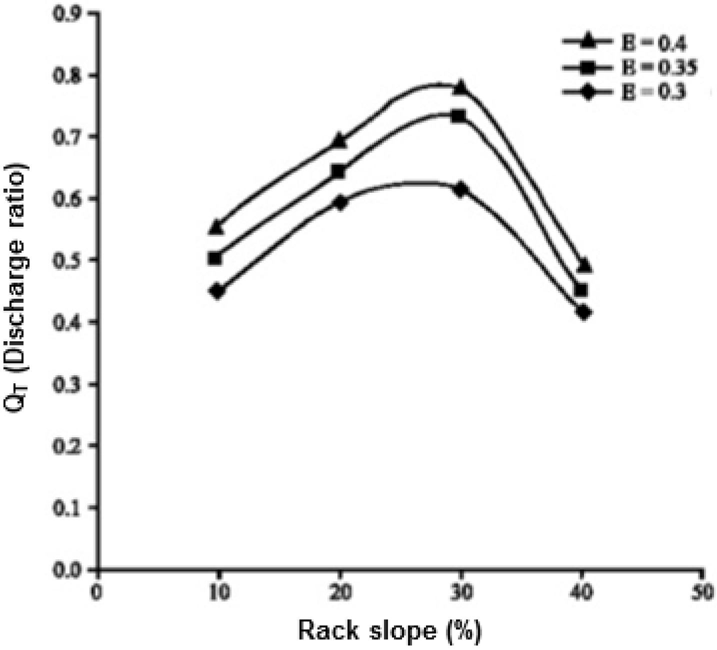

Figure 1.2: Values of discharge ratio against slope for three different rack openings: No sediment in the flume (Kamanbedast, A. A., Bejestan, M. S., 2008)

Yılmaz (2008) conducted a series of experiments in a rectangular model 7.0 m long and 1.98 m wide to investigate the hydraulic characteristics of Tyrolean weirs at the Hydromechanics Laboratory. The Tyrolean screens were made of aluminum bars having 1 cm diameter circular cross sections. The experiments were conducted with and without sediments and were repeated for three clear distances between bars, e; 3 mm, 6 mm and 10 mm, and three angles of rack inclination; 4.8°, 9.6° and 14.5°. Variations of the discharge coefficient $C_{d,}$ the ratio of the diverted discharge to the total water discharge, $[(q_w)_i/(q_w)_T]$, and the dimensionless wetted rack length , L_2/e, with relevant dimensionless parameters were plotted. From these figures, for a given main channel discharge, the amount of the diverted discharge for a Tyrolean screen of known rack length, rack inclination and bar opening within the limits of the parameters tested in that study can be determined.

To investigate the hydraulic characteristics of Tyrolean type water-intake structures, Sahiner (2012) conducted a series of experiments at the Hydromechanics Laboratory as a continuation of Yılmaz's study in the same rectangular model 7.0 m long and 1.98 m wide. In this experimental study, the diverted flow from the main channel through the intake structure having metallic racks and perforated plates of different types were measured. The experiments were conducted in two stages. In the first stage, the tests were carried out with only steel racks having three different bar openings and slopes, and in the second stage, perforated screens of three different circular openings and screen slopes were used. Applying dimensional analysis to the related parameters of the system the dimensionless terms were defined for the water capture efficiency and the discharge coefficient of the system, and their variations with the relevant parameters were presented. Using these diagrams, one can determine the amount of water to be diverted by a Tyrolean weir of known geometry from a main channel of known discharge.

In the Water Measurement Manual of Water Resources Research Laboratory of United States Department of the Interior Bureau of Reclamation (2012), the discharge equation for a submerged rectangular orifice is determined by the equation given below:

$$Q = C_c C_{vf} C_{va} A\sqrt{2g(h_1 - h_2)} \quad (1.2)$$

where Q is the discharge passing through the orifice, C_c is the coefficient of contraction, C_{vf} is the coefficient of velocity caused by friction loss, C_{va} is the coefficient to account for exclusion of the approach velocity head from the equation, A is the area of the orifice, g is gravitational acceleration, h_1 is the upstream head and h_2 is the downstream head.

$C_c C_{vf} C_{va}$ is called the discharge coefficient which has been determined experimentally to be 0.61 for rectangular irrigation weirs. The coefficient of contraction has the most influence on the discharge coefficient. Moreover, if the difference between upstream and downstream heads or water surface elevations is called the differential head, $\Delta h= h_1-h_2$,the modified equation is given as:

$$Q = C_d A\sqrt{2g\Delta h} \quad (1.3)$$

CHAPTER 2

THEORETICAL STUDY

2.1 Introduction

The theoretical studies about the performance of the circular bottom intake orifices were presented in this chapter. An expression for the discharge coefficient was derived by using some theoretical formulas. Moreover, another coefficient and some other dimensionless parameters were obtained from the dimensional analysis.

2.2 Derivation of the Discharge Coefficient for Circular Bottom Intake Orifices

According to the definition sketch given in Figure 2.1, the energy (Bernoulli) equation can be written along a streamline passing through two points; the one is on top of section (1) and the other one is at the center of the orifice at section (2) (2_A, 2_B, 2_C, 2_D, or 2_E) assuming that the velocity profile is uniform over the flow depth at section (1), there is no surface tension effect and the energy loss is negligible, as:

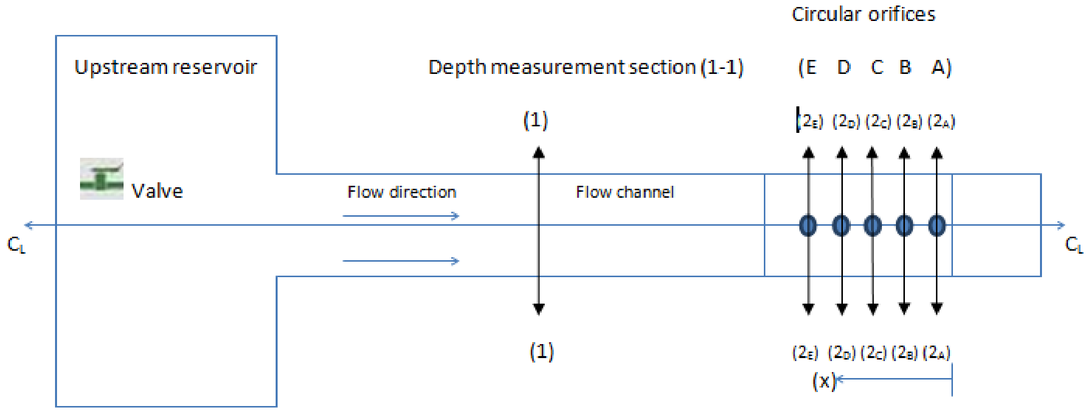

(a) Top view

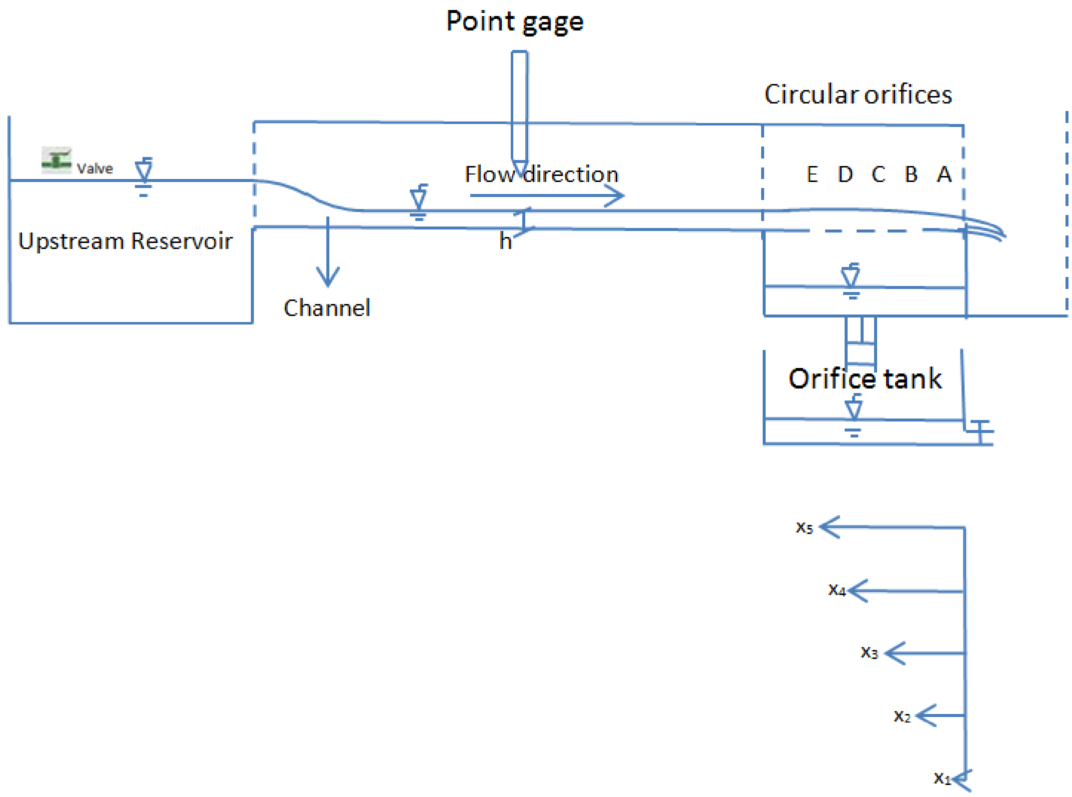

(b) Side view

Figure 2.1: Definition sketch for a Tyrolean weir having circular orifices (a) Top view (b) Side view

$$h+\frac{V_T^2}{2g}=\frac{V_0^2}{2g} \quad \text{……………………………………………………………………} (2.1)$$

where h is the flow depth at section (1), V_T and V_0 are flow velocities at sections (1) and (2), respectively, and g is gravitational acceleration.

By assuming the channel bottom as the datum and stating that

$$V_T=\frac{Q_T}{A_T} \quad \text{……………………………………………………………………….. } (2.2)$$

where Q_T is the total discharge in the main channel and A_T is the total flow area at the depth measurement section (A_T=h.w, where w is the width of the main channel). The theoretical velocity at the orifice can be written as

$$V_0=\sqrt{2g(h+\frac{V_T^2}{2g})} \quad \text{………………………………………………………………...} (2.3)$$

The theoretical discharge passing through the orifice, $(Q_0)_{theoretical}$ or $(Q_0)_{the.}$, can be calculated as

$$(Q_0)_{the.}=A_0V_0=A_0\sqrt{2g(h+\frac{V_T^2}{2g})} \quad \text{…………………………………………………… } (2.4)$$

where A_0 is the circular orifice area and

$$A_0=\frac{\pi D^2}{4} \quad \text{…………………………………………………………………………… } (2.5)$$

where D is the orifice diameter.

After that, in order to find the discharge coefficient C_D, the measured discharge passing from the orifice during the time period t in the experiment, $(Q_0)_{mea.}$ is divided by $(Q_0)_{the}$. So,

$$C_D=\frac{(Q_o)_{mea.}}{(Q_0)_{the.}} \quad \text{…………………………………………………………………………. } (2.6)$$

It should be emphasized that C_D is the only discharge coefficient in this study in order to find the relationship between $(Q_0)_{mea.}$ and $(Q_0)_{the.}$. The variation of C_D with the related dimensionless parameters will be presented at the end of the following section.

2.3 Application of Dimensional Analysis to the Problem of Flow through Circular Orifices

For the circular bottom intake orifices of which the hydraulic and geometric parameters are described in Figure 2.1, the following equation for the diverted discharge, $(Q_0)_{mea.}$, through the circular bottom intake orifices can be written as a function of the appropriate variables, assuming that surface tension effects, effects of viscosity and fluid compressibility are negligible.

$(Q_0)_{mea..}= f(V_T, h, D, w, x, \theta, g, \rho, \mu)$……………………..……………………………….. (2.7)

where V_T is the flow velocity at the depth measurement section of the channel, h is the flow depth at the depth measurement section of the channel, D is the orifice diameter, w is the width of the channel, x is the distance from the free fall of the channel at the exit section to the center of the circular orifice, θ is the slope of the screen on which the orifice is located, g is the gravitational acceleration, ρ is the density of water and μ is the viscosity of water.

By selecting ρ, V_T and h as the repeating variables and applying the Buckingham's π theorem, the dimensionless terms given in Equation 2.8 are obtained.

$$\frac{(Q_0)_{mea..}}{h^2 V_T} = f\left(\frac{D}{h}, \frac{x}{h}, \frac{w}{h}, Fr, Re, \theta\right) \quad (2.8)$$

where Fr is the Froude number, $Fr = \frac{V_T}{\sqrt{gh}}$, and Re is the Reynolds number, $Re = \frac{\mu}{\rho V_T h}$.

Since the width of the main channel, w, is constant in this study and any parameter related to the main channel discharge will not be studied, the term of w/h can be dropped from Equation 2.8. In open channel flows, the effect of Re on the flow parameters is negligible compared to Fr. Therefore; Re in Equation 2.8 can also be removed. Eventually, Equation 2.8 can be written as

$$(Q_0)_{mea.} = V_T h^2 K \quad (2.9)$$

where K=f(D/h, x/h, Fr, θ)

Since the discharge coefficient C_D presented in Equation 2.6 and the parameter K given in Equation 2.9 are both practically describe the similar discharge coefficients, one can also express C_D as a function of the dimensionless parameters given in Equation 2.9 as;

$$C_D = f\left(\frac{D}{h}, \frac{x}{h}, Fr, \theta\right) \quad (2.10)$$

In Chapter 4, the variation of K and C_D with the related dimensionless terms stated above will be presented.

CHAPTER 3

EXPERIMENTAL SETUP AND PROCEDURE

3.1 Experimental Setup

To investigate the hydraulics of circular bottom intake orifices, a physical model was constructed at the Hydromechanics Laboratory at METU. The model consists of a reservoir at the upstream which was about 0,6 m in length, 1.60 m in width and about 0.5 m in depth, a water intake pipe, an open channel, a screen of bottom intake structure, a point gage for measurement of water surface level in the channel with 1 mm precision and a reservoir at the downstream which was 1 m in length, 1 m in width and 0.50 m in depth, (Figures 3.1-3.9). Water was taken from the constant-head reservoir by a pipe 5 cm in diameter and the discharge was controlled with a hand-controlled valve. The head-discharge curve of the experimental setup was prepared after measuring the discharge volumetrically at various flow depths recorded at the flow depth measurement section by a series of experiments conducted before the experiments of the circular bottom intake orifices. Water coming into the system from the pipe was firstly collected in the upstream reservoir to reduce the turbulence of the flow and to provide a smooth flow towards the channel. To determine the water depth in the channel, at a location 1.28 meter downstream from the radial inlet section of the channel, a point gage was placed in the middle of the channel. The channel's length, width and slope were 3 m, 0.30 m and 0.001, respectively.

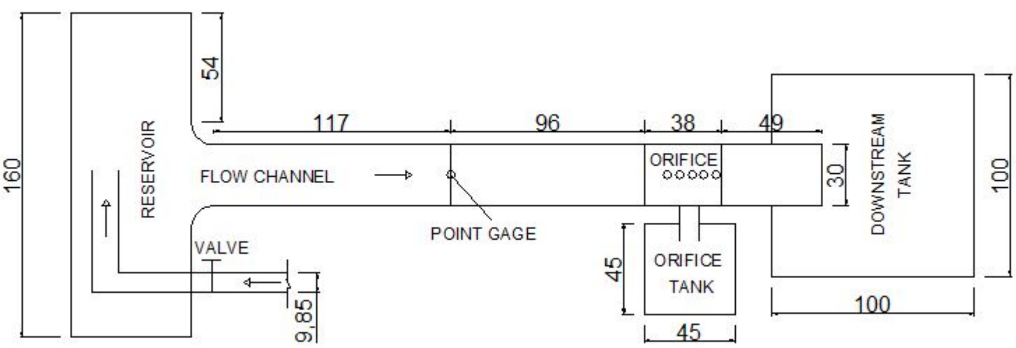

Figure 3.1: Top view of the experimental setup (all dimensions are in cm.)

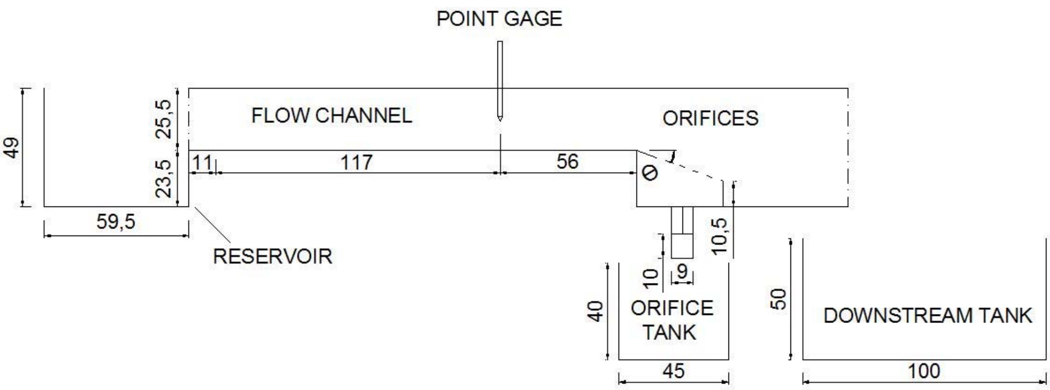

Figure 3.2: Side view of the experimental setup at orifice angle of θ (all dimensions are in cm.)

Figure 3.3: General view of the experimental setup

Figure 3.4: Top view of the circular bottom intake orifices

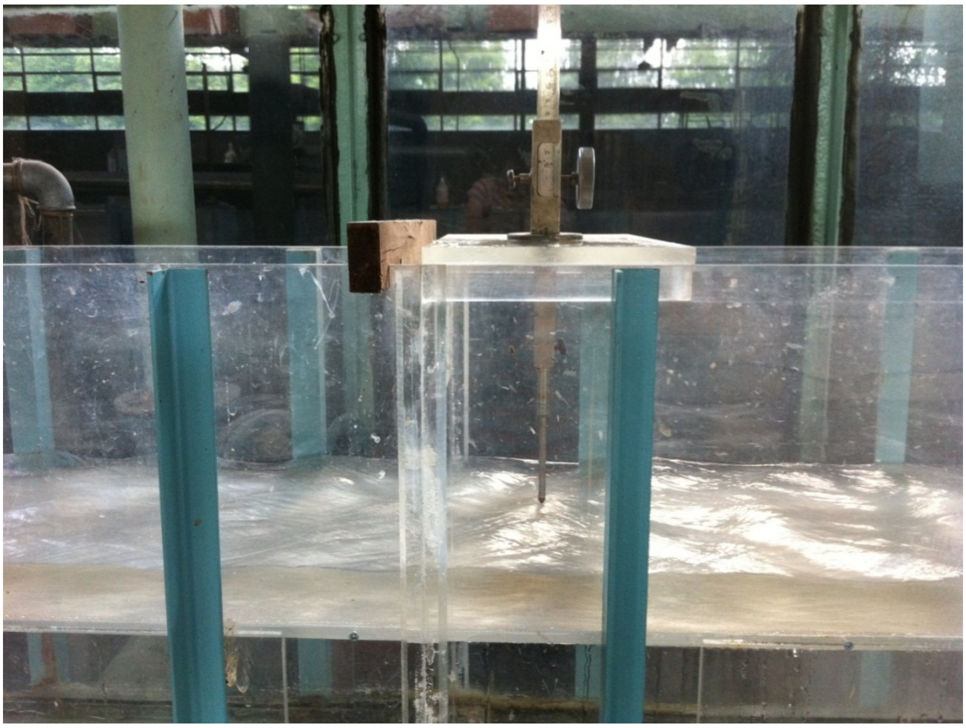

Figure 3.5: View of the point gage used in the flow depth measurements

Figure 3.6: View of the downstream reservoir where water is collected

Figure 3.7: Side view of the upstream reservoir and hand-controlled valve on the discharge pipe

Figure 3.8: General view of the tank in which water coming from the orifices is collected

Figure 3.9: Bottom intake structure with multiple circular bottom intake orifices on the screen

The screen of the circular bottom intake orifices was located at the downstream of the channel before the free fall. The elevation difference between upstream and downstream sections of the screen was 23.50 cm. The screen was made of fiber glass transparent material, about 3 mm in thickness. The experiments were conducted for five different orifice diameters (D_1=1.0 cm, D_2=1.5 cm, D_3=2.0 cm, D_4=3.0 cm and D_5=4.0 cm) and for three different screen slopes (θ_1 = 0°, θ_2 = 10° and θ_3 = 20°). The circular orifices were located on the screen. In Figures 3.10-3.12, the photographs of the screens used in the experiments with all slopes are showed with all details. At the bottom of the screen, there is a collection channel which is 0.30 m wide, 0.38 m long, 0.24 m high and has a slope of about 0.01.Water and sediment coming into the bottom intake structure are directed to the sediment trap reservoir through the collection channel, but in this study, as defined above, the effects of sediment to the hydraulics of circular bottom intake orifices was not investigated, only water flow was considered.

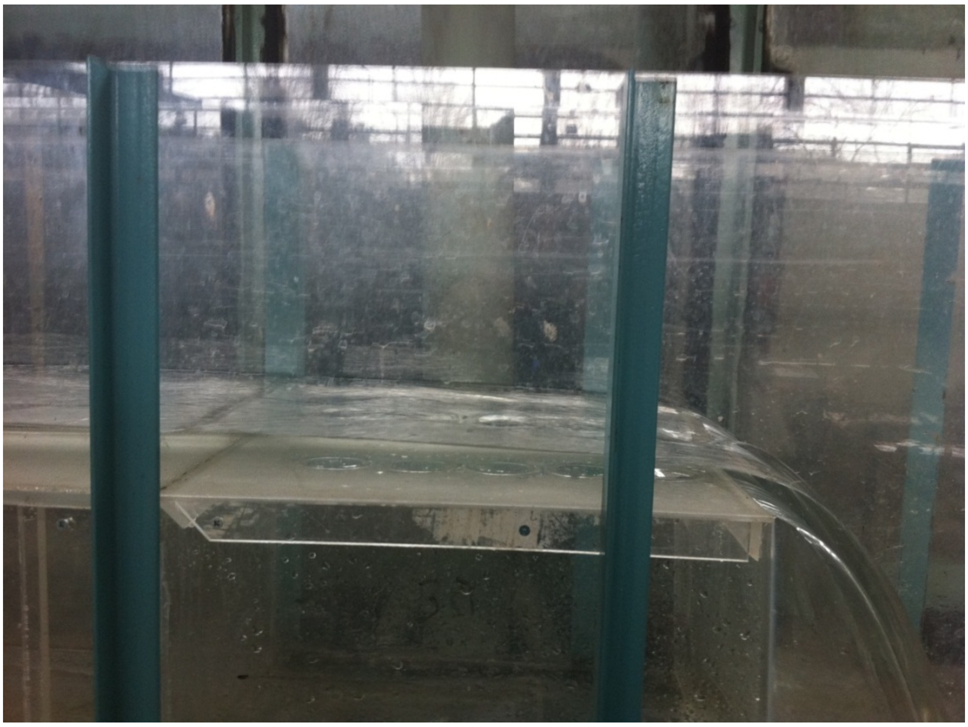

Figure 3.10: Bottom intake structure with a slope of θ_1 = 0°

Figure 3.11: Bottom intake structure with a slope of $\theta_2 = 10°$

Figure 3.12: Bottom intake structure with a slope of $\theta_3 = 20°$

3.2 Experimental Procedure

3.2.1 Discharge Measurements in the Channel

A set of experiments was conducted to find the discharge calibration curves of the channel with respect to flow depth before placing the circular orifices on the screen. In the first step, a small amount of water was given to the system from the water intake pipe by opening the hand-controlled valve, and after waiting for about 5 minutes in order to eliminate the waves on the water surface in the channel, the stage of the water surface at the upstream section of the channel with the point gage which is in 0.1 mm precision was recorded. Then, the flow depth was found by subtracting the bottom stage of the channel from the stage of the water surface at the upstream section of the channel. The discharge of the water intake pipe was measured volumetrically by collecting the incoming water into the downstream reservoir over a certain time period. After that, the discharge was increased gradually with the valve at the end of the intake pipe and the other measurements were taken for a wide range of discharge with the same procedure mentioned above. The measured discharges, named as "total discharge Q_T", and the corresponding flow depths, h, measured at the depth measurement section, used in the derivation of the discharge rating curve are presented in Table 3.1. Afterwards, the polynomial curve given by Equation 3.1 was driven with a correlation coefficient of R^2=0.999 (Figure 3.13).

$Q_T=0.035h^3-0.015h^2+0.760h-0.650$ ……………………………………..……………..(3.1)

which is valid for 1.3 cm $\leq$ h $\leq$4.6 cm.

Table 3.1: Measured Q_T and h values used in forming the discharge rating curve of the experimental setup

Test no	h(cm)	Q_T (lt/sec)
1	1.3	0.39
2	1.5	0.59
3	1.9	0.96
4	2.6	1.86
5	3.3	2.99
6	3.65	3.60
7	4.1	4.65
8	4.6	5.95

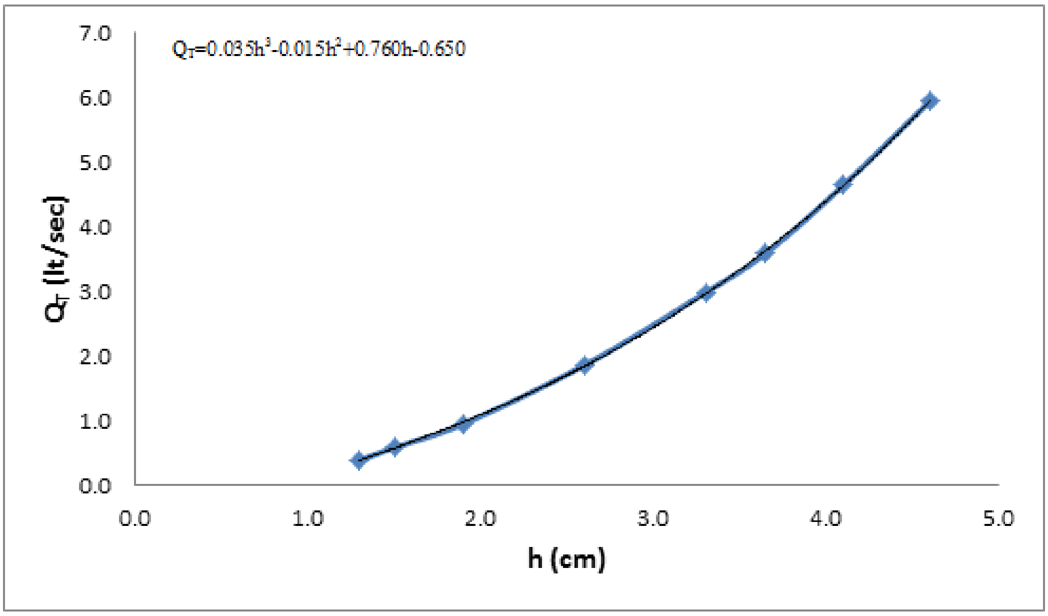

Figure 3.13: Discharge rating curve for the channel

3.2.2 Discharge Measurements in the Circular Bottom Intake Orifices

In order to measure the discharges passing through the circular bottom intake orifices on the screen, a series of experiments was carried out on the model. There were 5 circular openings or orifices on the screen from downstream to upstream name as A, B, C, D and E, respectively (Figure 2.1). The screen of the model was manufactured in such a way that at each location of the orifices stated above, A, B, C, D and E, five circular orifices having different diameters, 1.0 cm, 1.5 cm, 2.0 cm, 3.0 cm and 4.0 cm, but the same center could be located. To do this, first, on the screen, the circular holes of 4.0 cm diameter were opened at the locations of A, B, C, D and E. Then, portable circular cabs having 1.0 cm, 1.5 cm, 2.0 cm, 3.0 cm and 4.0 cm diameter circular openings were made from plexiglas. Therefore, the diameters of the circular orifices at a desired location could easily be changed from 1.0 cm up to 4.0 cm by placing the appropriate portable caps. At each predetermined location; A, B, C, D and E; totally five orifices of different diameters could be formed (Table 3.2).

The location of the orifice center from the downstream end of the screen which is designated by x is an important parameter for the amount of water to be diverted by the orifice to the collection channel. Since there are 5 different locations along the centerline of the screen to locate the orifices, there are 5 different x values for the experimental setup, which are presented in Table 3.2.

Table 3.2: Locations of orifices from the free fall section of the model, x_i (Figure 2.1).

Orifice location	Diameters of the orifices tested, D (cm)	x_i (cm)
A	1.0, 1.5, 2.0, 3.0, 4.0	3
B	1.0, 1.5, 2.0, 3.0, 4.0	9
C	1.0, 1.5, 2.0, 3.0, 4.0	15
D	1.0, 1.5, 2.0, 3.0, 4.0	21
E	1.0, 1.5, 2.0, 3.0, 4.0	27

The x values tabulated in Table 3.2, x_1, x_2, x_3, x_4 and x_5 are the distances measured from the downstream end (free fall section) of the screen to the center of the circular orifices, A, B, C, D and E, respectively (Figure 2.1).

The main purpose of the experiments was to investigate the water capture efficiencies of the orifices at different places, diameters and slopes. In the experiments, at the first step, the valve at the end of the water intake pipe was opened slowly and the upstream reservoir was filled with water. The flow depth in the channel, h, was stabled at about 1.30 cm and the screen slope, θ, was kept at θ_1 (θ_1=0°). Then, one orifice with a certain diameter such as A5 was opened to divert water. The other orifices were closed with portable caps. After that, for a definite volume of water diverted by the orifice, the elapsed time was measured with a chronometer with split second precision. When the definite volume was divided by the elapsed time, the measured discharge passing from the orifice during time, t in the experiment could be found. Later, it was divided by the calculated discharge of the orifice determined by using the theoretical formulas, and finally, the discharge coefficient, C_D, was calculated (Equation 2.6). This procedure was applied for other orifices that were B5, C5, D5 and E5, in return. In the following stage, the orifice diameters were changed like A4, B4, C4, D4, E4, A3, B3, C3, D3, E3, A2, B2, C2, D2, E2, A1, B1, C1, D1 and E1, respectively. After the first stage was completed for the first flow depth, the flow depth was increased by opening the valve a little more. 6 flow depths which were ranged from 1.30 cm to 4.50 cm were used in the experiments. When the experiments were completed for no slope screen, the slope of the screen was changed as θ_2, and θ_3 (θ_2=10° and θ_3=20°), respectively. The procedure of the no slope screens was applied for 10° and 20° slope screens, too. For each slope, 150 experiments and totally 450 experiments were conducted. The experimental procedure was similar for each screen having different orifices (A, B, C, D and E), different angle of inclinations (θ_1=0°, θ_2=10° and θ_3=20°) and different orifice diameters (D_1=1.0 cm, D_2=1.5 cm, D_3=2.0 cm, D_4=3.0 cm and D_5=4.0 cm). All of the measured quantities were presented in tabular forms in Appendix A.

As of extra concern, the procedure mentioned above was also applied for multiple circular orifices. In other words, all circular orifices were opened simultaneously and the experiments were performed with three different flow depths ranged from 1.30 cm to 2.70 cm for each screen having different orifices (A, B, C, D and E), different angle of inclinations (θ_1=0°, θ_2=10° and θ_3=20°) and different orifice diameters (D_1=1.0 cm, D_2=1.5 cm, D_3=2.0 cm,

D_4=3.0 cm and D_5=4.0 cm) because the capacity of the model was not suitable for flow depths larger than 2,70 cm in multiple orifices. The main objective in this extra study was to have an idea about the efficiency of the multiple circular bottom intake orifices in diverting water from the flow channel to the collection channel. All of the measured quantities were presented in tabular forms in Appendix B.

CHAPTER 4

ANALYSIS OF THE EXPERIMENTAL DATA AND DISCUSSION OF THE RESULTS

4.1 Introduction

In this chapter the data obtained from the experiments; discharge coefficients, C_D, coefficients obtained from dimensional analysis, K, and the dimensionless variables obtained from dimensional analysis were analyzed and the relationships between the relevant parameters were presented with graphs.

4.2 The Studies Related to the Single Circular Bottom Intake Orifice on the Screen

In this section, the results of the experimental studies carried out on the single circular bottom intake orifices on the screen with different locations, slopes and diameters were presented.

4.2.1 Relationship between Discharge Coefficient, C_D, and the Related Dimensionless Parameters for Single Circular Bottom Intake Orifices on the Screen

The relationship between C_D and the relevant dimensionless parameters are given by Equation 2.10.

Figures 4.1-4.5 show the variation of C_D values with the dimensionless variable, D/h, for all single circular bottom intake orifices tested at the locations of A, B, C, D and E, respectively at 0° slope condition of the bottom intake screen. The general trends of all the data given in these figures are very similar; C_D values are above 1.0 for D/h less than about 0.5 and then C_D values decrease as D/h values get larger than 0.5 and attain the value of about 0.2 for the value of D/h about 3.0. Except the zone of D/h between 0.5 and about 1.25; the C_D data of the orifices of different diameters at a given location fall almost on a single curve in such a way that C_D values increase as the orifice diameter decrease. Only for the orifices of diameters 1.0 cm, C_D values greater than 1.0 are obtained.

Figures 4.6-4.10 show the variation of C_D with the dimensionless variable D/h for all circular bottom intake orifices having different orifice diameters, D, separately at 10° slope condition of the bottom intake screen. In these figures, it is seen that, different than Figures 4.1-4.5, the data of C_D for each orifice tested follow different trends. At orifices of small diameters C_D increases at different rates with increasing D/h. As the orifice diameter increases, C_D values start decreasing with increasing D/h. The C_D data of the orifices with larger diameters, D= 3 cm and 4 cm, almost coincide with each other.

Figures 4.11-4.15 show the variation of C_D values with the dimensionless variable D/h for all circular bottom intake orifices that have the different orifice diameters, D, separately at 20°

slope condition of the bottom intake screen. The C_D of each orifice at a given location follows different trends in these figures. While C_D values of the small-diameter orifices increase rapidly with increasing D/h, as the orifice diameter gets larger, C_D values increase gradually with increasing D/h and then start decreasing slowly.

Finally, it can be concluded that the circular orifices with the smallest diameters give the largest C_D values for the range of D/h values tested in this study regardless of the screen inclination.

For a bottom intake screen of known; slope θ, orifice diameter D, flow depth at the depth measurement section of the channel h and the distance from the free fall section of the bottom intake screen to the center of the circular orifice x, one can easily determine the diverted measured discharge passing from the orifice after determining the C_D value from one of the relevant figures and then substituting its value in Equation 2.6.

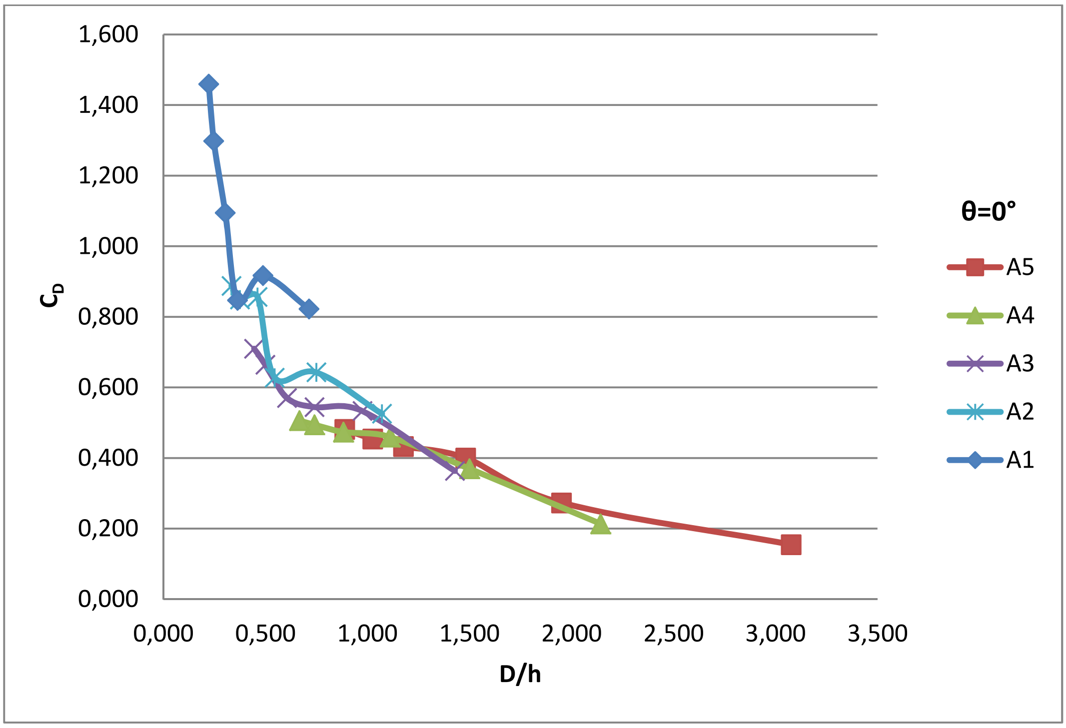

Figure 4.1: Discharge coefficient versus D/h for the orifice A with different D values at θ=0°

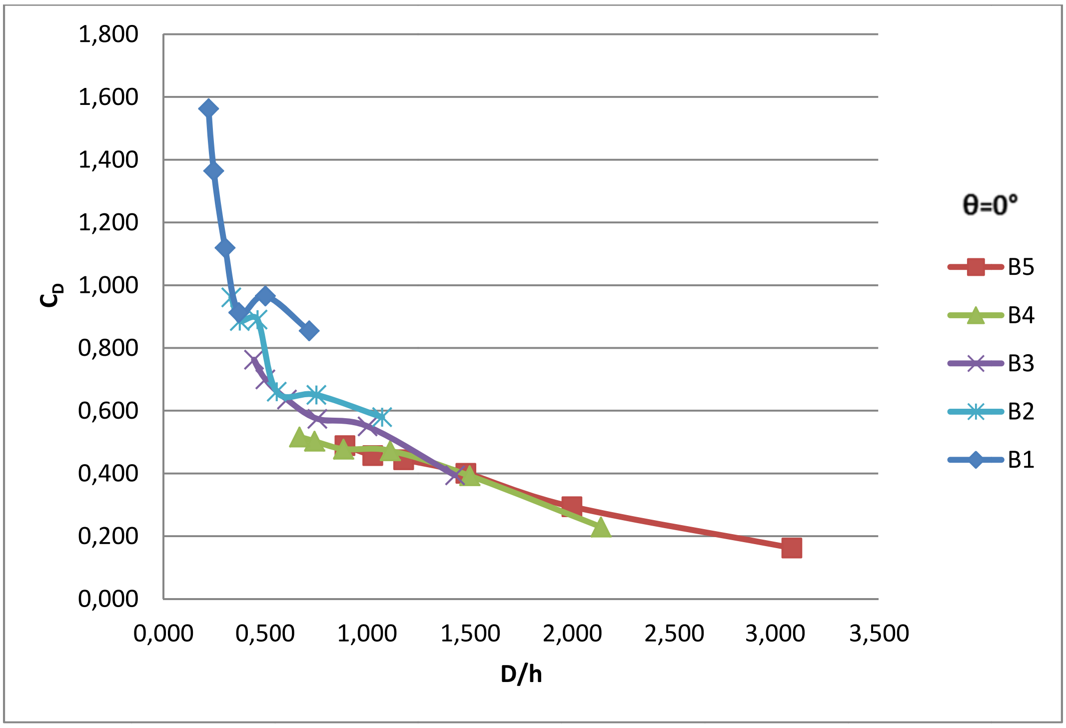

Figure 4.2: Discharge coefficient versus D/h for the orifice B with different D values at θ=0°

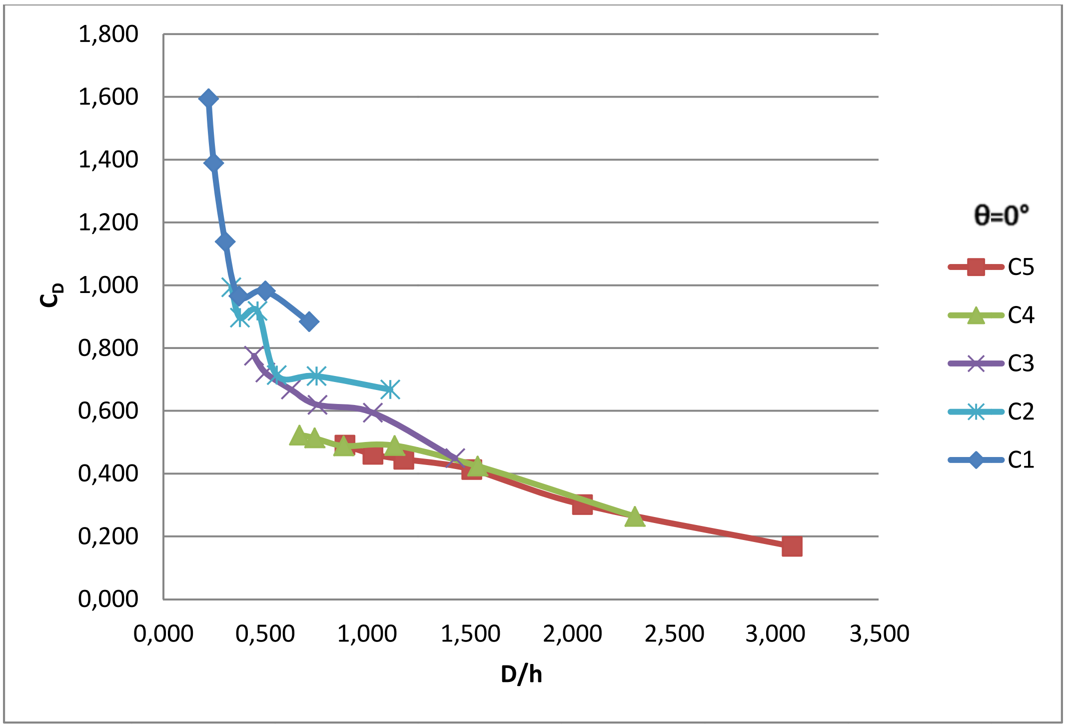

Figure 4.3: Discharge coefficient versus D/h for the orifice C with different D values at θ=0°

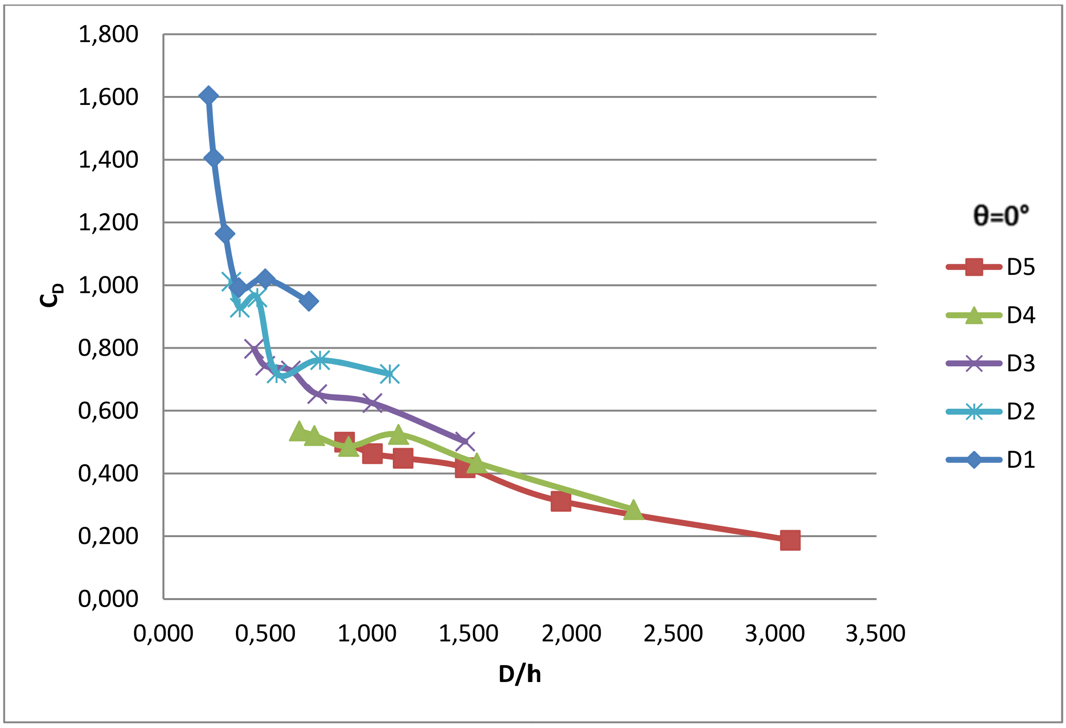

Figure 4.4: Discharge coefficient versus D/h for the orifice D with different D values at θ=0°

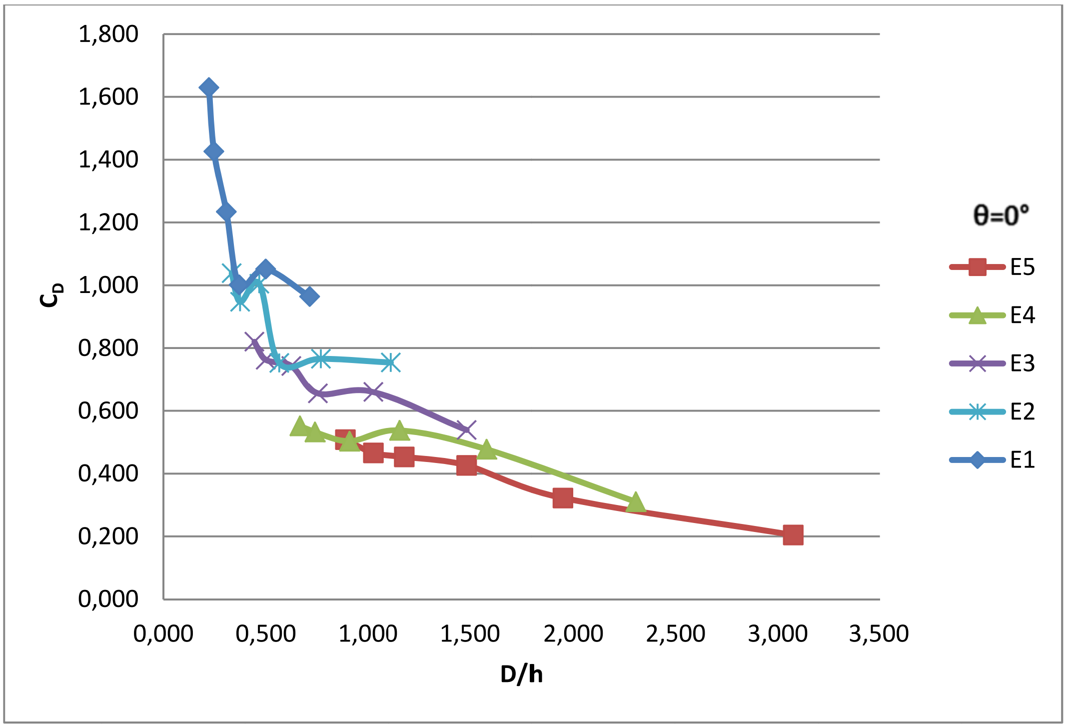

Figure 4.5: Discharge coefficient versus D/h for the orifice E with different D values at θ=0°

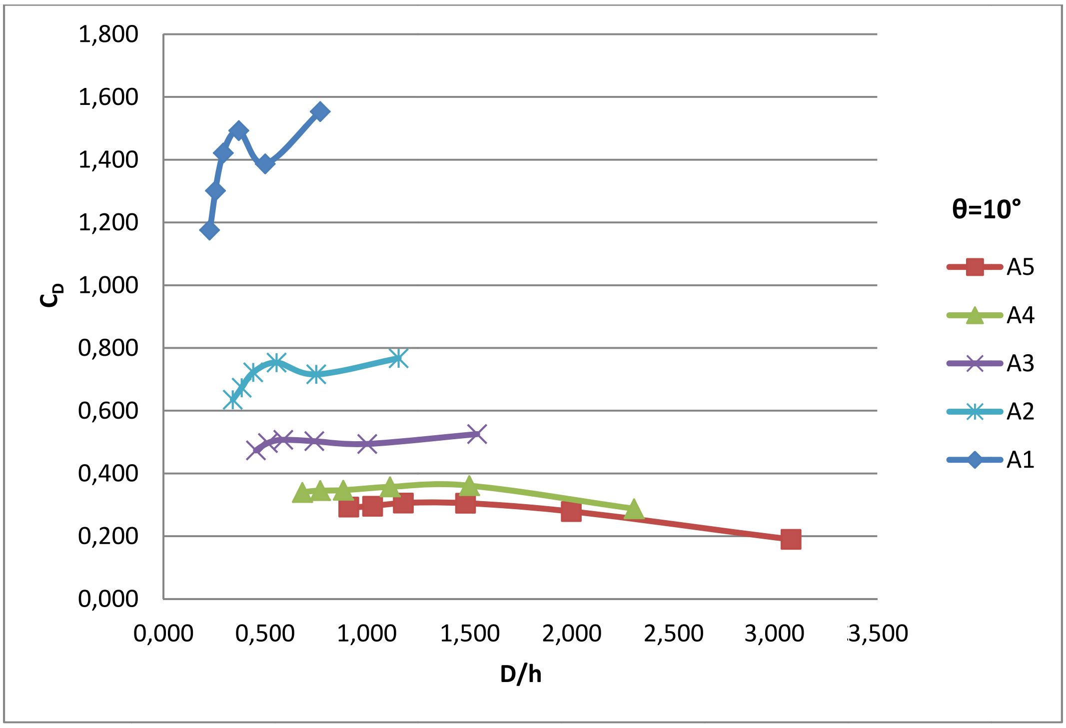

Figure 4.6: Discharge coefficient versus D/h for the orifice A with different D values at θ=10°

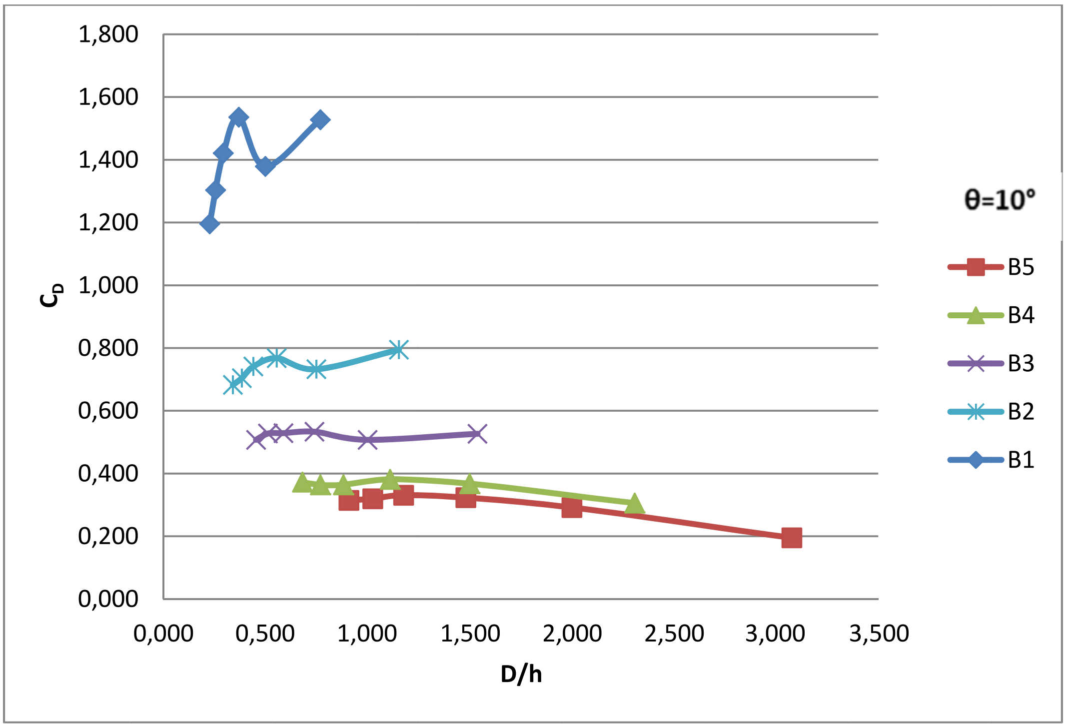

Figure 4.7: Discharge coefficient versus D/h for the orifice B with different D values at θ=10°

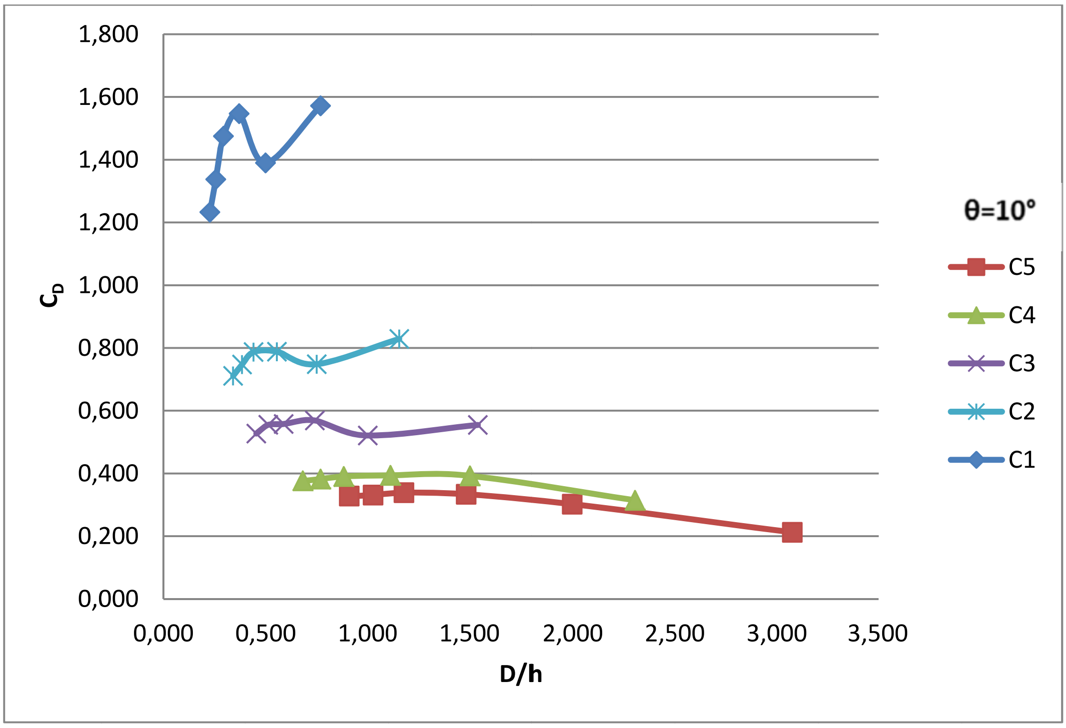

Figure 4.8: Discharge coefficient versus D/h for the orifice C with different D values at θ=10°

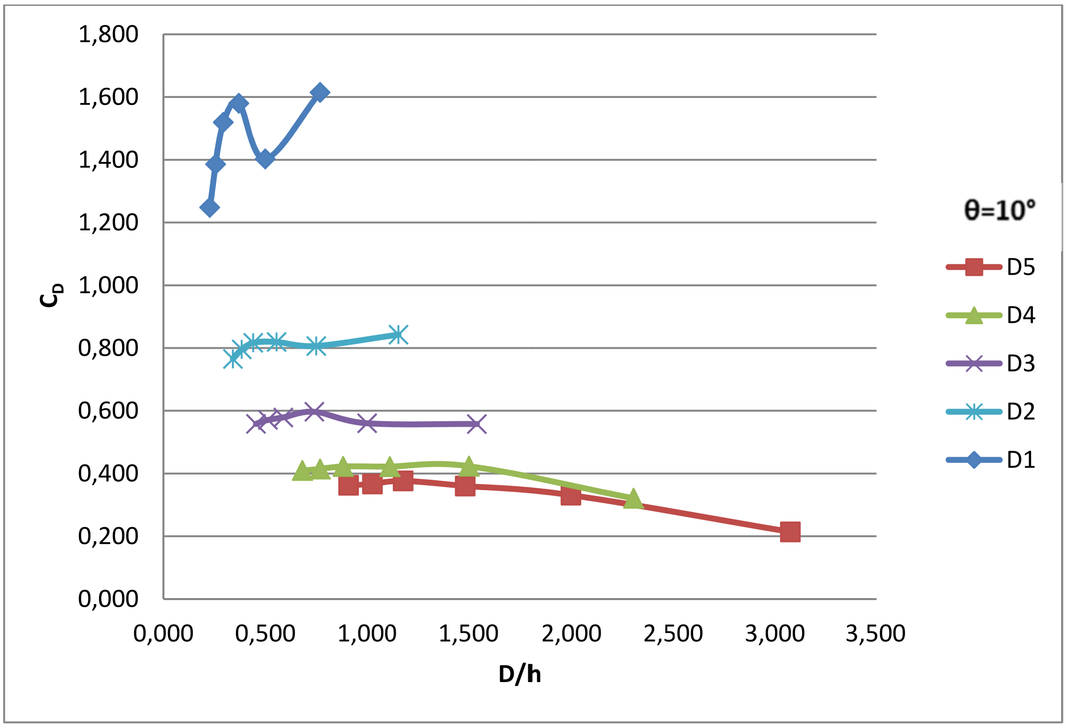

Figure 4.9: Discharge coefficient versus D/h for the orifice D with different D values at θ=10°

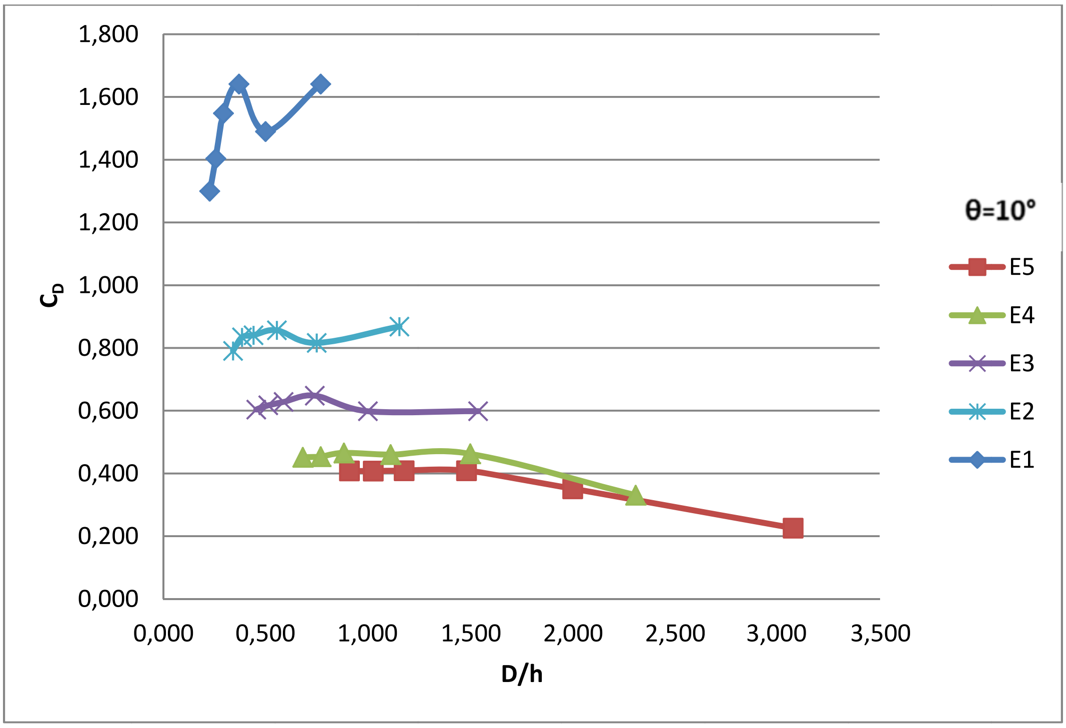

Figure 4.10: Discharge coefficient versus D/h for the orifice E with different D values at θ=10°

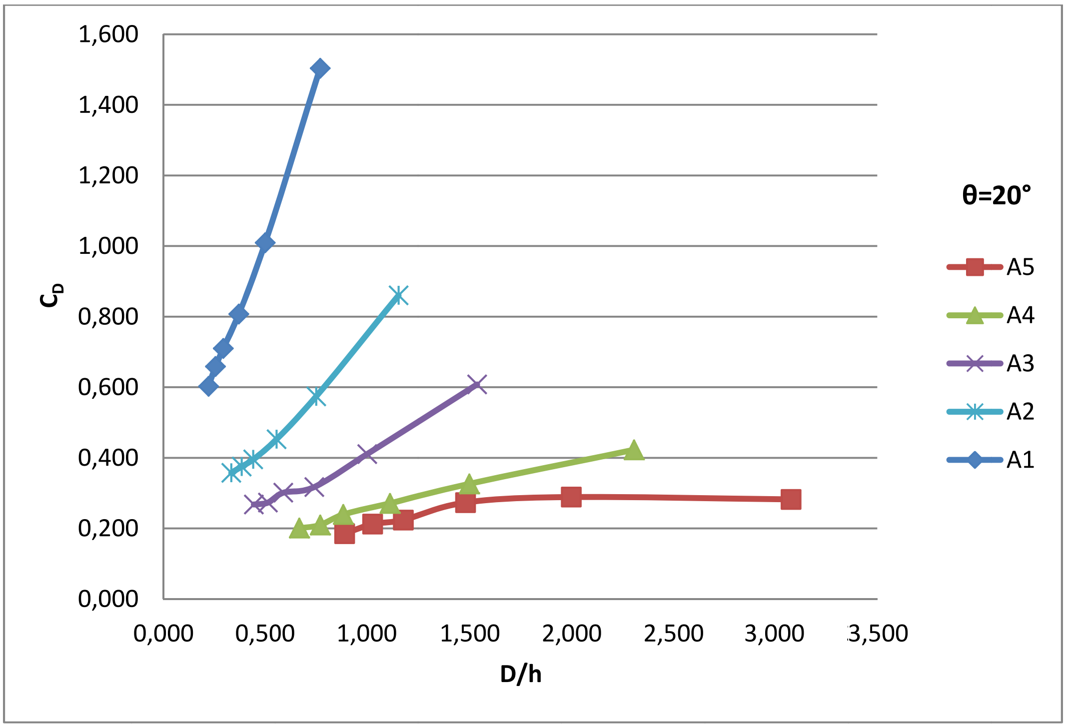

Figure 4.11: Discharge coefficient versus D/h for the orifice A with different D values at θ=20°

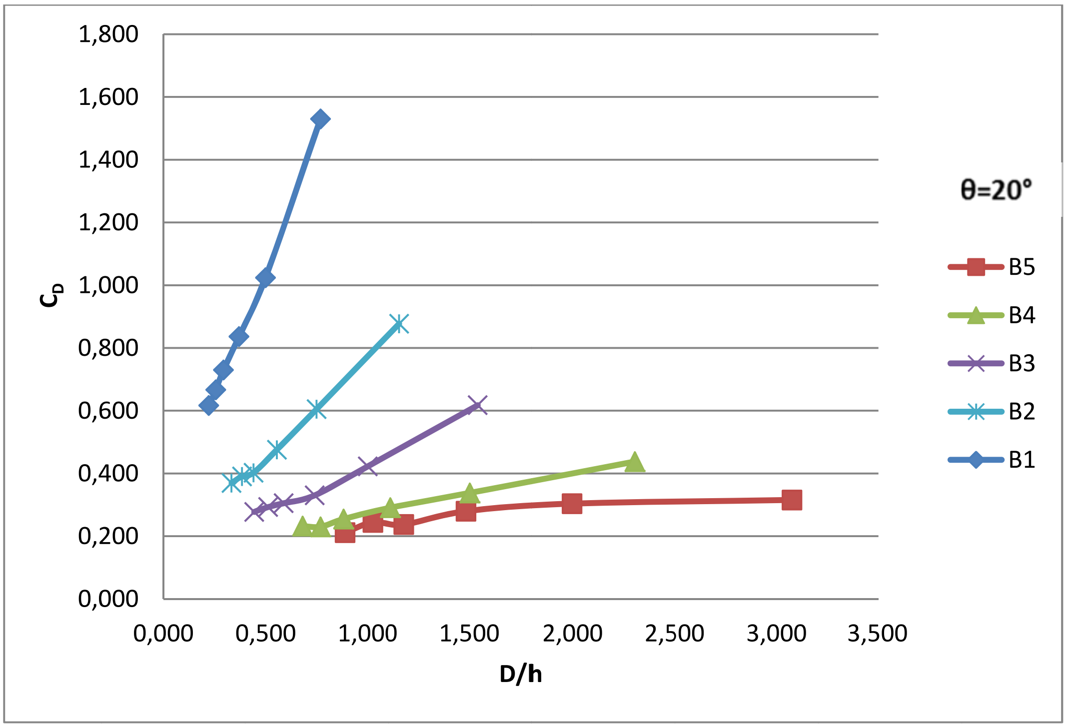

Figure 4.12: Discharge coefficient versus D/h for the orifice B with different D values at θ=20°

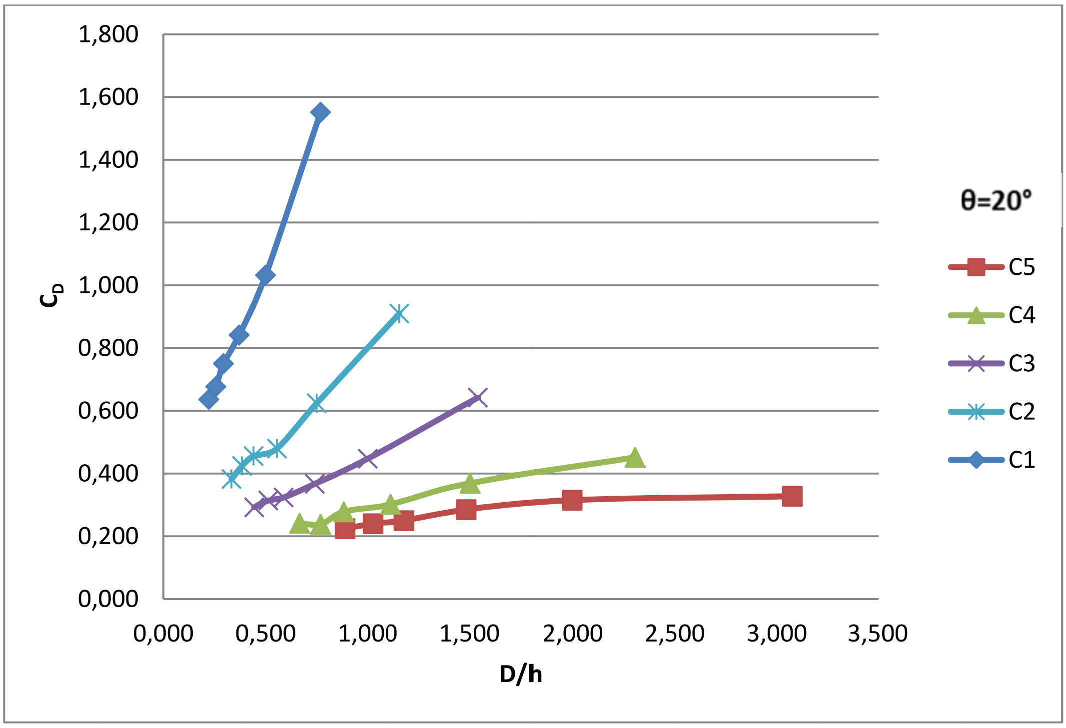

Figure 4.13: Discharge coefficient versus D/h for the orifice C with different D values at θ=20°

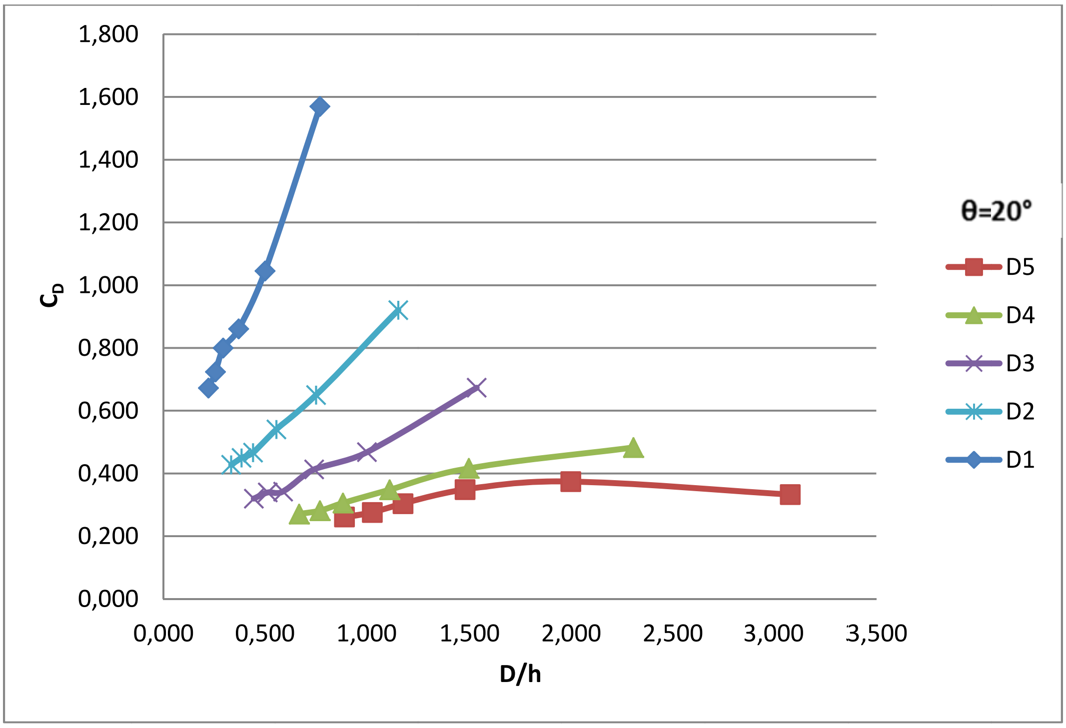

Figure 4.14: Discharge coefficient versus D/h for the orifice D with different D values at θ=20°

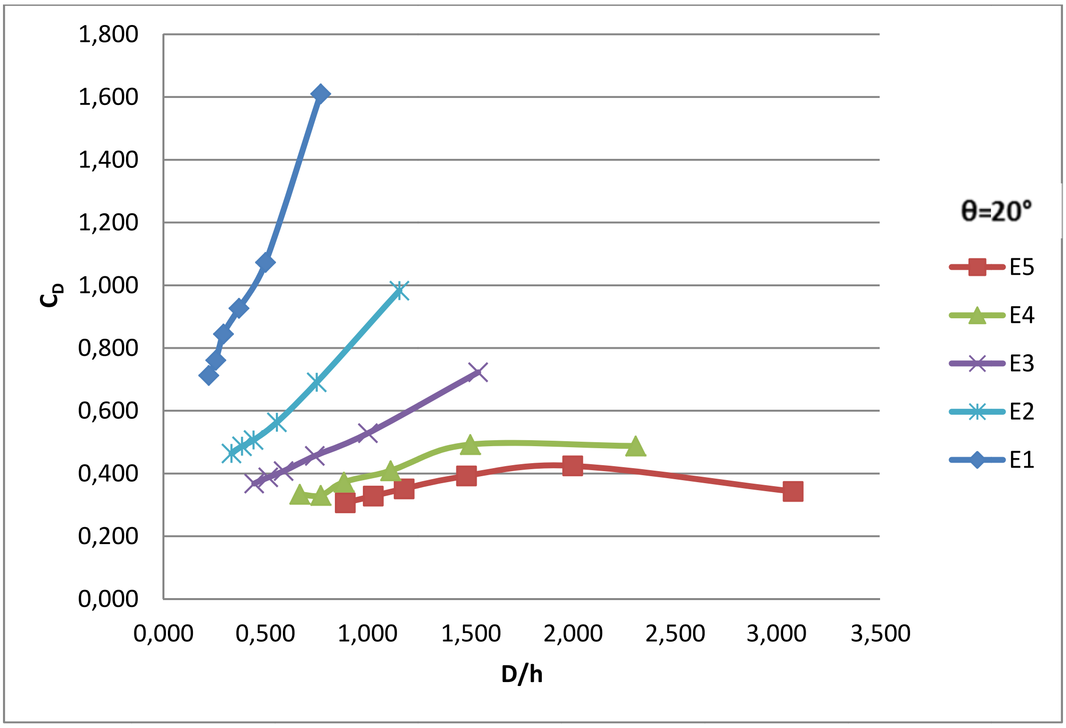

Figure 4.15: Discharge coefficient versus D/h for the orifice E with different D values at θ=20°

Figures 4.16-4.20 show the variation of C_D with the dimensionless variable, x/h for all circular bottom intake orifices that have different distances from the free fall at the end of the bottom intake screen to the center of each circular orifice (x), separately at 0° slope condition of the bottom intake screen. These figures also indicate that at a given location for an orifice of known diameter if the flow depth decreases, C_D values decrease. For a given x/h, C_D values of an orifice closer to the free fall section of the bottom intake screen is smaller than the others which are far away than the free fall section. This is due to the higher flow depth over the orifices which are far away from the free fall section than these orifices closer to the free fall section. Another important point, one can state from these figures is that as the diameters of the orifices get smaller, their C_D values increase for a given x/h.

Figures 4.21-4.25 and Figures 4.26-4.30 show the variation of C_D with the dimensionless variable x/h for all circular bottom intake orifices that have different distances from the free fall at the end of the bottom intake screen to the center of the circular orifice, x, separately at 10° and 20° slopes conditions of the bottom intake screen, respectively. In all these figures, it is not easy to say that the relation between C_D and x/h for the orifices tested are similar to each other, as the screen slope changes from 10° to 20°. While the trend of the data given in Figures 4.21 and 4.22 are very similar to those in Figures 4.16 and 4.17 of the screen of θ=0°, the trends of the data of orifices having smaller diameters (Figures 4.23-4.25) are absolutely different than those of corresponding figures (Figures 4.18-4.20). As the slope of the screen is further increased, θ=20°, C_D values increase with increasing x/h for orifices of constant diameter at a given location.

Finally, it can be concluded that the circular orifices with small diameters give the largest C_D values for the range of x/h values tested regardless of the rack inclination.

For a bottom intake rack of known slope θ, orifice diameter D, flow depth at the channel h, the distance from the free fall section of the screen at the orifice to the center of the circular orifice x, one can easily determine the measured discharge passing from the orifice in the experiment after determining C_D value from one of the relevant figures and then substituting its value in Equation 2.6.

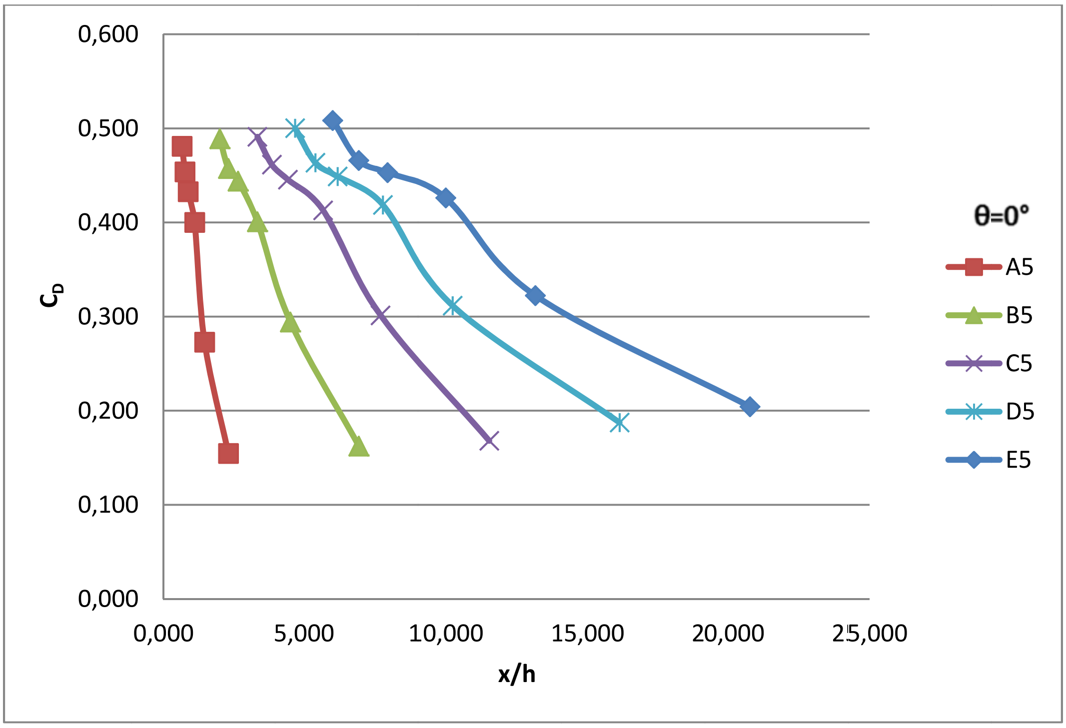

Figure 4.16: Discharge coefficient versus x/h for D=4 cm with different x values at θ=0°

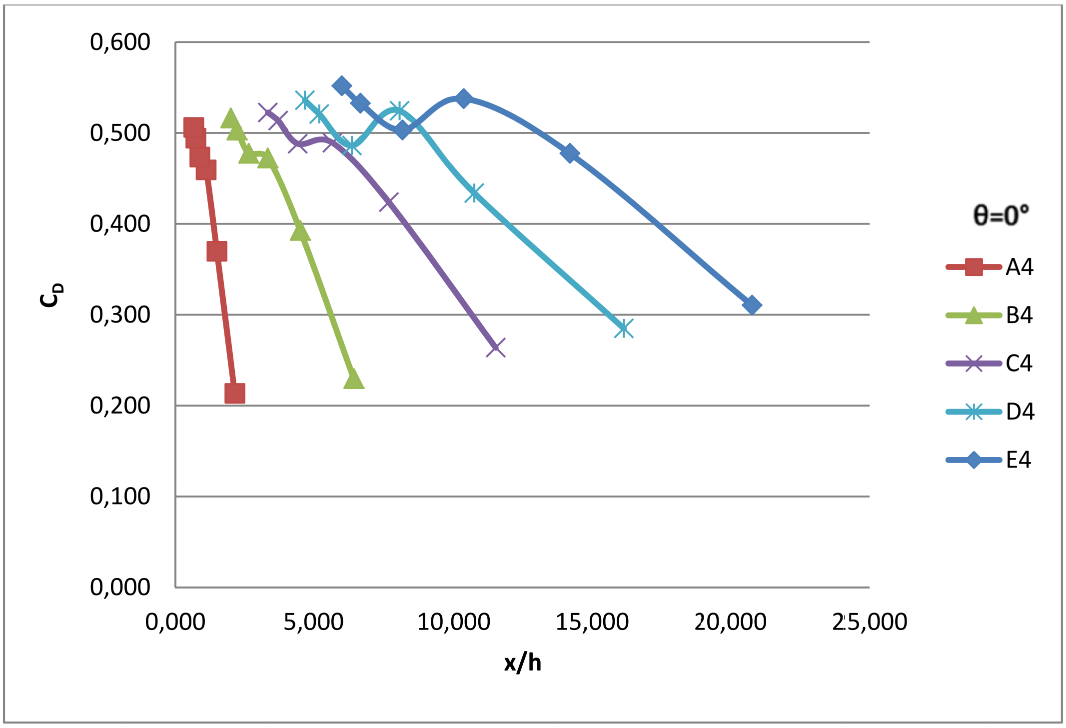

Figure 4.17: Discharge coefficient versus x/h for D=3 cm with different x values at θ=0°

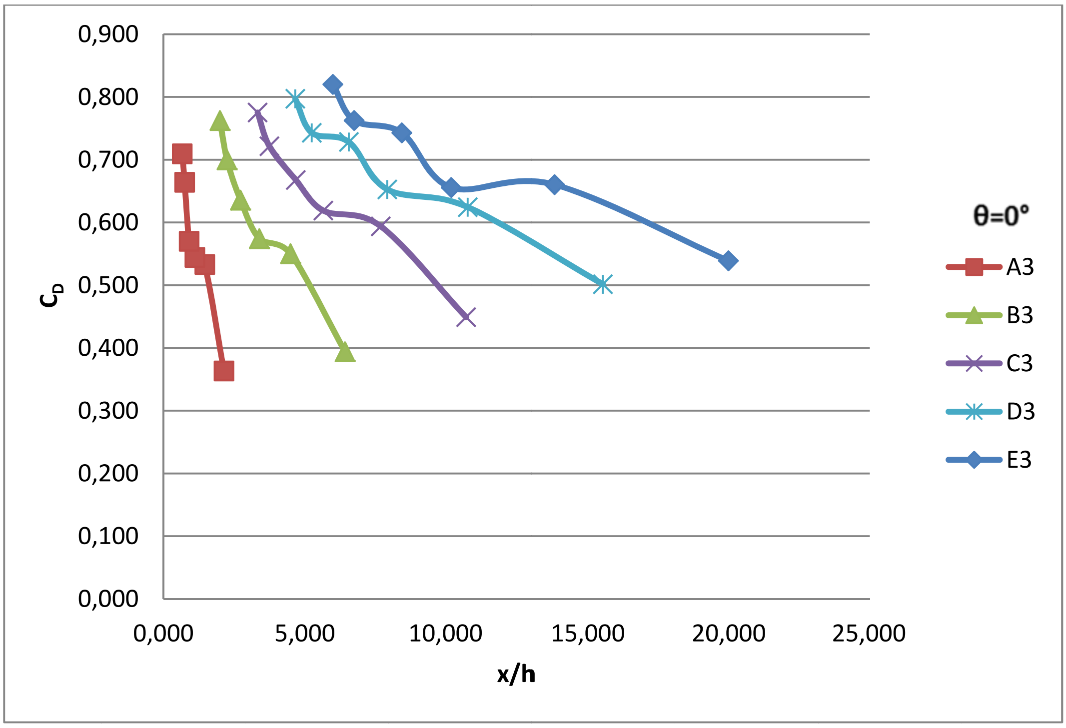

Figure 4.18: Discharge coefficient versus x/h for D=2 cm with different x values at θ=0°

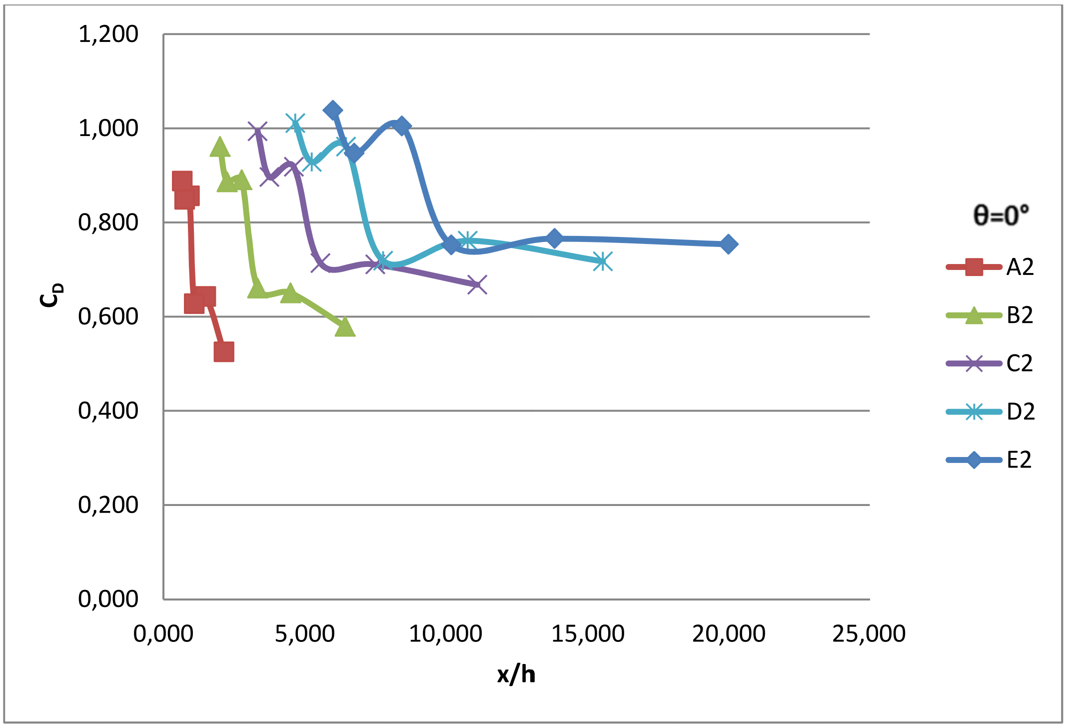

Figure 4.19: Discharge coefficient versus x/h for D=1.5 cm with different x values at θ=0°

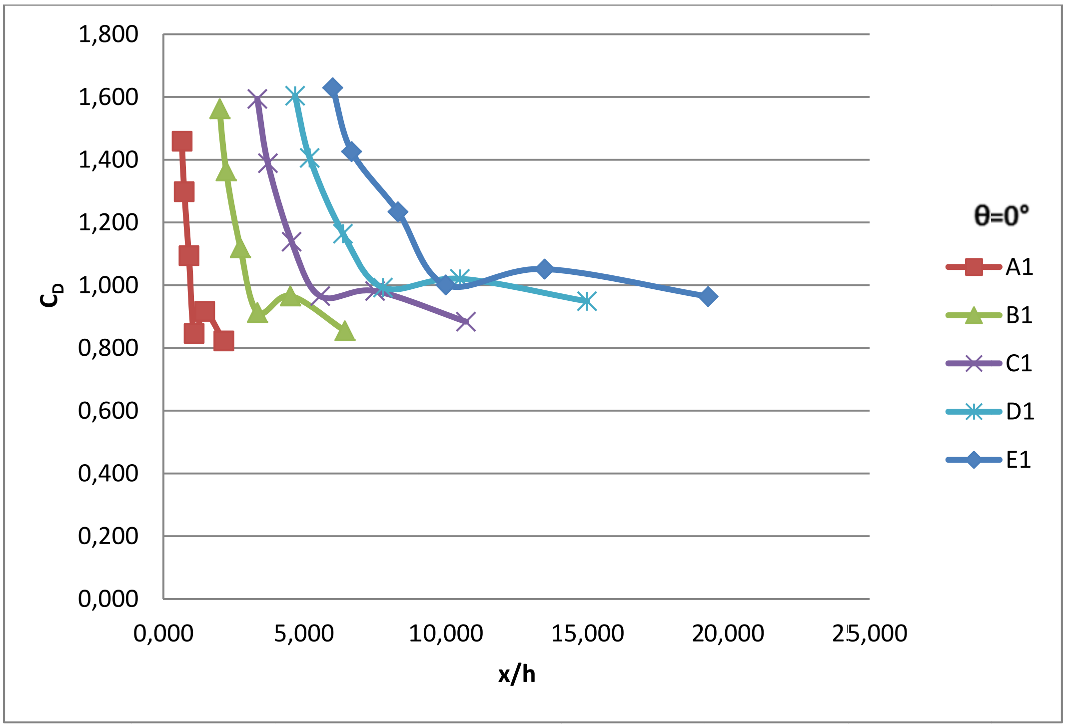

Figure 4.20: Discharge coefficient versus x/h for D=1 cm with different x values at θ=0°

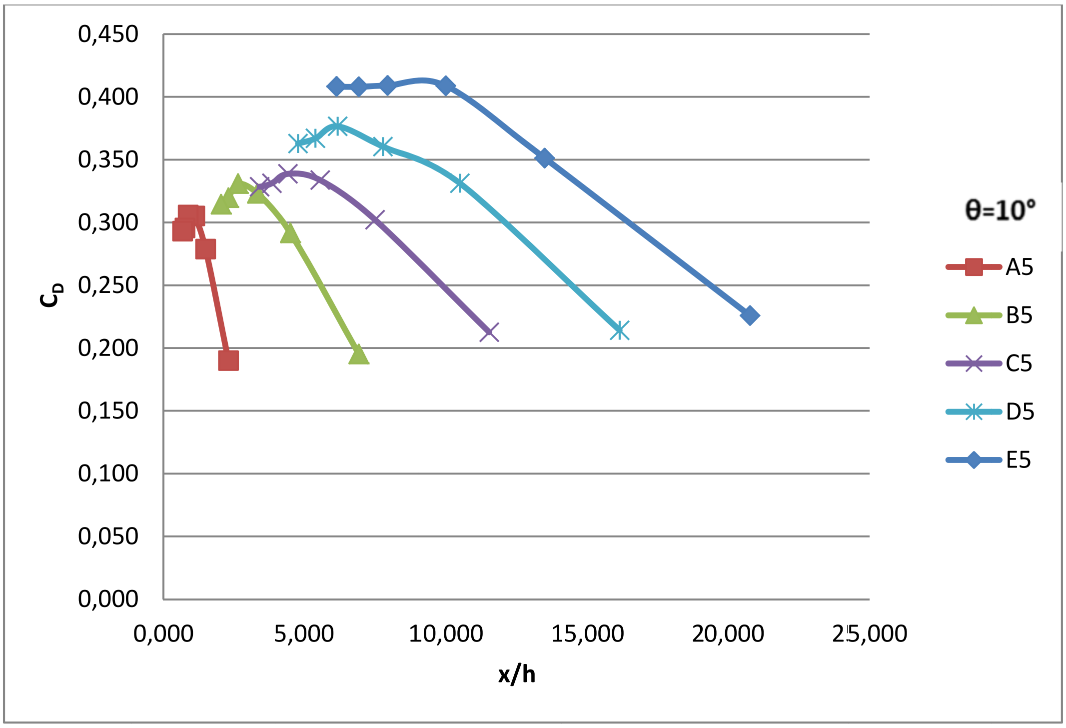

Figure 4.21: Discharge coefficient versus x/h for D=4 cm with different x values at θ=10°

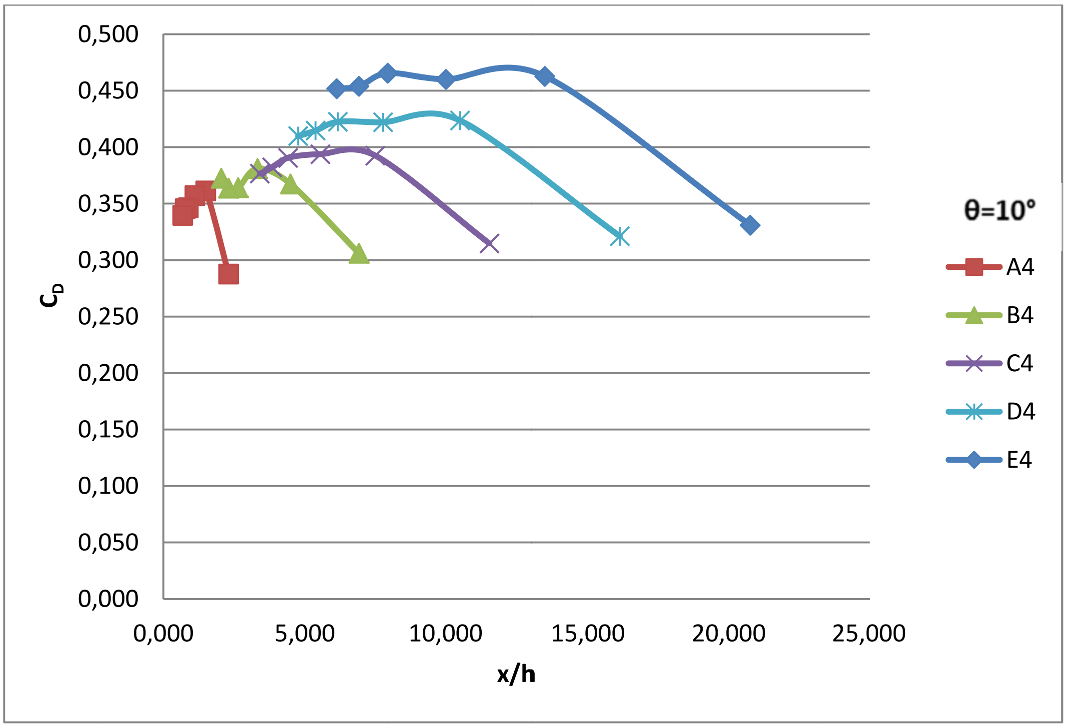

Figure 4.22: Discharge coefficient versus x/h for D=3 cm with different x values at θ=10°

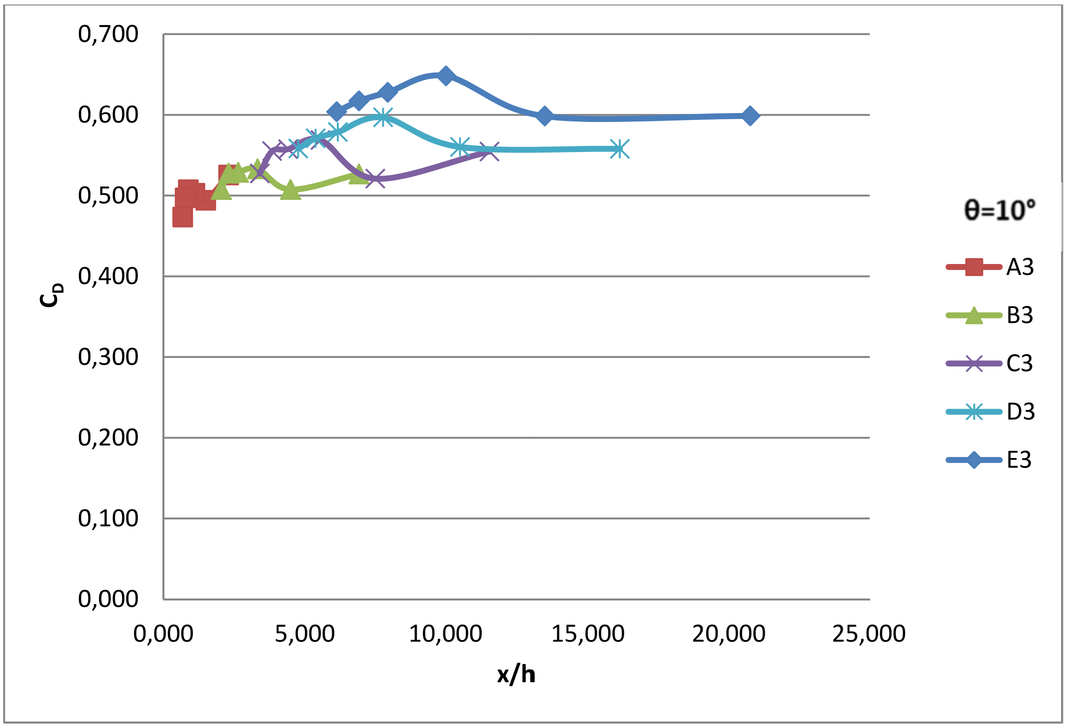

Figure 4.23: Discharge coefficient versus x/h for D=2 cm with different x values at θ=10°

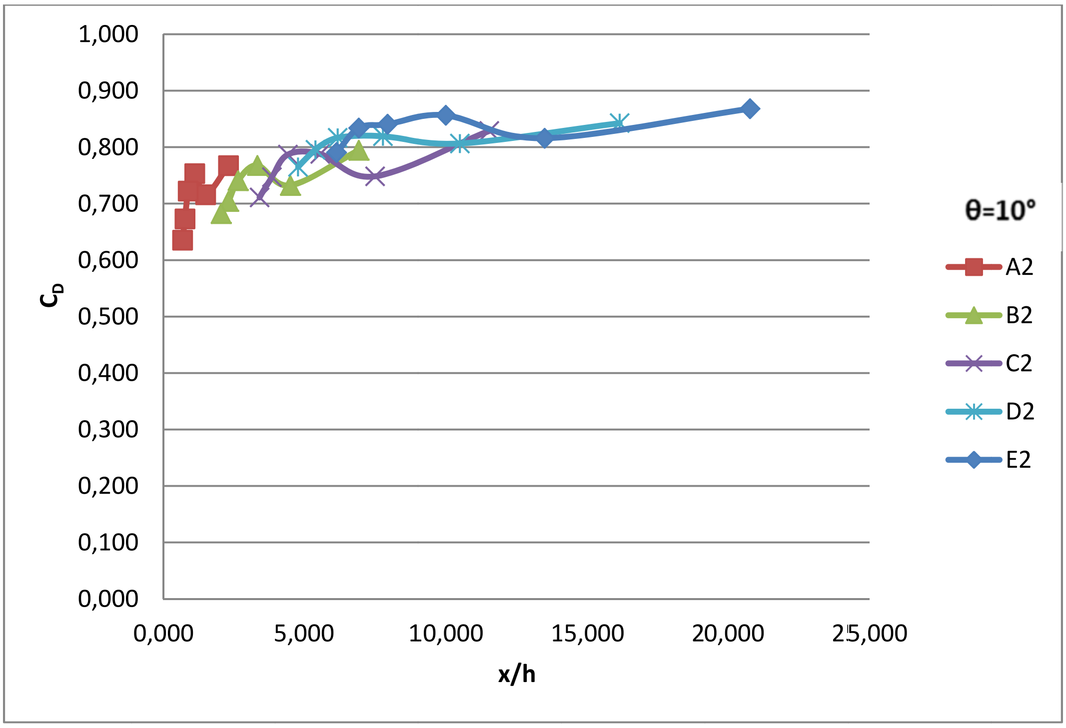

Figure 4.24: Discharge coefficient versus x/h for D=1.5 cm with different x values at θ=10°

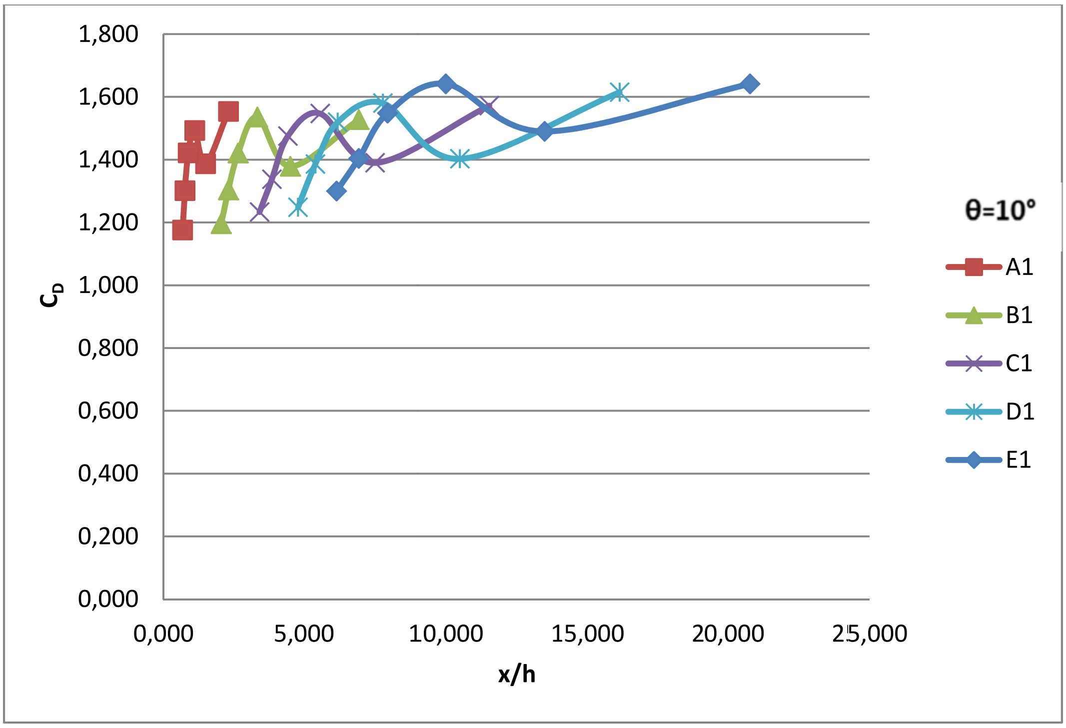

Figure 4.25: Discharge coefficient versus x/h for D=1 cm with different x values at θ=10°

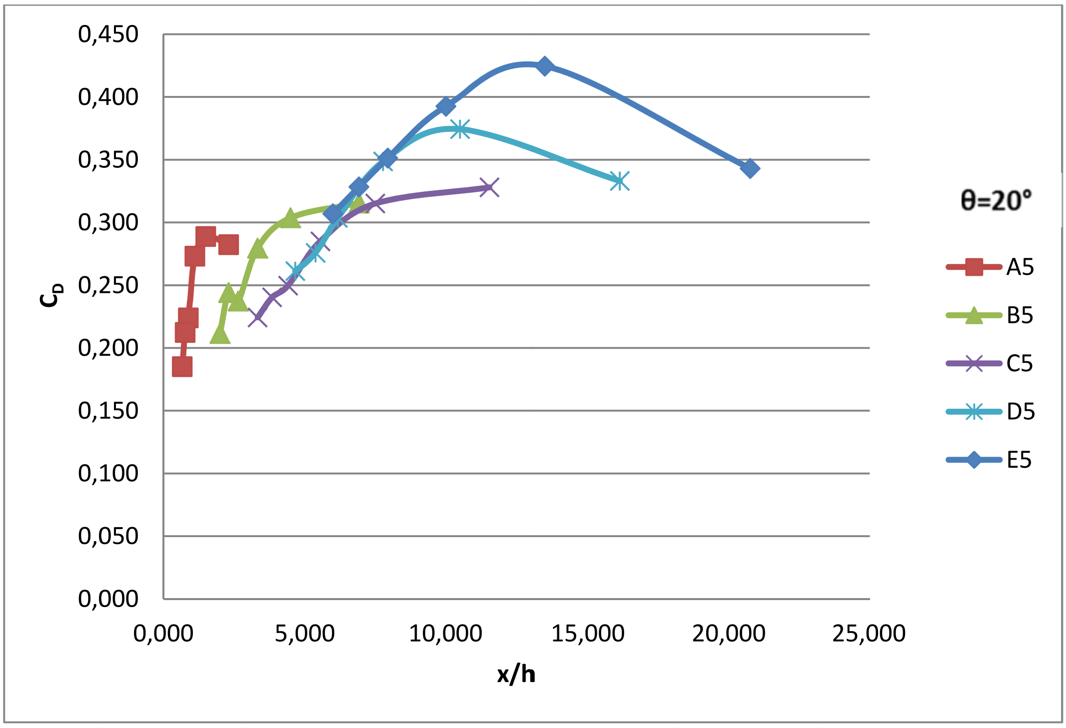

Figure 4.26: Discharge coefficient versus x/h for D=4 cm with different x values at θ=20°

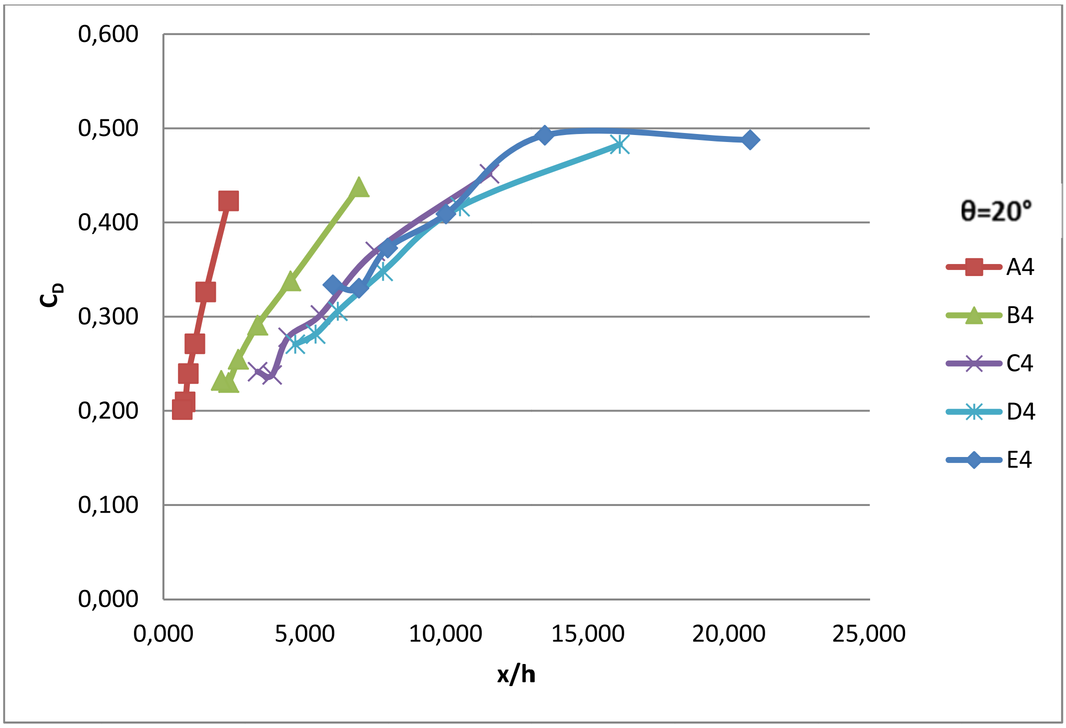

Figure 4.27: Discharge coefficient versus x/h for D=3 cm with different x values at θ=20°

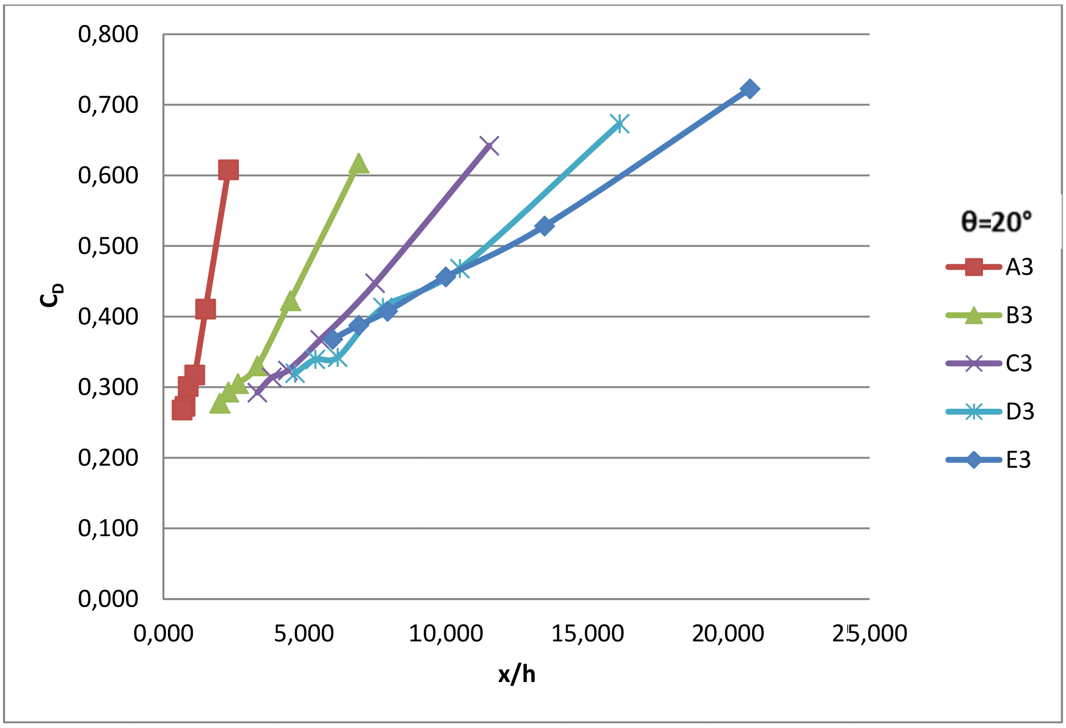

Figure 4.28: Discharge coefficient versus x/h for D=2 cm with different x values at θ=20°

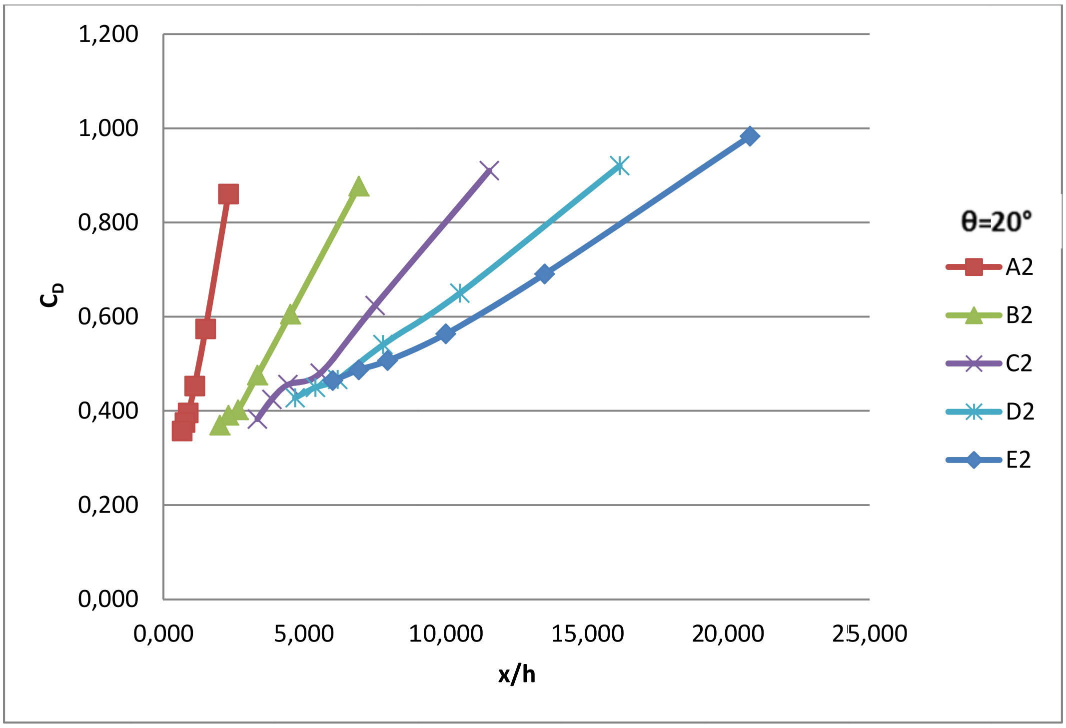

Figure 4.29: Discharge coefficient versus x/h for D=1.5 cm with different x values at θ=20°

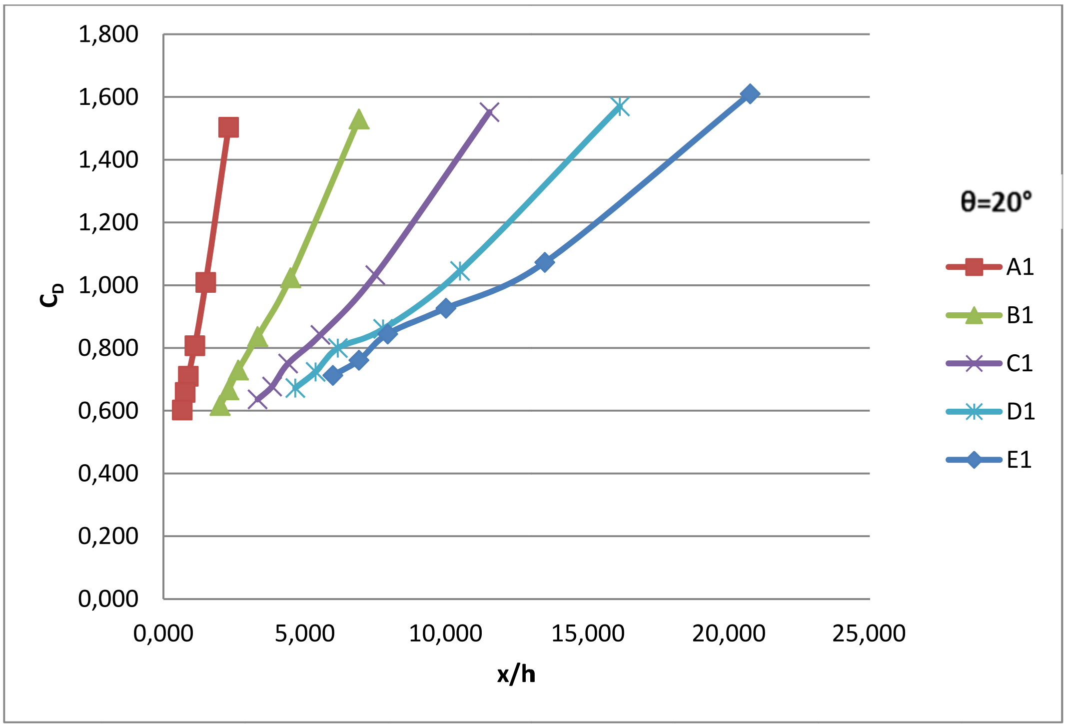

Figure 4.30: Discharge coefficient versus x/h for D=1 cm with different x values at θ=20°

Variation of C_D with Fr for the circular orifices of varying diameters located at a fixed location on the bottom intake screen of θ=0° is shown in Figures 4.31-4.35. When the general trends of the data given on these figures are examined, it is seen that C_D increases with increasing Fr for an orifice of known diameter. Maximum C_D values are obtained at maximum Fr. For a given Fr, C_D value of the orifice increases as the orifice diameter gets smaller. The orifice of the diameter D=1.0 cm always yields the highest C_D values while the orifice of diameter D=4.0 cm gives the minimum C_D values. Figures 4.36-4.40 show the variation of C_D with Fr for the orifices of constant diameter but varying locations on the bottom intake screen of θ=0°. These figures clearly reveal that for a given Fr the orifices closer to the free fall section of the screen yield smaller C_D values than those which are far away from the free fall section.

Figures 4.41-4.45 show the relationship between C_D and Fr for the circular orifices of varying diameters located at a fixed location on the bottom intake screen of θ=10°. In all these figures, it is observed that except the orifice of D=1.0 cm, in the other orifices C_D slightly decrease or increase with increasing Fr as a function of orifice diameter. For the orifice of D=1.0 cm, one may say that C_D generally has a decreasing tendency with increasing Fr.

Figures 4.46-4.50 present the data of C_D versus Fr for the orifices of the same diameters located at different locations on the bottom outlet screen of θ=10°. From these figures, it can be concluded that as the location of the orifice increases from the free fall section of the screen, the C_D value of the orifice increases for a given Fr.

The data of C_D versus Fr are presented in Figures 4.51-4.60 for the bottom outlet of θ=20°. From these figures, it can be pointed out that C_D values of the orifices of known diameter decrease as Fr increases.

Finally, it can be concluded that the circular orifices with small diameters give the largest C_D values for the range of Fr values tested regardless of the rack inclination.

For a bottom intake rack of known slope θ, orifice diameter D, flow depth at the channel h, the distance from the free fall section of the screen at the orifice to the center of the circular orifice x, one can easily determine the measured discharge passing from the orifice in the experiment after determining C_D value from one of the relevant figures and then substituting its value in Equation 2.6.

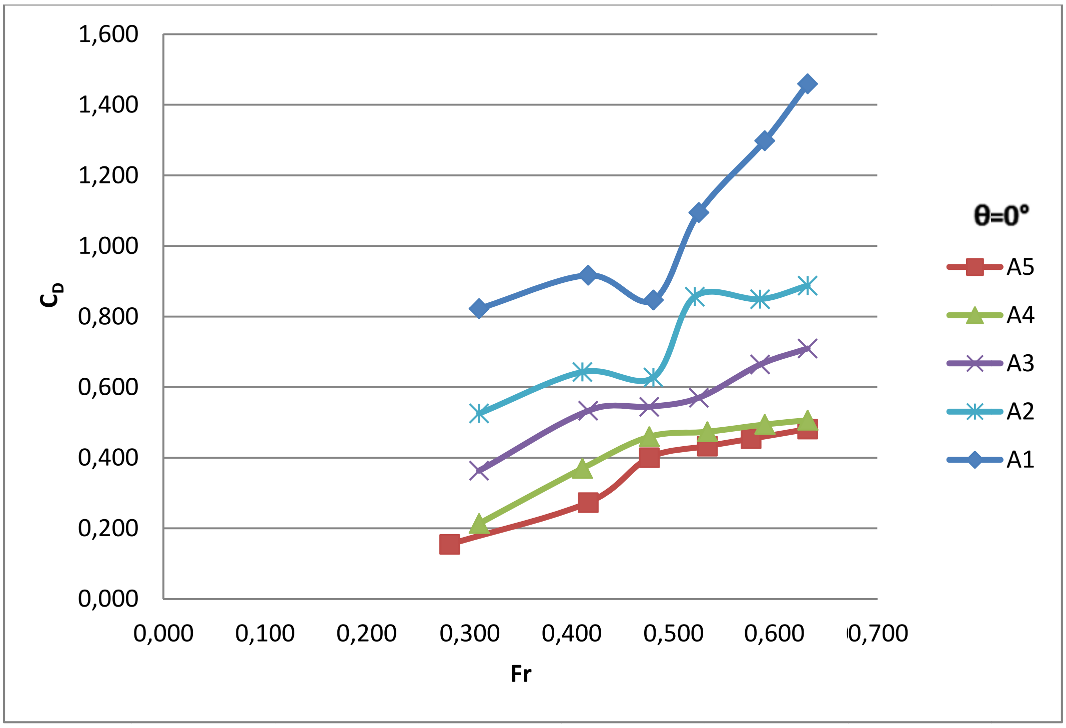

Figure 4.31: Discharge coefficient versus Fr for the orifice A with different D values at θ=0°

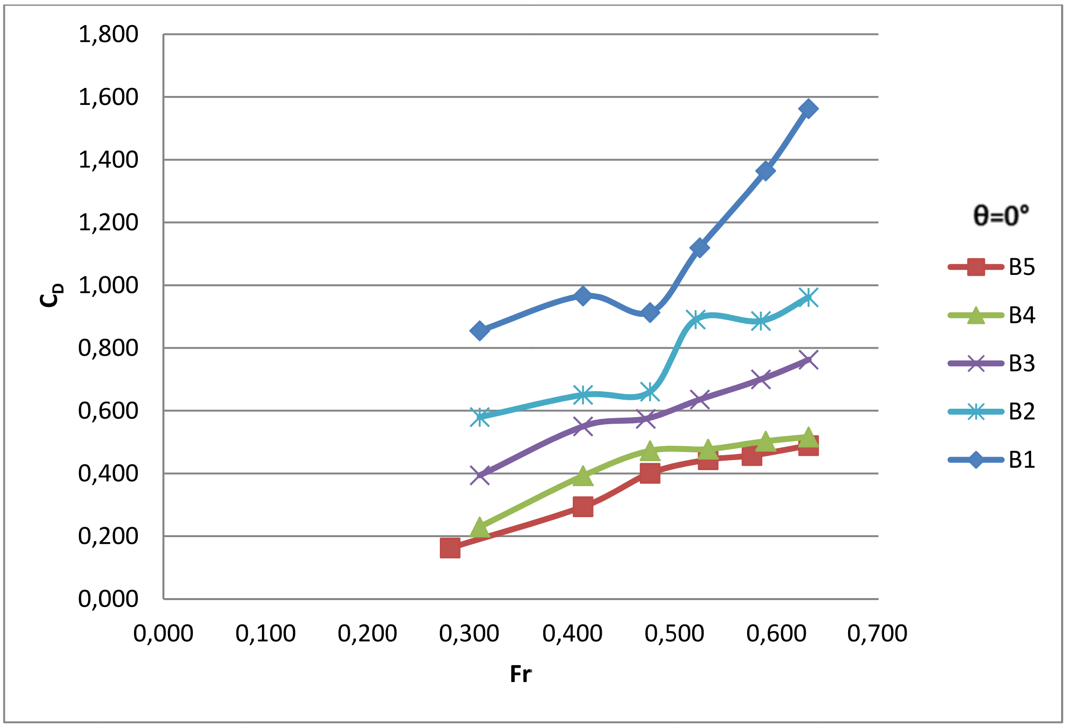

Figure 4.32: Discharge coefficient versus Fr for the orifice B with different D values at θ=0°

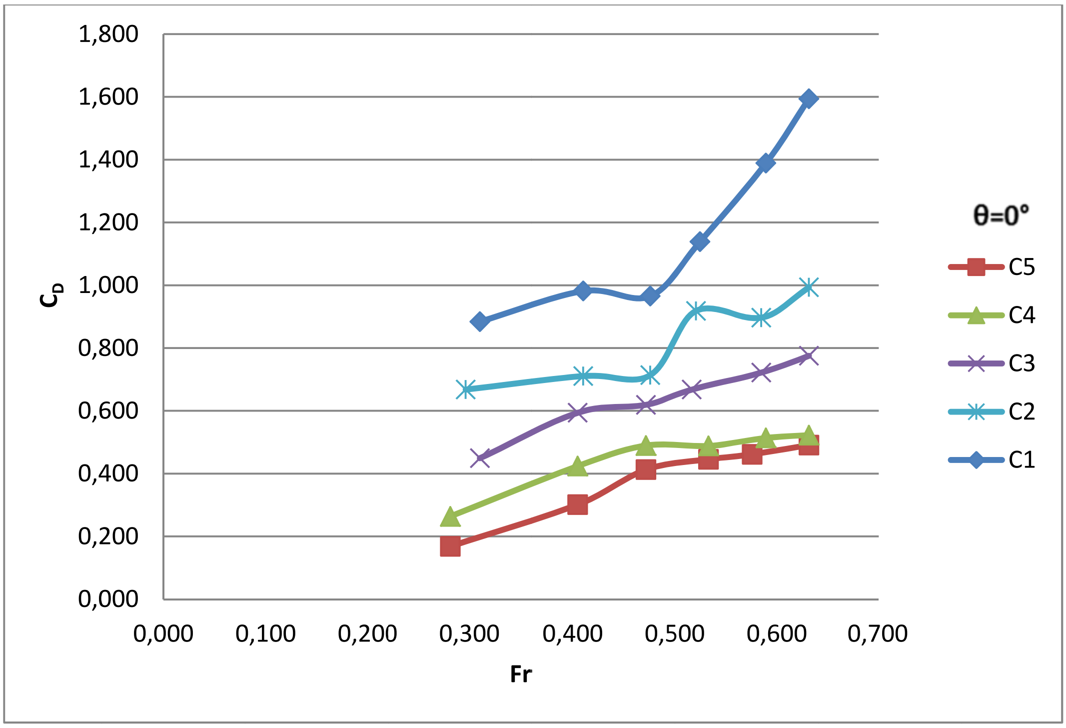

Figure 4.33: Discharge coefficient versus Fr for the orifice C with different D values at θ=0°

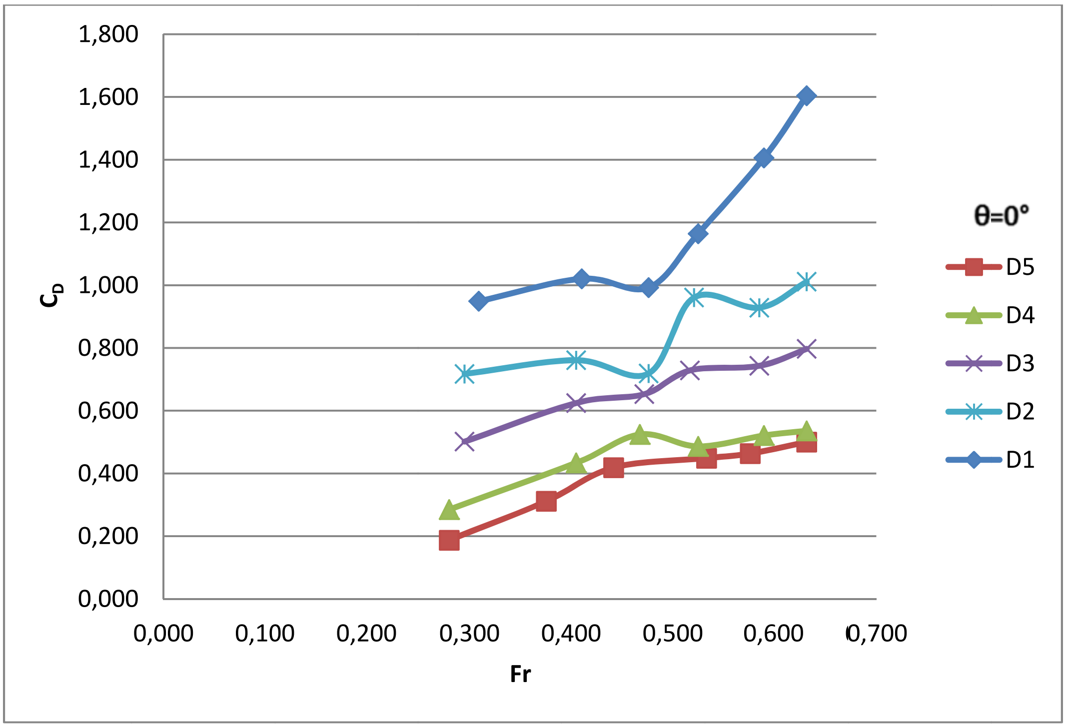

Figure 4.34: Discharge coefficient versus Fr for the orifice D with different D values at θ=0°

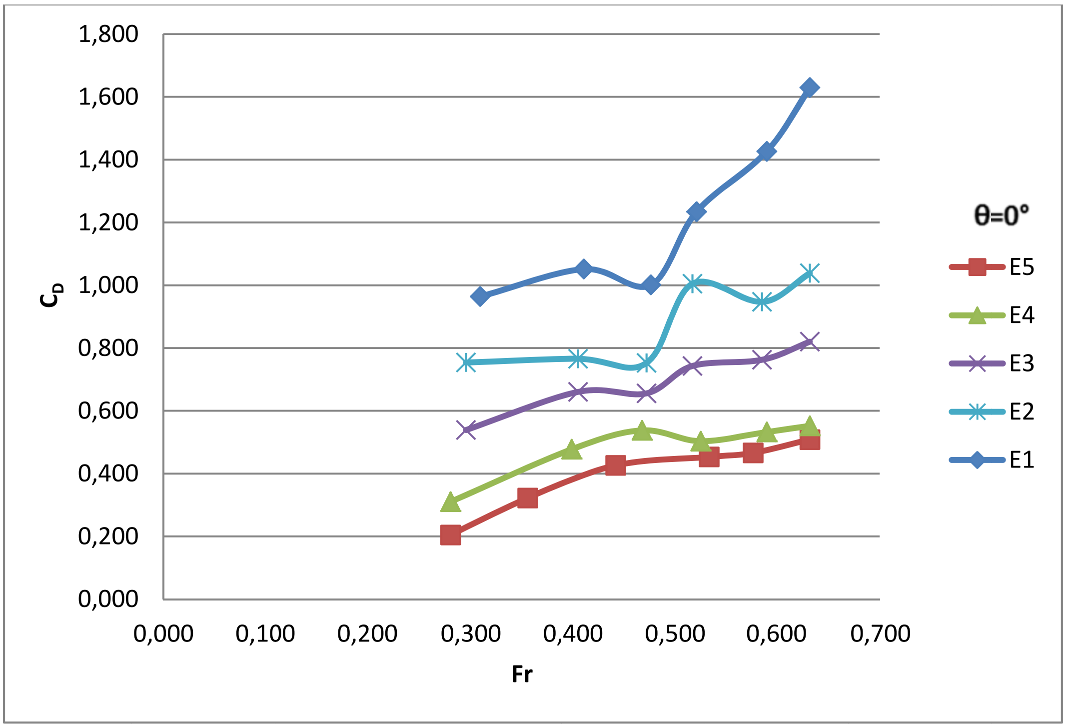

Figure 4.35: Discharge coefficient versus Fr for the orifice E with different D values at θ=0°

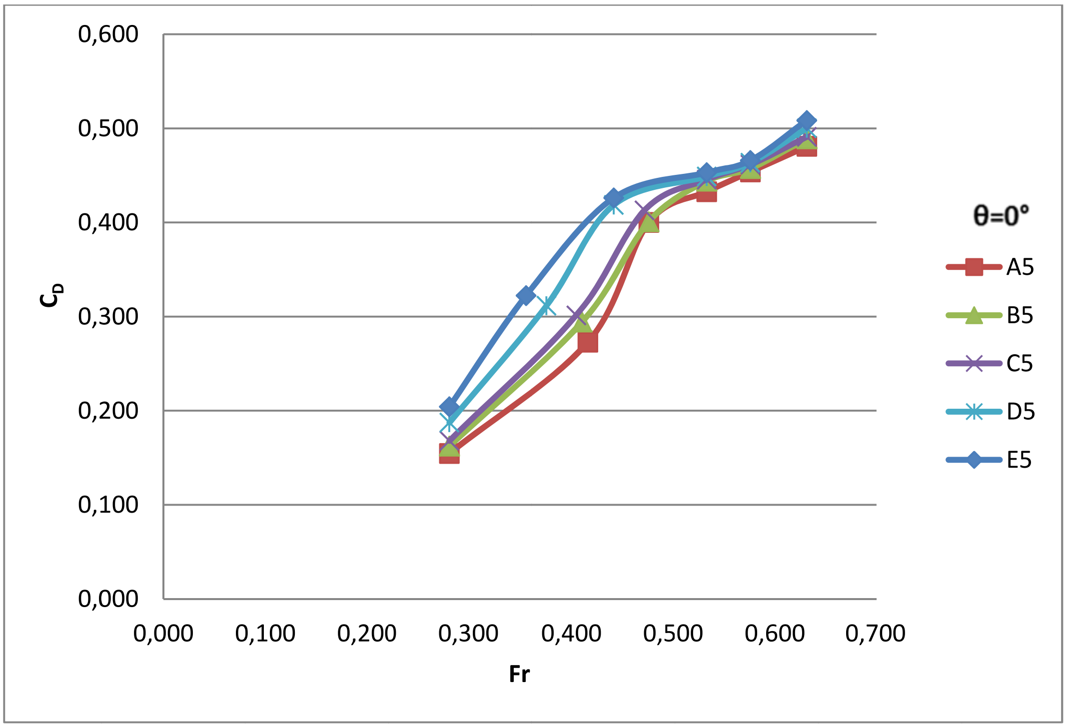

Figure 4.36: Discharge coefficient versus Fr for D=4 cm with different x values at θ=0°

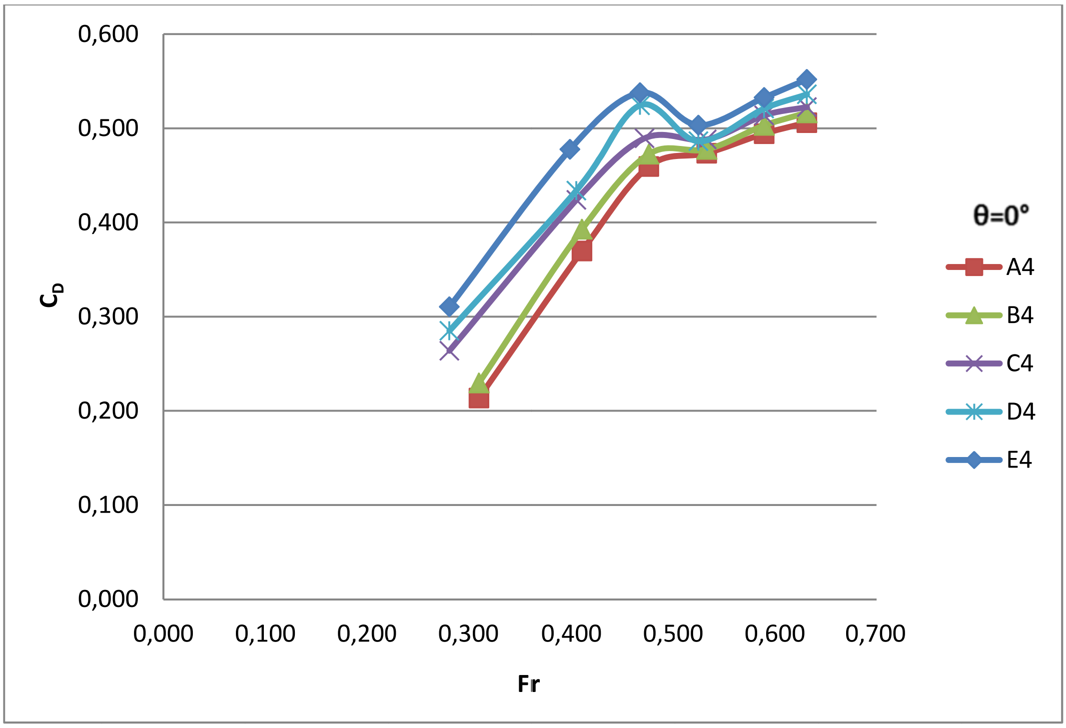

Figure 4.37: Discharge coefficient versus Fr for D=3 cm with different x values at θ=0°

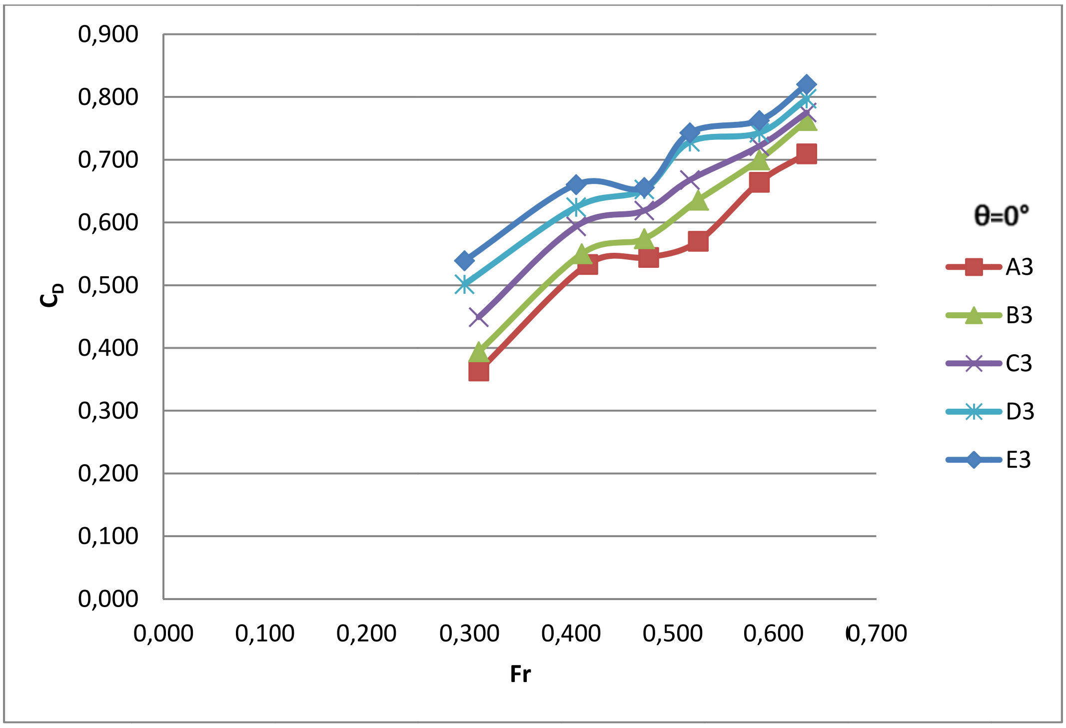

Figure 4.38: Discharge coefficient versus Fr for D=2 cm with different x values at θ=0°

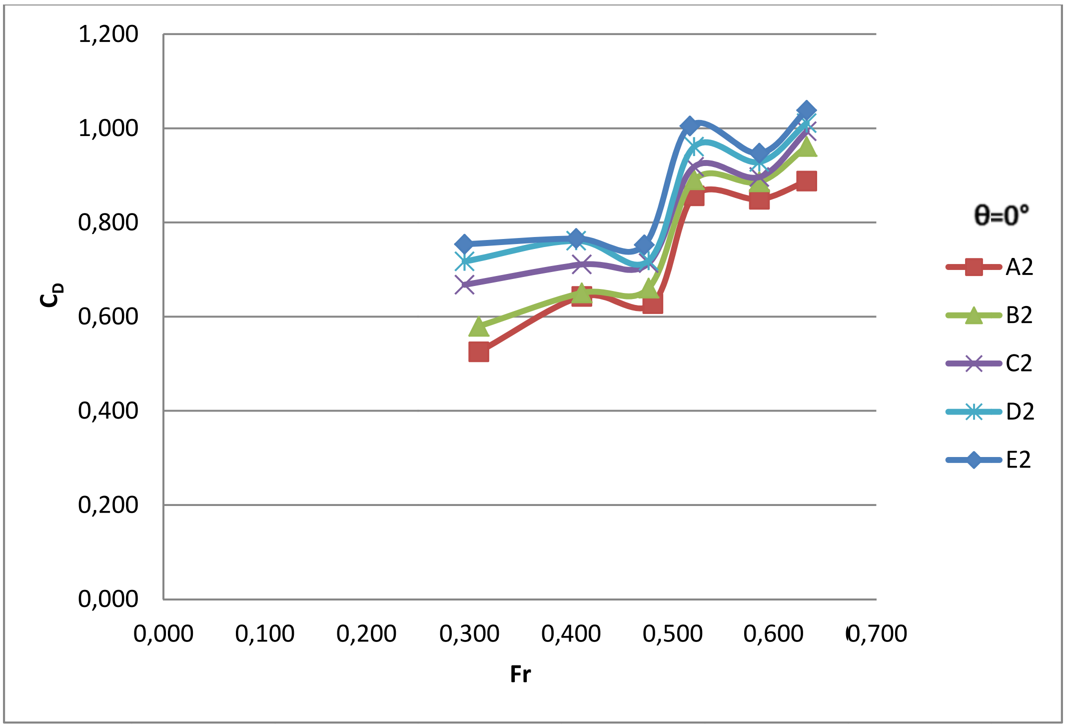

Figure 4.39: Discharge coefficient versus Fr for D=1.5 cm with different x values at θ=0°

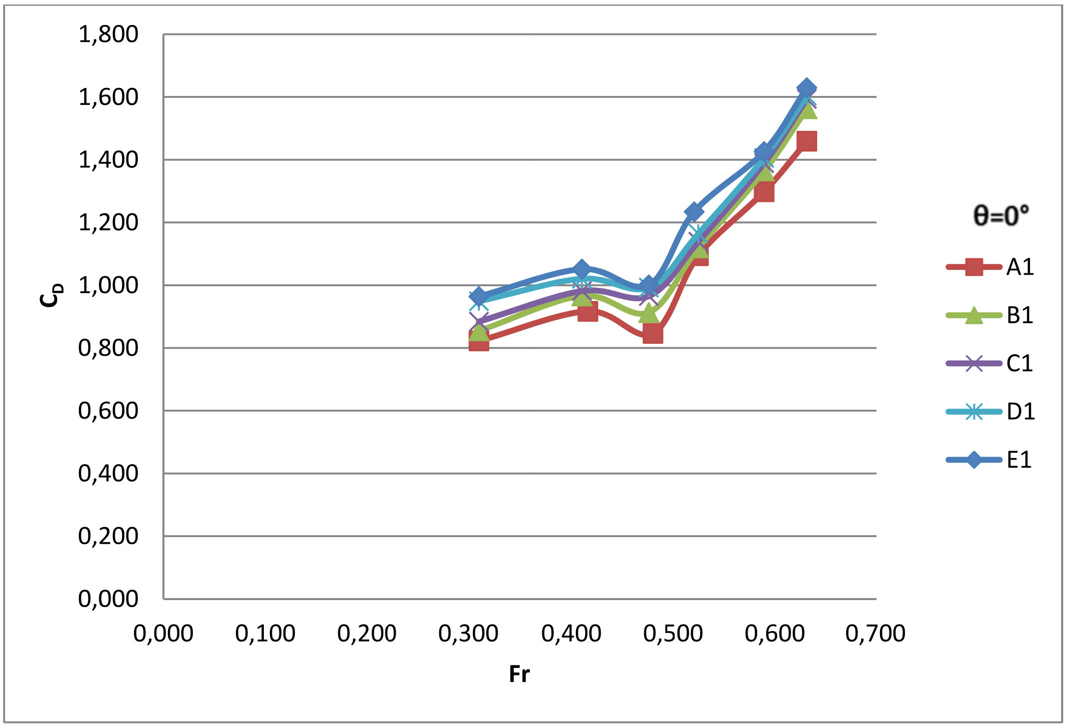

Figure 4.40: Discharge coefficient versus Fr for D=1 cm with different x values at θ=0°

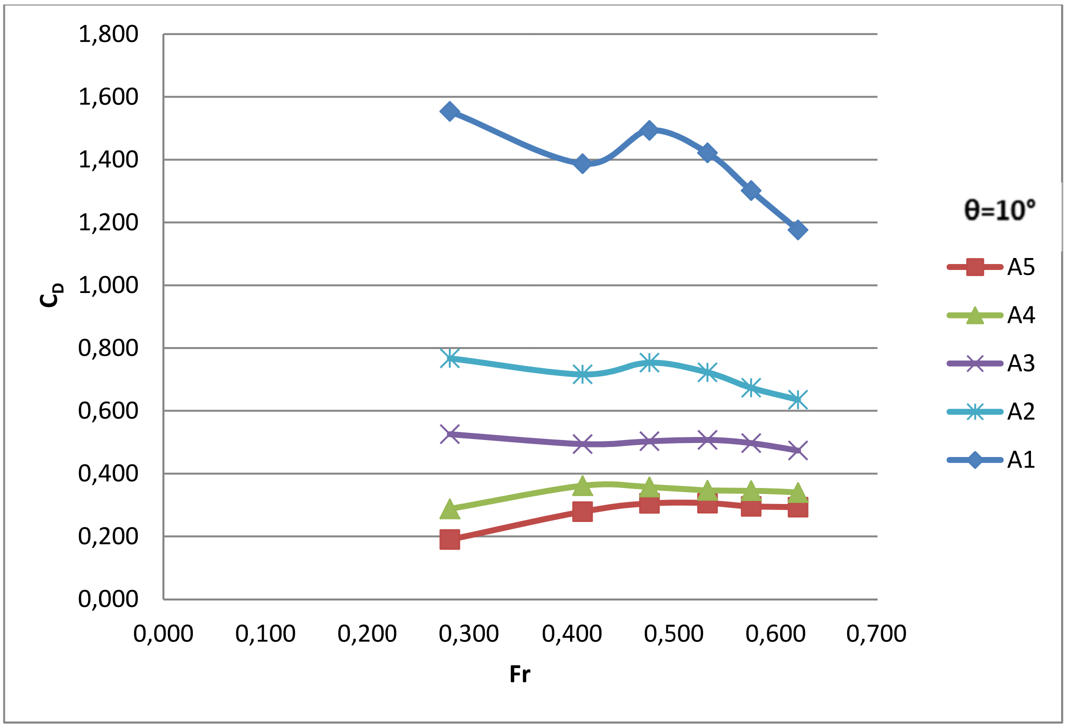

Figure 4.41: Discharge coefficient versus Fr for the orifice A with different D values at θ=10°

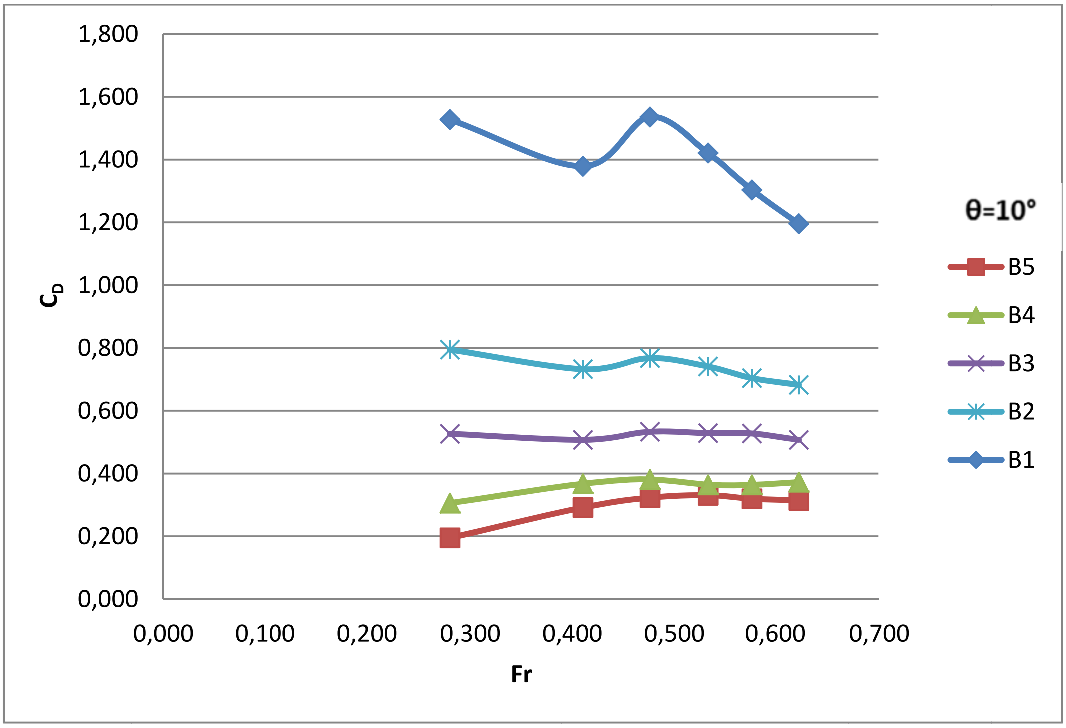

Figure 4.42: Discharge coefficient versus Fr for the orifice B with different D values at θ=10°

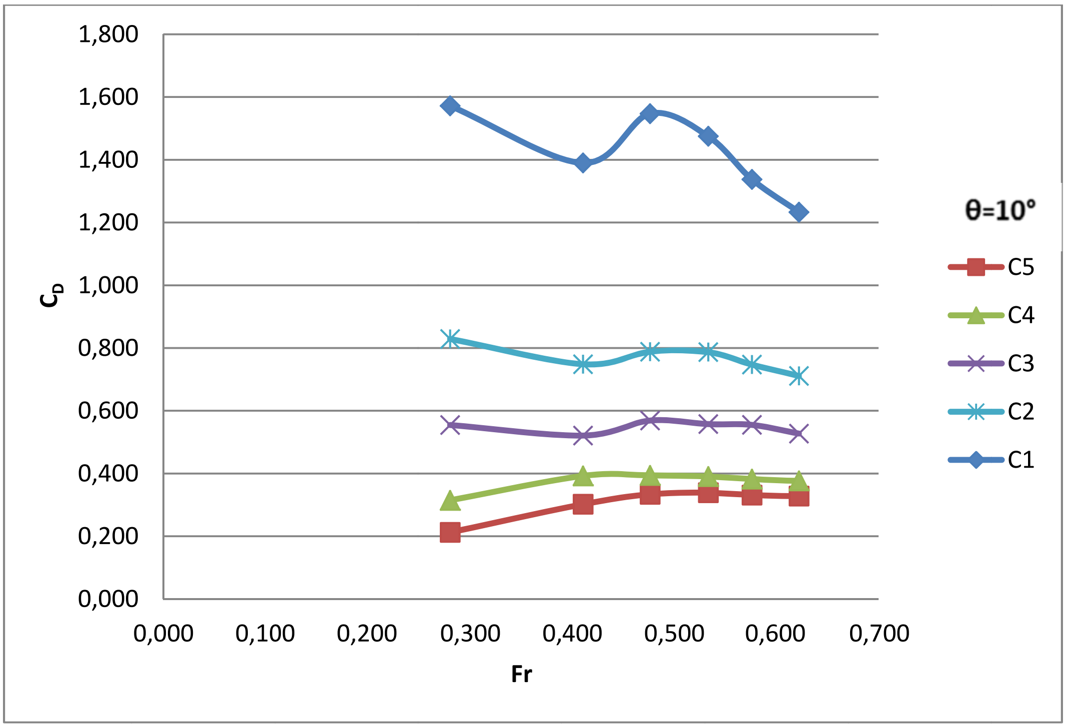

Figure 4.43: Discharge coefficient versus Fr for the orifice C with different D values at θ=10°

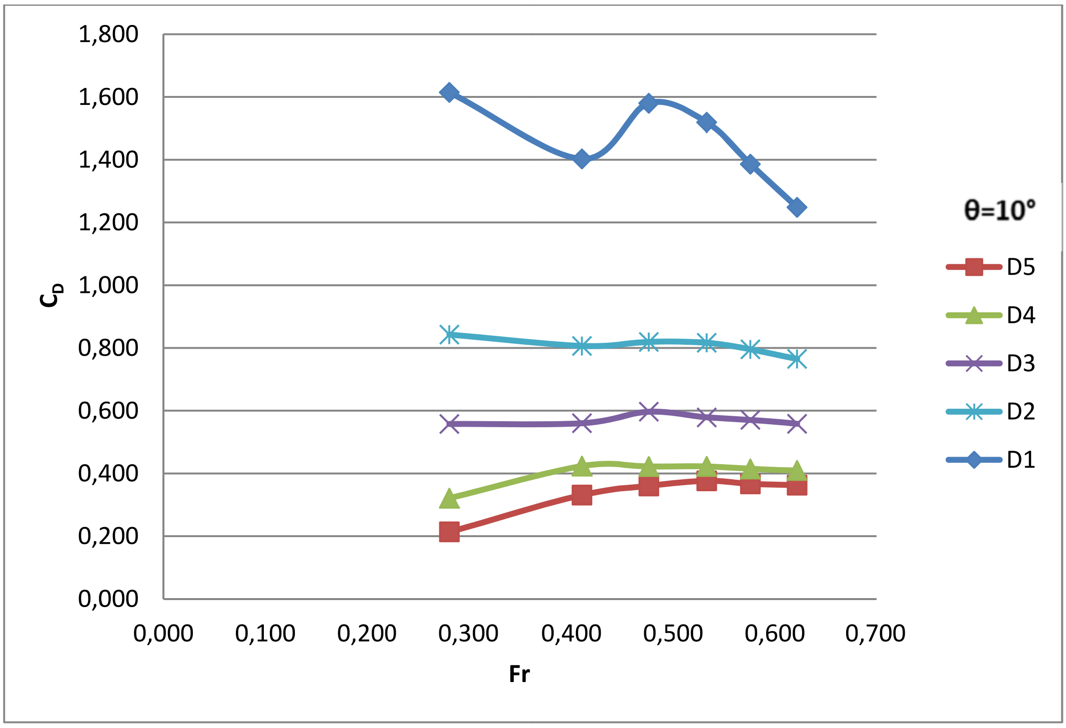

Figure 4.44: Discharge coefficient versus Fr for the orifice D with different D values at θ=10°

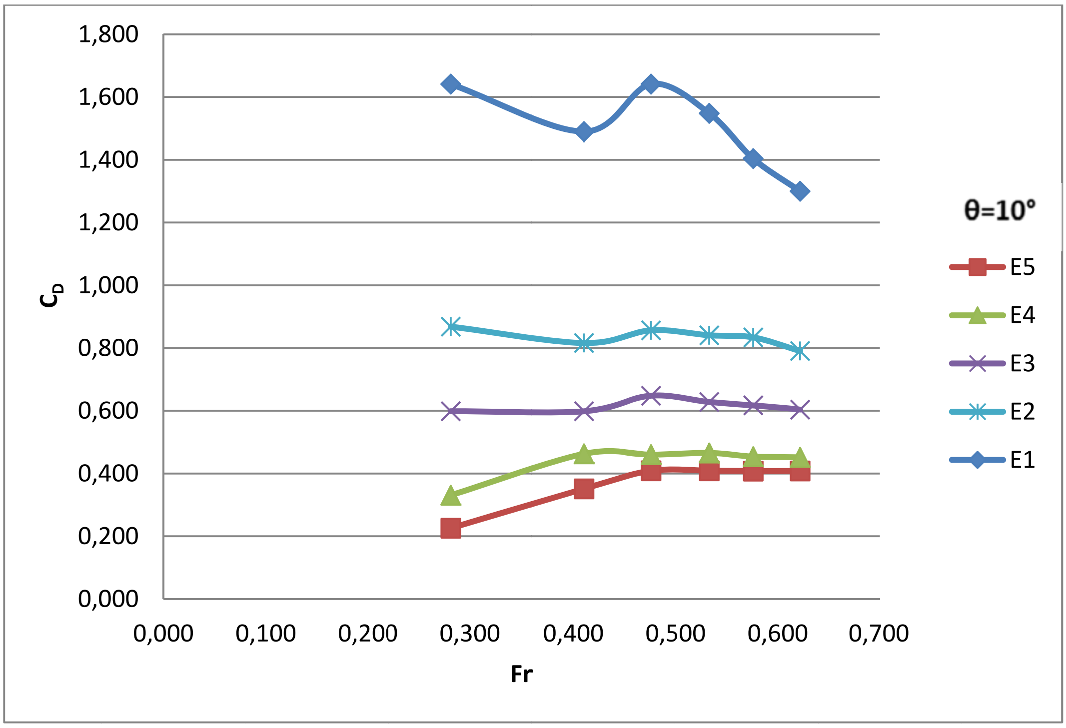

Figure 4.45: Discharge coefficient versus Fr for the orifice E with different D values at θ=10°

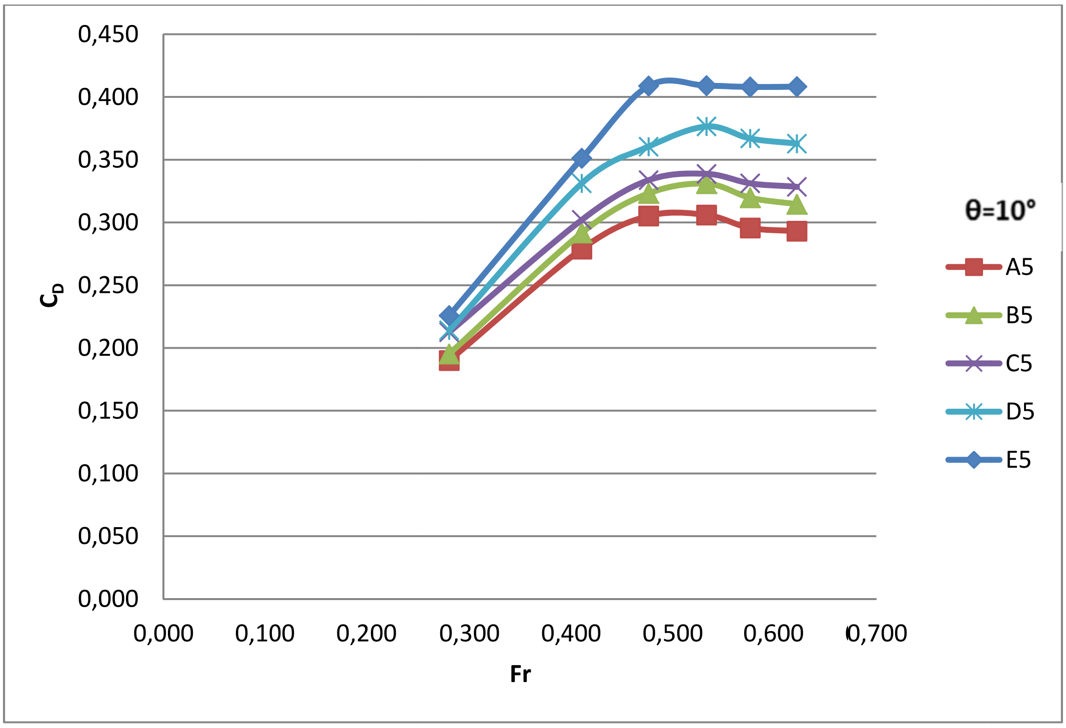

Figure 4.46: Discharge coefficient versus Fr for D=4 cm with different x values at θ=10°

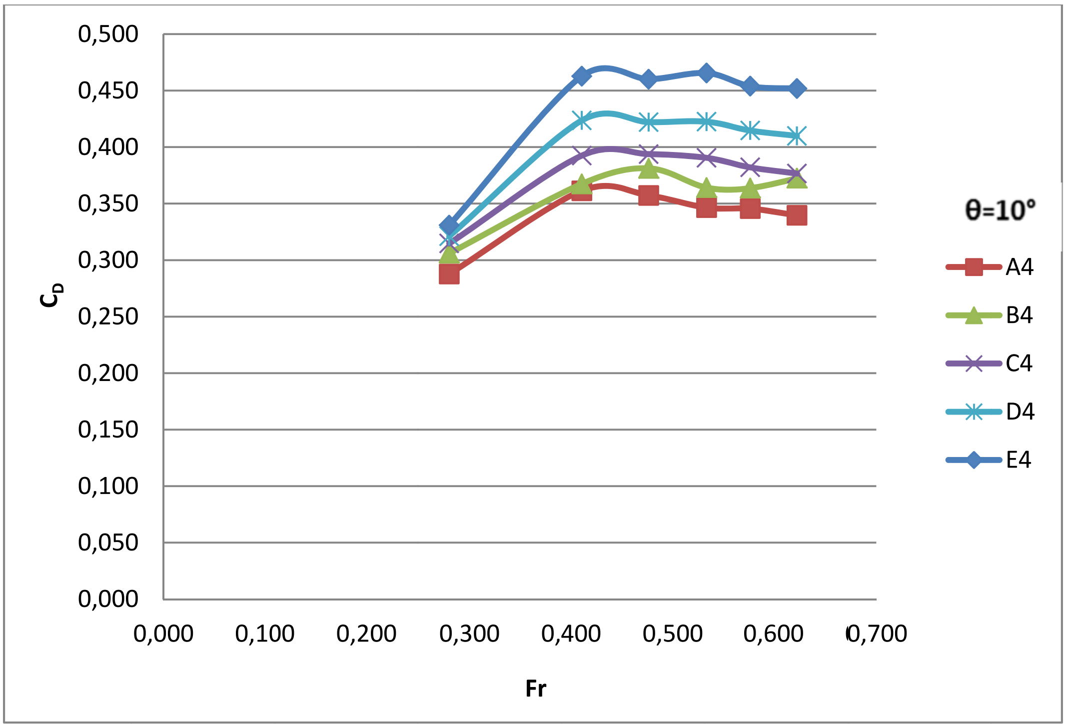

Figure 4.47: Discharge coefficient versus Fr for D=3 cm with different x values at θ=10°

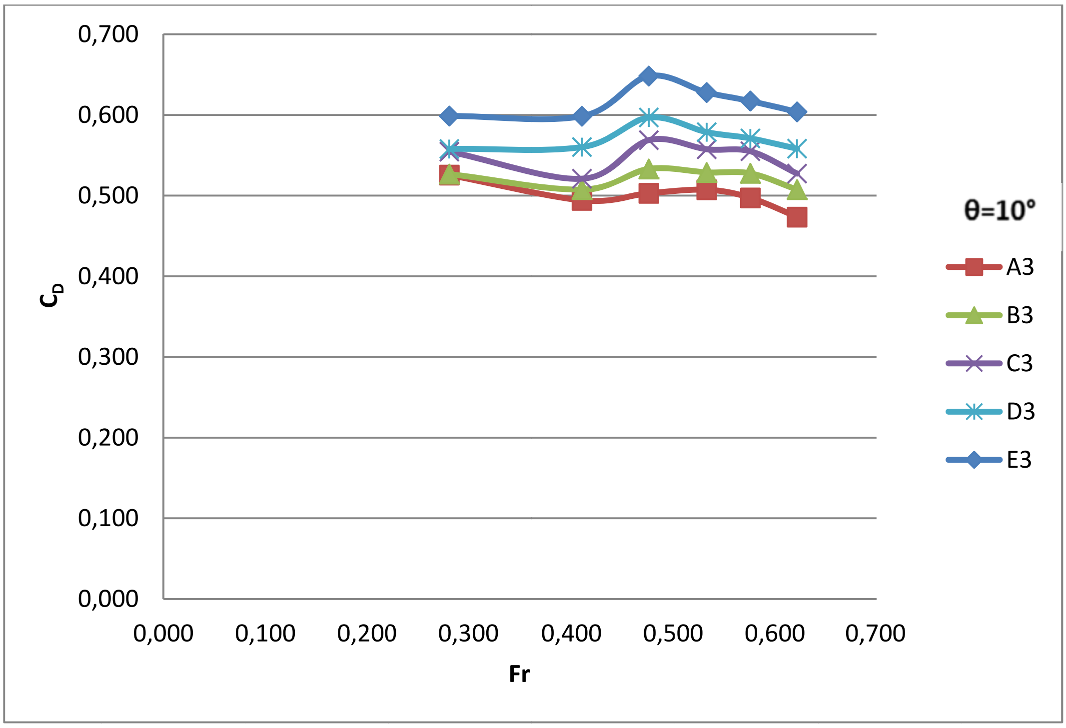

Figure 4.48: Discharge coefficient versus Fr for D=2 cm with different x values at θ=10°

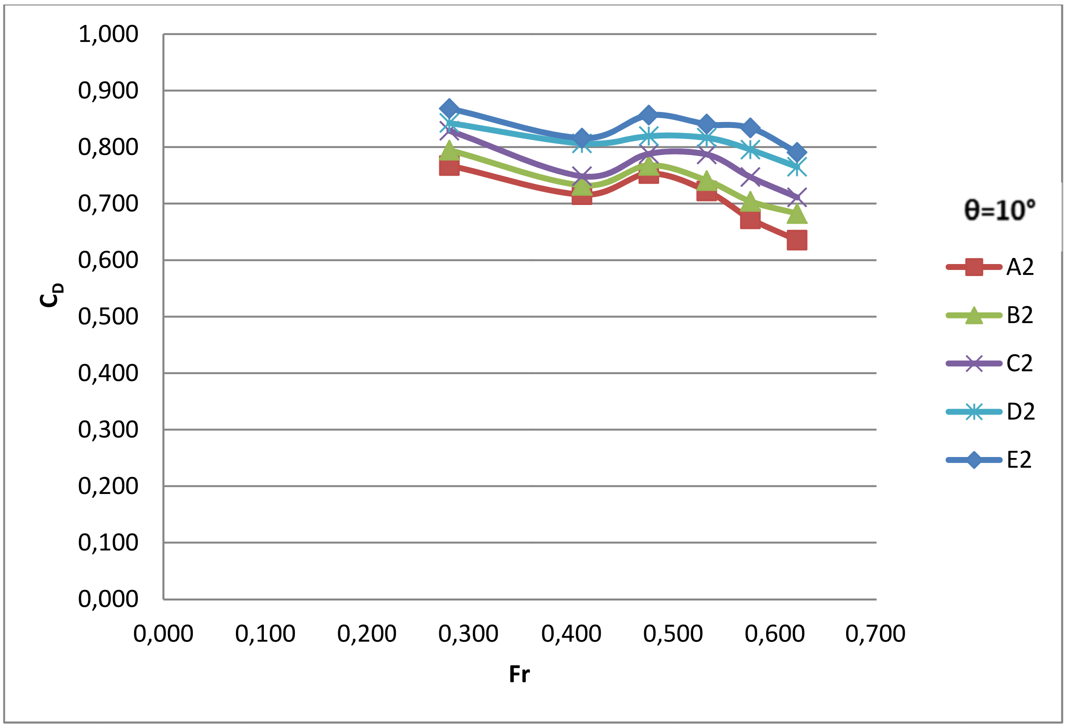

Figure 4.49: Discharge coefficient versus Fr for D=1.5 cm with different x values at θ=10°

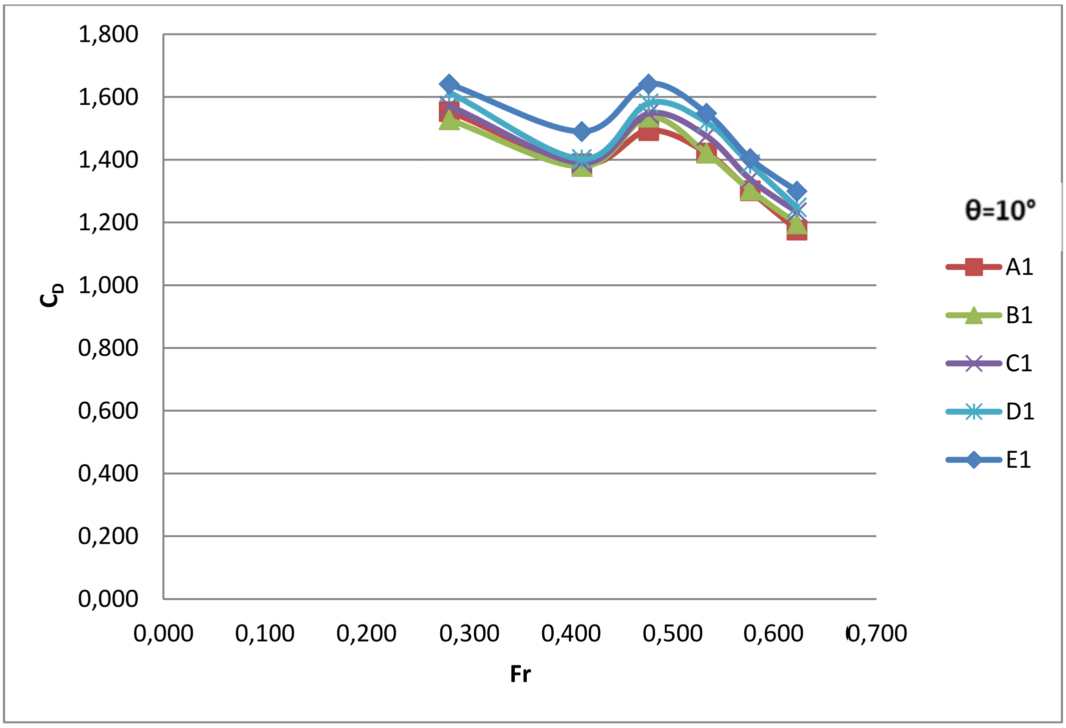

Figure 4.50: Discharge coefficient versus Fr for D=1 cm with different x values at θ=10°

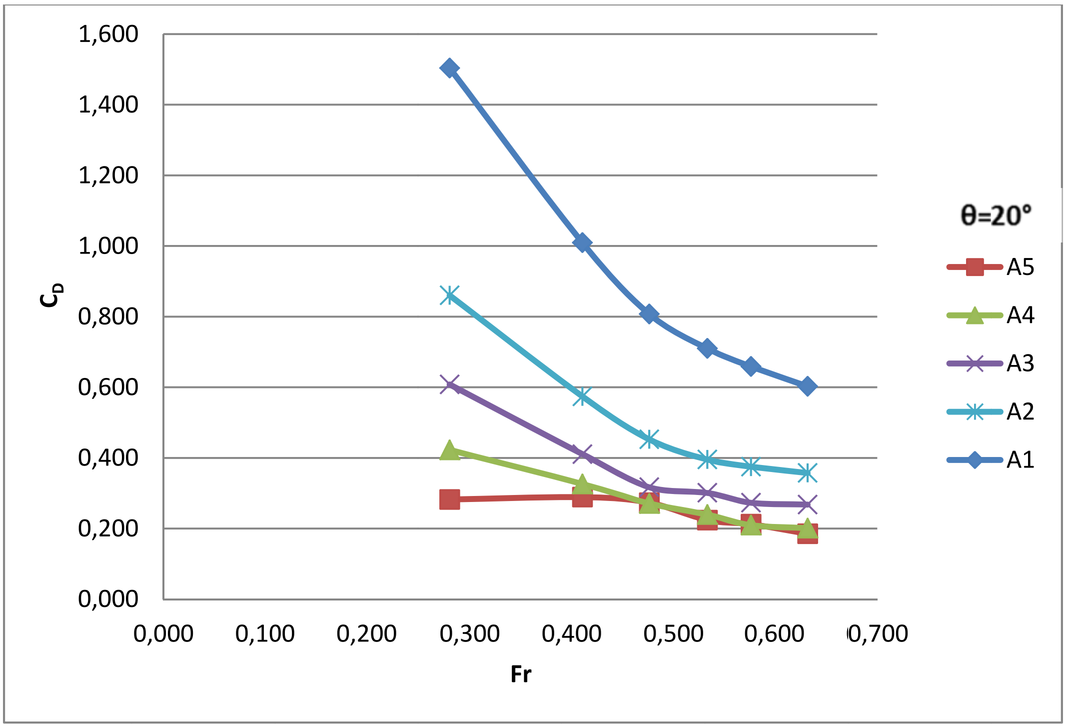

Figure 4.51: Discharge coefficient versus Fr for the orifice A with different D values at θ=20°

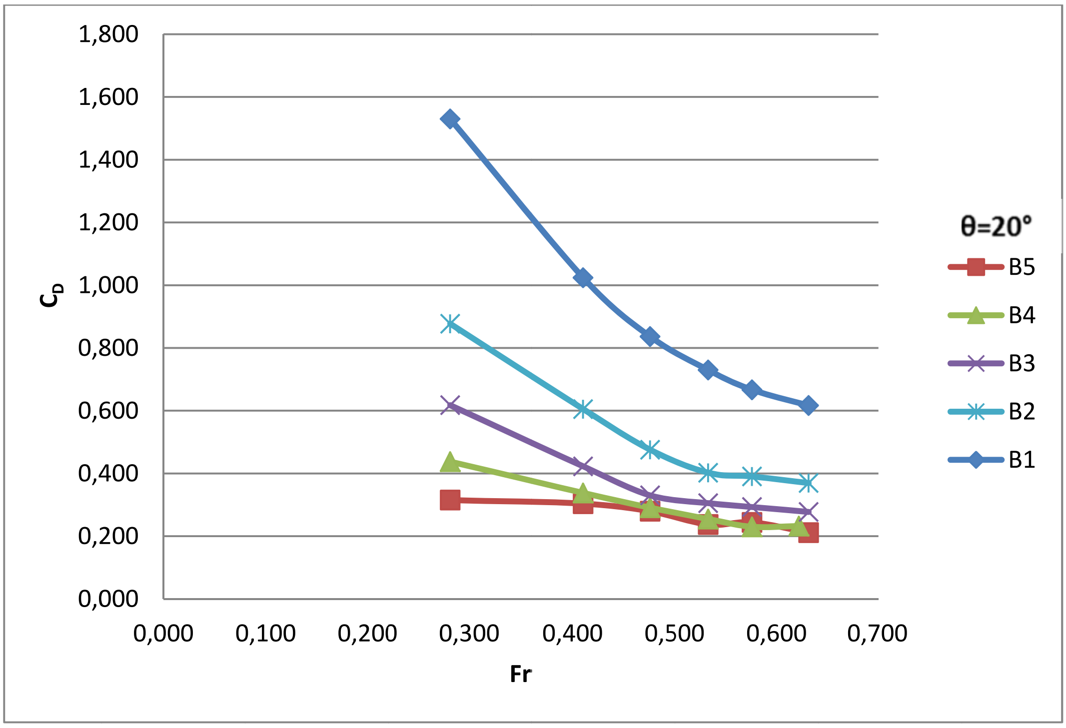

Figure 4.52: Discharge coefficient versus Fr for the orifice B with different D values at θ=20°

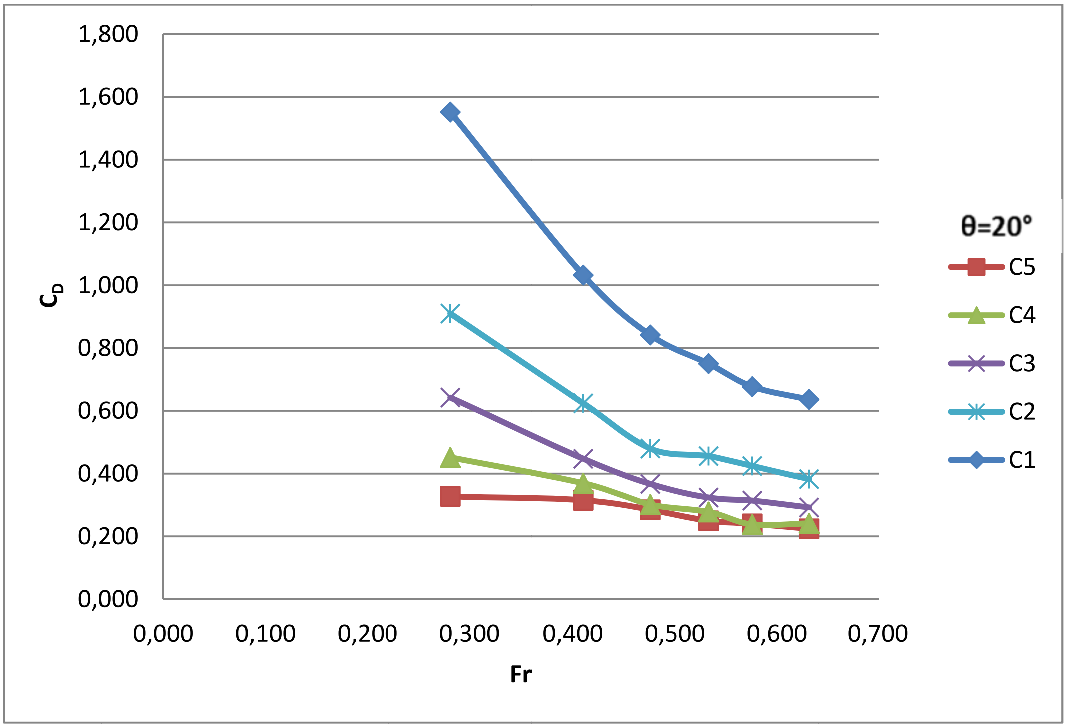

Figure 4.53: Discharge coefficient versus Fr for the orifice C with different D values at θ=20°

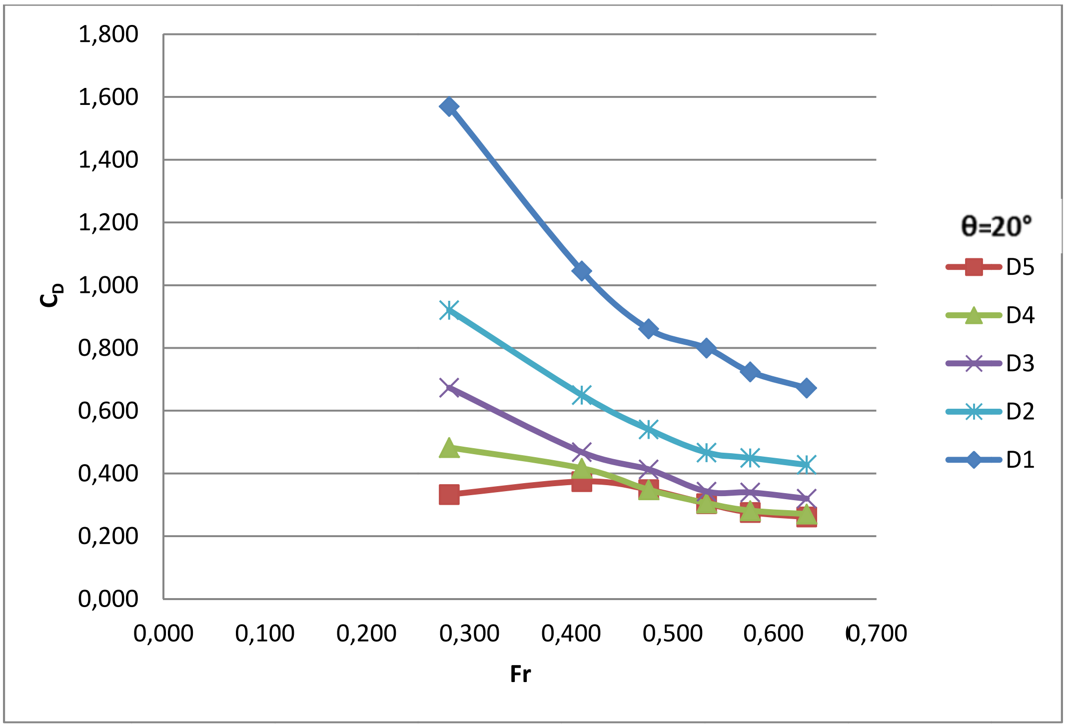

Figure 4.54: Discharge coefficient versus Fr for the orifice D with different D values at θ=20°

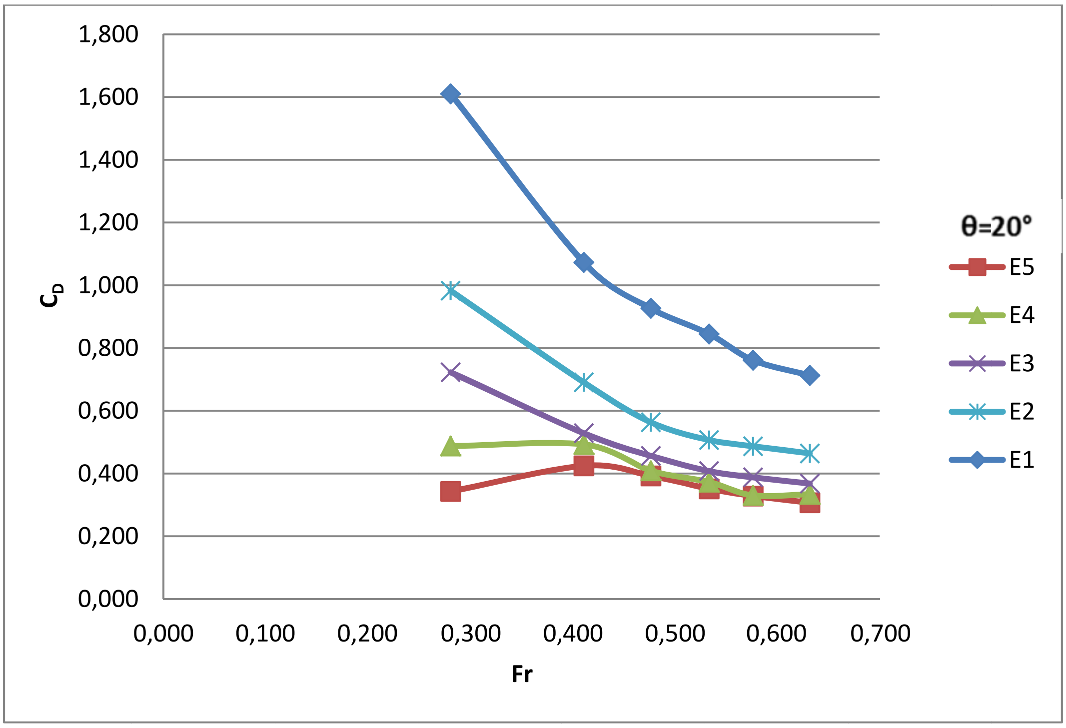

Figure 4.55: Discharge coefficient versus Fr for the orifice E with different D values at θ=20°

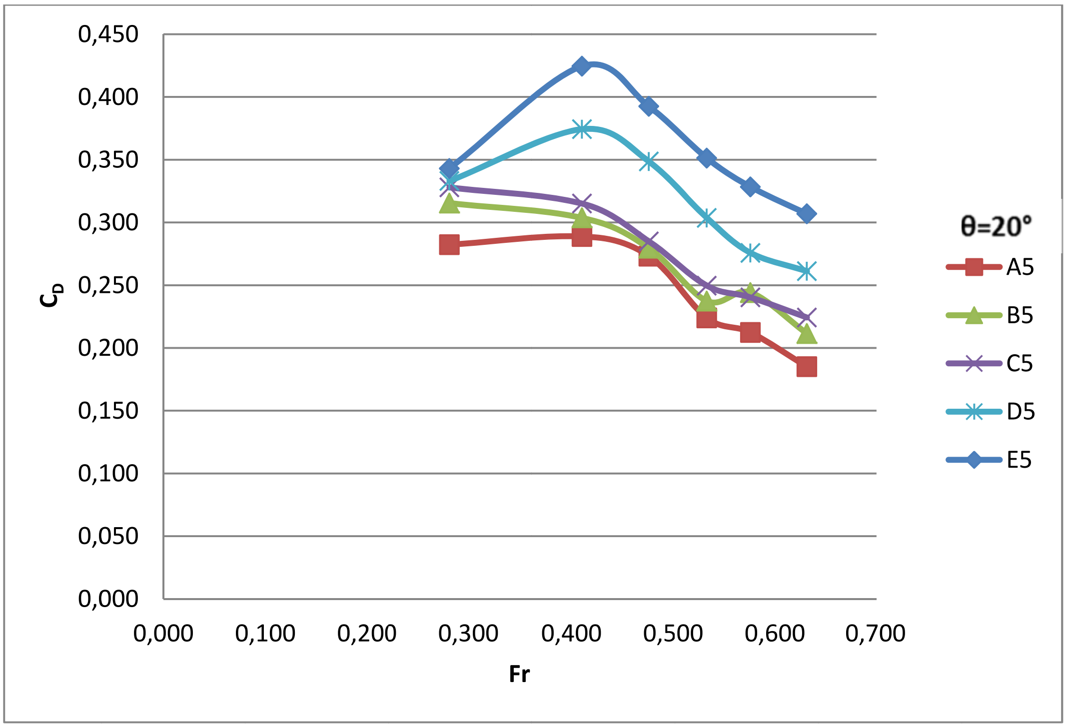

Figure 4.56: Discharge coefficient versus Fr for D=4 cm with different x values at θ=20°

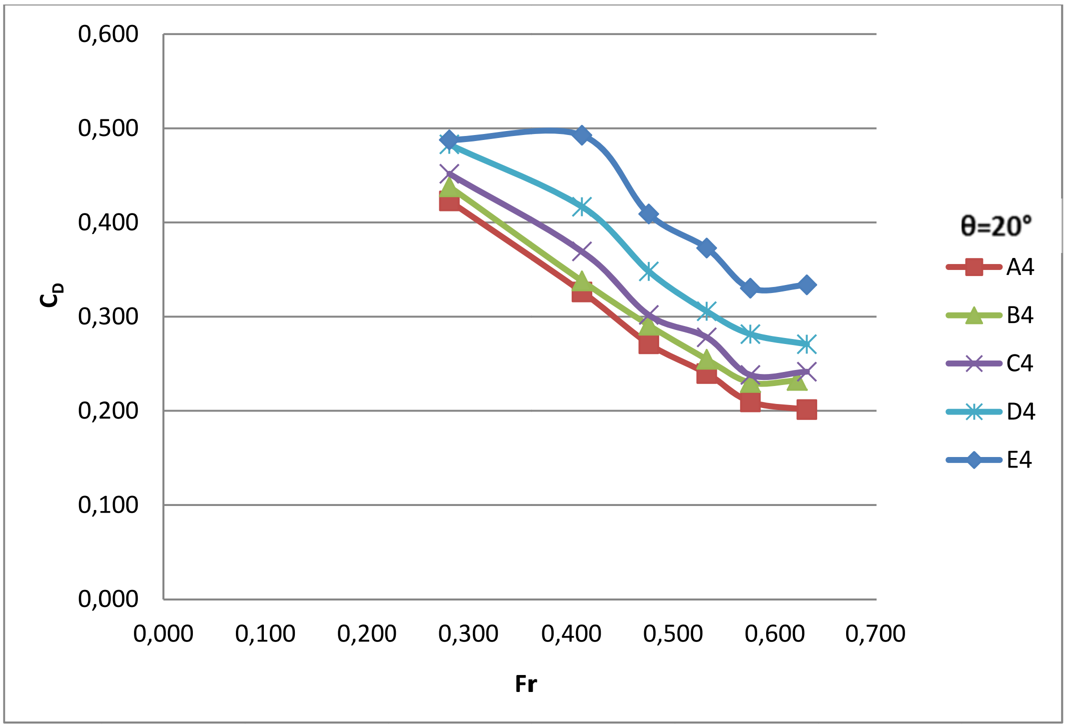

Figure 4.57: Discharge coefficient versus Fr for D=3 cm with different x values at θ=20°

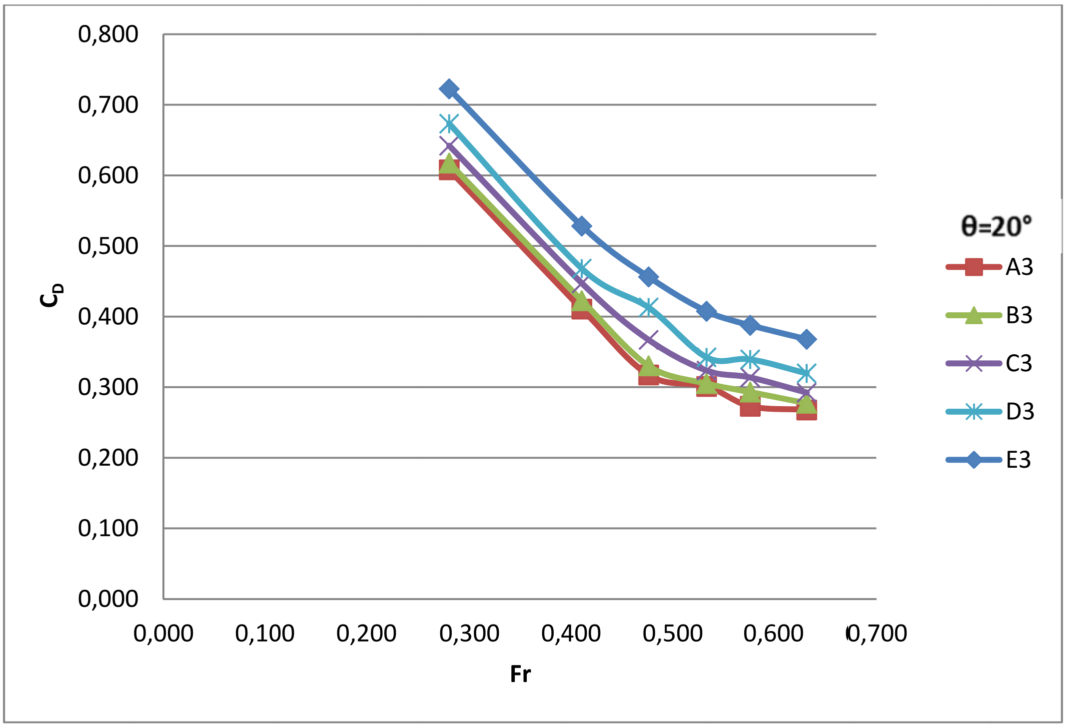

Figure 4.58: Discharge coefficient versus Fr for D=2 cm with different x values at θ=20°

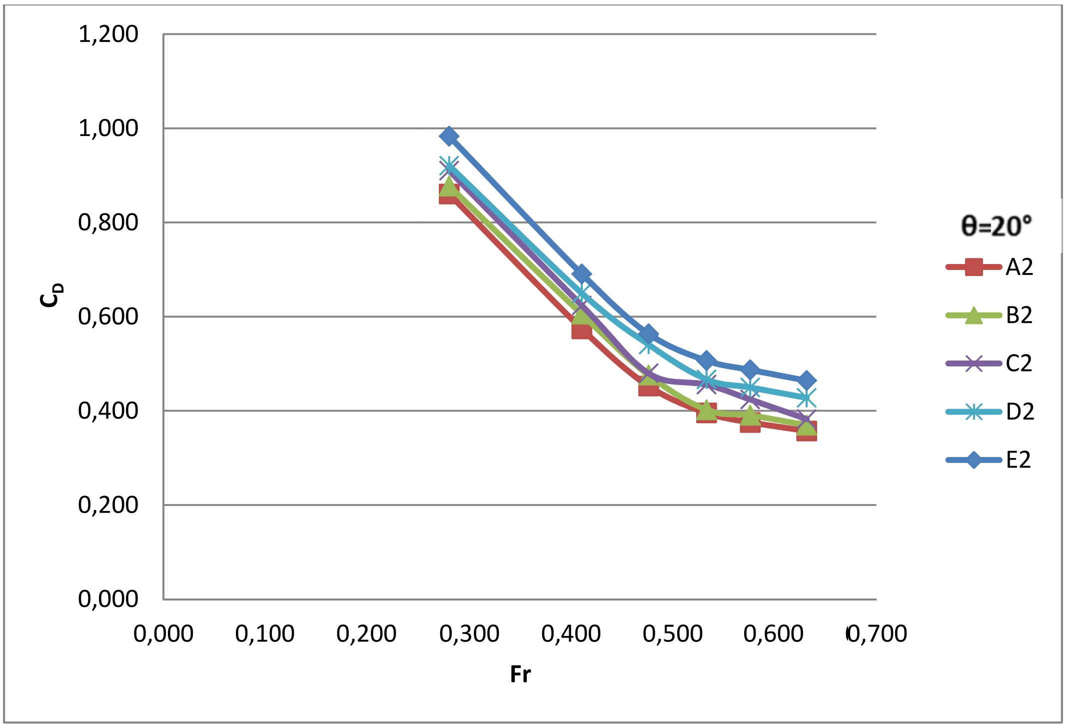

Figure 4.59: Discharge coefficient versus Fr for D=1.5 cm with different x values at θ=20°

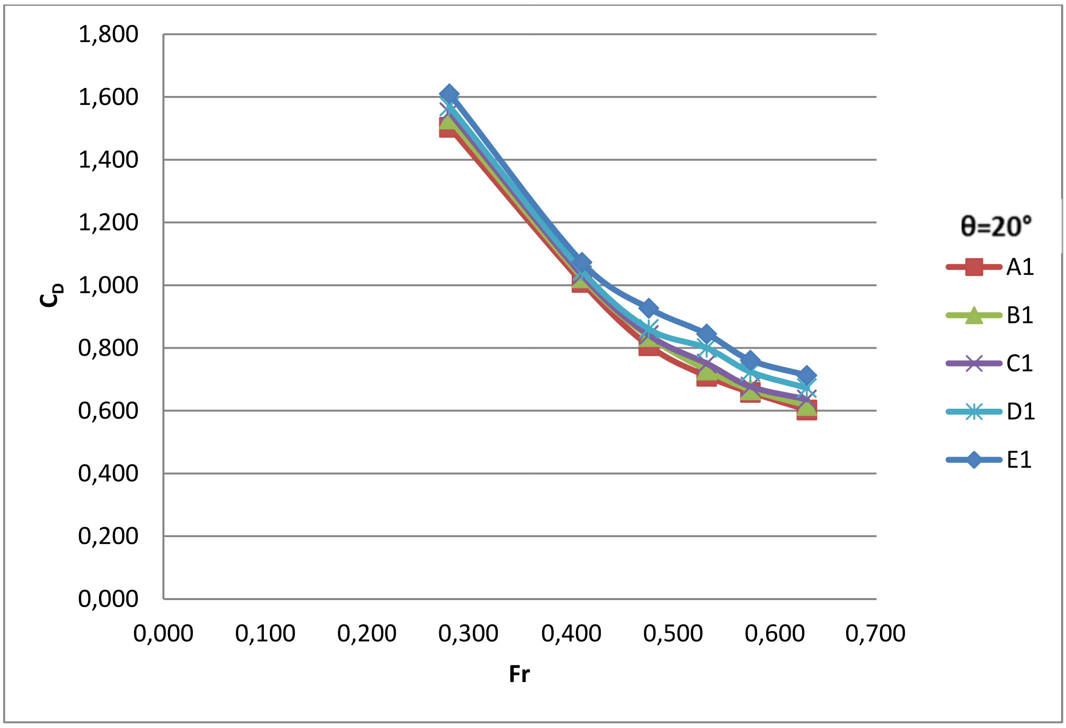

Figure 4.60: Discharge coefficient versus Fr for D=1 cm with different x values at θ=20°

From the inspection of Figures 4.1-4.60, it can be concluded that the value of C_D for a given orifice type decreases as the slope of the screen increases under the same upstream flow conditions that is for the same D/h, x/h and Fr.

4.2.2 Empirical Relationship between C_D and Related Parameters with respect to Screen Slopes

To show the relationship between C_D and the relevant parameters stated in Equation 2.10, regression analysis may be applied to the available data after defining the empirical equation as below:

At θ=0°,

$$C_D = k\left(\frac{D}{h}\right)^l \left(\frac{x}{h}\right)^m (Fr)^n \qquad (4.1)$$

where k, l, m and n are the empirical coefficients and defined as k=0.333, l= -0.824, m=0.079, n= -0.343, with a correlation coefficient of R^2=0.937. The plot of C_D values calculated from Equation 4.1, $(C_D)_{calculated}$, versus the measured C_D values, $(C_D)_{measured}$, is presented in Figure 4.61. The calculated C_D data lay between ±30% error lines.

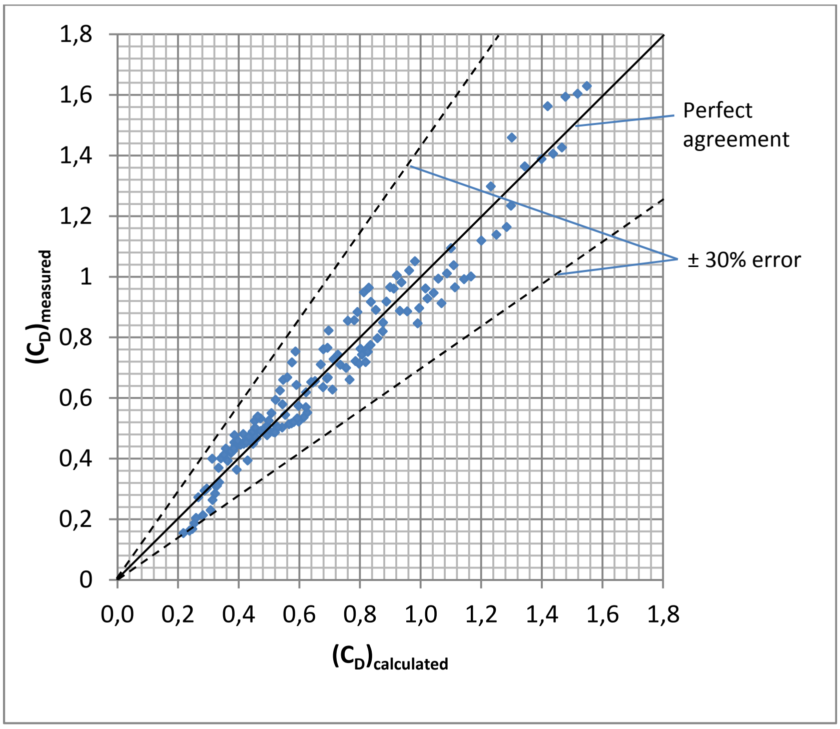

Figure 4. 61: Comparison of measured and calculated C_D values at θ=0°

At θ=10°,

$$C_D = 0.128(\frac{D}{h})^{-1.071}(\frac{x}{h})^{0.088}(Fr)^{-1,435} \quad \text{……………..……………..………………………(4.2)}$$

with a correlation coefficient of R^2=0.924. The plot of C_D values calculated from Equation 4.2, $(C_D)_{calculated}$ versus the measured C_D values, $(C_D)_{meaasured}$, is presented in Figure 4.62. The calculated C_D data lay between ±30% error lines.

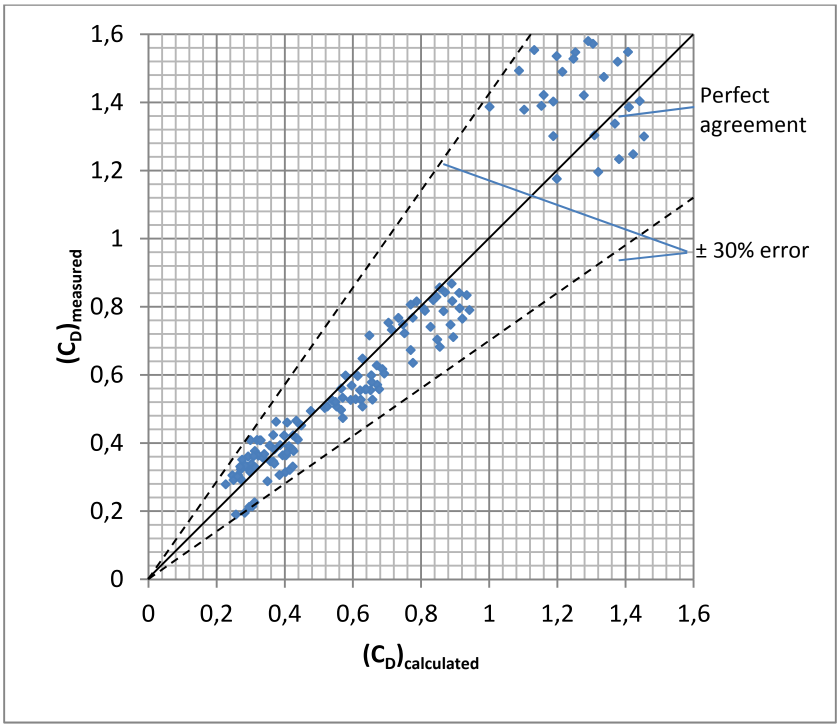

Figure 4. 62: Comparison of measured and calculated C_D values at θ=10°

At θ=20°,

$$C_D = 0.069\left(\frac{D}{h}\right)^{-0.786}\left(\frac{x}{h}\right)^{0,121}(Fr)^{-1,908} \qquad \text{……………..……………………………………(4.3)}$$

with a correlation coefficient of R^2=0.896. The plot of C_D values calculated from Equation 4.3, $(C_D)_{calculated}$ versus the measured C_D values, $(C_D)_{meaasured}$, is presented in Figure 4.63. The calculated C_D data lay between ±30% error lines.

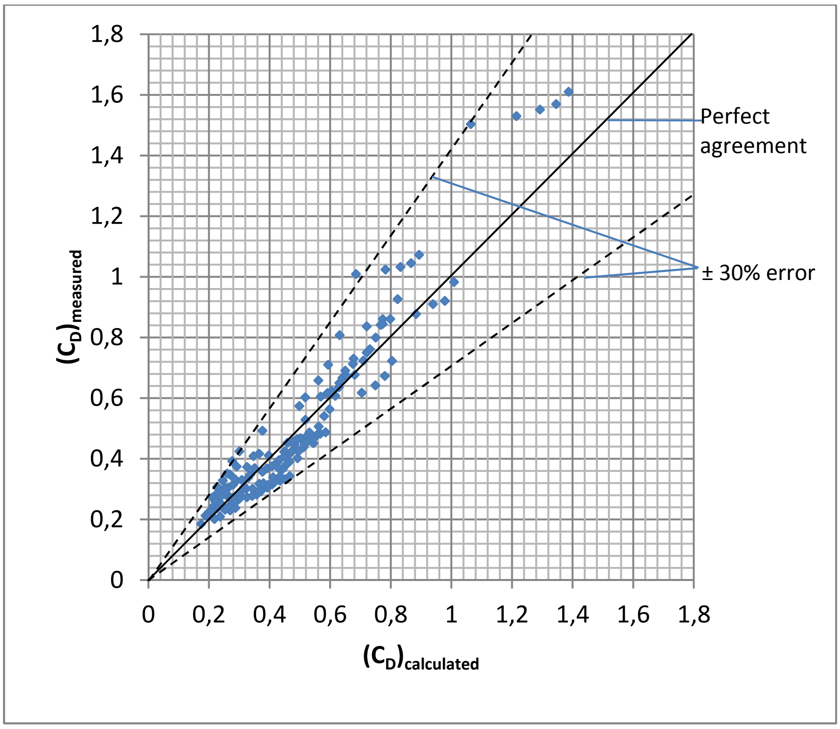

Figure 4. 63: Comparison of measured and calculated C_D values at θ=20°

4.2.3 Relationship between Coefficient K and the Related Dimensionless Parameters for a Single Circular Bottom Intake Orifice on the Screen

The relationship between K and the relevant dimensionless parameters are given by Equation 2.9.

Figures 4.64-4.68 show the variation of K with the dimensionless variable D/h for all the circular bottom intake orifices tested at the locations of A, B, C, D and E, respectively at 0° slope condition of the bottom intake screen. When the curves in Figures 4.64-4.68 are examined, almost in each figure, it is seen that the general trend of the data points for a given orifice diameter D is the same; as D/h values increase, K values almost linearly increase and attain maximum values at the largest D/h values. For a given D/h, as the diameter of the orifice increases at a given location, the corresponding K value decreases.

Figures 4.69-4.73 and Figures 4.74-78 show the variation of K with the dimensionless variable, D/h for all circular bottom intake orifices tested when they are located on the screens having the slopes of 10° and 20°, respectively. The variations of K with D/h in all these figures are very similar to those given in Figures 4.64-4.68.

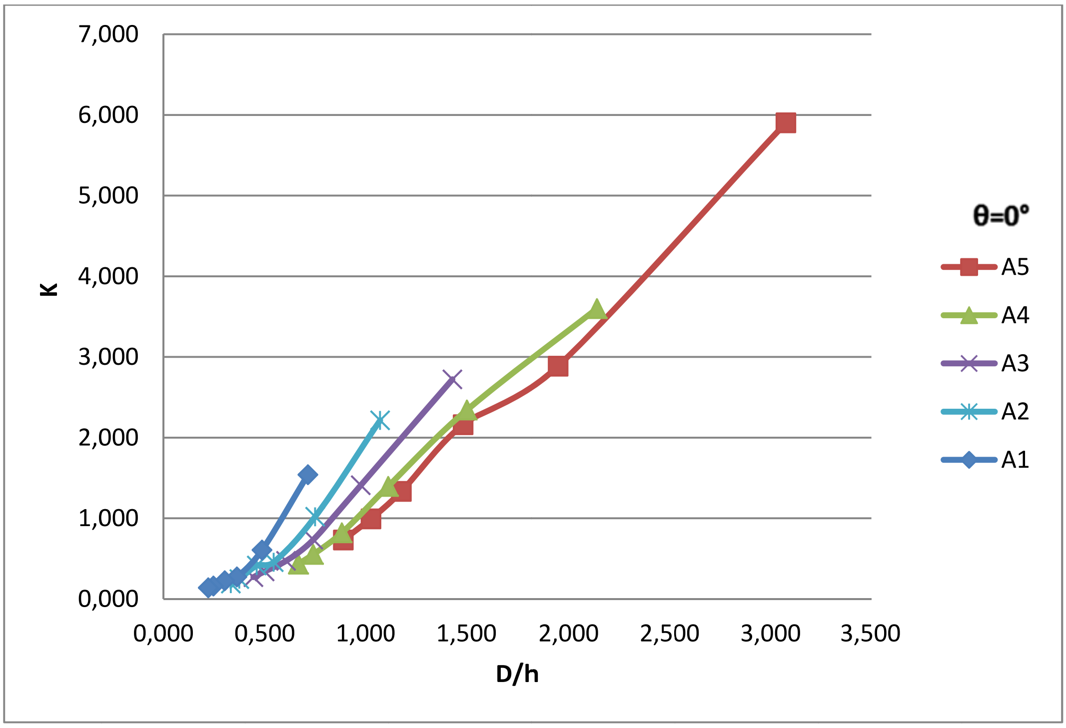

Figure 4.64: K versus D/h for the orifice A with different D values at θ=0°

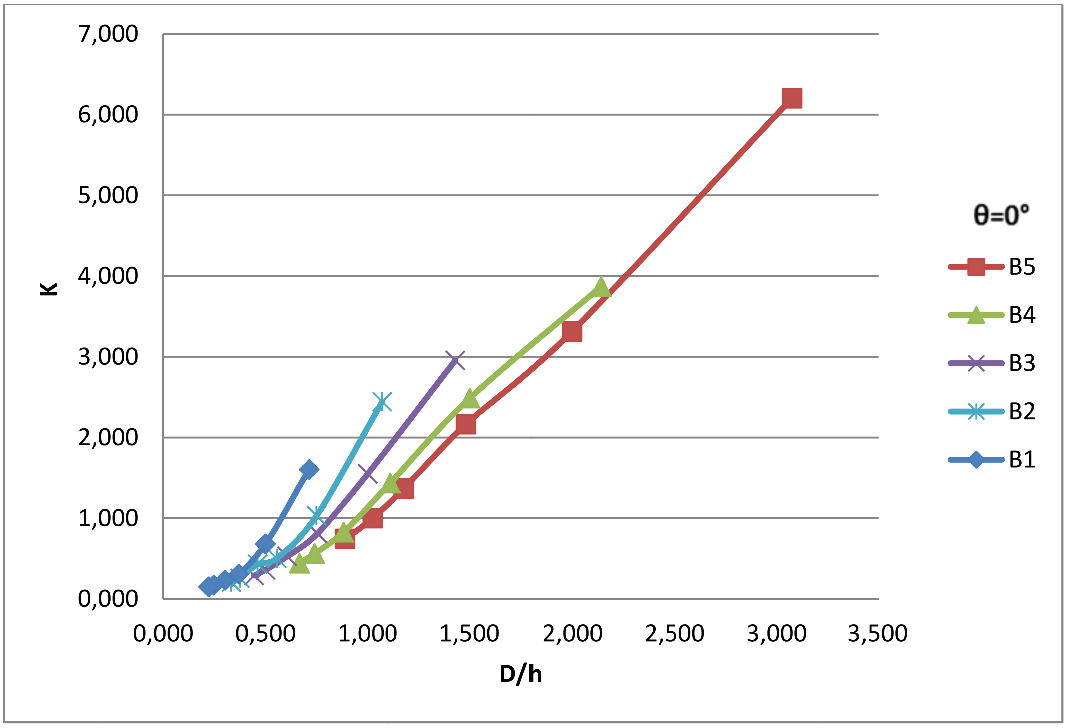

Figure 4.65: K versus D/h for the orifice B with different D values at θ=0°

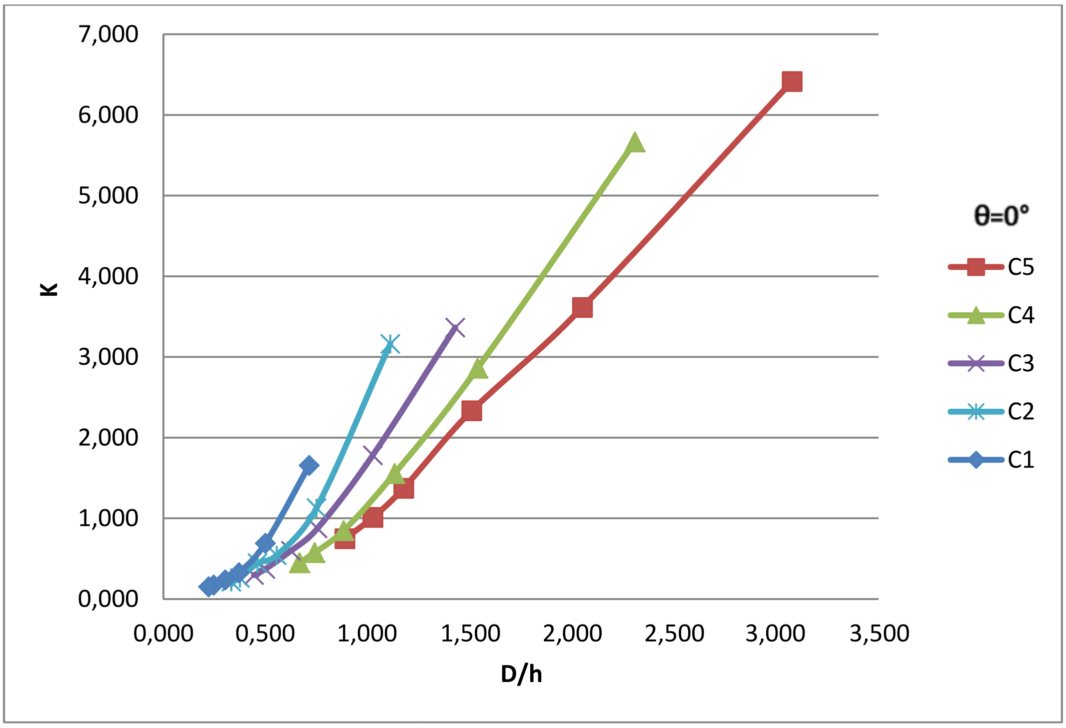

Figure 4.66: K versus D/h for the orifice C with different D values at θ=0°

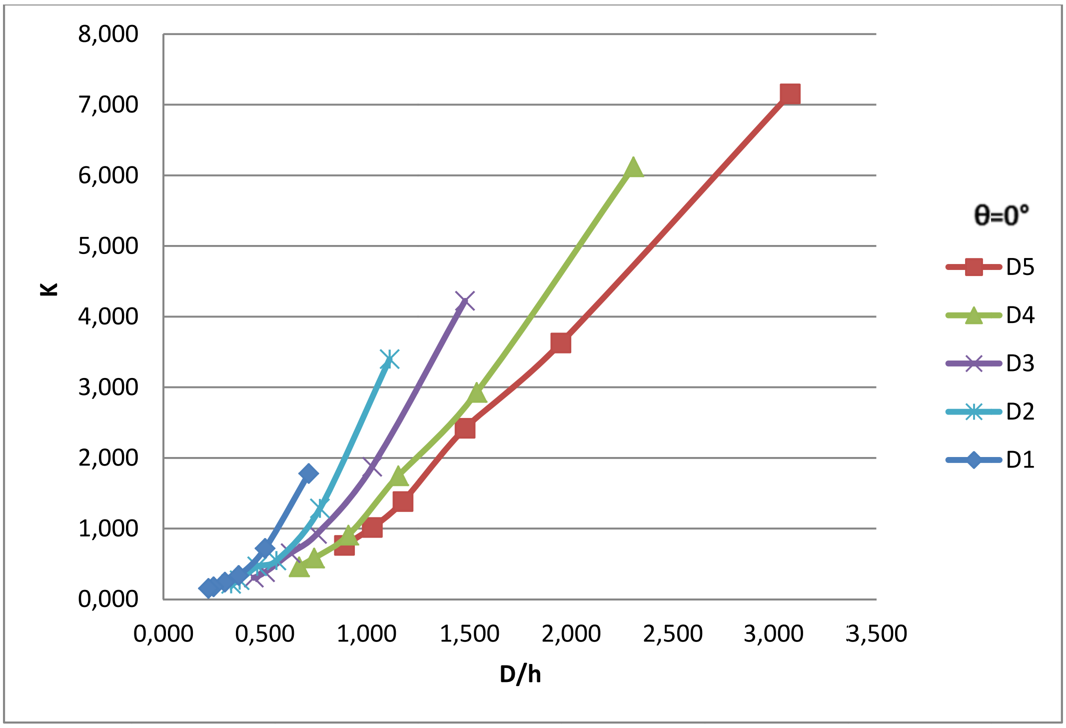

Figure 4.67: K versus D/h for the orifice A with different D values at θ=0°

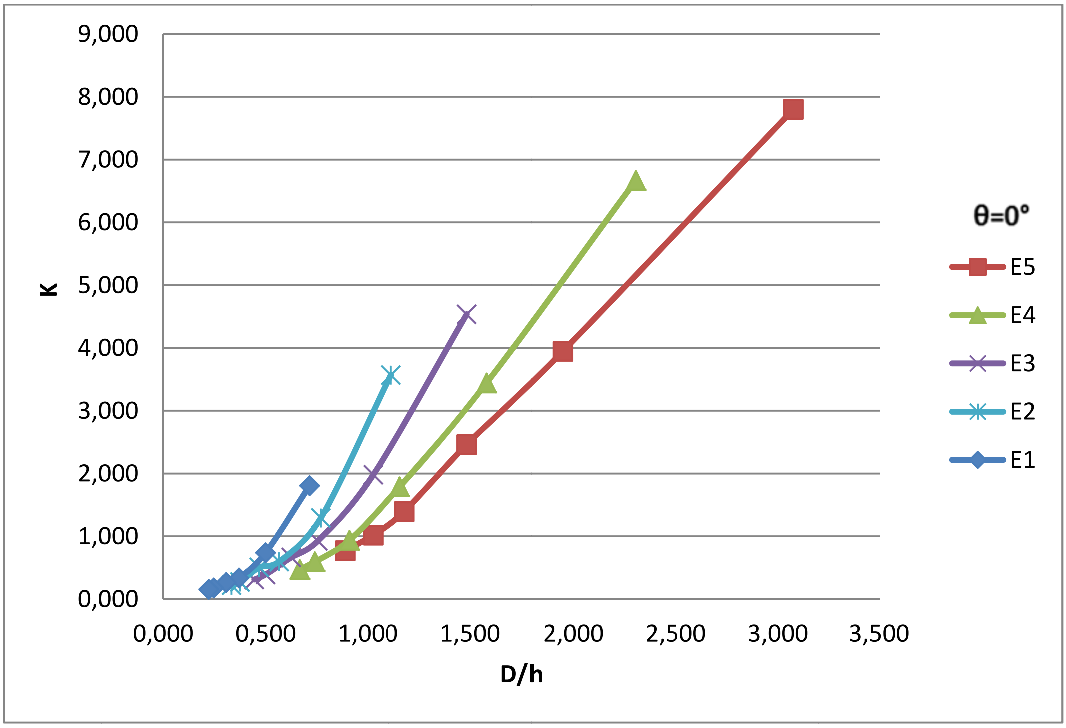

Figure 4.68: K versus D/h for the orifice E with different D values at θ=0°

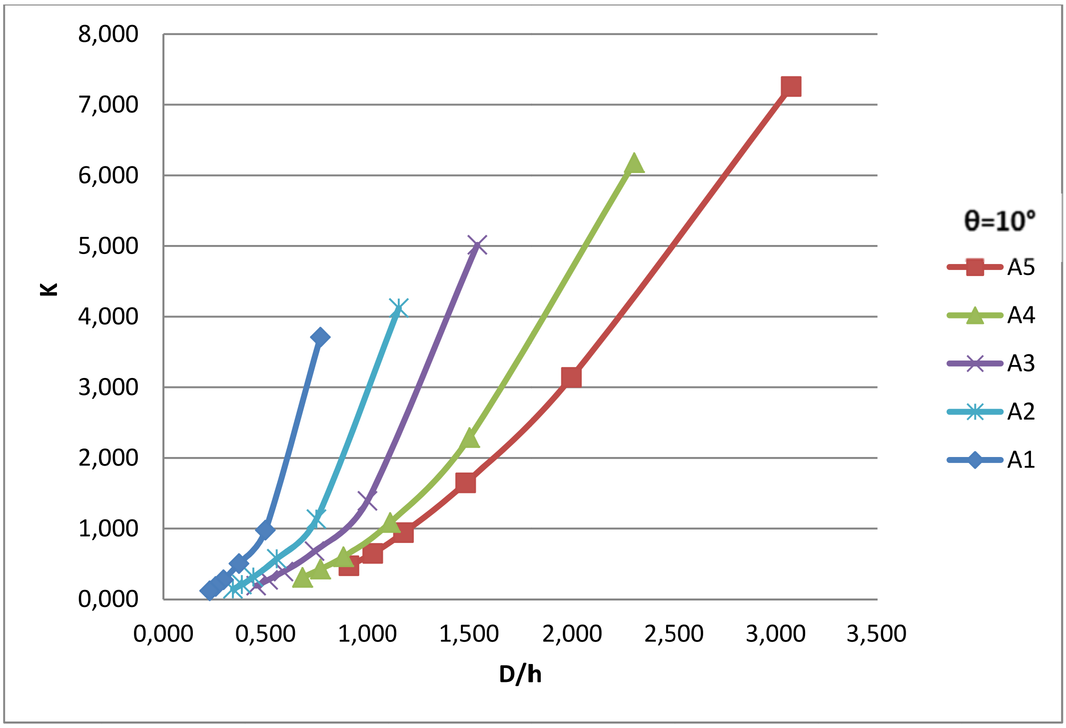

Figure 4.69: K versus D/h for the orifice A with different D values at θ=10°

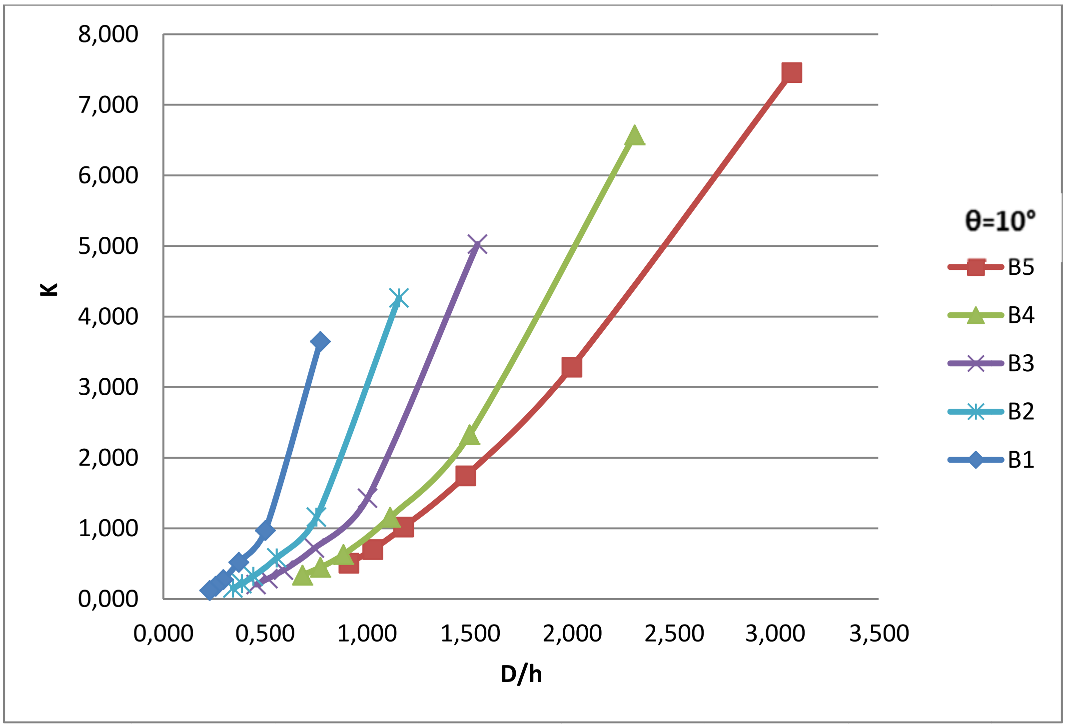

Figure 4.70: K versus D/h for the orifice B with different D values at θ=10°

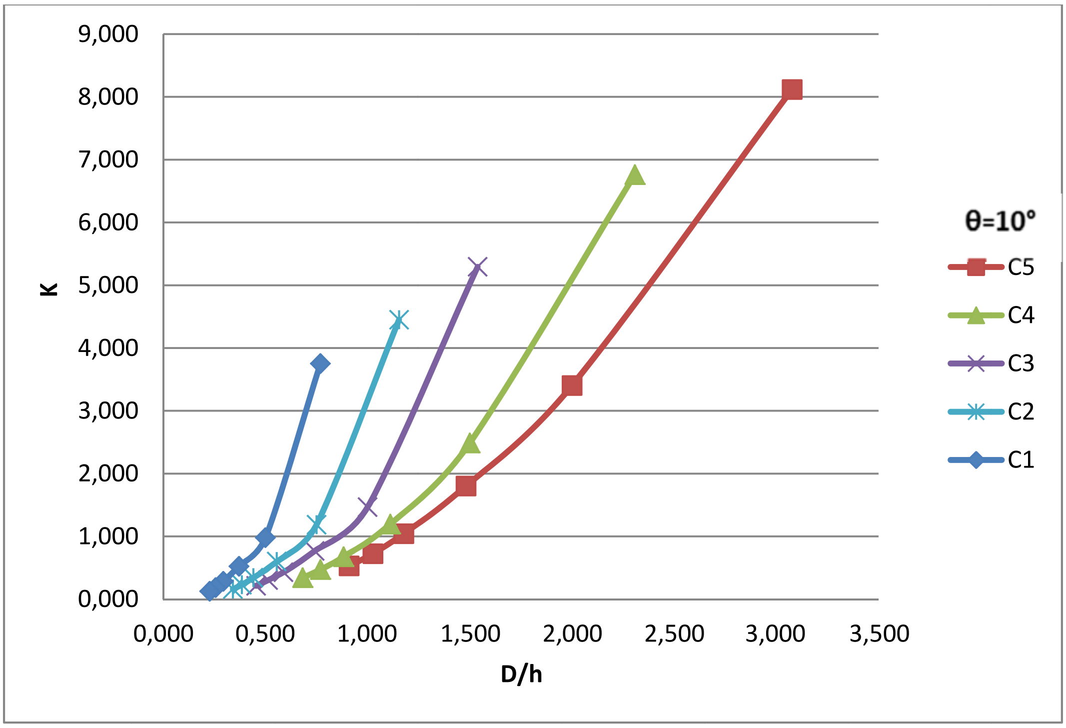

Figure 4.71: K versus D/h for the orifice C with different D values at θ=10°

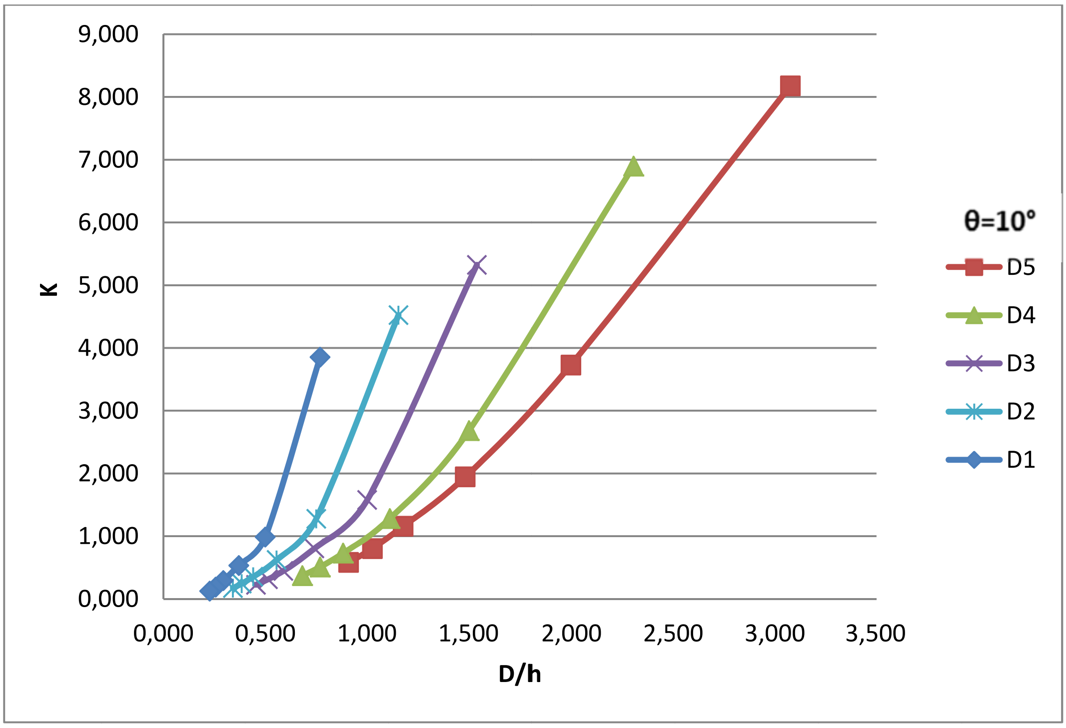

Figure 4.72: K versus D/h for the orifice D with different D values at θ=10°

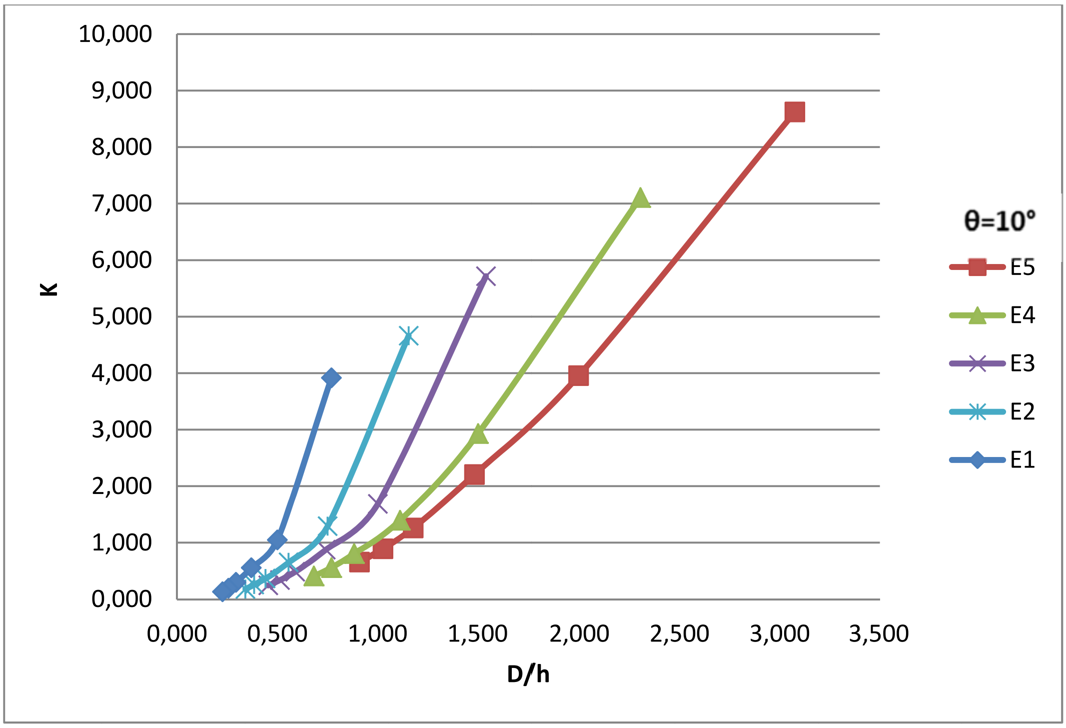

Figure 4.73: K versus D/h for the orifice E with different D values at θ=10°

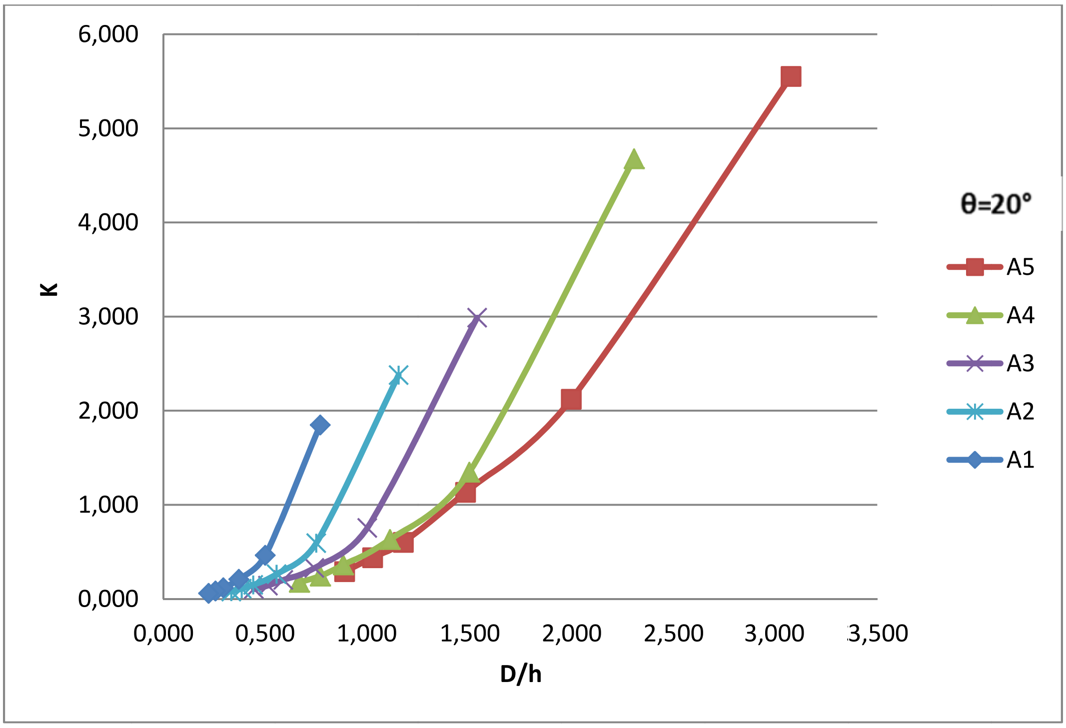

Figure 4.74: K versus D/h for the orifice A with different D values at θ=20°

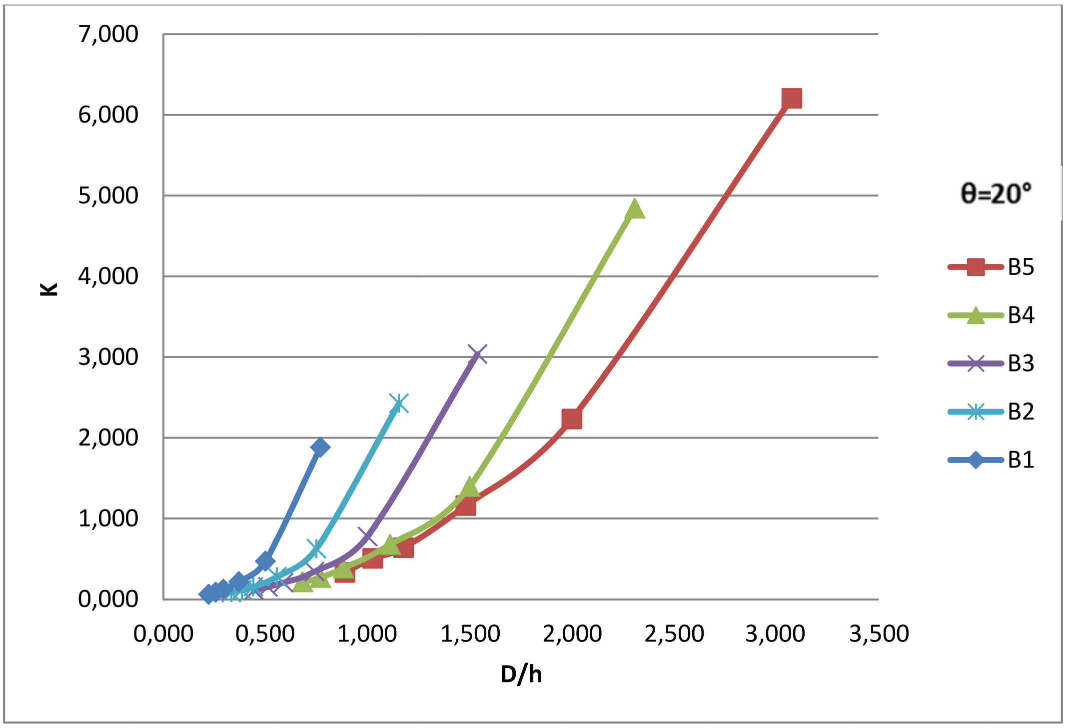

Figure 4.75: K versus D/h for the orifice B with different D values at θ=20°

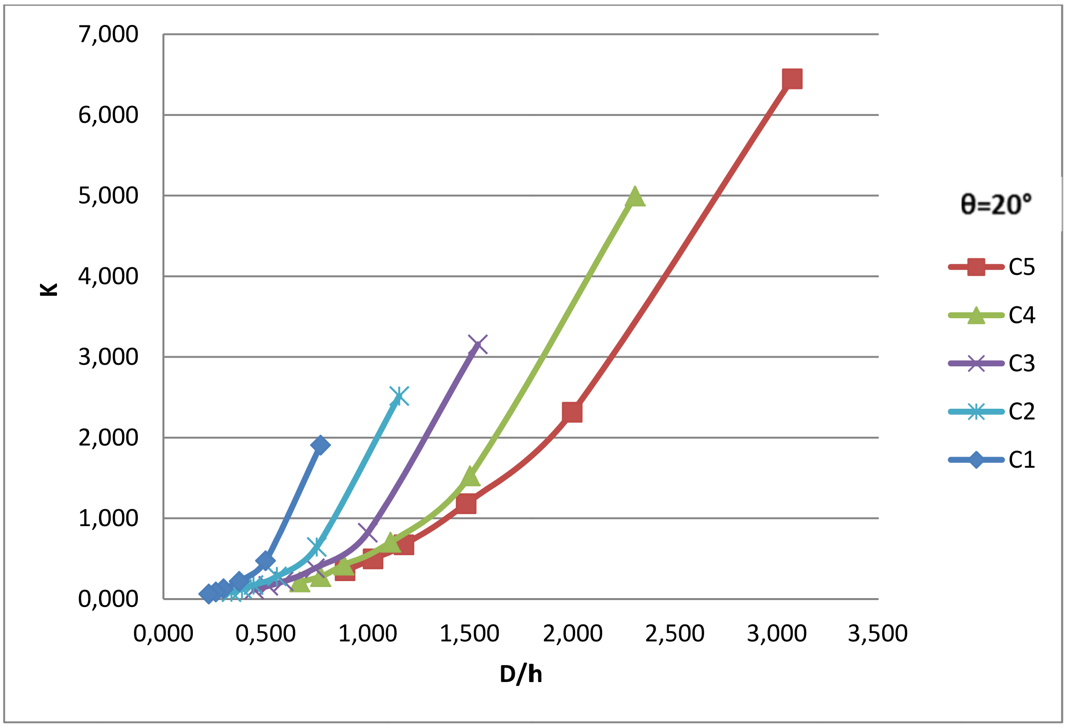

Figure 4.76: K versus D/h for the orifice C with different D values at θ=20°

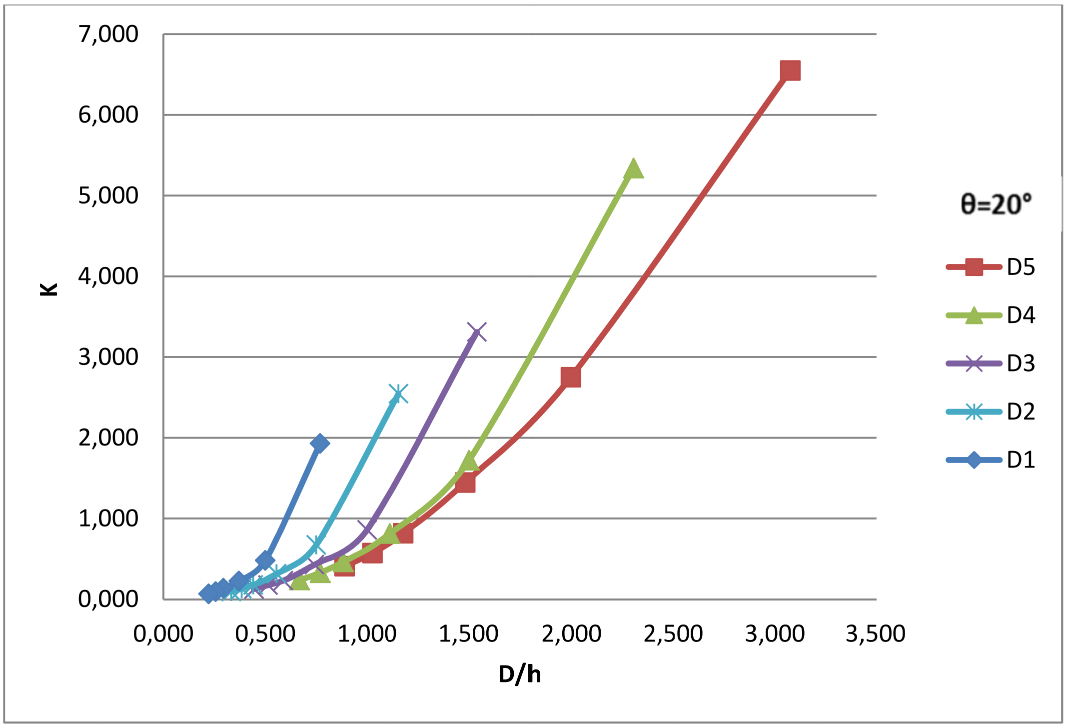

Figure 4.77: K versus D/h for the orifice D with different D values at θ=20°

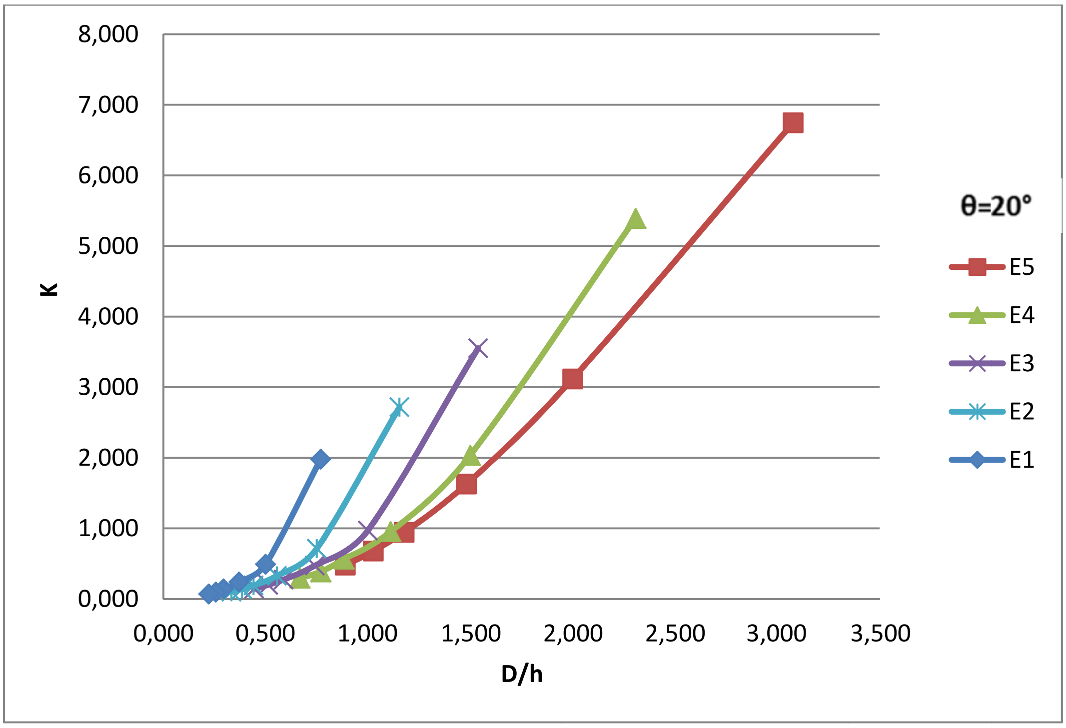

Figure 4.78: K versus D/h for the orifice E with different D values at θ=20°

Figures 4.79-4.83 show the effect of orifice location on K values for screens of θ=0°. From these figures, it is seen that for all the orifices tested K values increase with increasing x/h. Since the x value of a given orifice is fixed, as h decreases, K increases. It can also be concluded that for a given x/h, K value increases as the location of the orifice approaches to the free fall section of the screen.

The similar conclusions can also be made for the data of K versus x/h plotted for the screens of θ=10° and θ=20°, Figures 4.84-4.88 and Figures 4.89-4.93, respectively.

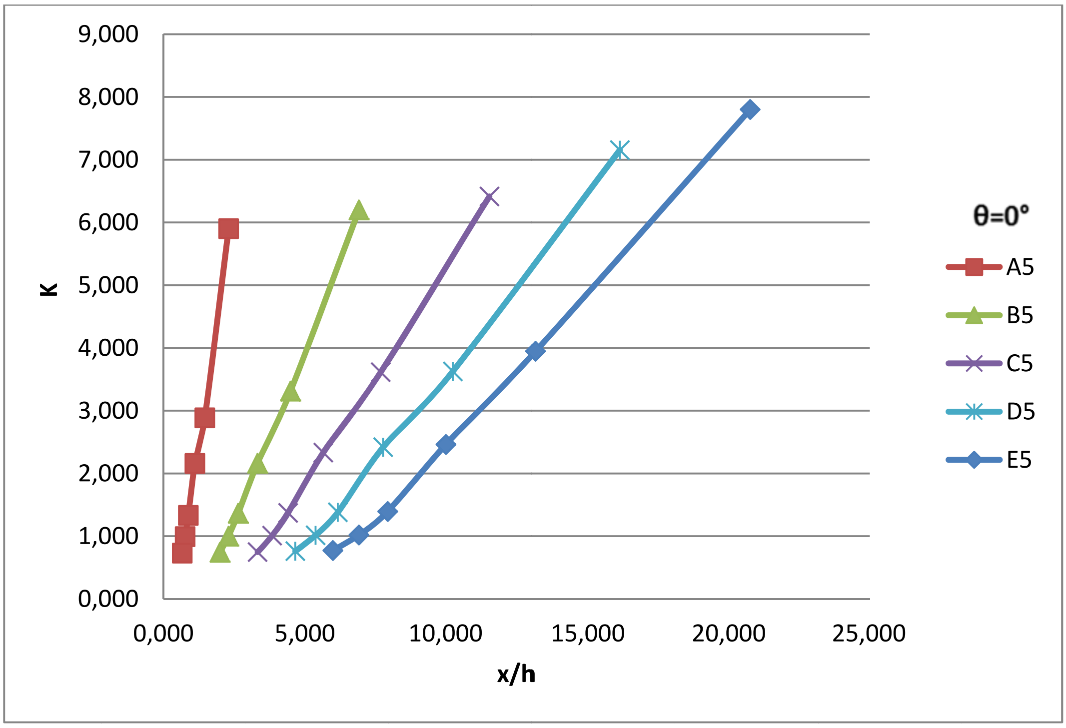

Figure 4.79: K versus x/h for D=4 cm with different x values at θ=0°

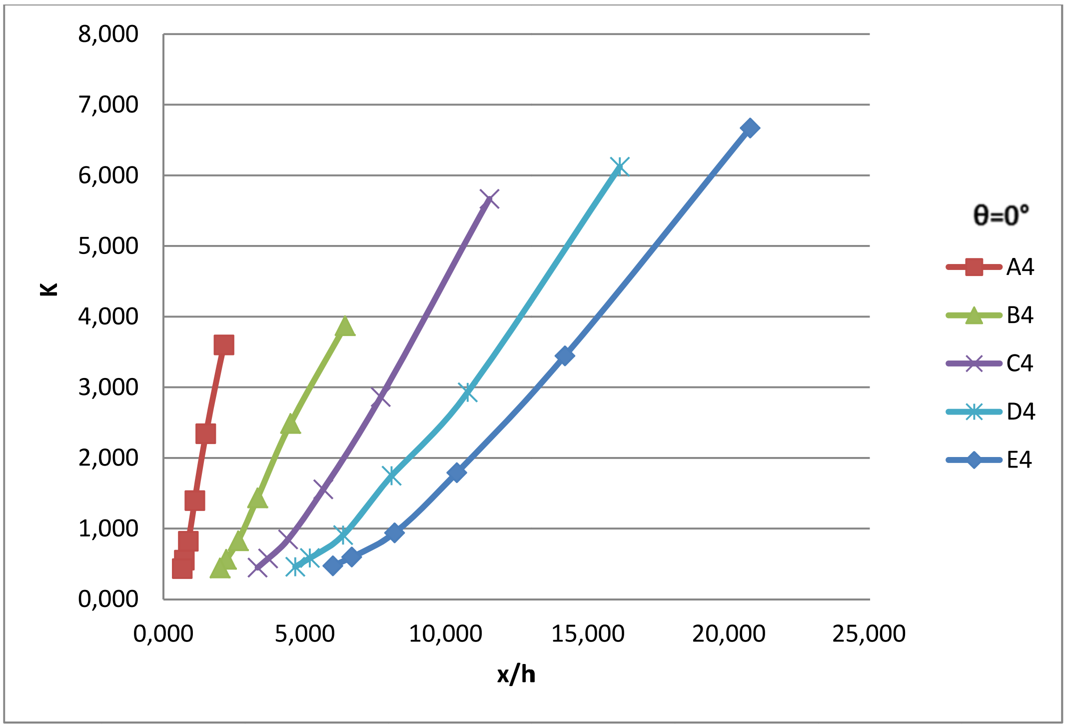

Figure 4.80: K versus x/h for D=3 cm with different x values at θ=0°

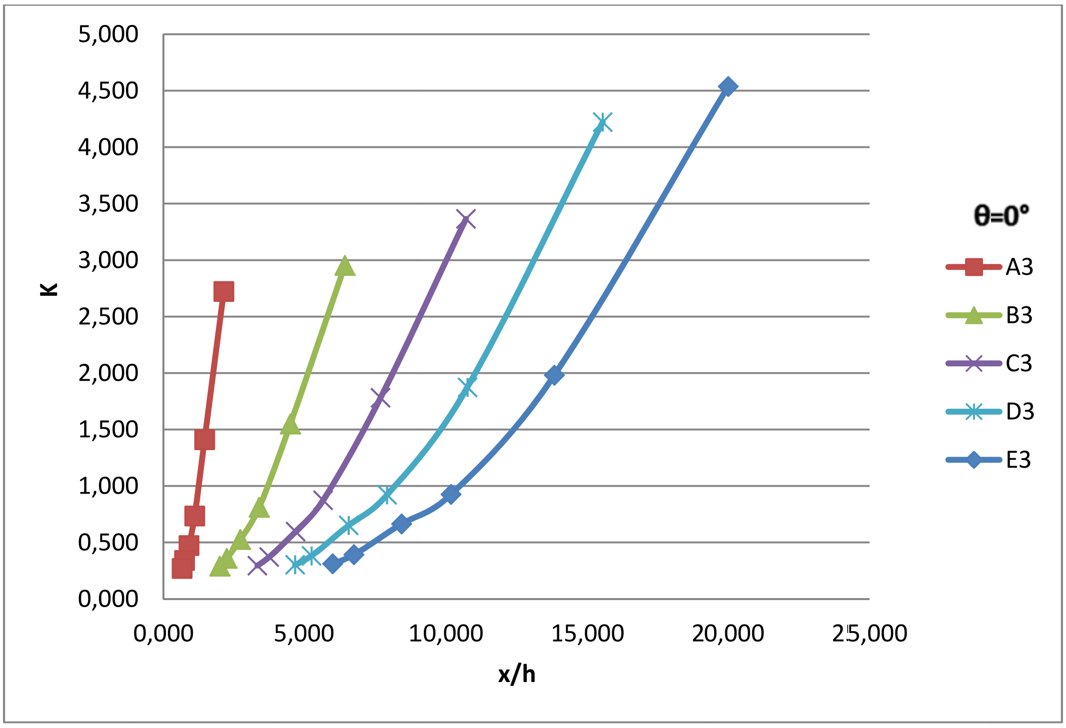

Figure 4.81: K versus x/h for D=2 cm with different x values at θ=0°

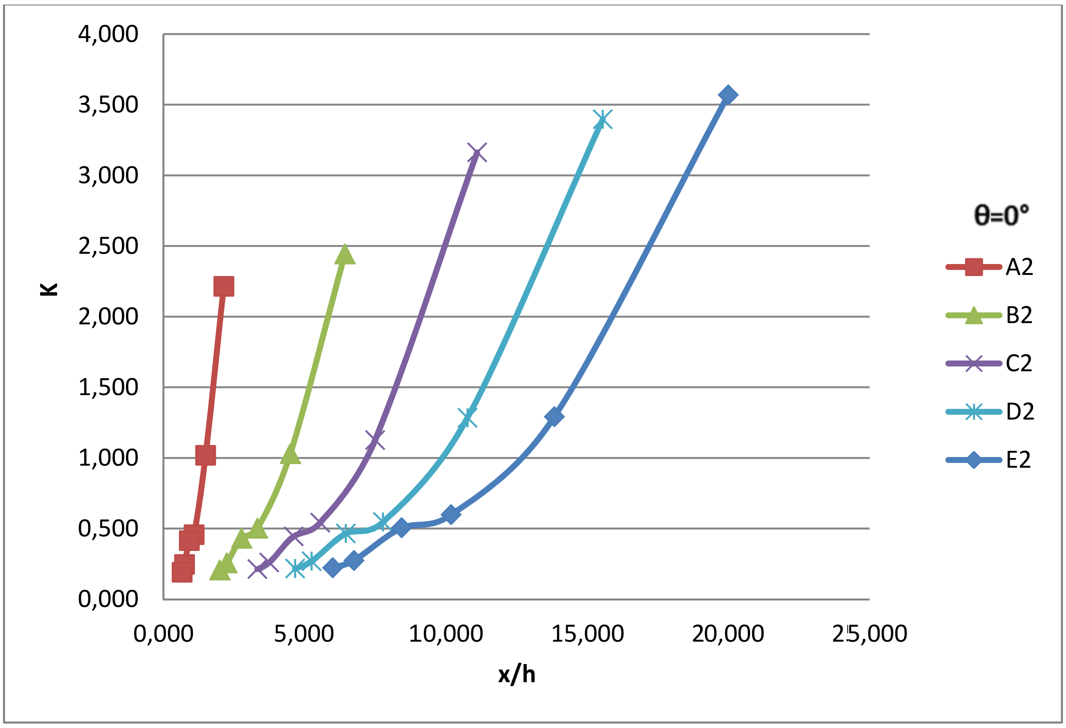

Figure 4.82: K versus x/h for D=1.5 cm with different x values at θ=0°

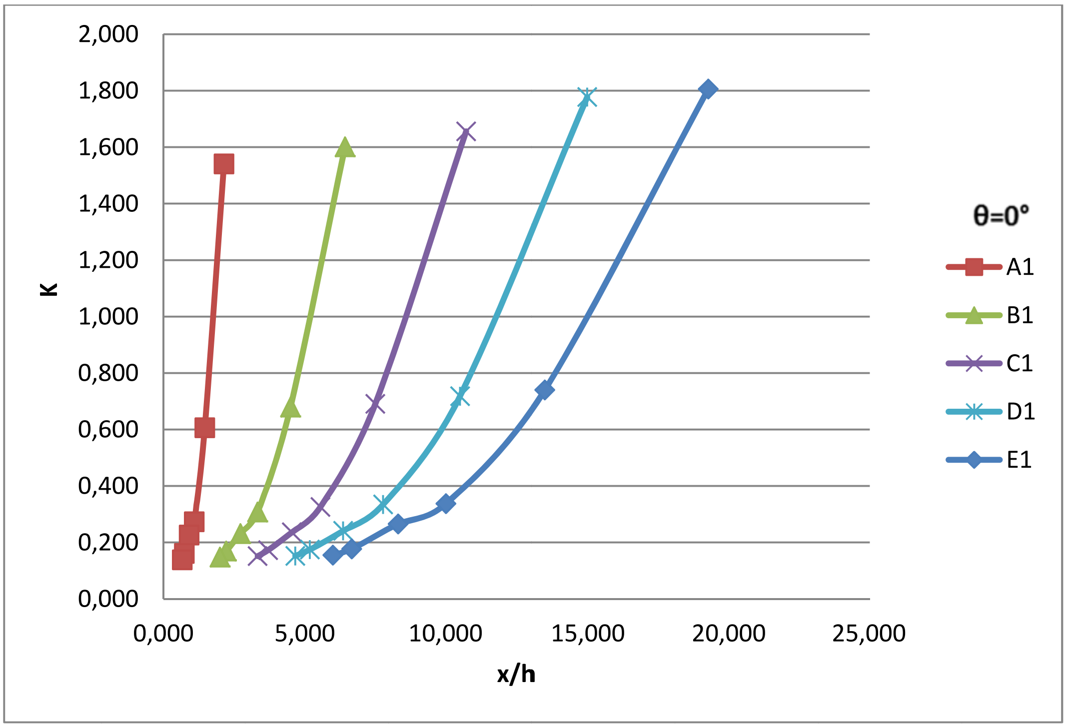

Figure 4.83: K versus x/h for D=1 cm with different x values at θ=0°

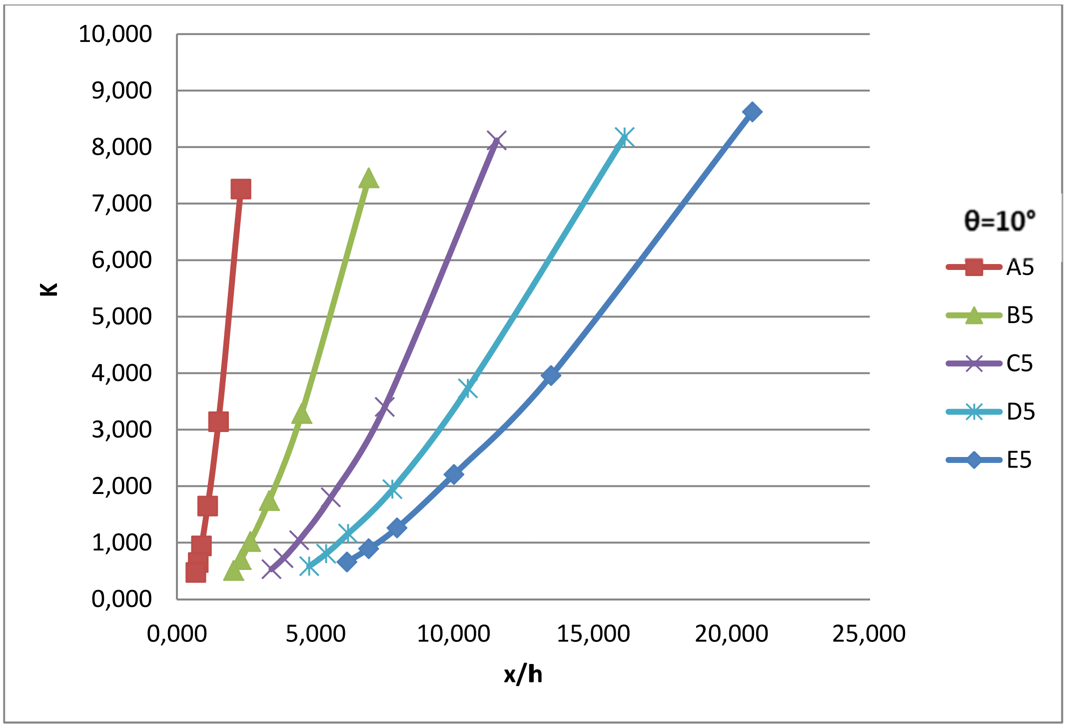

Figure 4.84: K versus x/h for D=4 cm with different x values at θ=10°

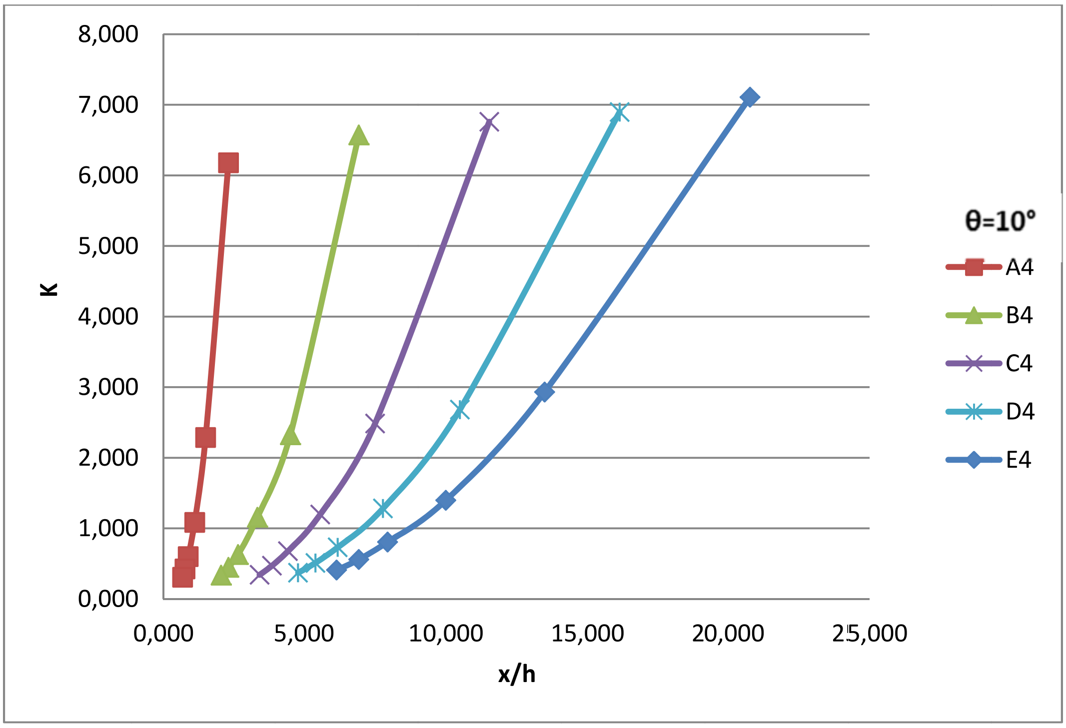

Figure 4.85: K versus x/h for D=3 cm with different x values at θ=10°

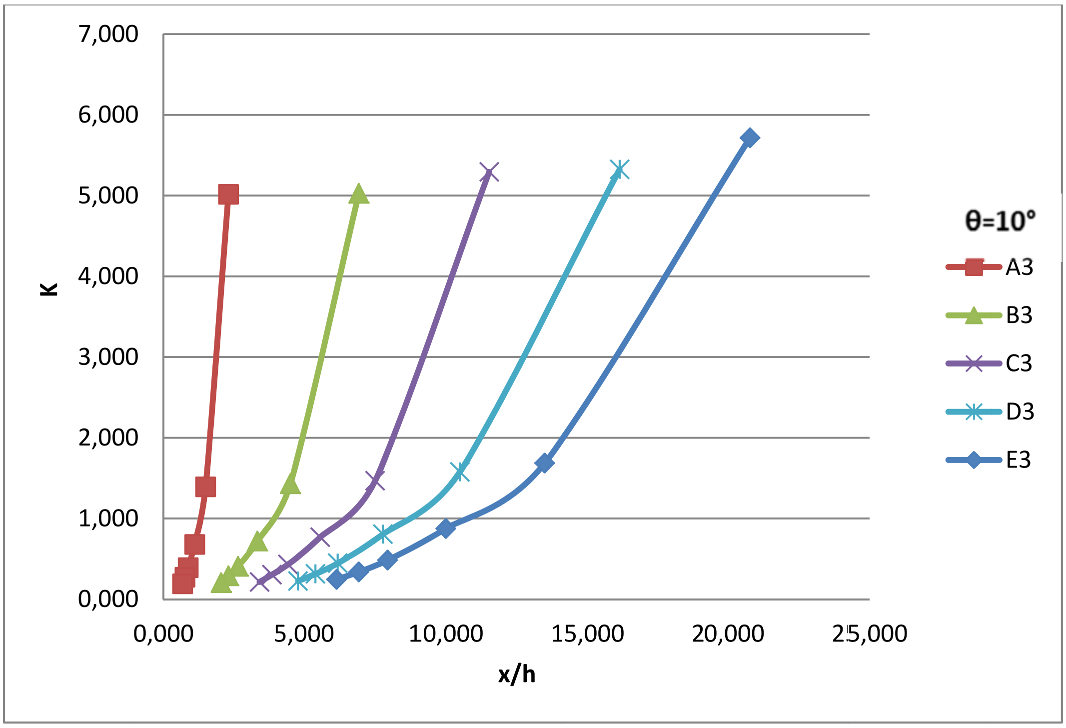

Figure 4.86: K versus x/h for D=2 cm with different x values at θ=10°

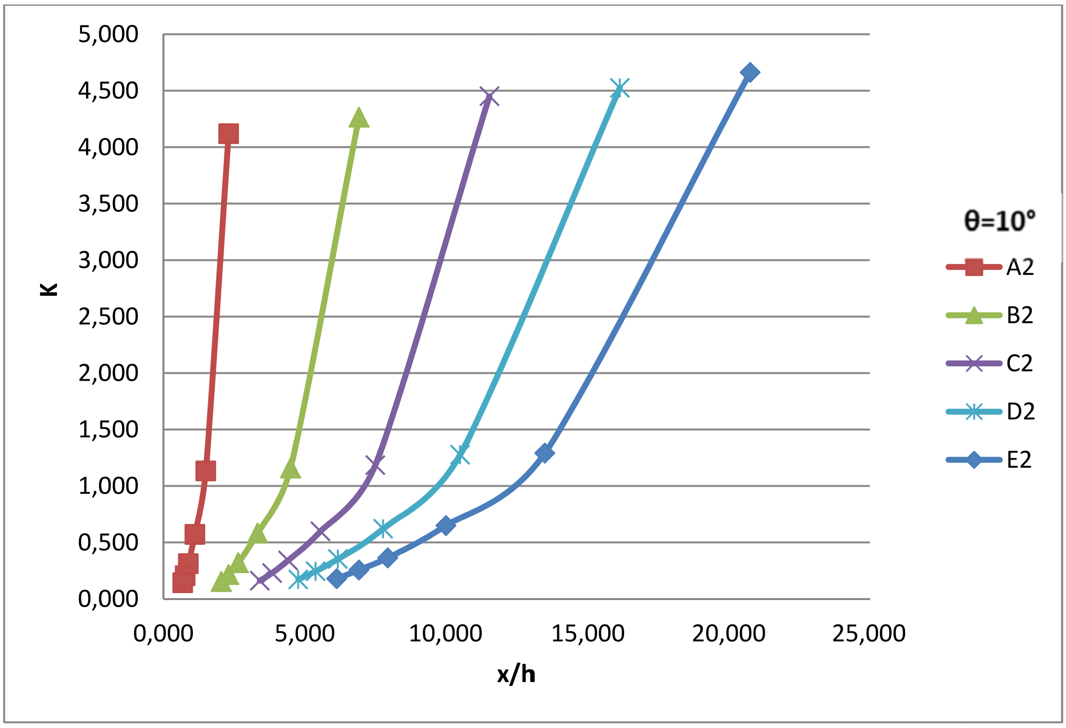

Figure 4.87: K versus x/h for D=1.5 cm with different x values at θ=10°

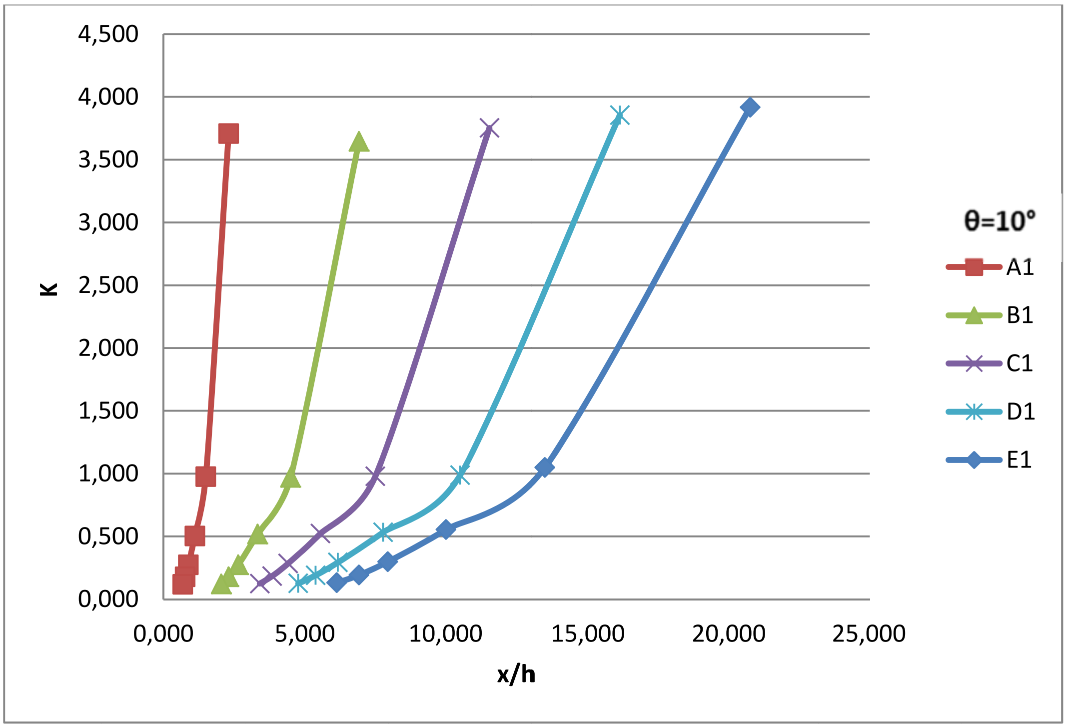

Figure 4.88: K versus x/h for D=1 cm with different x values at θ=10°

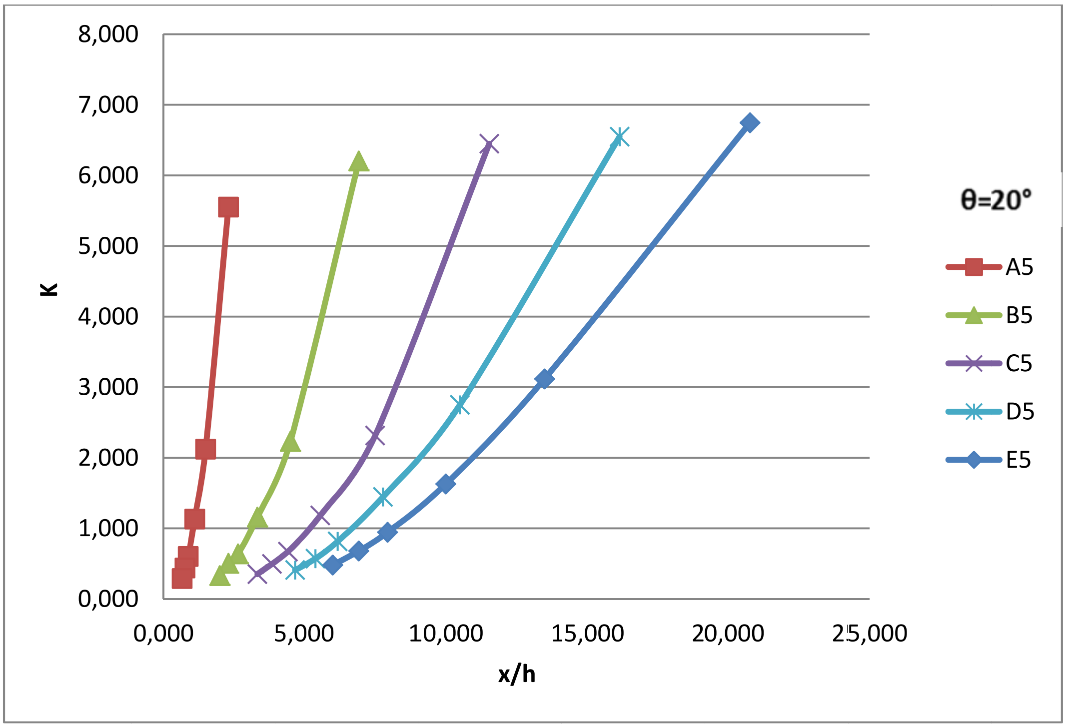

Figure 4.89: K versus x/h for D=4 cm with different x values at θ=20°

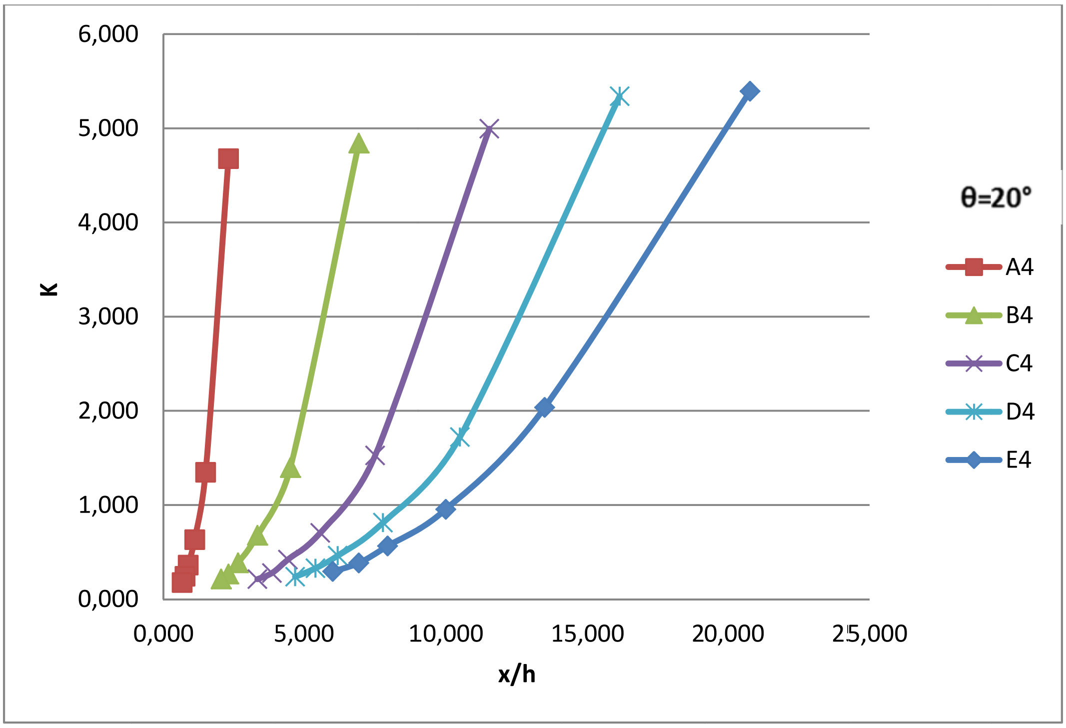

Figure 4.90: K versus x/h for D=3 cm with different x values at θ=20°

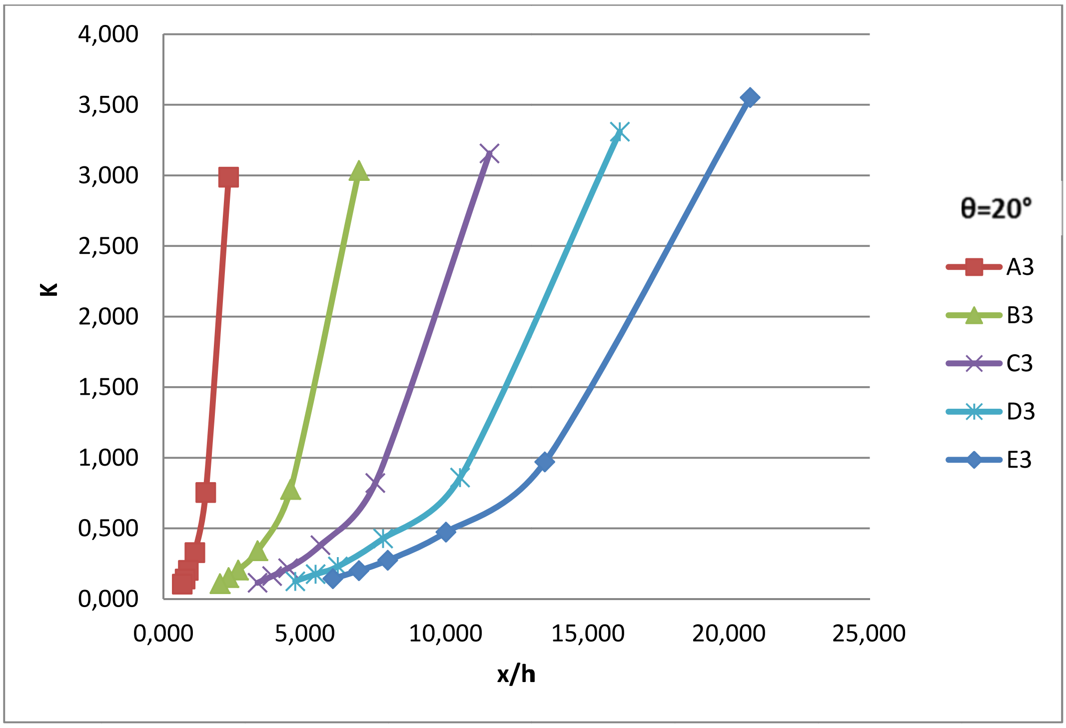

Figure 4.91: K versus x/h for D=2 cm with different x values at θ=20°

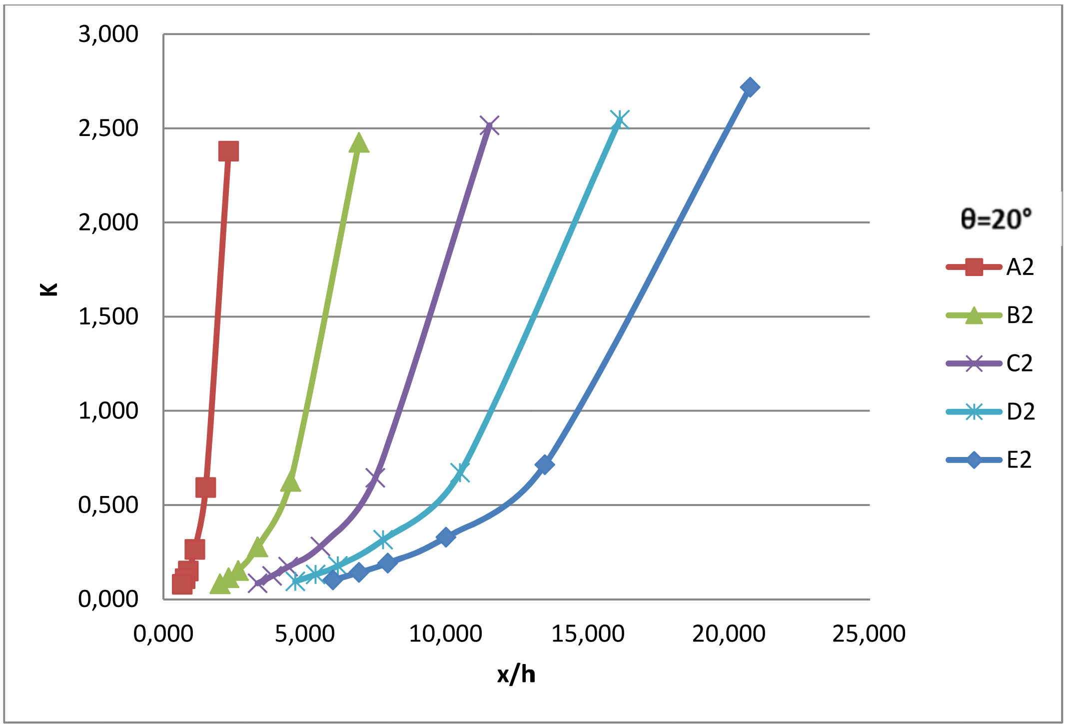

Figure 4.92: K versus x/h for D=1.5 cm with different x values at θ=20°

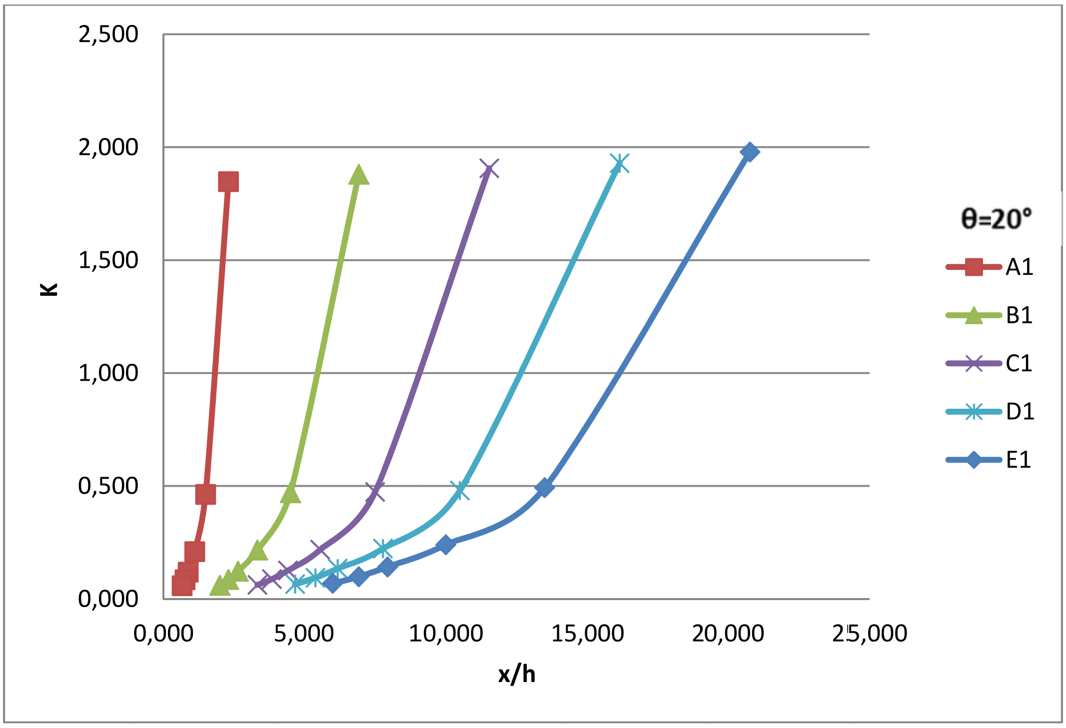

Figure 4.93: K versus x/h for D=1 cm with different x values at θ=20°

Figures 4.94-4.98 present the data of K and Fr for the orifices of varying diameters located at a fixed location on the bottom intake screens of θ=0°. All these figures show that at small Fr values, K values are large and decreases as Fr increase for an orifice of constant diameter. The variation of K with increasing Fr gets smaller as Fr gets larger. For a given Fr, the value of K increases as the diameter of the orifice increases.

Figures 4.99-4.103 show the variation of K with Fr for the orifices of the same diameters located at various locations on the bottom intake screen of θ=0°. In all these figures, it is seen that K values of an orifice of given diameter and location decrease with increasing Fr. For the Froude numbers less than about 0.4, K values vary with the location of the orifices for a given value of Fr. On the other hand, for the Froude numbers larger than about 0.4, all the data of K for the orifices of the same diameter but located at various locations collapse almost on the same curve. As the orifice diameter gets smaller, almost all of the K data of the orifices of the same diameter become independent of the location of the orifice.

Figures 4.104-4.113 and Figures 4.114-4.123 present the variation of K with Fr for all of the orifices tested with the bottom intake screens of θ=10° and θ=20°, respectively. Except the slopes of the screens, the general trends of all K data are very similar to those of screens having the bottom slope of θ=0°.

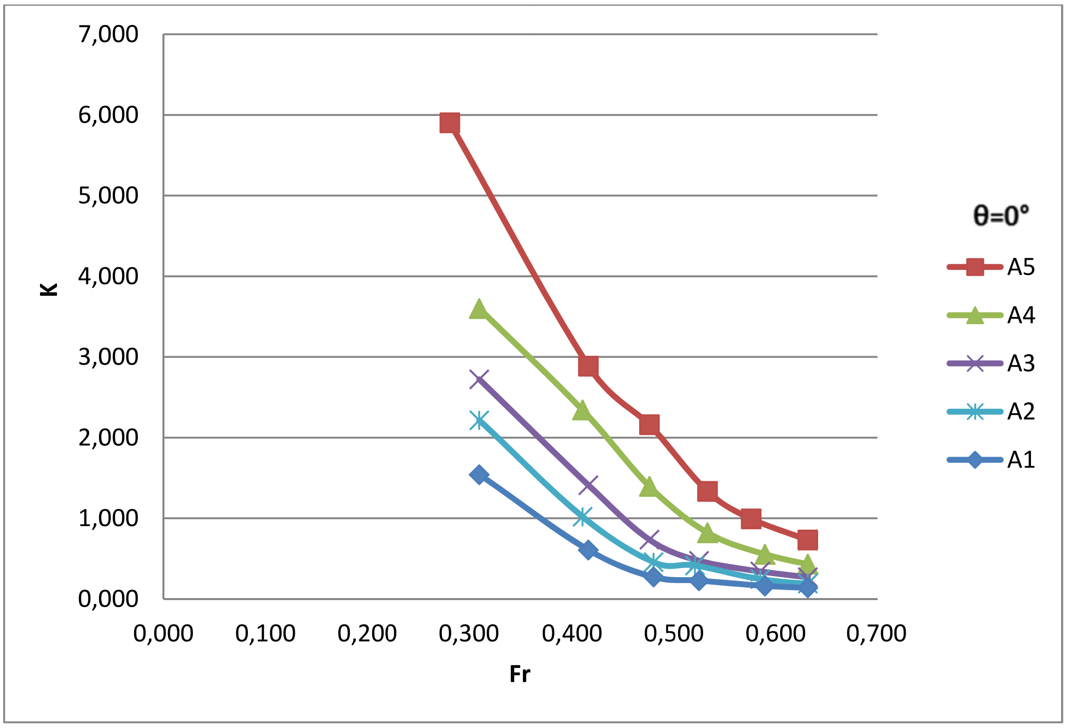

Figure 4.94: K versus Fr for the orifice A with different D values at θ=0°

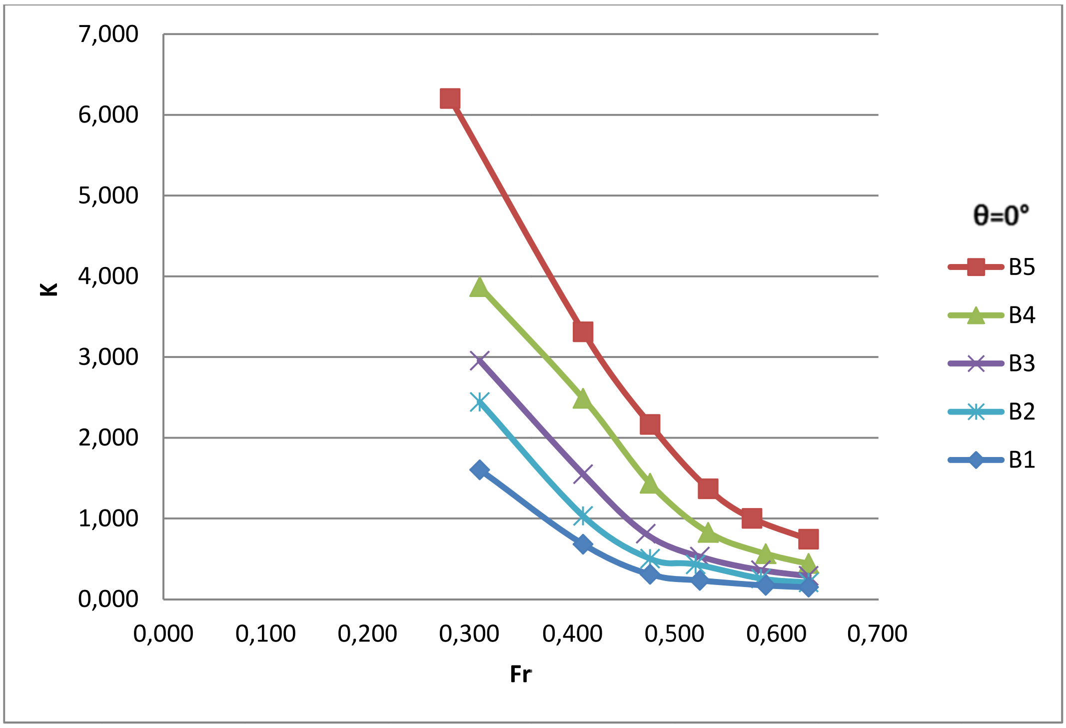

Figure 4.95: K versus Fr for the orifice B with different D values at θ=0°

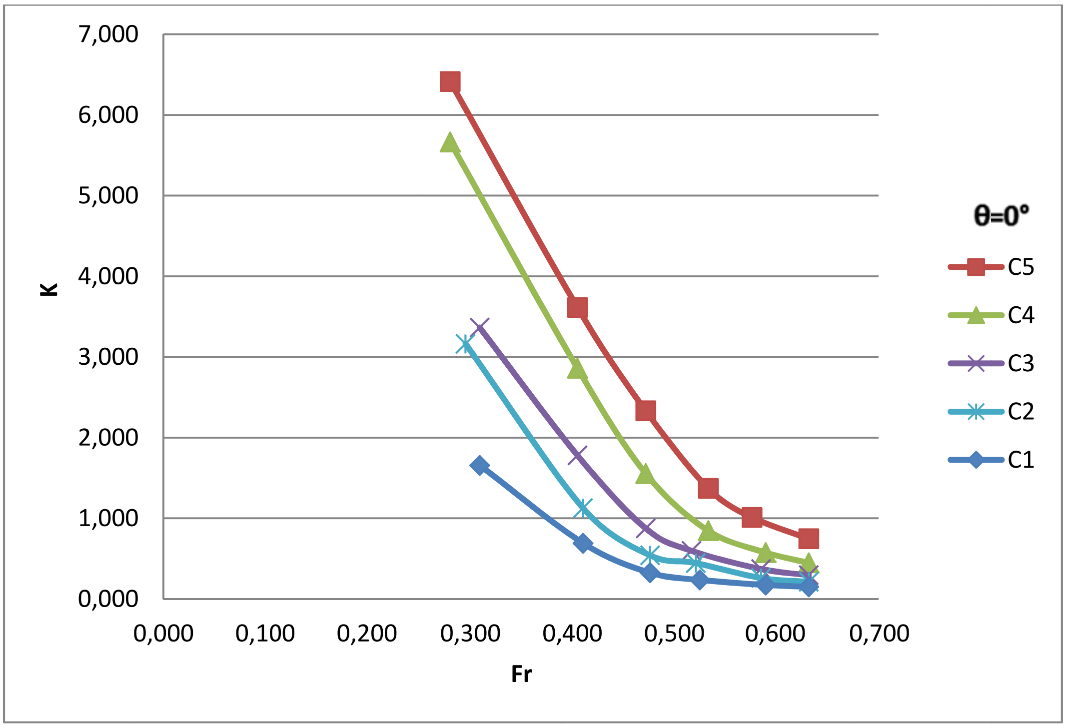

Figure 4.96: K versus Fr for the orifice C with different D values at θ=0°

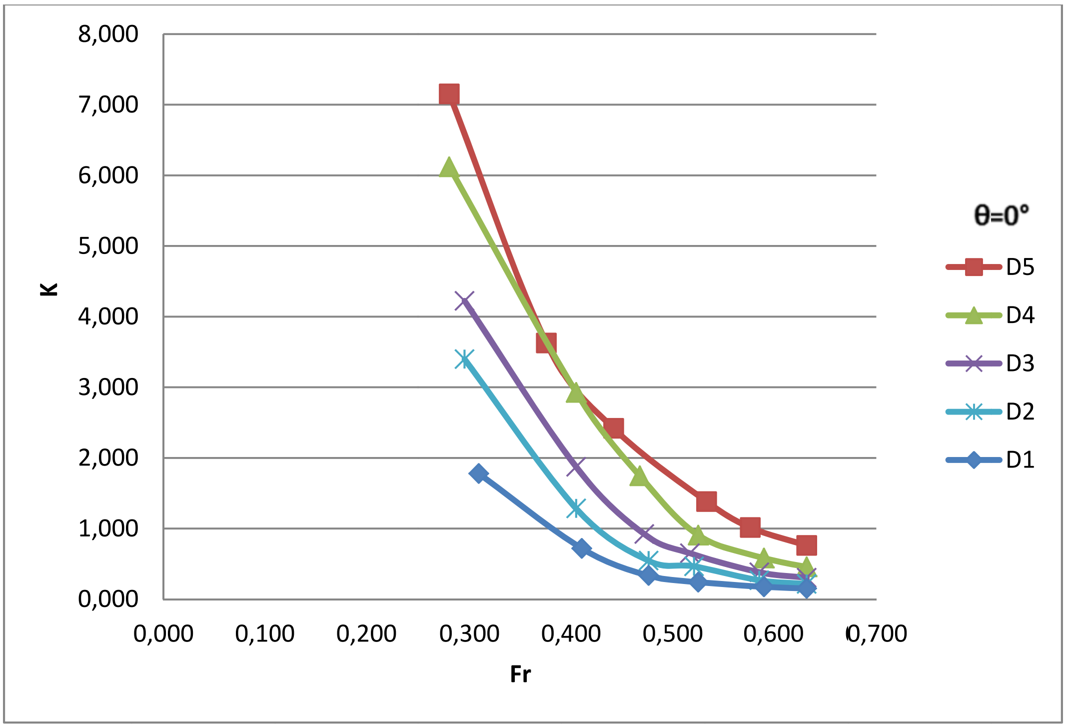

Figure 4.97: K versus Fr for the orifice D with different D values at θ=0°

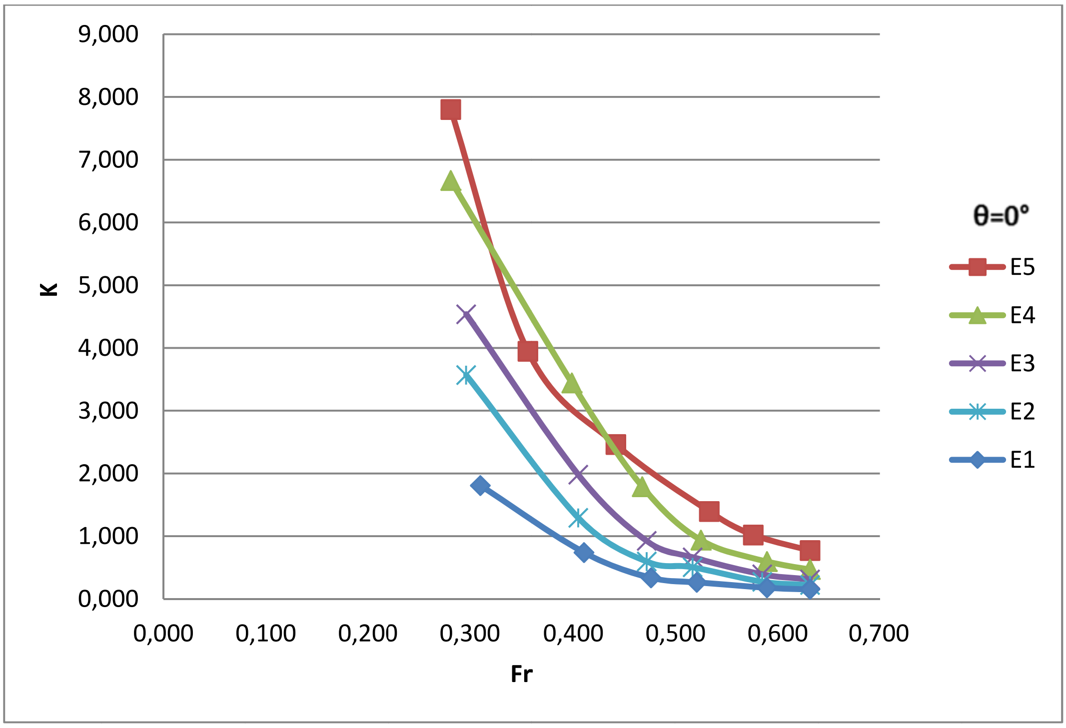

Figure 4.98: K versus Fr for the orifice E with different D values at θ=0°

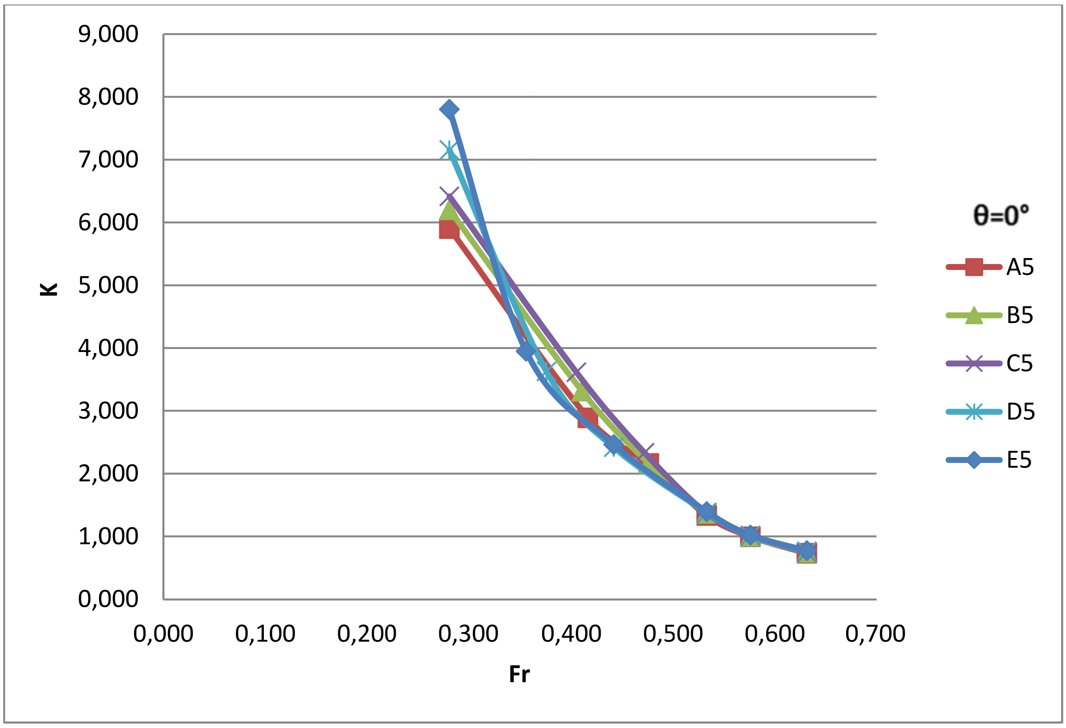

Figure 4.99: K versus Fr for D=4 cm with different x values at θ=0°

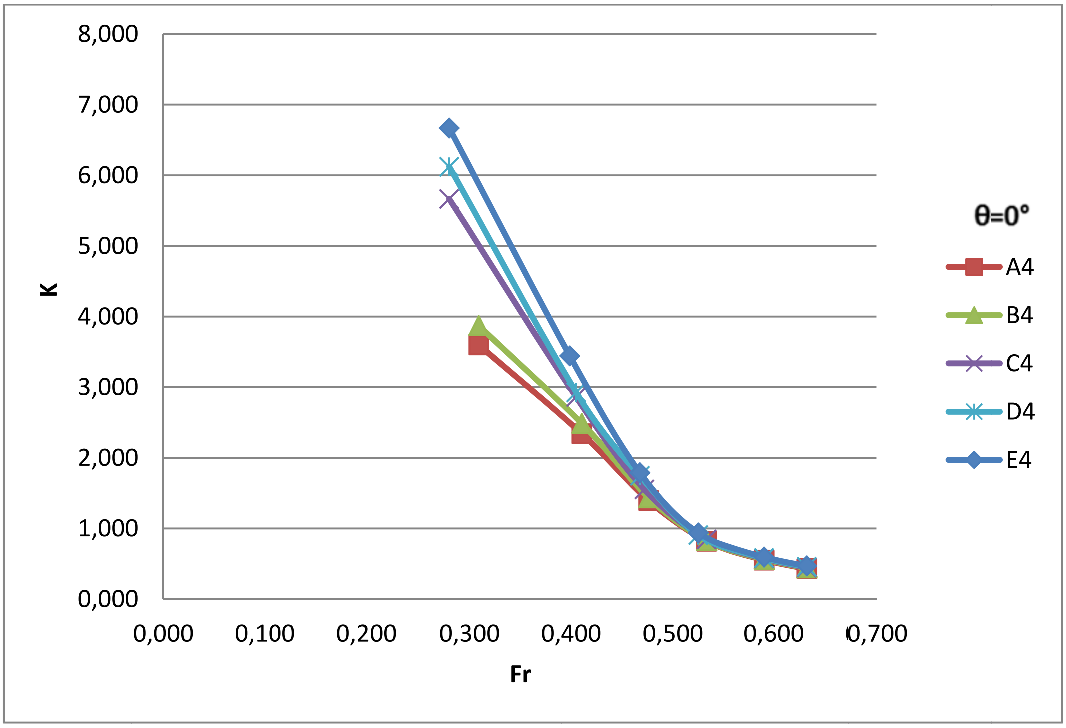

Figure 4.100: K versus Fr for D=3 cm with different x values at θ=0°

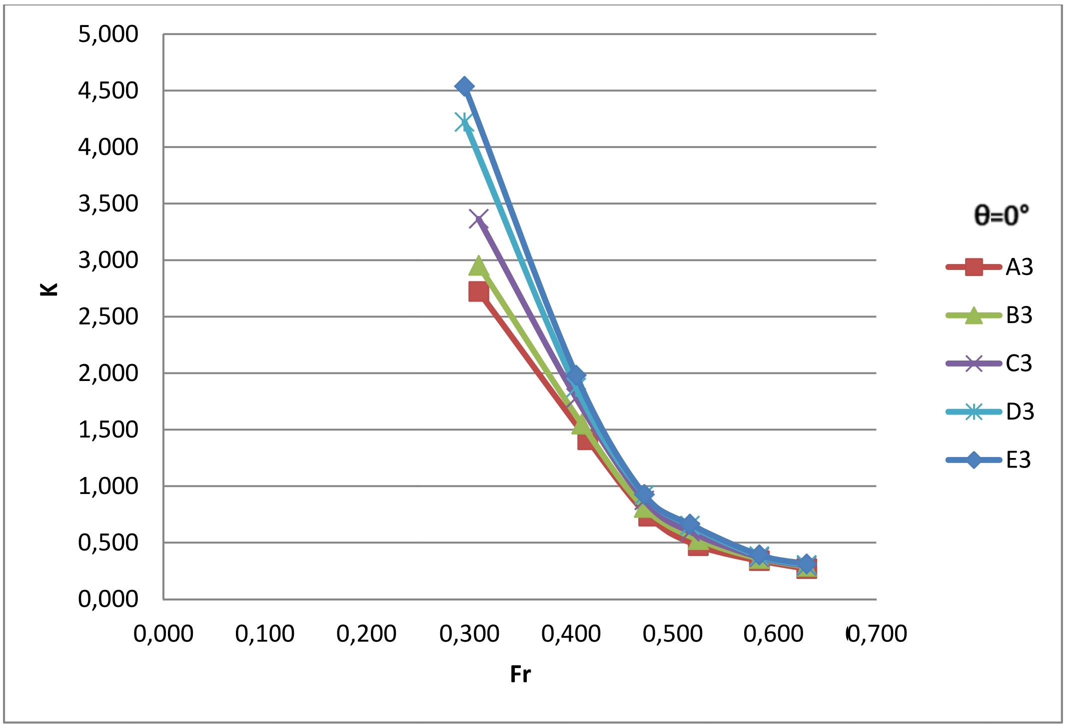

Figure 4.101: K versus Fr for D=2 cm with different x values at θ=0°

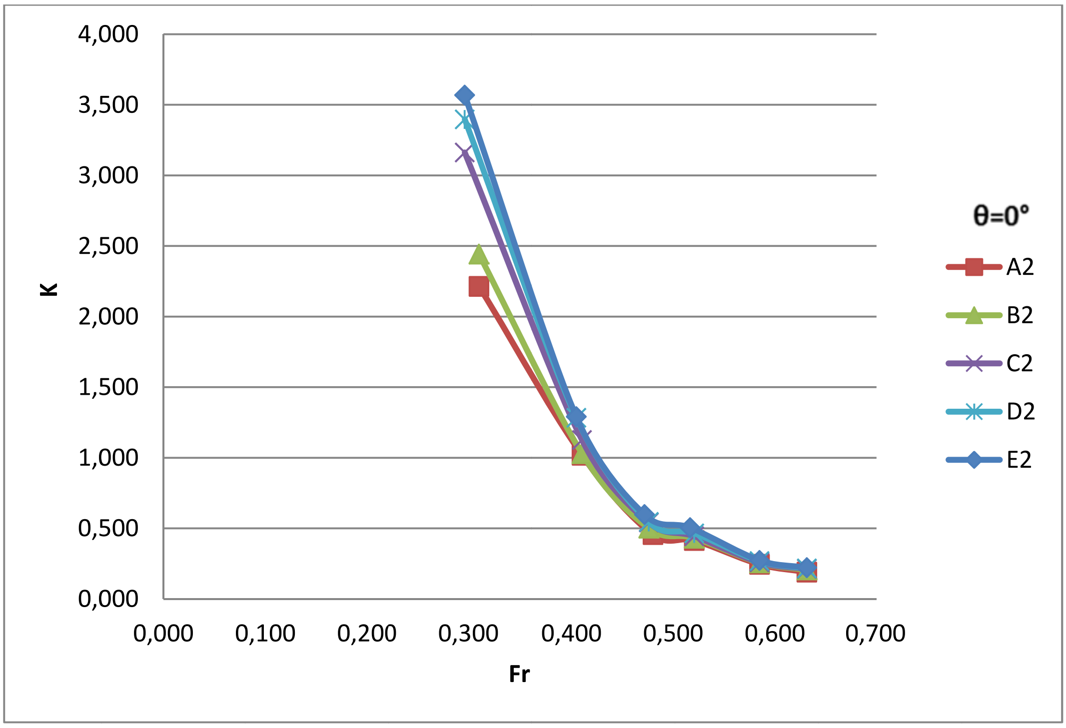

Figure 4.102: K versus Fr for D=1.5 cm with different x values at θ=0°

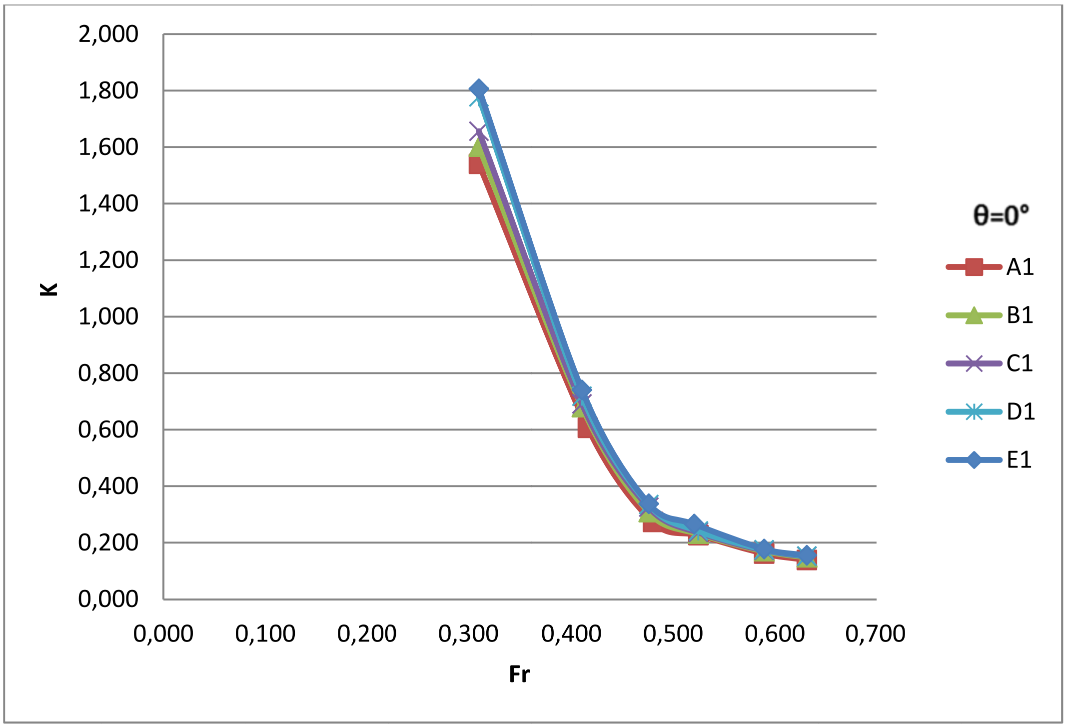

Figure 4.103: K versus Fr for D=1 cm with different x values at θ=0°

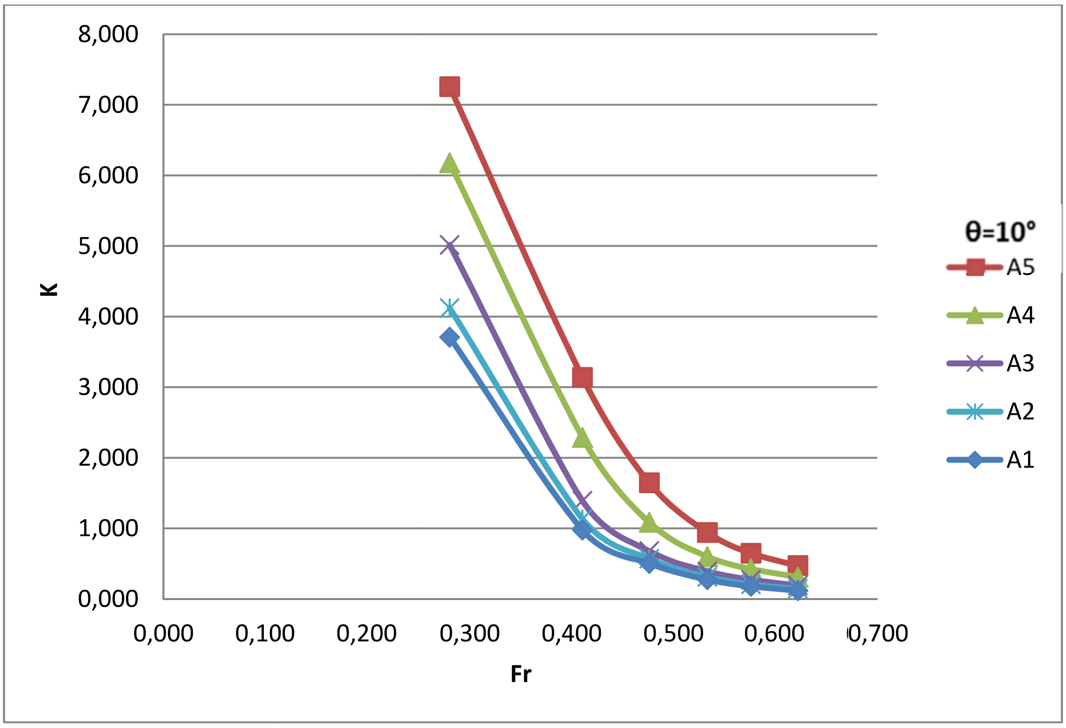

Figure 4.104: K versus Fr for the orifice A with different D values at θ=10°

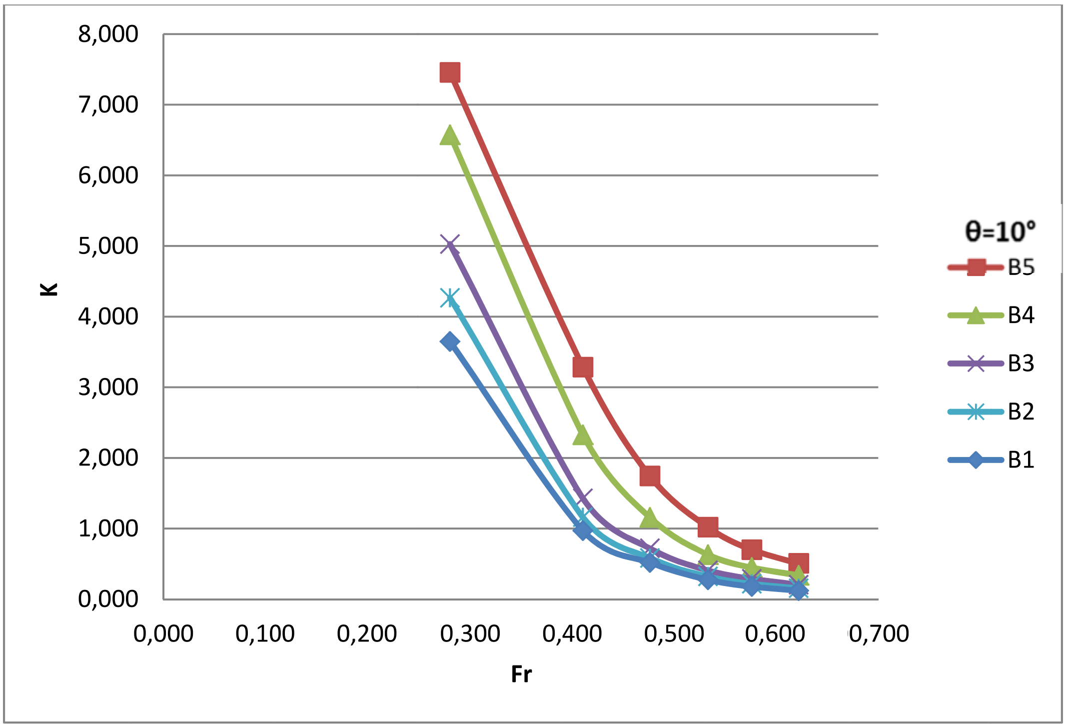

Figure 4.105: K versus Fr for the orifice B with different D values at θ=10°

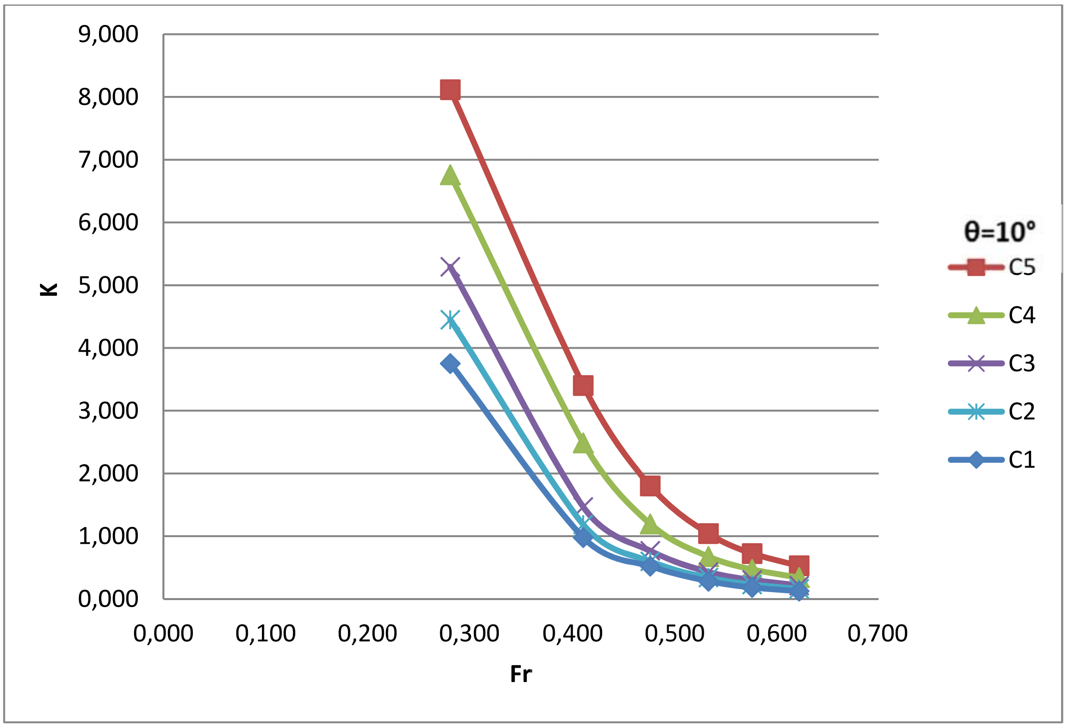

Figure 4.106: K versus Fr for the orifice C with different D values at θ=10°

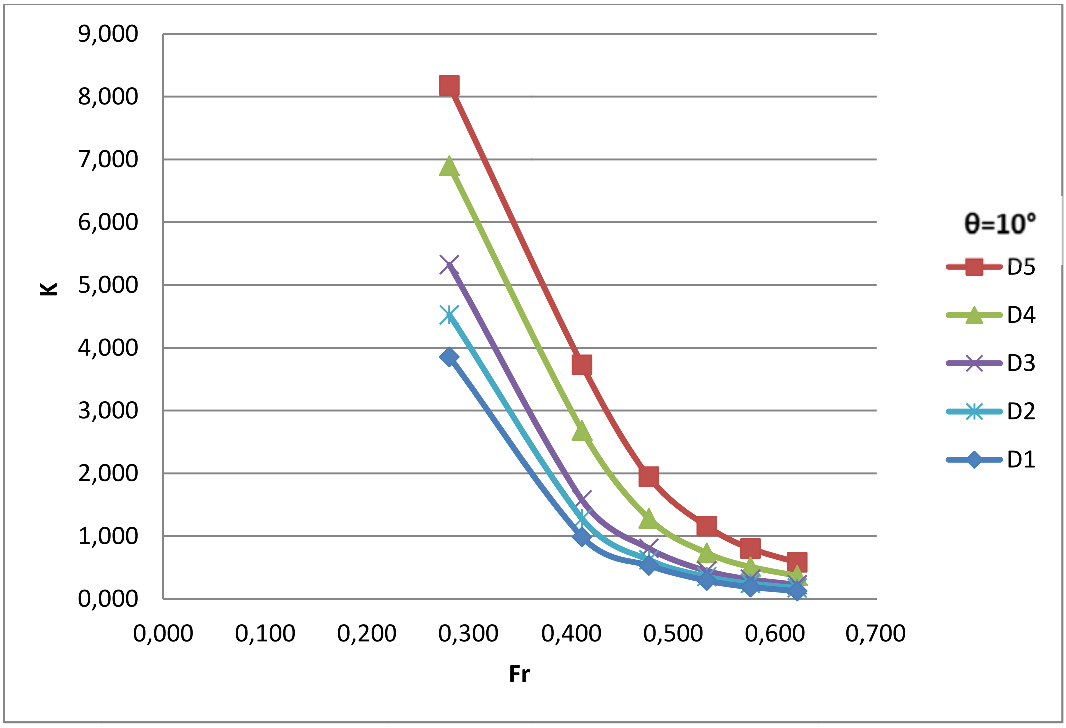

Figure 4.107: K versus Fr for the orifice D with different D values at θ=10°

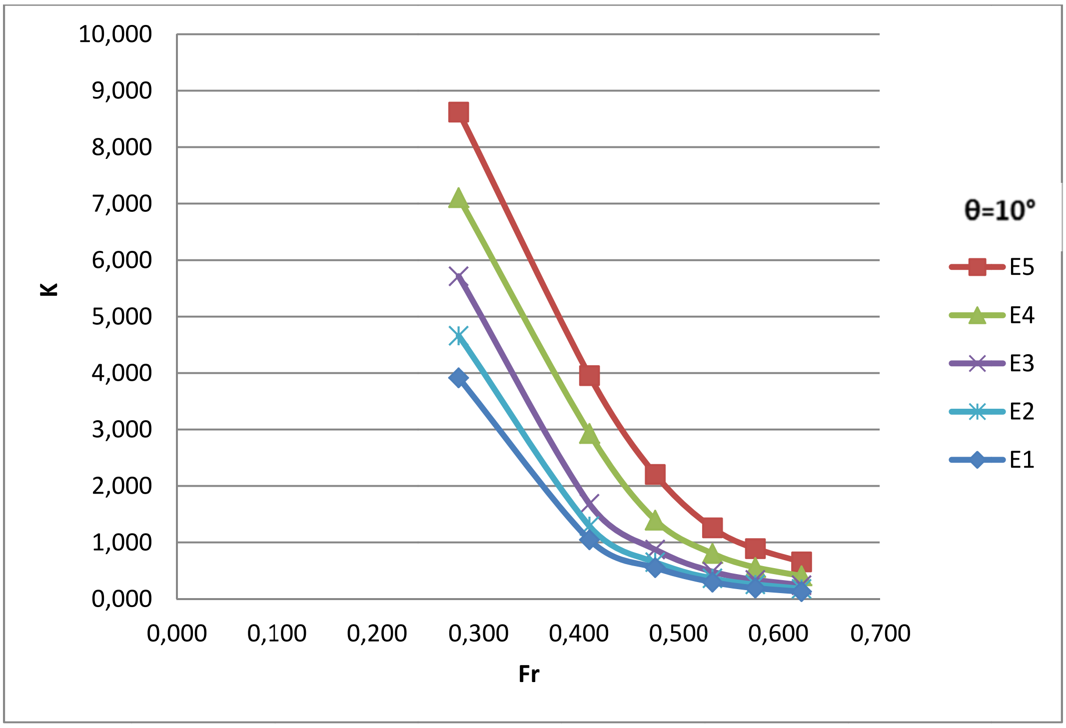

Figure 4.108: K versus Fr for the orifice E with different D values at θ=10°

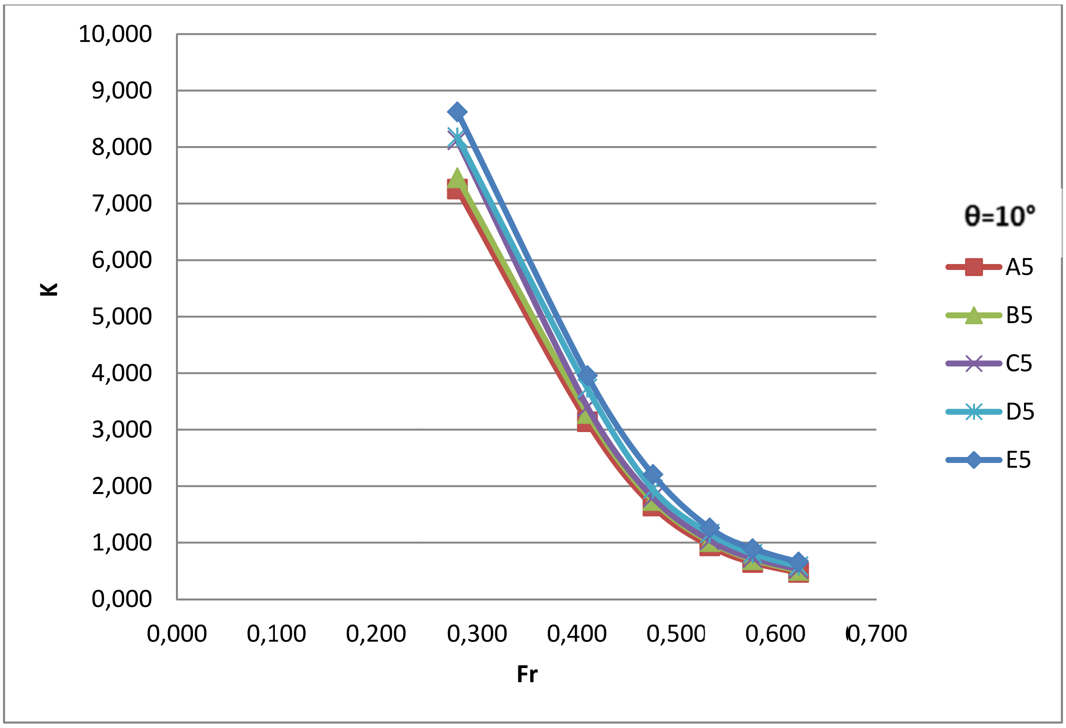

Figure 4.109: K versus Fr for D=4 cm with different x values at θ=10°

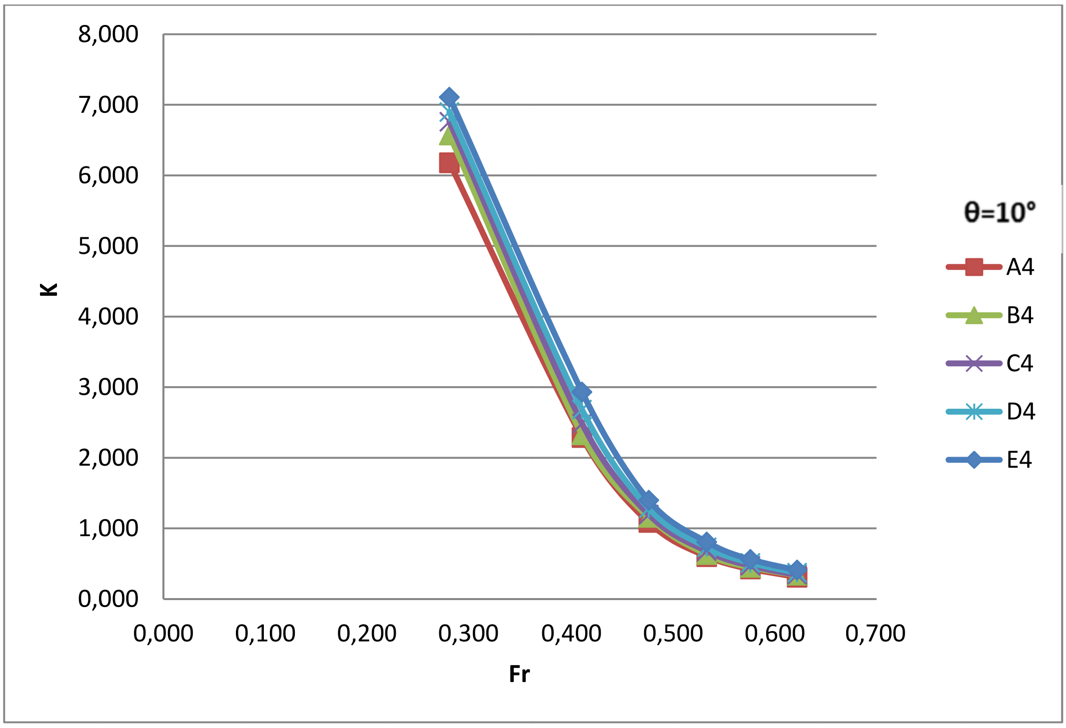

Figure 4.110: K versus Fr for D=3 cm with different x values at θ=10°

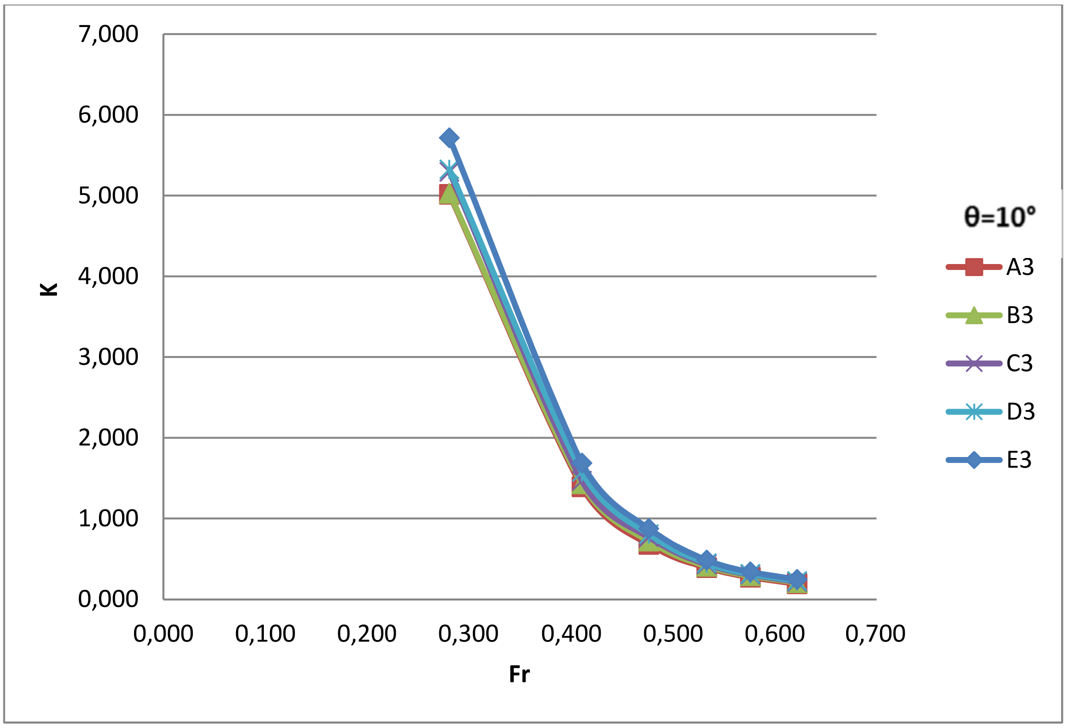

Figure 4.111: K versus Fr for D=2 cm with different x values at θ=10°

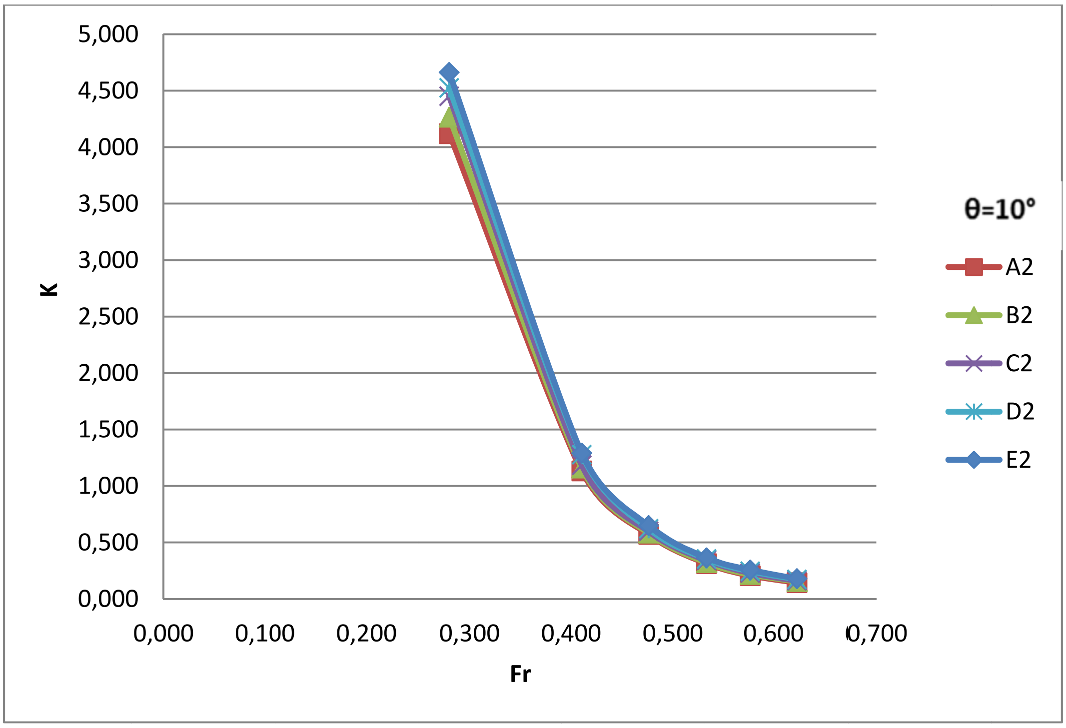

Figure 4.112: K versus Fr for D=1.5 cm with different x values at θ=10°

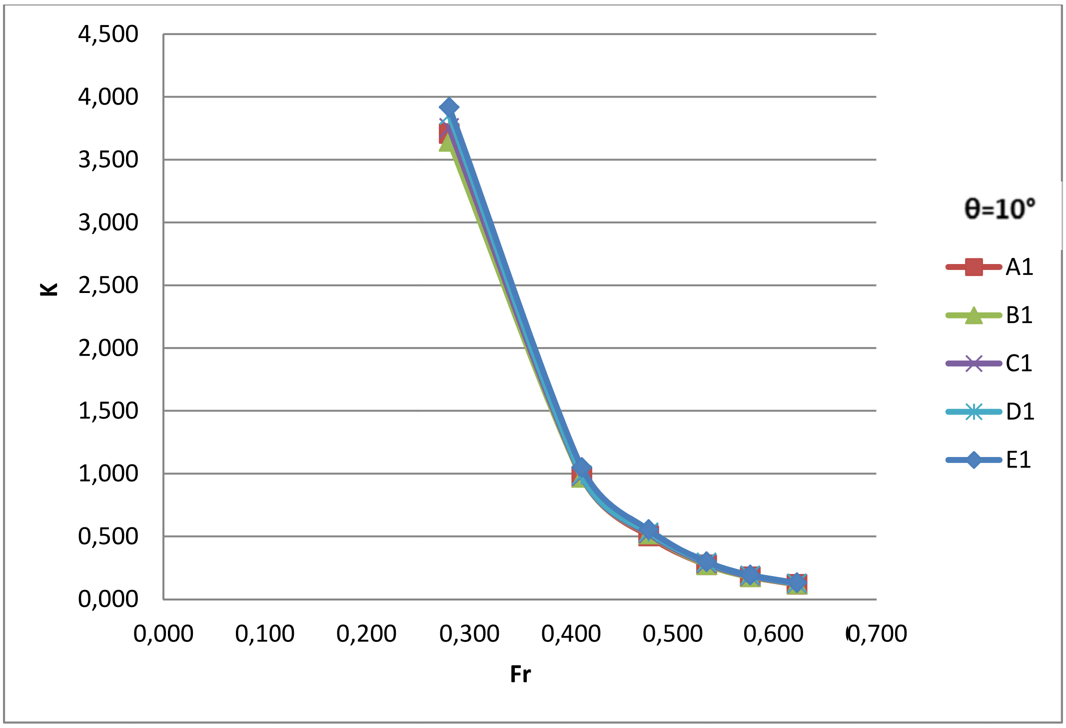

Figure 4.113: K versus Fr for D=1 cm with different x values at θ=10°

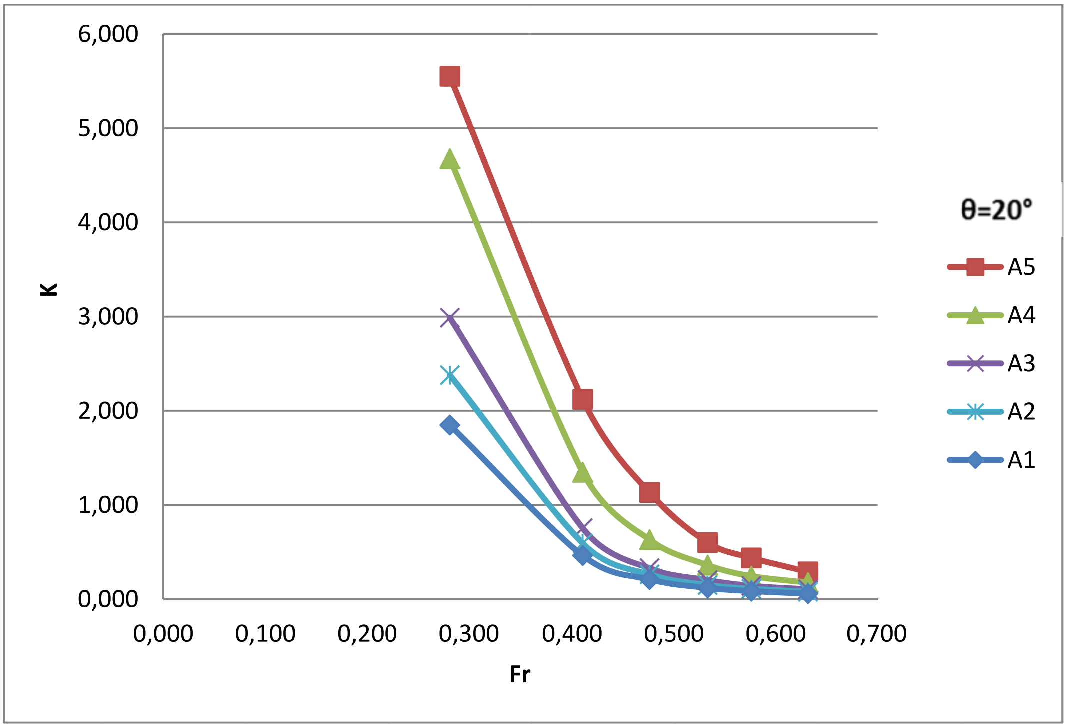

Figure 4.114: K versus Fr for the orifice A with different D values at θ=20°

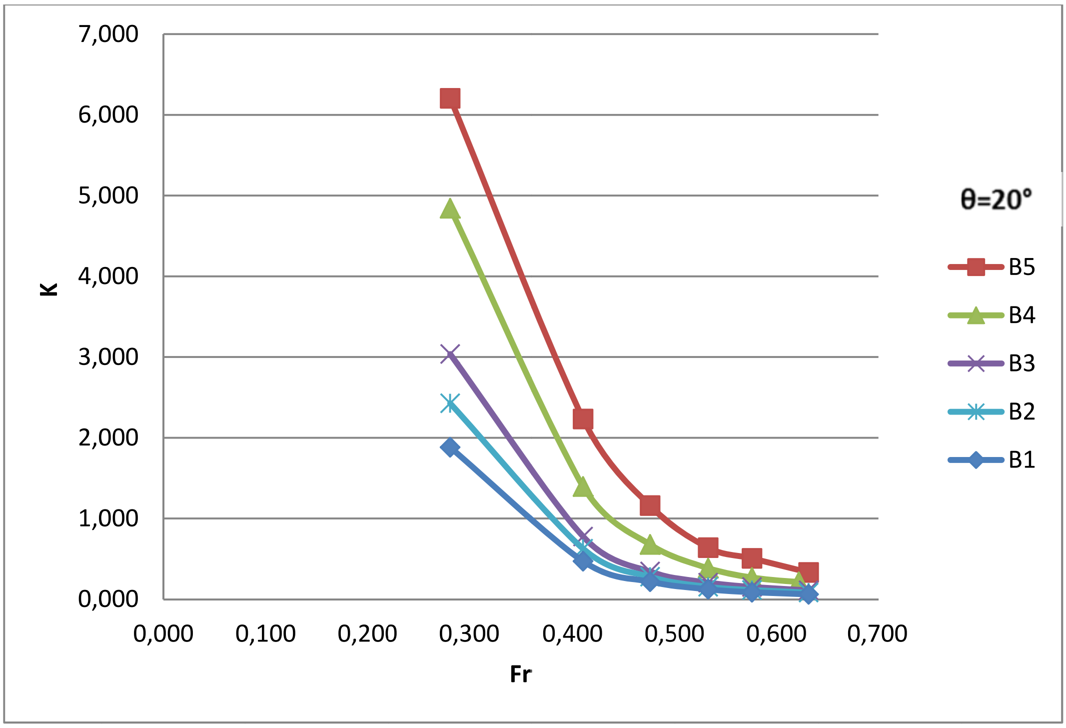

Figure 4.115: K versus Fr for the orifice B with different D values at θ=20°

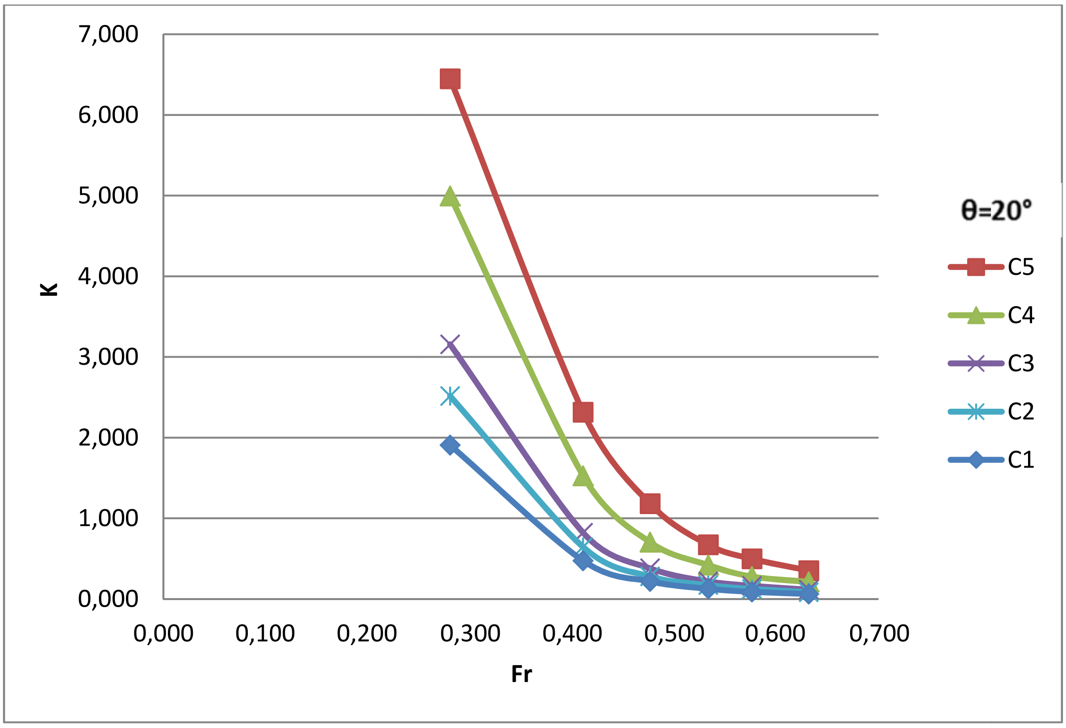

Figure 4.116: K versus Fr for the orifice C with different D values at θ=20°

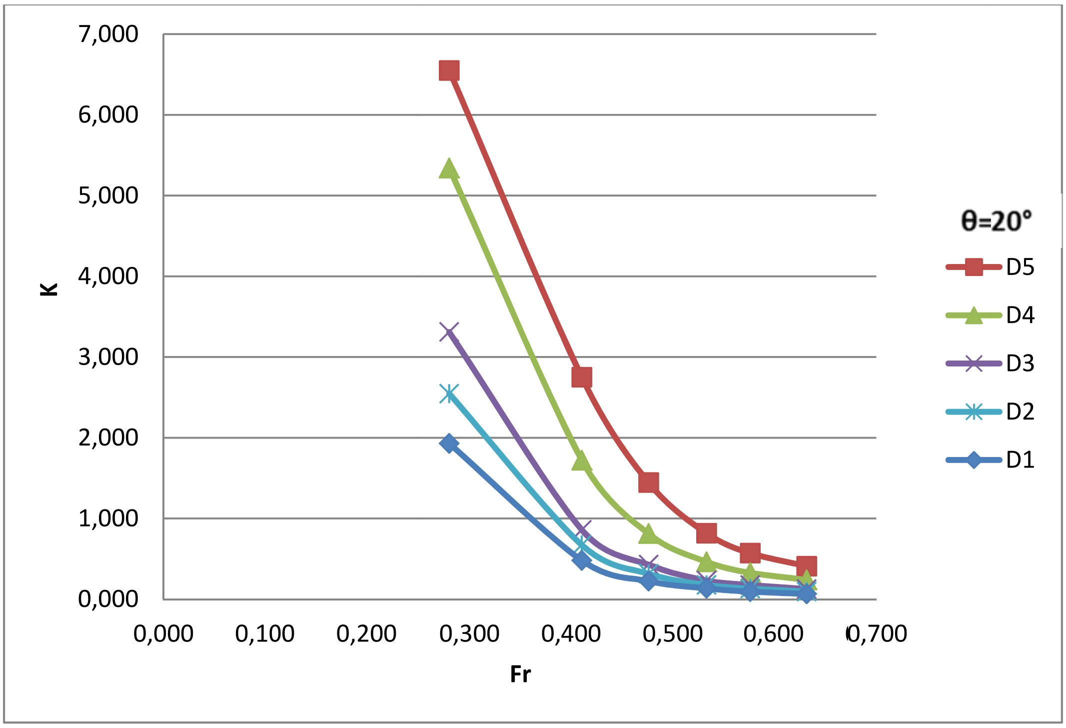

Figure 4.117: K versus Fr for the orifice D with different D values at θ=20°

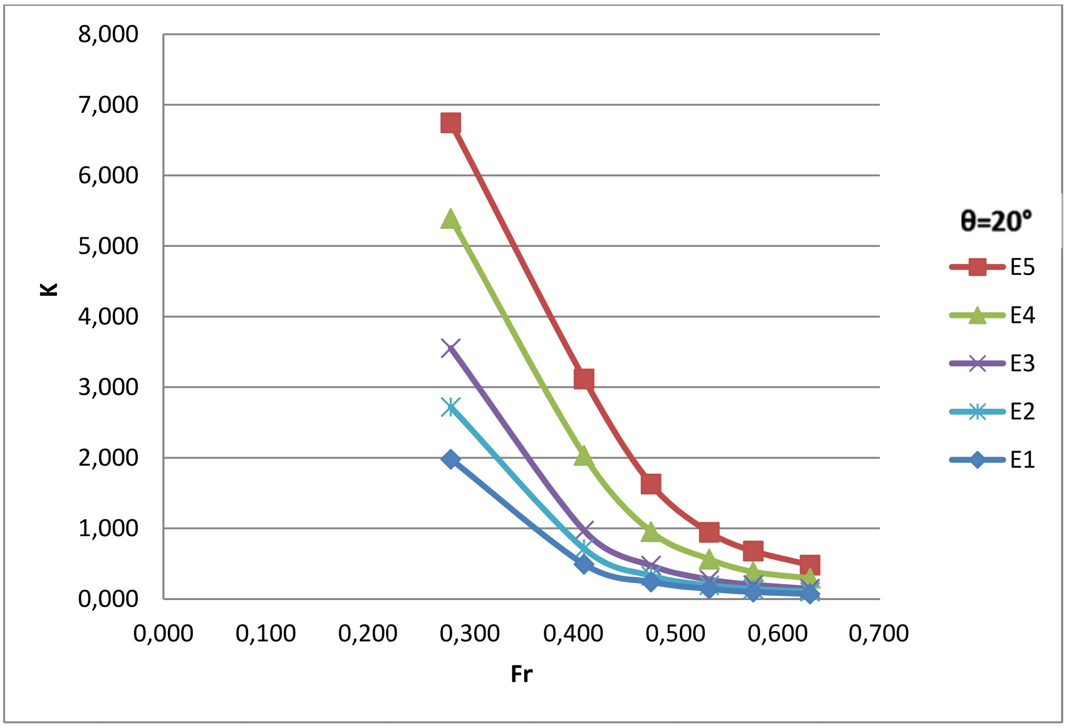

Figure 4.118: K versus Fr for the orifice E with different D values at θ=20°

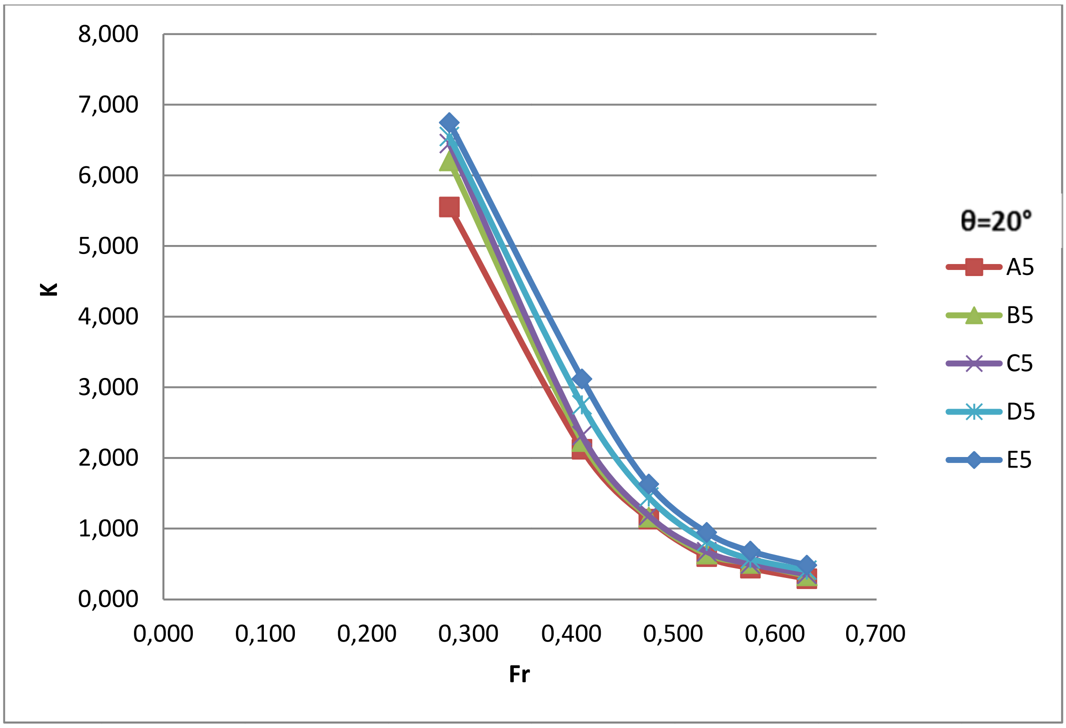

Figure 4.119: K versus Fr for D=4 cm with different x values at θ=20°

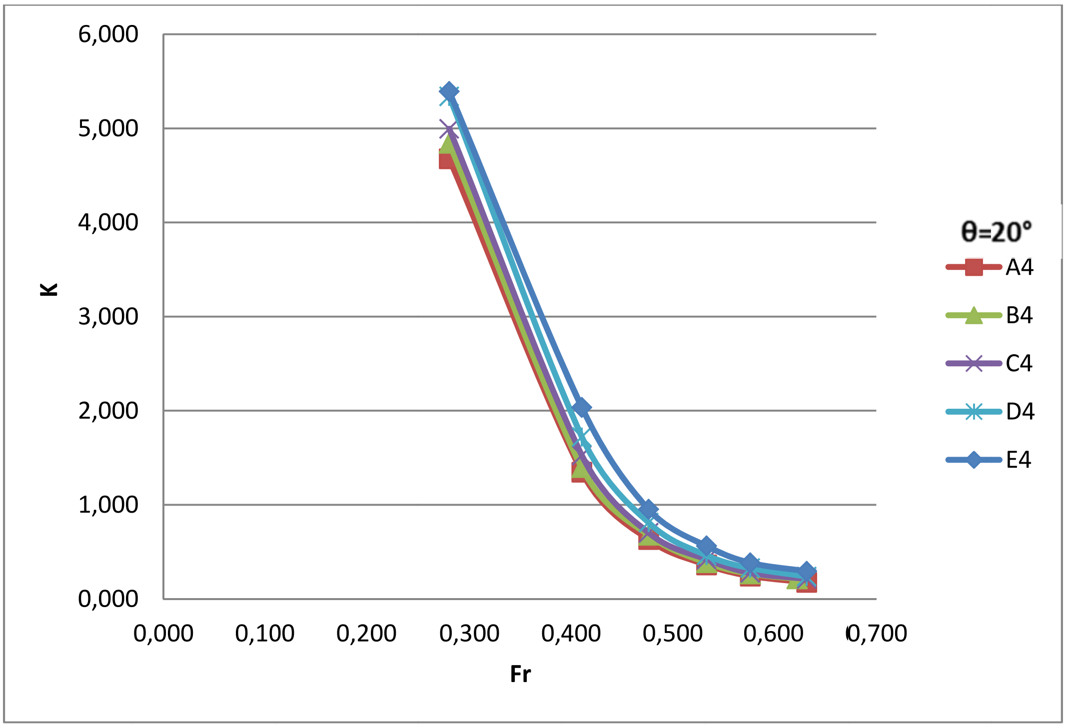

Figure 4.120: K versus Fr for D=3 cm with different x values at θ=20°

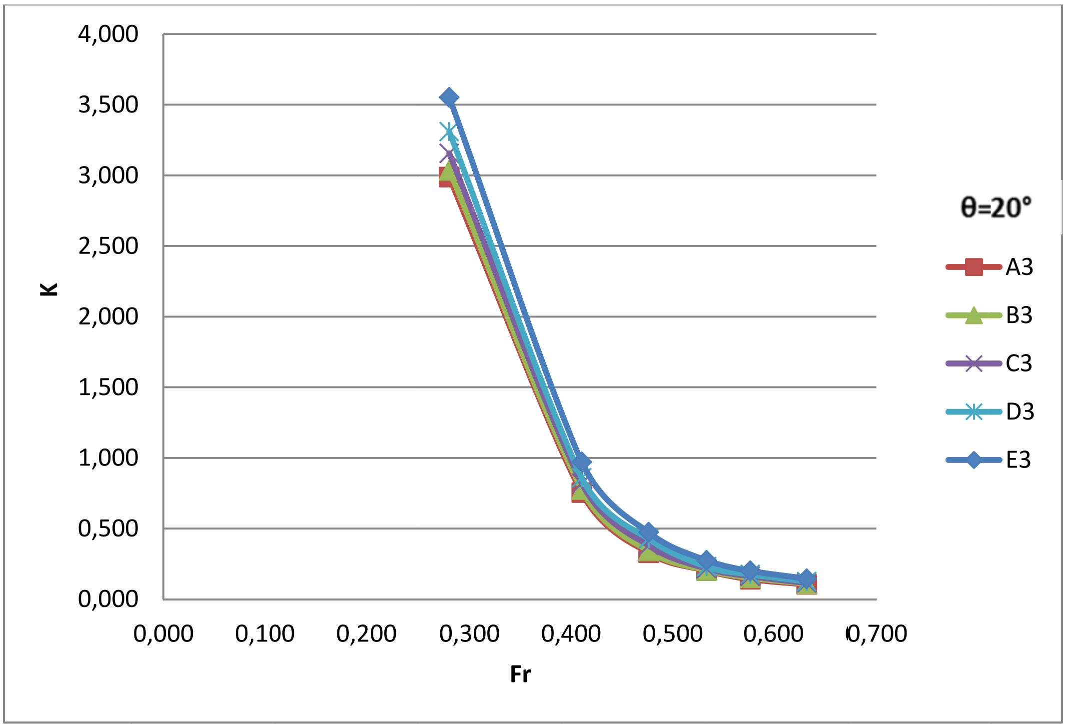

Figure 4.121: K versus Fr for D=2 cm with different x values at θ=20°

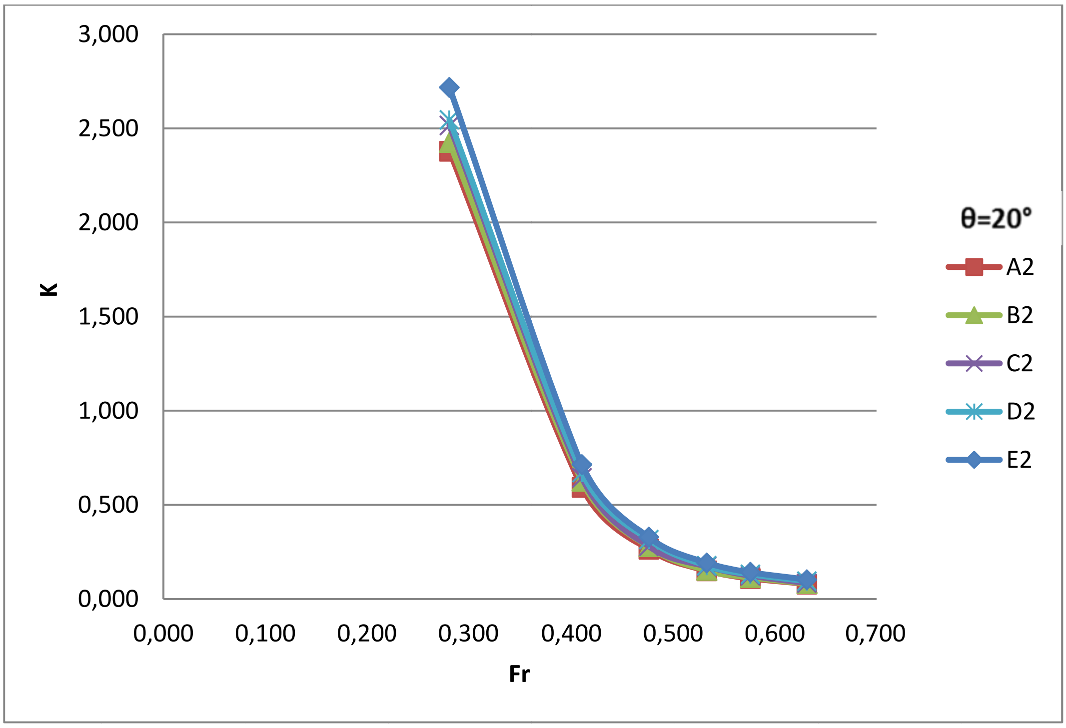

Figure 4.122: K versus Fr for D=1.5 cm with different x values at θ=20°

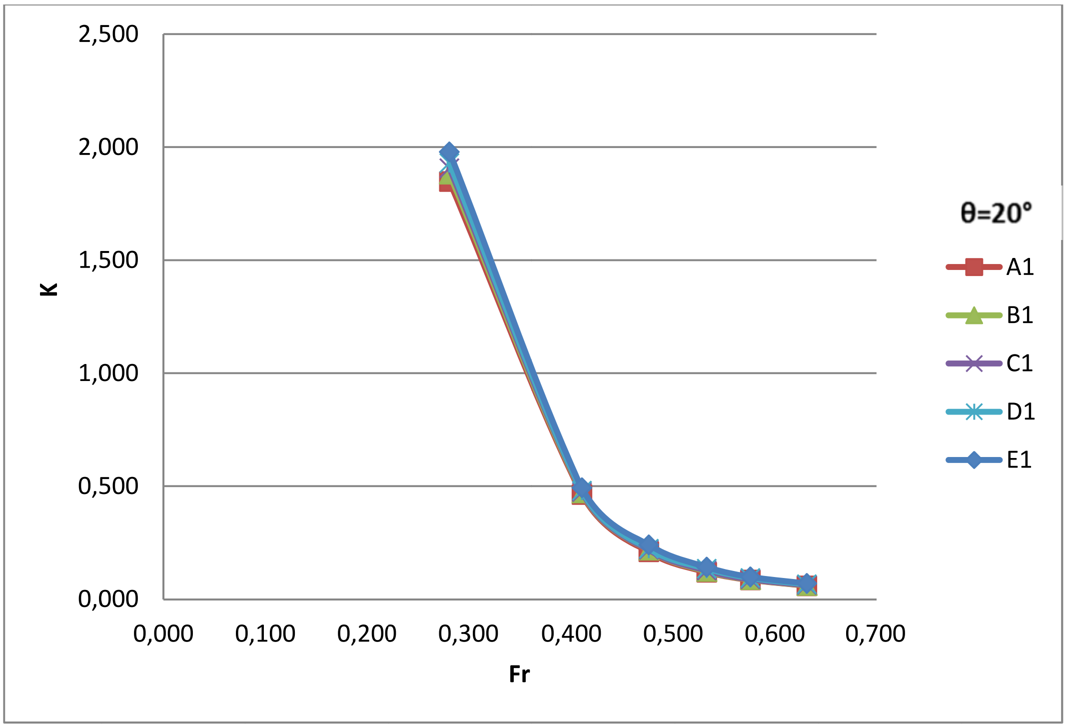

Figure 4.123: K versus Fr for D=1 cm with different x values at θ=20°

From the analysis of Figures 4.64-4.123, it can be stated that the value of K for a given orifice type, in general, decreases as the slope of the screen increases under the same upstream flow conditions that is for the same D/h, x/h and Fr.

4.2.4 Empirical Relationship between K and Related Parameters with respect to Screen Slopes

In order to derive an empirical equation for K as a function of D/h, x/h and Fr, regression analysis was applied to the available related data and the following equations were determined.

At θ=0°,

$$K = 0.419\left(\frac{D}{h}\right)^{1.176}\left(\frac{x}{h}\right)^{0.079}(Fr)^{-1.253} \qquad \text{...(4.4)}$$

with a correlation coefficient of R^2=0.987.

K values obtained from measurements and calculated from Equation 4.4 are presented in Figure 4.124. This figure shows that all the data lies between ± 30% error lines.

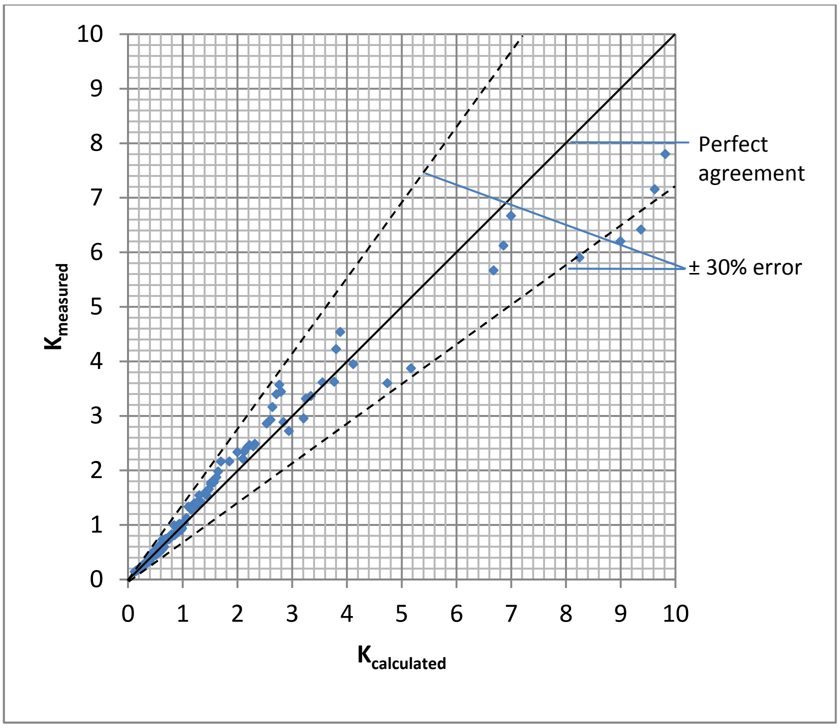

Figure 4. 124: Comparison of measured and calculated K values at θ=0°

At θ=10°,

$$K = 0.161(\frac{D}{h})^{0.928}(\frac{x}{h})^{0.088}(Fr)^{-2.352} \quad \text{………………..……………………………….(4.5)}$$

With a correlation coefficient of R^2=0.983.

K values obtained from measurements and calculated from Equation 4.5 are presented in Figure 4.125. This figure shows that all the data lies between ± 30% error lines.

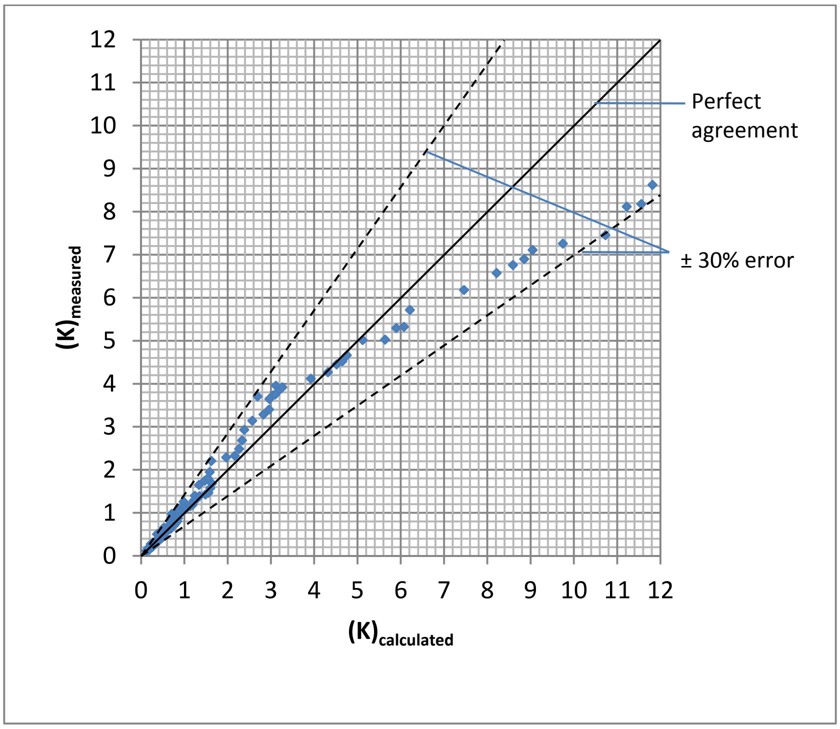

Figure 4. 125: Comparison of measured and calculated K values at θ=10°

At θ=20°,

$$K = 0.129(\frac{D}{h})^{1.205}(\frac{x}{h})^{0.117}(Fr)^{-1.970} \quad \text{………………..……………………………….(4.6)}$$

with a correlation coefficient of R^2= 0.896.

K values obtained from measurements and calculated from Equation 4.6 are presented in Figure 4.126. These figures show that all the data lies between ± 30% error lines.

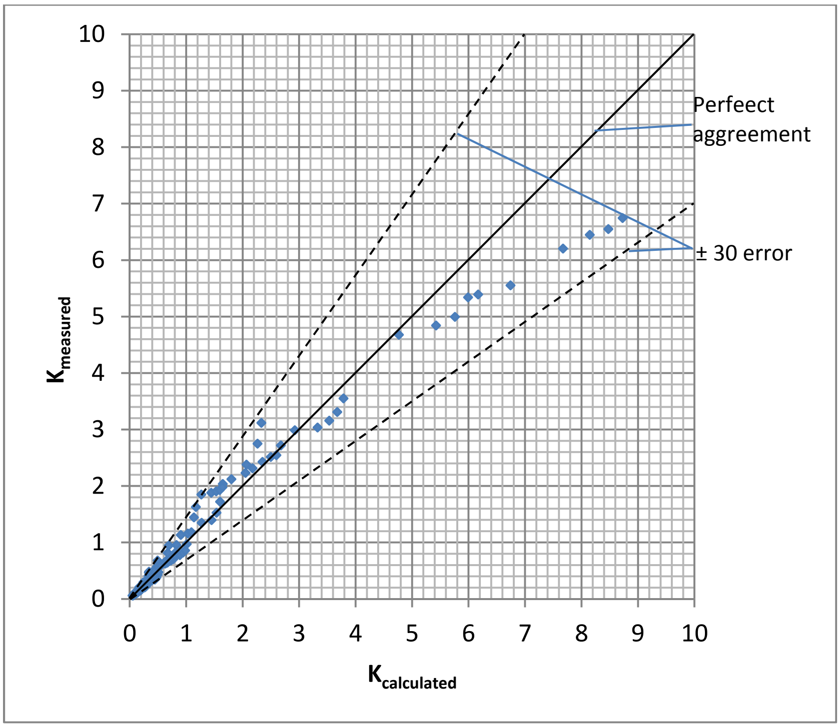

Figure 4. 126: Comparison of measured and calculated K values at θ=20°

4.3 Studies related to the Multiple Bottom Intake Orifices on the Screen

In this section, the results of the experimental studies carried out on the multiple circular bottom intake orifices located along the centerline of the screen at different diameters and slopes are presented. The maximum number of the circular bottom intake orifices with the same diameters located on the screen for each set of the experiments is 5. During experiments, all of the 5 orifices having the same diameter were kept open. In these series of experiments, only those orifices having the diameters of 1 cm, 1.5 cm and 2 cm were tested due to the limited discharge capacity of the model used in this study. Therefore, only the data of aforementioned orifices were presented in the following figures as a function of the related dimensionless parameters.

4.3.1 Relationship between Discharge Coefficient C_D and the Related Dimensionless Parameters for Multiple Circular Bottom Intake Orifices on the Screen

The relationship between C_D and the relevant dimensionless parameters are given by Equation 2.10.

Figures 4.127-4.129 show variation of C_D with the dimensionless variable D/h for the circular bottom intake orifices having the orifice diameters of 1 cm, 1.5 cm and 2 cm at screen slopes of 0°, 10° and 20°, respectively. In general, in all these figures, the distribution of C_D versus D/h data for each model tested; A1-E1, A2-E2 and A3-E3 are very similar to each other regardless of the screen slope. The model of minimum orifice diameter, A1-E1, always produces maximum C_D values. As the orifice diameter gets larger, C_D values decrease. Except the screen of θ=20°, in the other screens, in general, C_D values decrease with increasing D/h. In the model which has the screen slope of θ=20°, C_D values first increase with increasing D/h and then start decreasing (Figure 4.129). From these figures, it is also observed that as the slope of the screen increases, C_D values of the model of the same orifice diameter get smaller.

The relationship between C_D and Fr is presented in Figures 4.130-4.132 for the multiple circular bottom intake orifices tested. The general trend of the data of the screens of θ=0° and θ=10°, Figure 4.130 and 4.131, are very similar. C_D values first increase with increasing Fr up to certain values and then for larger Fr values, C_D values do not change significantly. For the model of the largest screen slope, θ=20° (Figure 4.132), the variation of C_D with Fr is different for the model of A1-E1; C_D rapidly varies with increasing Fr up to the value of about 0.5, and then the rate of decrease of C_D with increasing Fr decreases. On the other hand, for the other curves, A2-E2 and A3-E3, C_D values increase with increasing Fr up to the value of about 0.45 and then start decreasing with increasing Fr by following a similar trend as the data of the models of A1-E1 and A2-E2.

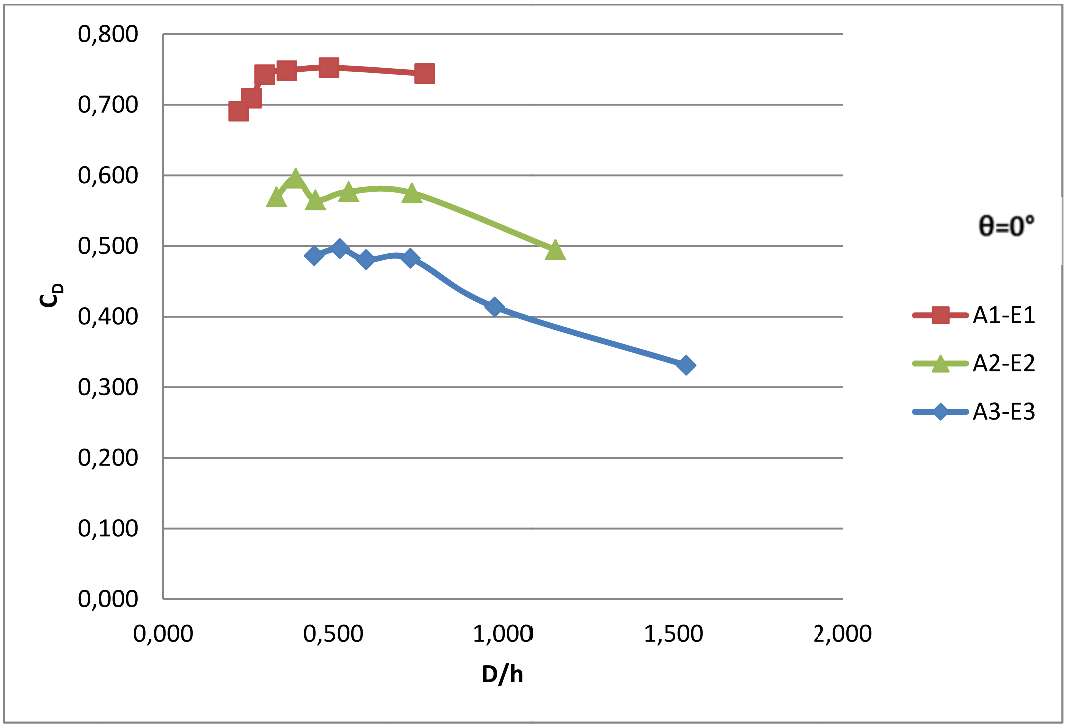

Figure 4.127: Discharge coefficient versus D/h for multiple orifices with different D values at θ=0°

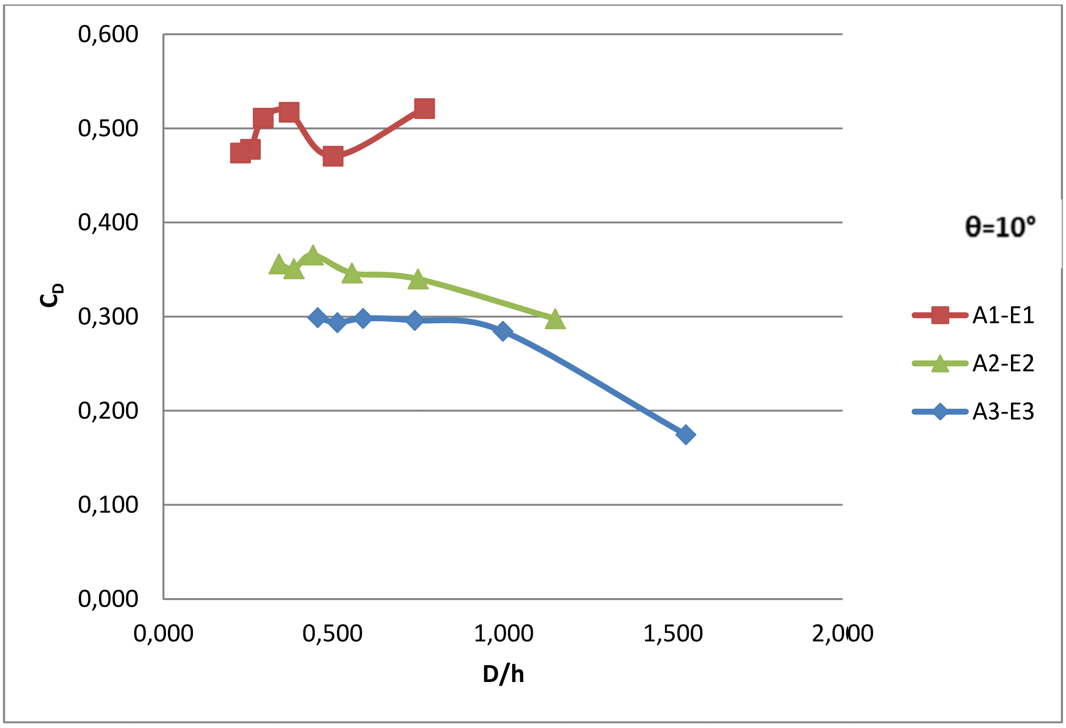

Figure 4.128: Discharge coefficient versus D/h for multiple orifices with different D values at θ=10°

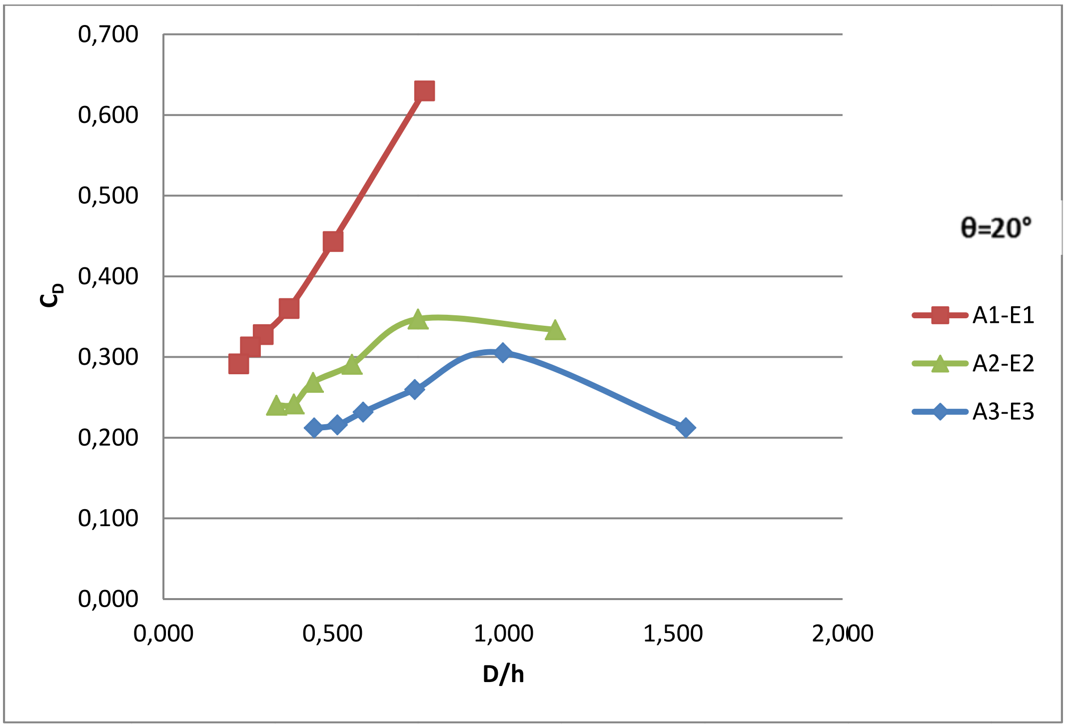

Figure 4.129: Discharge coefficient versus D/h for multiple orifices with different D values at θ=20°

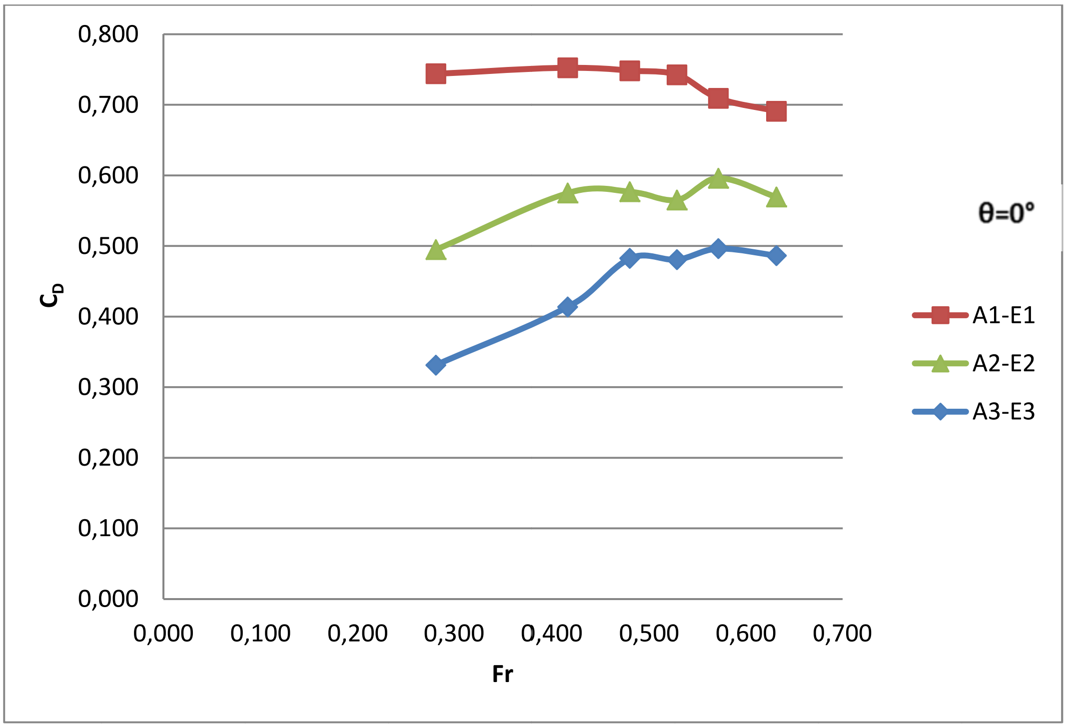

Figure 4.130: Discharge coefficient versus Fr for multiple orifices with different D values at θ=0°

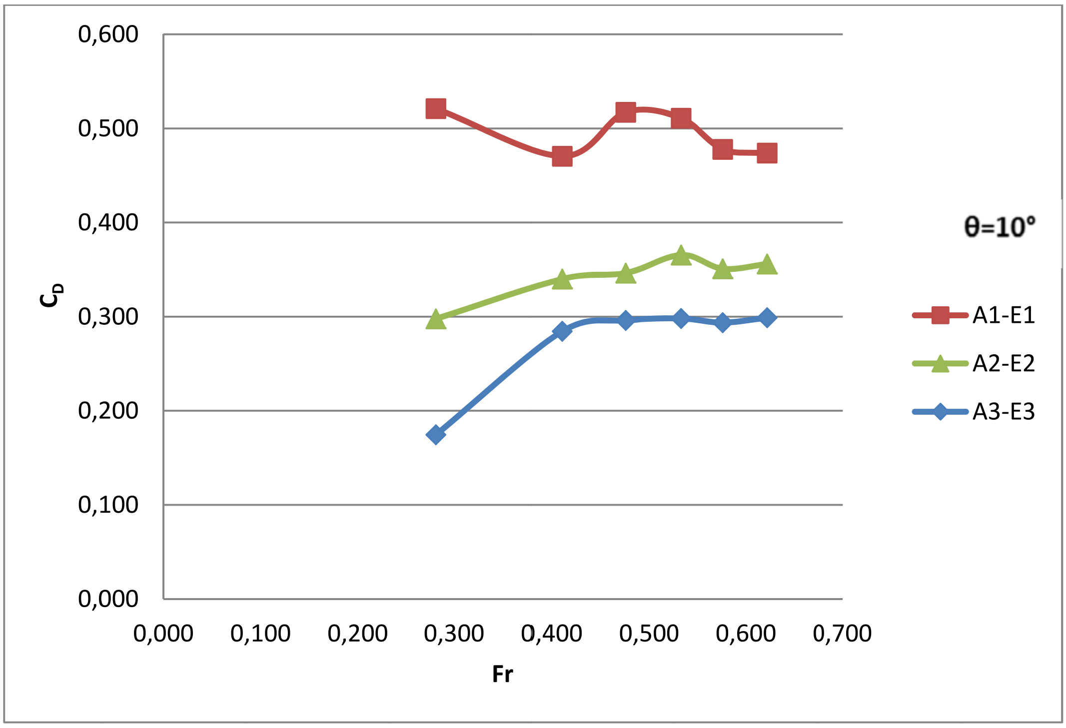

Figure 4.131: Discharge coefficient versus Fr for multiple orifices with different D values at θ=10°

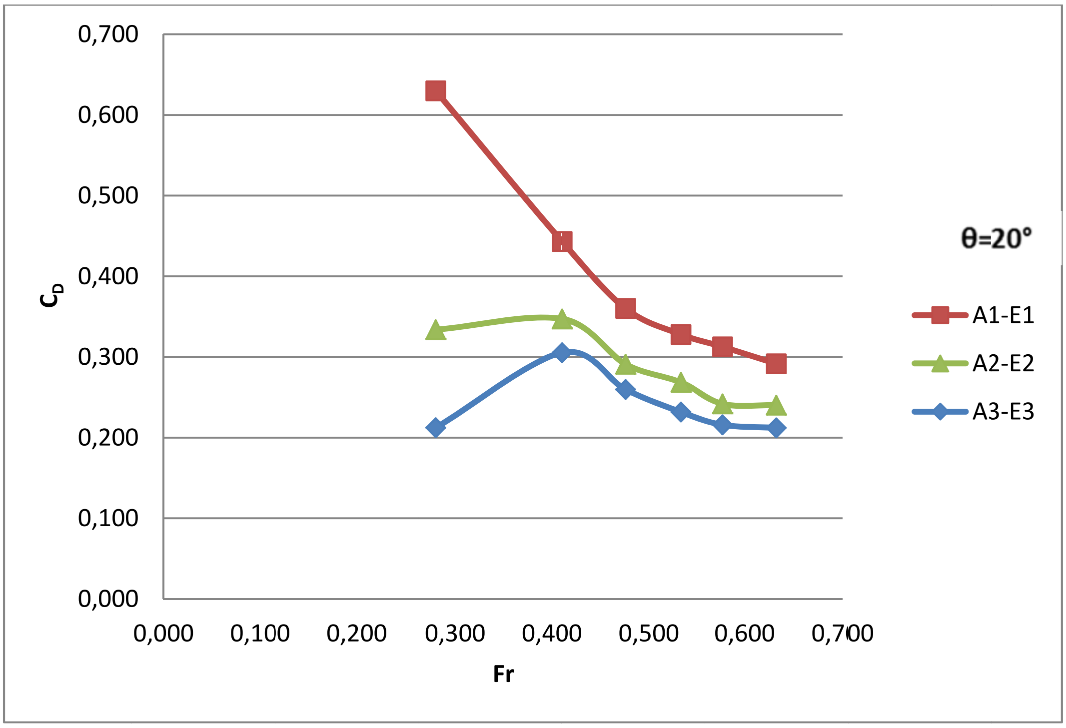

Figure 4.132: Discharge coefficient versus Fr for multiple orifices with different D values at θ=20°

From the inspection of Figures 4.127-4.132, it can be concluded that the value of C_D for a given orifice set such as A1-E1, A2-E2, or A3-E3, in general decreases as the slope of the screen increases under the same upstream flow conditions that are for the same D/h and Fr.

4.3.2 Empirical Relationship between C_D and Related Parameters with respect to Screen Slopes for Multiple Circular Bottom Intake Orifices

In order to derive an empirical equation for C_D as a function of D/h and Fr, regression analysis was applied to the available related data and the following equations were determined.

At θ=0°,

$$C_D = 0.193\left(\frac{D}{h}\right)^{-0.678}(Fr)^{-0.847} \quad \text{...(4.7)}$$

with a correlation coefficient of R^2=0.834.

C_D values; obtained from measurements and calculated from Equation 4.7 are presented in Figure 4.133. From this figure, it is seen that all the data lies between ± 20% error lines.

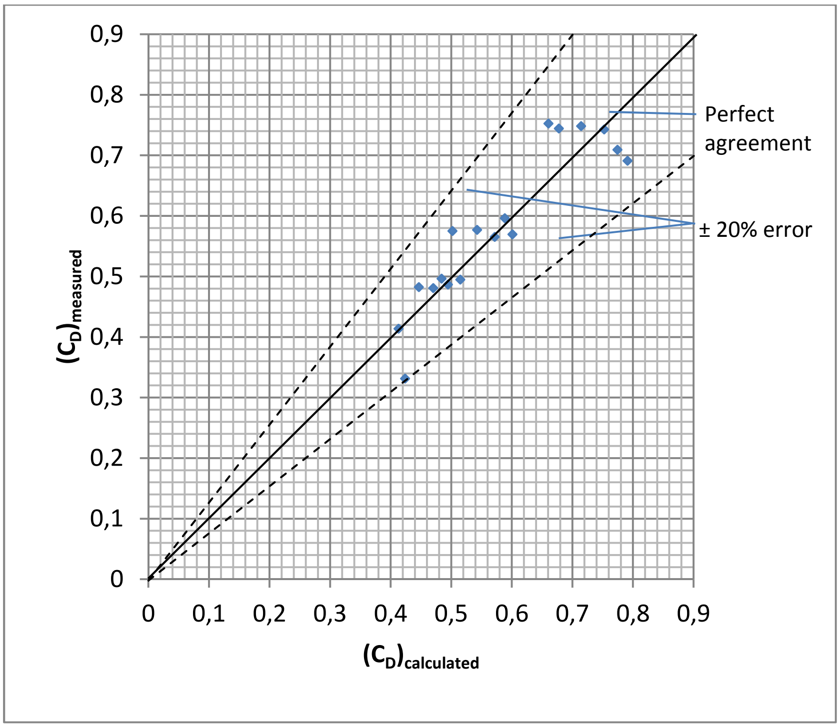

Figure 4. 133: Comparison of measured and calculated C_D values for multiple circular bottom intake orifices at θ=0°

At θ=10°,

$$C_D = 0.097(\frac{D}{h})^{-0.827}(Fr)^{-1.027} \qquad \text{...(4.8)}$$

with a correlation coefficient of R^2=0.81.

C_D values; obtained from measurements and calculated from Equation 4.8 are presented in Figure 4.134. From this figure, it is seen that all the data lies between ± 30% error lines.

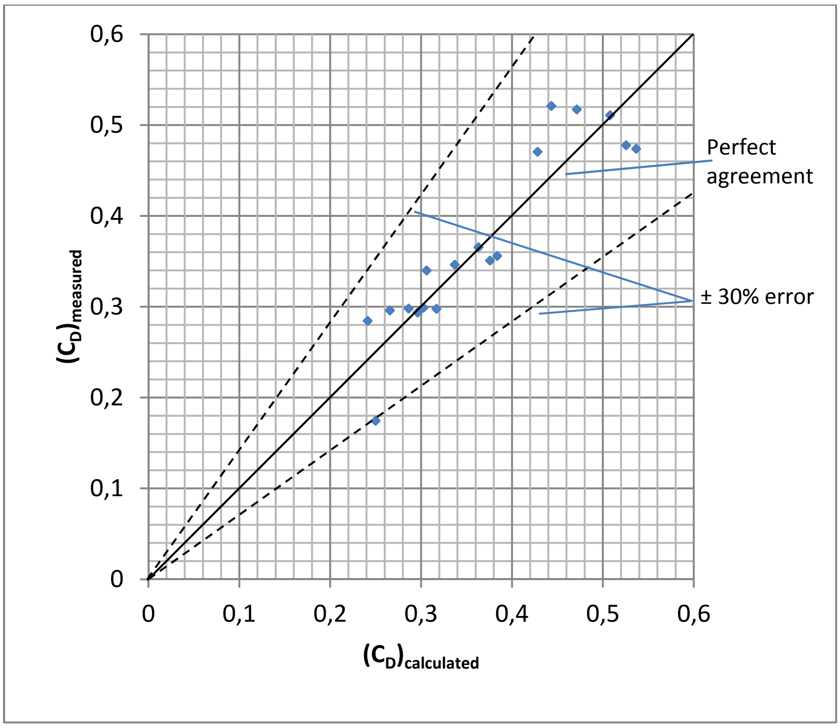

Figure 4. 134: Comparison of measured and calculated C_D values for multiple circular bottom intake orifices at θ=10°

At θ=20°,

$$C_D = 0.066(\frac{D}{h})^{-0.612}(Fr)^{-1.464} \qquad \text{(4.9)}$$

with a correlation coefficient of R^2=0.677.

C_D values; obtained from measurements and calculated from Equation 4.9 are presented in Figure 4.135. This figure implies that all the data lies between ± 30% error lines.

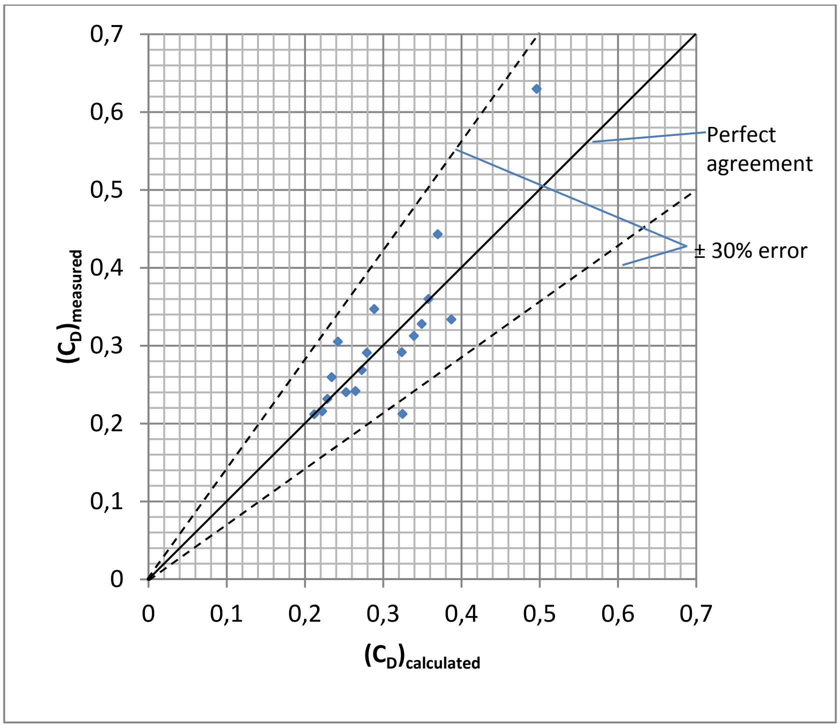

Figure 4. 135: Comparison of measured and calculated C_D values for multiple circular bottom intake orifices at θ=20°

4.3.3 Relationship between Coefficient K and the Related Dimensionless Parameters for Multiple Circular Bottom Intake Orifices on the Screen

The relationship between K and the relevant dimensionless parameters are given by Equation 2.9.

Figures 4.136-4.138 show variation of K with the dimensionless variable D/h for the circular bottom intake orifices having the orifice diameters of 1 cm, 1.5 cm and 2 cm at the screens with the slopes of 0°, 10° and 20°, respectively. These figures reveal that K rapidly increases with increasing D/h for any orifice series tested. As the orifice diameter decreases, the related data set moves towards left by yielding smaller K values for a given D/h. If the slope of the bottom intake screen increases, K value of an orifice series of known diameter decreases for a given D/h.

Figures 4.139-4.141 show the variation of K with the dimensionless variable Fr for all circular bottom intake orifices having the orifice diameters of 1 cm, 1.5 cm and 2 cm at the screens with the slopes of 0°, 10° and 20°, respectively. From these figures, it can be concluded that K values decrease with increasing Fr for the orifice series tested. For a given Fr, K values increase as the diameters of the orifices on the orifice series tested increase. The effect of screen slope on the values of K is the same as stated above for the parameter of D/h when the screen slope increases.

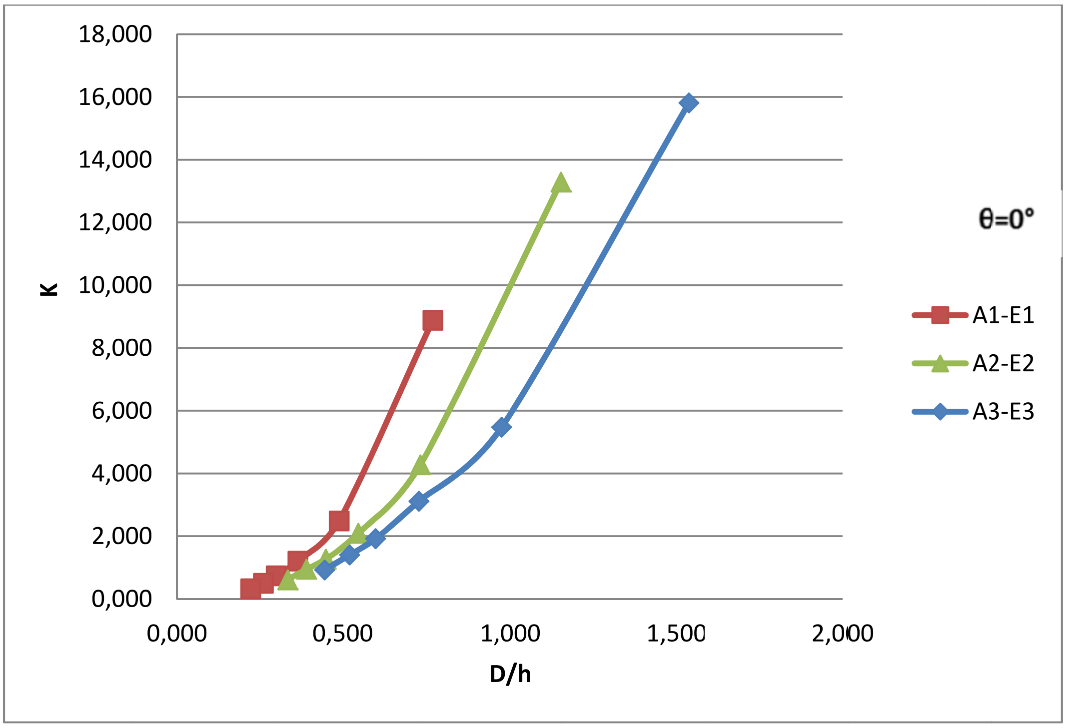

Figure 4.136: K versus D/h for multiple orifices with different D values at θ=0°

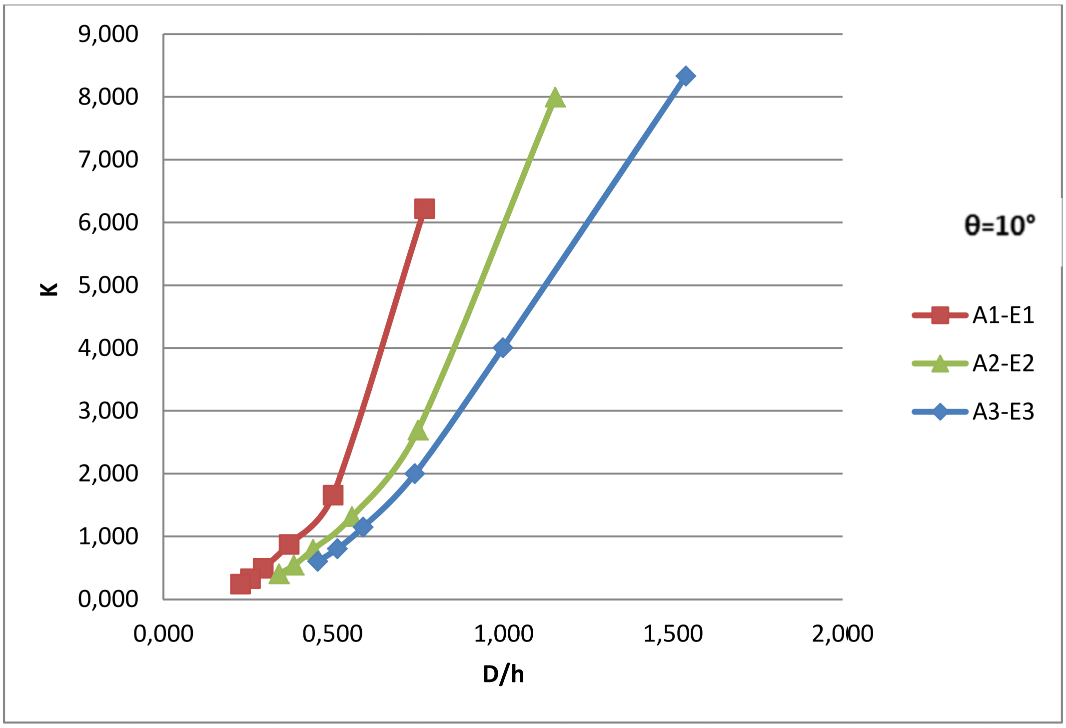

Figure 4.137: K versus D/h for multiple orifices with different D values at θ=10°

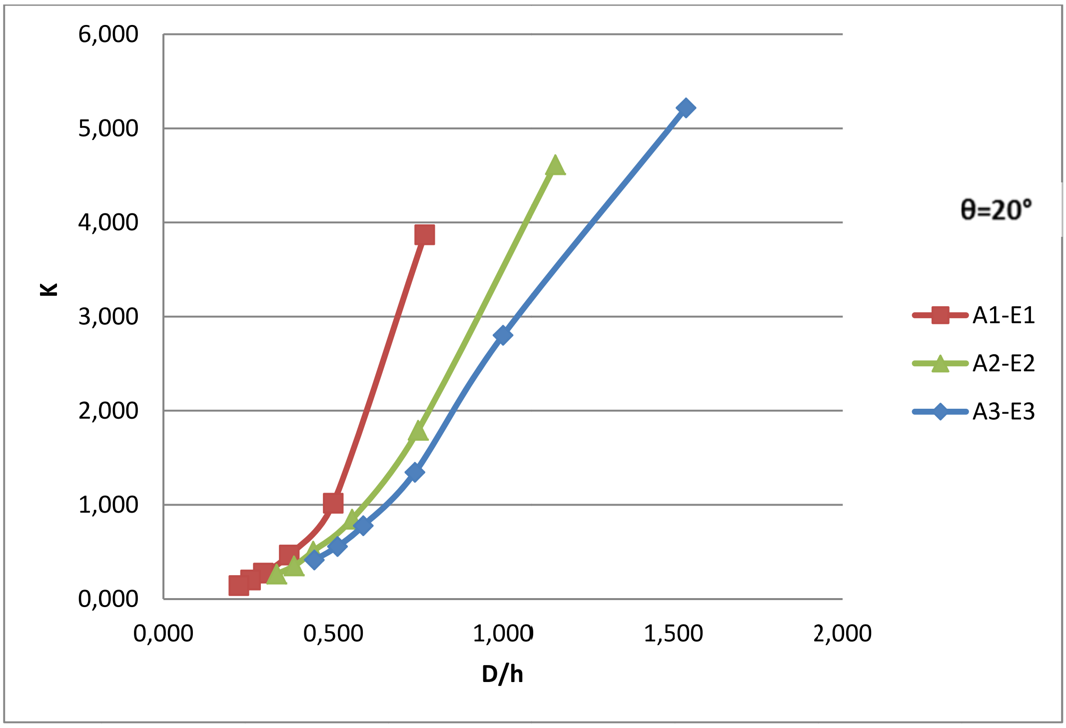

Figure 4.138: K versus D/h for multiple orifices with different D values at θ=20

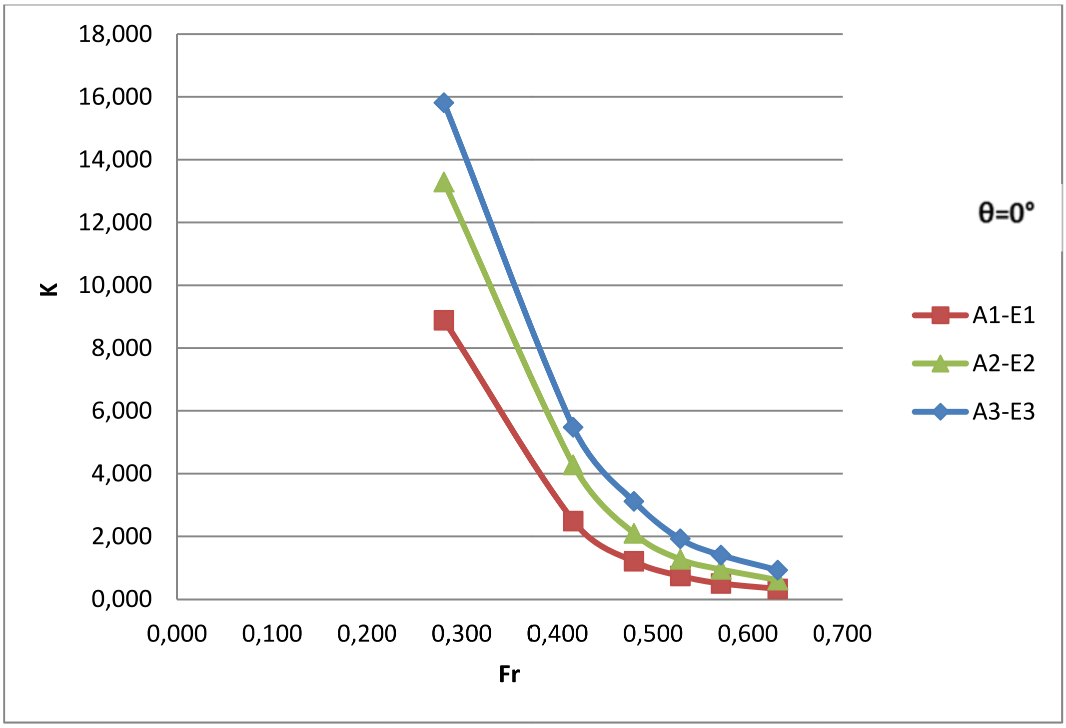

Figure 4.139: K versus Fr for multiple orifices with different D values at θ=0°

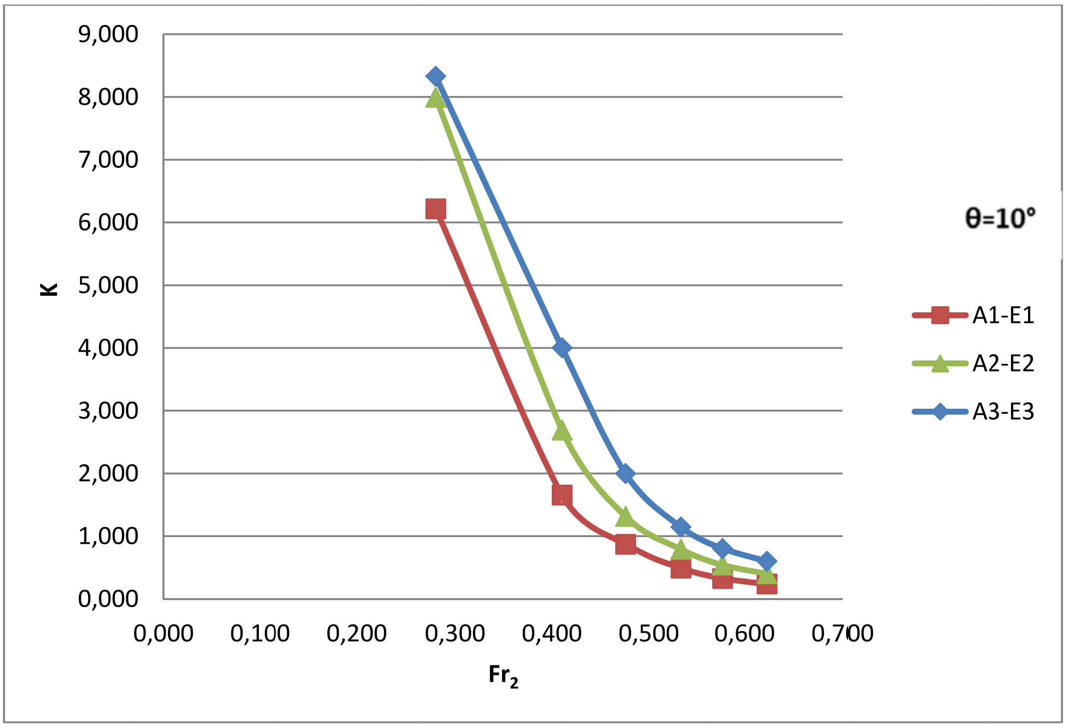

Figure 4.140: K versus Fr for multiple orifices with different D values at θ=10°

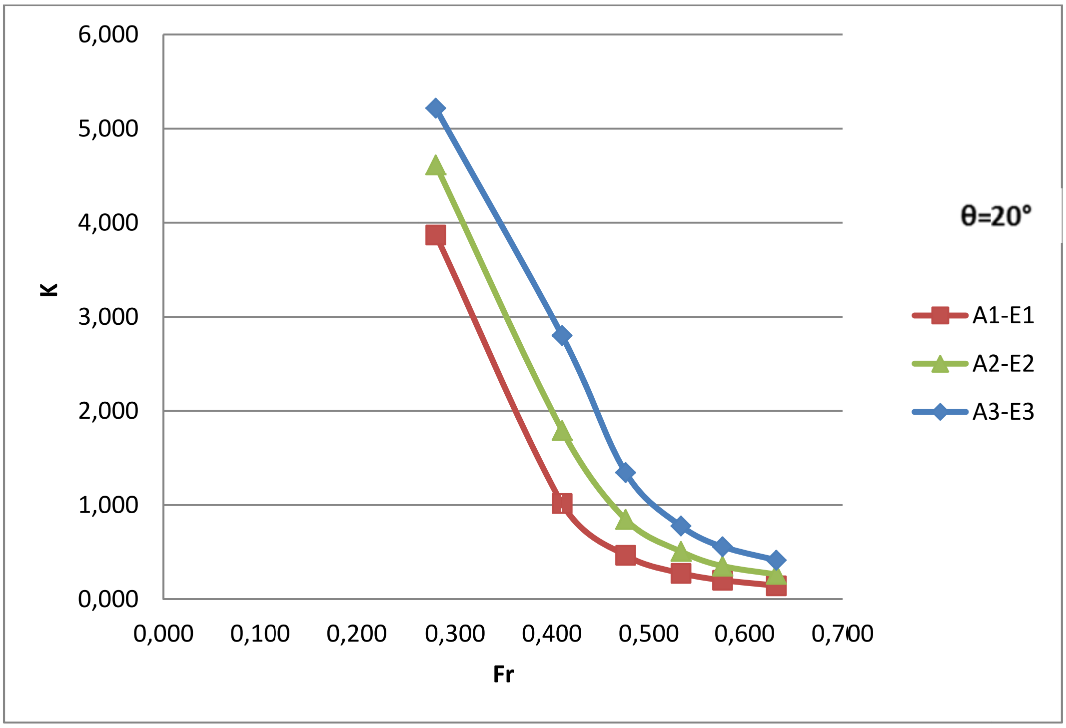

Figure 4.141: K versus Fr for multiple orifices with different D values at θ=20°

From the analysis of Figures 4.136-4.141, it can be pointed out that the value of K for a given orifice set such as A1-E1, A2-E2, or A3-E3, in general, decreases under the same upstream flow conditions that are for the same D/h and Fr.

4.3.4 Empirical Relationship between K and Related Parameters with respect to Screen Slopes for Multiple Circular Bottom Intake Orifices

In order to derive an empirical equation for K as a function of D/h and Fr, regression analysis was applied to the available related data and the following equation was determined.

At θ=0°,

$$K = 1.209\left(\frac{D}{h}\right)^{1.320}(Fr)^{-1.766} \qquad \text{(4.10)}$$

with a correlation coefficient of R^2=0.993.

K values; obtained from measurements and calculated from Equation 4.10 are presented in Figure 4.142. From this figure, it is seen that all the data lies between ± 20% error lines.

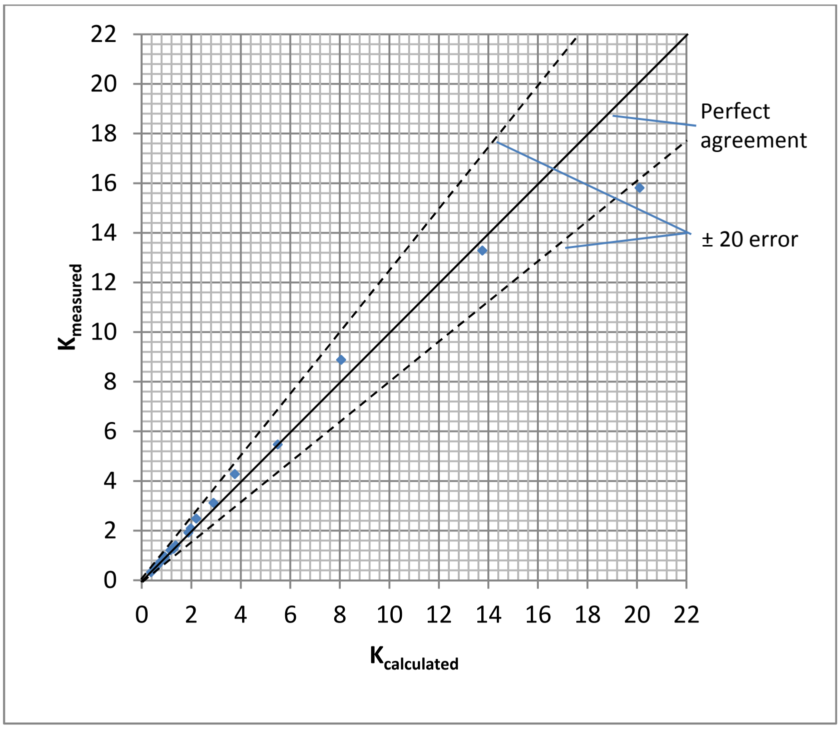

Figure 4. 142: Comparison of measured and calculated K values for multiple circular bottom intake orifices at θ=0°

At θ=10°,

$$K = 0.604(\frac{D}{h})^{1.170}(Fr)^{-1.946} \quad \text{..(4.11)}$$

with a correlation coefficient of R^2=0.988.

K values; obtained from measurements and calculated from Equation 4.11 are presented in Figure 4.143. From these figures, it is seen that all the data lies between ± 30% error lines.

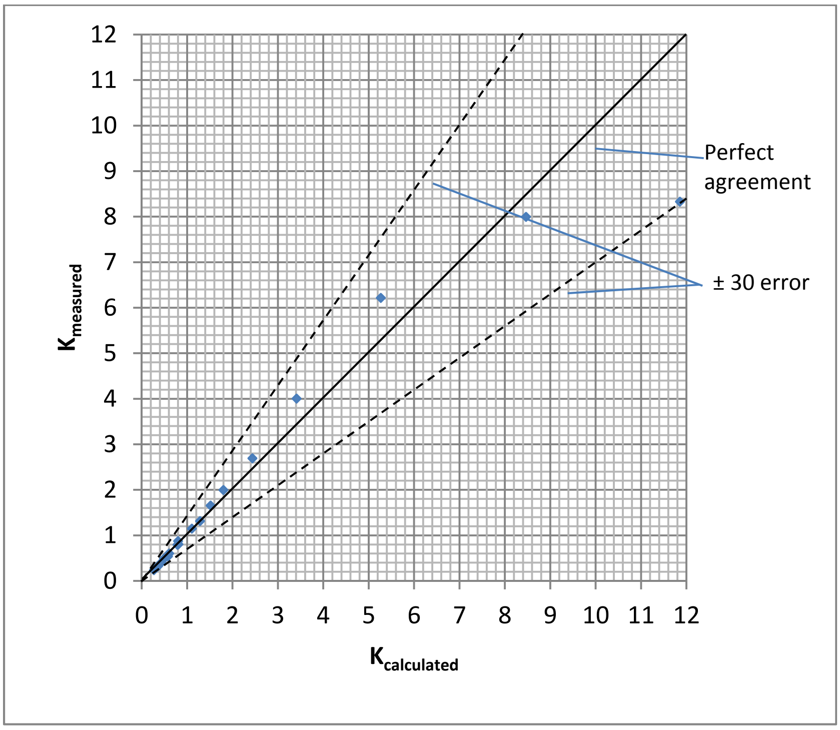

Figure 4. 143: Comparison of measured and calculated K values for multiple circular bottom intake orifices at θ=10°

At θ=20°,

$$K = 0.593(\frac{D}{h})^{1.364}(Fr)^{-1.545} \quad \text{..(4.12)}$$

with a correlation coefficient of R^2=0.985.

K values; obtained from measurements and calculated from Equation 4.12 are presented in Figure 4.144. From this figure, it is seen that all the data lies between ± 30% error lines.

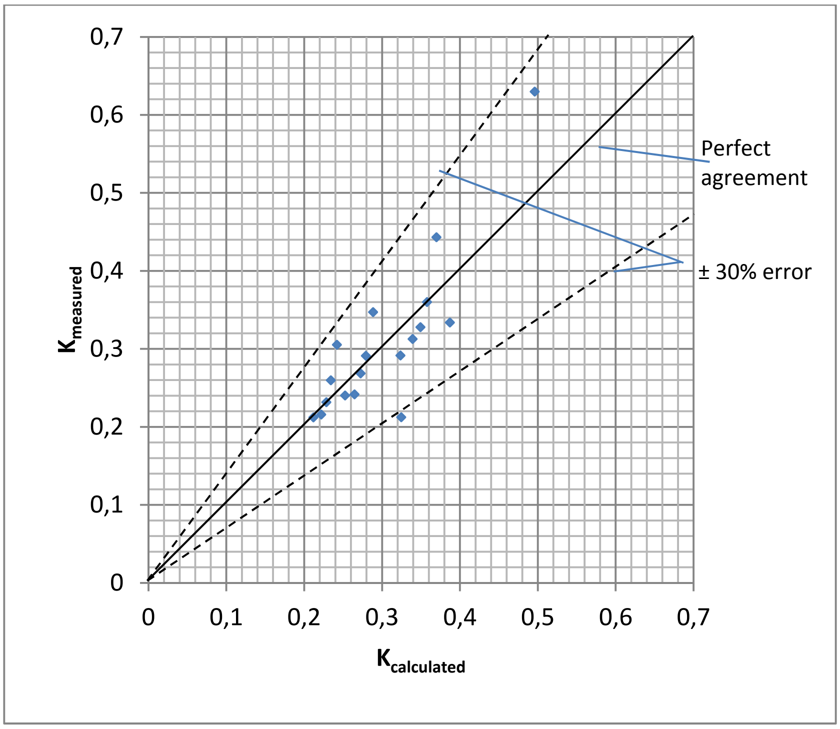

Figure 4. 144: Comparison of measured and calculated K values for multiple circular bottom intake orifices at θ=20°

4.4 Numerical Examples for the Application of the Relationships for Single and Multiple Circular Bottom Intake Orifices Presented in the Study

In Tables 4.1-4.6, some numerical examples are presented to show the application of the derived empirical equations in this study to determine the coefficients C_D and K, and the corresponding orifice discharges. At the end of the tables, the errors made in the calculations of orifice discharges are given.

For the given examples, the errors made in the calculations of the single circular orifice discharges using the coefficients of C_D and K vary between 0.040-0.468 and 0.049-0.450, respectively, for the screen of θ=0°. As the slope of the screen increases from θ=0° to θ=10° and θ=20°, the corresponding errors vary between 0.025-0.380 and 0.021-0.374 for θ=10°, respectively and between 0.044- 0.320 and 0.017-0.258 for θ=20°, respectively (Equation 4.13). Furthermore, the same errors made in the calculations of the multiple circular orifice discharges using the coefficients of C_D and K vary between 0.026-0.090 and 0.029-0.094, respectively, for the screen of θ=0°. As the slope of the screen increases from θ=0° to θ=10° and θ=20°, the corresponding errors vary between 0.010-0.146 and 0.005-0.155 for θ=10°, and between 0.033-0.217 and 0.003-0.246 for θ=20°, respectively (Equation 4.13).

$$\Delta Q_0 = \left|(Q_0)_{mea.} - (Q_0)_{cal.}\right| \quad (4.13)$$

Table 4.1: Numerical examples for single circular orifices at θ=0°

Orifice type	h (cm)	V_T (m/s)	$(Q_0)_{mea.}$ (lt/s)	D/h	x/h	Fr	$(Q_0)_{the.}$ (lt/s)
A1	2.75	0.250	0.052	0.364	1.091	0.481	0.061
A3	3.30	0.299	0.154	0.606	0.909	0.525	0.270
B2	4.50	0.420	0.175	0.333	2.000	0.632	0.182
B4	2.70	0.245	0.256	1.111	3.333	0.476	0.543
C3	4.00	0.367	0.217	0.500	3.750	0.585	0.301
C5	1.30	0.100	0.109	3.077	11.538	0.281	0.647
D1	3.30	0.299	0.078	0.303	6.364	0.525	0.067
D2	1.35	0.108	0.067	1.111	15.556	0.296	0.093
E4	1.90	0.172	0.214	1.579	14.211	0.399	0.448
E5	1.90	0.160	0.265	1.951	13.171	0.356	0.822

Table 4.1 continued

Orifice type	$(C_D)_{mea.}$	$(C_D)_{cal.}$ (Eq. 4.1)	$(Q_0)_{cal.}$ (lt/s) (Eq.2.6)	$(\Delta Q_0)_{C_D}/(Q_0)_{mea.}$
A1	0.847	0.991	0.060	0.163
A3	0.570	0.623	0.168	0.092
B2	0.961	1.019	0.185	0.060
B4	0.472	0.433	0.235	0.081
C3	0.722	0.787	0.237	0.091
C5	0.168	0.247	0.160	0.468
D1	1.164	1.286	0.086	0.105
D2	0.717	0.576	0.054	0.201
E4	0.478	0.386	0.173	0.191
E5	0.322	0.335	0.276	0.040

Table 4.1 continued

Orifice type	$K_{mea.}$	$K_{cal.}$ (Eq. 4.4)	$(Q_0)_{cal.}$ (lt/s) (Eq.2.9)	$(\Delta Q_0)_K/(Q_0)_{mea.}$
A1	0.273	0.322	0.061	0.169
A3	0.472	0.517	0.168	0.094
B2	0.206	0.216	0.184	0.049
B4	1.435	1.322	0.236	0.078
C3	0.371	0.403	0.237	0.091
C5	6.415	9.353	0.158	0.450
D1	0.241	0.267	0.087	0.115
D2	3.397	2.708	0.053	0.205
E4	3.443	2.796	0.174	0.189
E5	3.948	4.112	0.238	0.104

Table 4.2: Numerical examples for single circular orifices at θ=10°

Orifice type	h (cm)	V_T (m/s)	$(Q_0)_{mea.}$ (lt/s)	D/h	x/h	Fr	$(Q_0)_{the.}$ (lt/s)
A1	2.70	0.245	0.090	0.370	1.111	0.476	0.060
A3	3.40	0.308	0.139	0.588	0.882	0.533	0.274
B2	4.40	0.409	0.122	0.341	2.045	0.622	0.179
B4	2.70	0.245	0.207	1.111	3.333	0.476	0.543
C3	3.90	0.356	0.165	0.513	3.846	0.576	0.297
C5	1.30	0.100	0.138	3.077	11.538	0.281	0.647
D1	3.40	0.308	0.104	0.294	6.176	0.533	0.069
D2	1.30	0.100	0.077	1.154	16.154	0.281	0.091
E4	2.00	0.182	0.213	1.500	13.500	0.411	0.461
E5	2.00	0.182	0.288	2.000	13.500	0.411	0.820

Table 4.2 continued

Orifice type	$(C_D)_{mea.}$	$(C_D)_{cal.}$ (Eq. 4.1)	$(Q_0)_{cal.}$ (lt/s) (Eq.2.6)	$(\Delta Q_0)_{C_D}/(Q_0)_{mea.}$
A1	1.493	1.087	0.065	0.275
A3	0.507	0.552	0.151	0.087
B2	0.683	0.853	0.153	0.251
B4	0.381	0.369	0.200	0.032
C3	0.555	0.650	0.193	0.170
C5	0.213	0.294	0.191	0.380
D1	1.519	1.375	0.095	0.088
D2	0.843	0.867	0.079	0.025
E4	0.463	0.373	0.172	0.192
E5	0.351	0.274	0.225	0.219

Table 4.2 continued

Orifice type	$K_{mea.}$	$K_{cal.}$ (Eq. 4.4)	$(Q_0)_{cal.}$ (lt/s) (Eq.2.9)	$(\Delta Q_0)_K/(Q_0)_{mea.}$
A1	0.504	0.370	0.066	0.265
A3	0.391	0.427	0.152	0.095
B2	0.155	0.193	0.153	0.253
B4	1.158	1.131	0.202	0.024
C3	0.304	0.357	0.193	0.172
C5	8.118	11.218	0.190	0.374
D1	0.293	0.267	0.095	0.087
D2	4.525	4.651	0.079	0.021
E4	2.931	2.388	0.174	0.184
E5	3.955	3.118	0.227	0.212

Table 4.3: Numerical examples for single circular orifices at θ=20°

Orifice type	h (cm)	V_T (m/s)	$(Q_0)_{mea.}$ (lt/s)	D/h	x/h	Fr	$(Q_0)_{the.}$ (lt/s)
A1	2.70	0.245	0.037	0.370	1.111	0.476	0.046
A3	3.40	0.308	0.072	0.588	0.882	0.533	0.239
B2	4.50	0.420	0.069	0.333	2.000	0.632	0.187
B4	2.70	0.245	0.121	1.111	3.333	0.476	0.417
C3	3.90	0.356	0.088	0.513	3.846	0.576	0.280
C5	1.30	0.100	0.109	3.077	11.538	0.281	0.333
D1	3.40	0.308	0.048	0.294	6.176	0.533	0.060
D2	1.30	0.100	0.043	1.154	16.154	0.281	0.047
E4	2.00	0.182	0.148	1.500	13.500	0.411	0.301
E5	2.00	0.182	0.227	2.000	13.500	0.411	0.535

Table 4.3 continued

Orifice type	$(C_D)_{mea.}$	$(C_D)_{cal.}$ (Eq. 4.1)	$(Q_0)_{cal.}$ (lt/s) (Eq.2.6)	$(\Delta Q_0)_{C_D}/(Q_0)_{mea.}$
A1	0.808	0.629	0.029	0.218
A3	0.301	0.343	0.082	0.138
B2	0.369	0.427	0.080	0.158
B4	0.291	0.303	0.126	0.044
C3	0.314	0.393	0.110	0.251
C5	0.328	0.432	0.144	0.320
D1	0.800	0.748	0.045	0.065
D2	0.921	0.973	0.046	0.063
E4	0.493	0.375	0.113	0.237
E5	0.425	0.299	0.160	0.295

Table 4.3 continued

Orifice type	$K_{mea.}$	$K_{cal.}$ (Eq. 4.4)	$(Q_0)_{cal.}$ (lt/s) (Eq.2.9)	$(\Delta Q_0)_K/(Q_0)_{mea.}$
A1	0.209	0.170	0.030	0.179
A3	0.202	0.232	0.082	0.145
B2	0.081	0.092	0.078	0.132
B4	0.679	0.728	0.130	0.074
C3	0.162	0.200	0.108	0.233
C5	6.449	8.111	0.137	0.258
D1	0.134	0.126	0.045	0.064
D2	2.545	2.588	0.044	0.017
E4	2.035	1.643	0.120	0.192
E5	3.118	2.324	0.169	0.255

Table 4.4: Numerical examples for multiple circular orifices at θ=0°

Orifice type	h (cm)	V_T (m/s)	$(Q_0)_{mea.}$ (lt/s)	D/h	Fr	$(Q_0)_{the.}$ (lt/s)
A1-E1	1.30	0.100	0.150	0.769	0.281	0.202
A2-E2	2.75	0.250	0.395	0.545	0.481	0.685
A3-E3	3.85	0.351	0.731	0.519	0.572	1.473

Table 4.4 continued

Orifice type	$(C_D)_{mea.}$	$(C_D)_{cal.}$ (Eq. 4.1)	$(Q_0)_{cal.}$ (lt/s) (Eq.2.6)	$(\Delta Q_0)_{C_D}/(Q_0)_{mea.}$
A1-E1	0.744	0.676	0.137	0.090
A2-E2	0.577	0.541	0.371	0.061
A3-E3	0.496	0.483	0.712	0.026

Table 4.4 continued

Orifice type	$K_{mea.}$	$K_{cal.}$ (Eq. 4.4)	$(Q_0)_{cal.}$ (lt/s) (Eq.2.9)	$(\Delta Q_0)_K/(Q_0)_{mea.}$
A1-E1	8.882	8.043	0.136	0.094
A2-E2	2.095	1.976	0.374	0.054
A3-E3	1.403	1.364	0.710	0.029

Table 4.5: Numerical examples for multiple circular orifices at θ=10°

Orifice type	h (cm)	V_T (m/s)	$(Q_0)_{mea.}$ (lt/s)	D/h	Fr	$(Q_0)_{the.}$ (lt/s)
A1-E1	1.30	0.100	0.105	0.769	0.281	0.202
A2-E2	2.70	0.245	0.235	0.556	0.476	0.679
A3-E3	3.90	0.356	0.436	0.513	0.576	1.484

Table 4.5 continued

Orifice type	$(C_D)_{mea.}$	$(C_D)_{cal.}$ (Eq. 4.1)	$(Q_0)_{cal.}$ (lt/s) (Eq.2.6)	$(\Delta Q_0)_{C_D}/(Q_0)_{mea.}$
A1-E1	0.521	0.444	0.090	0.146
A2-E2	0.346	0.338	0.229	0.024
A3-E3	0.294	0.297	0.441	0.010

Table 4.5 continued

Orifice type	$K_{mea.}$	$K_{cal.}$ (Eq. 4.4)	$(Q_0)_{cal.}$ (lt/s) (Eq.2.9)	$(\Delta Q_0)_K/(Q_0)_{mea.}$
A1-E1	6.218	5.253	0.089	0.155
A2-E2	1.315	1.289	0.230	0.021
A3-E3	0.804	0.809	0.438	0.005

Table 4.6: Numerical examples for multiple circular orifices at θ=20°

Orifice type	h (cm)	V_T (m/s)	$(Q_0)_{mea.}$ (lt/s)	D/h	Fr	$(Q_0)_{the.}$ (lt/s)
A1-E1	1.30	0.100	0.066	0.769	0.281	0.104
A2-E2	2.70	0.245	0.152	0.556	0.476	0.521
A3-E3	3.90	0.356	0.302	0.513	0.576	1.401

Table 4.6 continued

Orifice type	$(C_D)_{mea.}$	$(C_D)_{cal.}$ (Eq. 4.1)	$(Q_0)_{cal.}$ (lt/s) (Eq.2.6)	$(\Delta Q_0)_{C_D}/(Q_0)_{mea.}$
A1-E1	0.630	0.497	0.052	0.217
A2-E2	0.291	0.280	0.146	0.039
A3-E3	0.216	0.223	0.312	0.033

Table 4.6 continued

Orifice type	$K_{mea.}$	$K_{cal.}$ (Eq. 4.4)	$(Q_0)_{cal.}$ (lt/s) (Eq.2.9)	$(\Delta Q_0)_K/(Q_0)_{mea.}$
A1-E1	3.870	2.946	0.050	0.246
A2-E2	0.849	0.838	0.150	0.015
A3-E3	0.558	0.560	0.303	0.003

When ΔQ_0 values presented in Tables 4.1-4.3 and Tables 4.4-4.6 are compared with each other, it is seen that the errors made in the calculation of orifice discharges by using C_D and K are not much different from each other under the same given flow conditions and orifice.

CHAPTER 5

CONCLUSIONS AND FURTHER RECOMMENDATIONS

In this experimental study, the effects of the diameter, location and slope of the circular bottom intake orifices on the amount of diverted water from the channel under different flow conditions were investigated. Within the scope of this study, totally 504 experiments were conducted; 150 experiments with single circular orifices for each screen slope, $\theta_1=0°$, $\theta_2=10°$ and $\theta_3=20°$ and 18 experiments with multiple circular orifices for each screen slope, $\theta_1 = 0°$, $\theta_2=10°$ and $\theta_3=20°$. The procedures were the same for all the experiments. From the graphs drawn by using the calculated parameters, an expression for the discharge coefficient of the bottom intake structure, C_D and the other coefficient, K, were derived and their variations with the related dimensionless parameters were presented. From the analysis of the experimental results, the following conclusions can be drawn:

1) C_D values of an orifice on the bottom intake screen at a fixed location increase as the orifice diameter decreases regardless of the screen slope (Figure 4.1-4.15).
2) At a given location for an orifice of known diameter, if the flow depth decreases, C_D values decrease (Figure 4.16-4.20).
3) For a given x/h, C_D values of an orifice closer to the free fall section of the bottom intake screen is larger than the others which are far away from the free fall section regardless of the screen slope (Figure 4.16-4.30).
4) C_D values increase with increasing Fr for an orifice of constant diameter. C_D values increase for a given Fr if the orifice diameter gets smaller (Figure 4.31-4.35).
5) C_D values of the orifice of known diameter decreases as Fr increases if the slope of the bottom intake screen gets the value of $\theta=20°$ from $\theta=10°$ (Figure 4.51-4.60).
6) The empirical equations of C_D derived for the bottom intake screens of $\theta=0°$, 10° and 20° show that C_D values can be estimated with an error of ±30%.
7) The coefficient K increases with increasing D/h for an orifice of given diameter at a fixed location regardless of the bottom intake screen slope (Figure 4.64-4.78).
8) For the same D/h, the value of K increases as the orifice diameter gets smaller.
9) K values increase with increasing x/h for all the orifices tested having the screen slopes of $\theta=0°$, 10° and 20° (Figure 4.79-4.93).
10) The coefficient K decreases for an orifice of known diameter with increasing Fr. For a given Fr, the value of K increases as the diameter of the orifice increases (Figure 4.94-4.98).
11) For the orifices of small diameters, D=1 cm and 1.5 cm, the location of the orifice on the screen does not affect the variation of K with Fr much (Figure 4.102-4.103).
12) The slope of the bottom intake screen does not influence the variation of K with Fr significantly (Figure 4.104-4.123).

13) The empirical equations of K derived for the bottom intake screen of θ=0°, 10° and 20° show that K values can be estimated with an error of ± 30%.

14) For multiple orifices tested; A1-E1, A2-E2 and A3-E3, the values of C_D and K, in general, decrease as the slope of the screen increases under the same upstream flow conditions, that is for the same D/h and Fr.

15) The errors to be made in the calculation of discharges diverted from the channel by the empirical equations of C_D and K for single or multiple circular bottom intake orifices are almost in the same order under the given upstream flow conditions.

As a recommendation, it can be stated that the similar experiments should be conducted with single and multiple orifices of different diameters than those tested in this study in a channel of higher discharge capacity.

REFERENCES

- Brunella, S., Hager, W. H. and Minor, H.E., (2003),“Hydraulics of Bottom Intake”, J. of Hydraulic Engineering, ASCE 0733-9429.

- Kamanbedast, A. A., Bejestan, M. S., (2008),“Effects of Slope and Area Opening on the Discharge Ratio in Bottom Intake Structures”, Journal of Applies Sciences, ISSN 1812-5654.

- Oakdale Engineering web site, http://www.oakdaleengr.com/download.htm, last accessed on 15.08.2013.

- Sahiner, H., (2012),“Hydraulic Characteristics of Tyrolean Weirs Having Steel Racks and Circular-Perforated Entry”, Thesis Submitted in Partial Fulfillment of the Requirements for the Degree of Master of Science in the Department of Civil Engineering The Middle East Technical University, Ankara, Turkey.

- United States Department of the Interior Bureau of Reclamation, Water Resources Research Laboratory, Water Measurement Manual, Chapter 9. Retrieved September 6, 2012 from http://www.usbr.gov/pmts/hydraulics_lab/pubs/wmm/.

- Yılmaz, N. A., (2010),“Hydraulic Characteristics of Tyrolean Weirs”, Thesis Submitted in Partial Fulfillment of the Requirements for the Degree of Master of Science in the Department of Civil Engineering The Middle East Technical University, Ankara, Turkey.

APPENDIX A

MEASURED AND CALCULATED PARAMETERS FOR THE EXPERIMENTS PERFORMED WITH THE SINGLE CIRCULAR BOTTOM INTAKE ORIFICES

Table A.1: Experimental results related to circular orifice A5 for θ=0°

Experiment no	h (cm)	Q_T (lt/sec)	t (sec)	V (lt)	$(Q_o)_{mea.}$ (lt/s)	D (m)	A_T =h*w (m^2)	V_T=Q_T /A_T (m/s)	A_o =(π*D^2)/4 (m^2)
1	1.30	0.391	60.00	6.000	0.100	0.040	0.004	0.100	0.00126
2	2.05	1.149	26.47	6.000	0.227	0.040	0.006	0.187	0.00126
3	2.70	1.986	20.72	8.000	0.386	0.040	0.008	0.245	0.00126
4	3.40	3.142	16.85	8.000	0.475	0.040	0.010	0.308	0.00126
5	3.90	4.170	37.59	20.250	0.539	0.040	0.012	0.356	0.00126
6	4.50	5.666	32.55	20.250	0.622	0.040	0.014	0.420	0.00126

V_o =(2g(h+V_T^2/2g))^{0,5} (m/s)	$(Q_o)_{the.}$=A_0*V_0 (lt/s)	C_D=$(Q_o)_{mea.}$/$(Q_o)_{the.}$	K=$(Q_o)_{mea.}$/(V_T*h^2)	D/h	x/h	Fr=V_T/(g*h)^{0,5}
0.515	0.647	0.155	5.902	3.077	2.308	0.281
0.661	0.831	0.273	2.887	1.951	1.463	0.417
0.768	0.965	0.400	2.160	1.481	1.111	0.476
0.873	1.097	0.433	1.333	1.176	0.882	0.533
0.945	1.187	0.454	0.994	1.026	0.769	0.576
1.029	1.293	0.481	0.732	0.889	0.667	0.632

Table A.2: Experimental results related to circular orifice B5 for θ=0°

Experiment no	h (cm)	Q_T (lt/sec)	t (sec)	V (lt)	$(Q_o)_{mea.}$ (lt/s)	D (m)	A_T =h*w (m^2)	V_T=Q_T /A_T (m/s)	A_o =(π*D^2)/4 (m^2)
1	1.30	0.391	57.10	6.000	0.105	0.040	0.004	0.100	0.00126
2	2.00	1.092	24.88	6.000	0.241	0.040	0.006	0.182	0.00126
3	2.70	1.986	20.68	8.000	0.387	0.040	0.008	0.245	0.00126
4	3.40	3.142	16.43	8.000	0.487	0.040	0.010	0.308	0.00126
5	3.90	4.170	37.30	20.250	0.543	0.040	0.012	0.356	0.00126
6	4.50	5.666	32.02	20.250	0.632	0.040	0.014	0.420	0.00126

V_o =(2g(h+V_T^2/2g))^{0,5} (m/s)	$(Q_o)_{the.}$=A_0*V_0 (lt/s)	C_D=$(Q_o)_{mea.}$/$(Q_o)_{the.}$	K=$(Q_o)_{mea.}$/(V_T*h^2)	D/h	x/h	Fr=V_T/(g*h)^{0,5}
0.515	0.647	0.162	6.202	3.077	6.923	0.281
0.652	0.820	0.294	3.313	2.000	4.500	0.411
0.768	0.965	0.401	2.164	1.481	3.333	0.476
0.873	1.097	0.444	1.367	1.176	2.647	0.533
0.945	1.187	0.457	1.001	1.026	2.308	0.576
1.029	1.293	0.489	0.744	0.889	2.000	0.632

Table A.3: Experimental results related to circular orifice C5 for θ=0°

Experiment no	h (cm)	Q_T (lt/sec)	t (sec)	V (lt)	$(Q_o)_{mea.}$ (lt/s)	D (m)	$A_T=h*w$ (m^2)	$V_T=Q_T/A_T$ (m/s)	$A_o=(\pi*D^2)/4$ (m^2)
1	1.30	0.391	55.20	6.000	0.109	0.040	0.004	0.100	0.00126
2	1.95	1.037	24.63	6.000	0.244	0.040	0.006	0.177	0.00126
3	2.65	1.914	20.28	8.000	0.394	0.040	0.008	0.241	0.00126
4	3.40	3.142	16.37	8.000	0.489	0.040	0.010	0.308	0.00126
5	3.90	4.170	36.97	20.250	0.548	0.040	0.012	0.356	0.00126
6	4.50	5.666	31.89	20.250	0.635	0.040	0.014	0.420	0.00126

$V_o=(2g(h+V_T^2/2g))^{0,5}$ (m/s)	$(Q_o)_{the.}=A_0*V_0$ (lt/s)	$C_D=(Q_o)_{mea.}/(Q_o)_{the.}$	$K=(Q_o)_{mea.}/(V_T*h^2)$	D/h	x/h	$Fr=V_T/(g*h)^{0,5}$
0.515	0.647	0.168	6.415	3.077	11.538	0.281
0.643	0.809	0.301	3.614	2.051	7.692	0.405
0.760	0.955	0.413	2.333	1.509	5.660	0.472
0.873	1.097	0.446	1.372	1.176	4.412	0.533
0.945	1.187	0.461	1.010	1.026	3.846	0.576
1.029	1.293	0.491	0.747	0.889	3.333	0.632

Table A.4: Experimental results related to circular orifice D5 for θ=0°

Experiment no	h (cm)	Q_T (lt/sec)	t (sec)	V (lt)	$(Q_o)_{mea.}$ (lt/s)	D (m)	$A_T=h*w$ (m^2)	$V_T=Q_T/A_T$ (m/s)	$A_o=(\pi*D^2)/4$ (m^2)
1	1.30	0.391	49.50	6.000	0.121	0.040	0.004	0.100	0.00126
2	2.05	1.037	23.35	6.000	0.257	0.040	0.006	0.169	0.00126
3	2.70	1.843	19.94	8.000	0.401	0.040	0.008	0.228	0.00126
4	3.40	3.142	16.25	8.000	0.492	0.040	0.010	0.308	0.00126
5	3.90	4.170	36.81	20.250	0.550	0.040	0.012	0.356	0.00126
6	4.50	5.666	31.31	20.250	0.647	0.040	0.014	0.420	0.00126

$V_o=(2g(h+V_T^2/2g))^{0,5}$ (m/s)	$(Q_o)_{the.}=A_0*V_0$ (lt/s)	$C_D=(Q_o)_{mea.}/(Q_o)_{the.}$	$K=(Q_o)_{mea.}/(V_T*h^2)$	D/h	x/h	$Fr=V_T/(g*h)^{0,5}$
0.515	0.647	0.187	7.154	3.077	16.154	0.281
0.656	0.825	0.312	3.626	1.951	10.244	0.376
0.763	0.958	0.419	2.419	1.481	7.778	0.442
0.873	1.097	0.449	1.383	1.176	6.176	0.533
0.945	1.187	0.463	1.015	1.026	5.385	0.576
1.029	1.293	0.500	0.761	0.889	4.667	0.632

Table A.5: Experimental results related to circular orifice E5 for θ=0°

Experiment no	h (cm)	Q_T (lt/sec)	t (sec)	V (lt)	$(Q_o)_{mea.}$ (lt/s)	D (m)	A_T =h*w (m^2)	V_T=Q_T /A_T (m/s)	A_o =(π*D^2)/4 (m^2)
1	1.30	0.391	45.40	6.000	0.132	0.040	0.004	0.100	0.00126
2	2.05	0.982	22.65	6.000	0.265	0.040	0.006	0.160	0.00126
3	2.70	1.843	19.59	8.000	0.408	0.040	0.008	0.228	0.00126
4	3.40	3.142	16.10	8.000	0.497	0.040	0.010	0.308	0.00126
5	3.90	4.170	36.62	20.250	0.553	0.040	0.012	0.356	0.00126
6	4.50	5.666	30.80	20.250	0.657	0.040	0.014	0.420	0.00126

V_o =(2g(h+V_T^2/2g))^{0,5} (m/s)	$(Q_o)_{the.}$=A_0*V_0 (lt/s)	C_D=$(Q_o)_{mea.}$/$(Q_o)_{the.}$	K=$(Q_o)_{mea.}$/(V_T*h^2)	D/h	x/h	Fr=V_T/(g*h)^{0,5}
0.515	0.647	0.204	7.800	3.077	20.769	0.281
0.654	0.822	0.322	3.948	1.951	13.171	0.356
0.763	0.958	0.426	2.462	1.481	10.000	0.442
0.873	1.097	0.453	1.395	1.176	7.941	0.533
0.945	1.187	0.466	1.020	1.026	6.923	0.576
1.029	1.293	0.508	0.774	0.889	6.000	0.632

Table A.6: Experimental results related to circular orifice A4 for θ=0°

Experiment no	h (cm)	Q_T (lt/sec)	t (sec)	V (lt)	$(Q_o)_{mea.}$ (lt/s)	D (m)	A_T =h*w (m^2)	V_T=Q_T /A_T (m/s)	A_o =(π*D^2)/4 (m^2)
1	1.40	0.482	74.10	6.000	0.081	0.030	0.004	0.115	0.00071
2	2.00	1.092	35.19	6.000	0.171	0.030	0.006	0.182	0.00071
3	2.70	1.986	32.08	8.000	0.249	0.030	0.008	0.245	0.00071
4	3.40	3.142	27.38	8.000	0.292	0.030	0.010	0.308	0.00071
5	4.05	4.516	60.01	20.250	0.337	0.030	0.012	0.372	0.00071
6	4.50	5.666	55.01	20.250	0.368	0.030	0.014	0.420	0.00071

V_o =(2g(h+V_T^2/2g))^{0,5} (m/s)	$(Q_o)_{the.}$=A_0*V_0 (lt/s)	C_D=$(Q_o)_{mea.}$/$(Q_o)_{the.}$	K=$(Q_o)_{mea.}$/(V_T*h^2)	D/h	x/h	Fr=V_T/(g*h)^{0,5}
0.537	0.379	0.214	3.600	2.143	2.143	0.310
0.652	0.461	0.370	2.342	1.500	1.500	0.411
0.768	0.543	0.459	1.395	1.111	1.111	0.476
0.873	0.617	0.474	0.821	0.882	0.882	0.533
0.966	0.683	0.494	0.553	0.741	0.741	0.590
1.029	0.727	0.506	0.433	0.667	0.667	0.632

Table A.7: Experimental results related to circular orifice B4 for θ=0°

Experiment no	h (cm)	Q_T (lt/sec)	t (sec)	V (lt)	$(Q_o)_{mea.}$ (lt/s)	D (m)	A_T =h*w (m^2)	V_T=Q_T /A_T (m/s)	A_o =(π*D^2)/4 (m^2)
1	1.40	0.482	68.90	6.000	0.087	0.030	0.004	0.115	0.00071
2	2.00	1.092	33.13	6.000	0.181	0.030	0.006	0.182	0.00071
3	2.70	1.986	31.19	8.000	0.256	0.030	0.008	0.245	0.00071
4	3.40	3.142	27.15	8.000	0.295	0.030	0.010	0.308	0.00071
5	4.05	4.516	58.97	20.250	0.343	0.030	0.012	0.372	0.00071
6	4.50	5.666	53.91	20.250	0.376	0.030	0.014	0.420	0.00071

V_o =(2g(h+V_T^2/2g))^{0,5} (m/s)	$(Q_o)_{the.}$=A_0*V_0 (lt/s)	C_D=$(Q_o)_{mea.}$/$(Q_o)_{the.}$	K=$(Q_o)_{mea.}$/(V_T*h^2)	D/h	x/h	Fr=V_T/(g*h)^{0,5}
0.537	0.379	0.230	3.871	2.143	6.429	0.310
0.652	0.461	0.393	2.488	1.500	4.500	0.411
0.768	0.543	0.472	1.435	1.111	3.333	0.476
0.873	0.617	0.478	0.827	0.882	2.647	0.533
0.966	0.683	0.503	0.563	0.741	2.222	0.590
1.029	0.727	0.516	0.442	0.667	2.000	0.632

Table A.8: Experimental results related to circular orifice C4 for θ=0°

Experiment no	h (cm)	Q_T (lt/sec)	t (sec)	V (lt)	$(Q_o)_{mea.}$ (lt/s)	D (m)	A_T =h*w (m^2)	V_T=Q_T /A_T (m/s)	A_o =(π*D^2)/4 (m^2)
1	1.30	0.391	62.50	6.000	0.096	0.030	0.004	0.100	0.00071
2	1.95	1.037	31.12	6.000	0.193	0.030	0.006	0.177	0.00071
3	2.65	1.914	30.43	8.000	0.263	0.030	0.008	0.241	0.00071
4	3.40	3.142	26.56	8.000	0.301	0.030	0.010	0.308	0.00071
5	4.05	4.516	57.75	20.250	0.351	0.030	0.012	0.372	0.00071
6	4.50	5.666	53.28	20.250	0.380	0.030	0.014	0.420	0.00071

V_o =(2g(h+V_T^2/2g))^{0,5} (m/s)	$(Q_o)_{the.}$=A_0*V_0 (lt/s)	C_D=$(Q_o)_{mea.}$/$(Q_o)_{the.}$	K=$(Q_o)_{mea.}$/(V_T*h^2)	D/h	x/h	Fr=V_T/(g*h)^{0,5}
0.515	0.364	0.264	5.666	2.308	11.538	0.281
0.643	0.455	0.424	2.860	1.538	7.692	0.405
0.760	0.537	0.489	1.555	1.132	5.660	0.472
0.873	0.617	0.488	0.846	0.882	4.412	0.533
0.966	0.683	0.514	0.575	0.741	3.704	0.590
1.029	0.727	0.522	0.447	0.667	3.333	0.632

Table A.9: Experimental results related to circular orifice D4 for θ=0°

Experiment no	h (cm)	Q_T (lt/sec)	t (sec)	V (lt)	$(Q_o)_{mea.}$ (lt/s)	D (m)	A_T =h*w (m^2)	V_T=Q_T /A_T (m/s)	A_o =(π*D^2)/4 (m^2)
1	1.30	0.391	57.85	6.000	0.104	0.030	0.004	0.100	0.00071
2	1.95	1.037	30.41	6.000	0.197	0.030	0.006	0.177	0.00071
3	2.60	1.843	28.69	8.000	0.279	0.030	0.008	0.236	0.00071
4	3.30	2.958	27.12	8.000	0.295	0.030	0.010	0.299	0.00071
5	4.05	4.516	56.95	20.250	0.356	0.030	0.012	0.372	0.00071
6	4.50	5.666	51.94	20.250	0.390	0.030	0.014	0.420	0.00071

V_o =(2g(h+V_T^2/2g))^{0,5} (m/s)	$(Q_o)_{the.}$=A_0*V_0 (lt/s)	C_D=$(Q_o)_{mea.}$/$(Q_o)_{the.}$	K=$(Q_o)_{mea.}$/(V_T*h^2)	D/h	x/h	Fr=V_T/(g*h)^{0,5}
0.515	0.364	0.285	6.121	2.308	16.154	0.281
0.643	0.455	0.434	2.927	1.538	10.769	0.405
0.752	0.532	0.524	1.746	1.154	8.077	0.468
0.858	0.607	0.486	0.907	0.909	6.364	0.525
0.966	0.683	0.521	0.583	0.741	5.185	0.590
1.029	0.727	0.536	0.459	0.667	4.667	0.632

Table A.10: Experimental results related to circular orifice E4 for θ=0°

Experiment no	h (cm)	Q_T (lt/sec)	t (sec)	V (lt)	$(Q_o)_{mea.}$ (lt/s)	D (m)	A_T =h*w (m^2)	V_T=Q_T /A_T (m/s)	A_o =(π*D^2)/4 (m^2)
1	1.30	0.391	53.10	6.000	0.113	0.030	0.004	0.100	0.00071
2	1.90	0.982	28.02	6.000	0.214	0.030	0.006	0.172	0.00071
3	2.60	1.843	27.98	8.000	0.286	0.030	0.008	0.236	0.00071
4	3.30	2.958	26.20	8.000	0.305	0.030	0.010	0.299	0.00071
5	4.05	4.516	55.69	20.250	0.364	0.030	0.012	0.372	0.00071
6	4.50	5.666	50.44	20.250	0.401	0.030	0.014	0.420	0.00071

V_o =(2g(h+V_T^2/2g))^{0,5} (m/s)	$(Q_o)_{the.}$=A_0*V_0 (lt/s)	C_D=$(Q_o)_{mea.}$/$(Q_o)_{the.}$	K=$(Q_o)_{mea.}$/(V_T*h^2)	D/h	x/h	Fr=V_T/(g*h)^{0,5}
0.515	0.364	0.310	6.669	2.308	20.769	0.281
0.634	0.448	0.478	3.443	1.579	14.211	0.399
0.752	0.532	0.538	1.790	1.154	10.385	0.468
0.858	0.607	0.503	0.938	0.909	8.182	0.525
0.966	0.683	0.533	0.596	0.741	6.667	0.590
1.029	0.727	0.552	0.472	0.667	6.000	0.632

Table A.11: Experimental results related to circular orifice A3 for θ=0°

Experiment no	h (cm)	Q_T (lt/sec)	t (sec)	V (lt)	$(Q_o)_{mea.}$ (lt/s)	D (m)	A_T =h*w (m^2)	V_T=Q_T /A_T (m/s)	A_o =(π*D^2)/4 (m^2)
1	1.40	0.482	65.32	4.000	0.061	0.020	0.004	0.115	0.00031
2	2.05	1.149	54.19	6.000	0.111	0.020	0.006	0.187	0.00031
3	2.70	1.986	45.69	6.000	0.131	0.020	0.008	0.245	0.00031
4	3.30	2.958	52.05	8.000	0.154	0.020	0.010	0.299	0.00031
5	4.00	4.398	40.00	8.000	0.200	0.020	0.012	0.367	0.00031
6	4.50	5.666	43.59	10.000	0.229	0.020	0.014	0.420	0.00031

V_o =(2g(h+V_T^2/2g))^{0,5} (m/s)	$(Q_o)_{the.}$=A_0*V_0 (lt/s)	C_D=$(Q_o)_{mea.}$/$(Q_o)_{the.}$	K=$(Q_o)_{mea.}$/(V_T*h^2)	D/h	x/h	Fr=V_T/(g*h)^{0,5}
0.537	0.169	0.363	2.722	1.429	2.143	0.310
0.661	0.208	0.533	1.410	0.976	1.463	0.417
0.768	0.241	0.544	0.735	0.741	1.111	0.476
0.858	0.270	0.570	0.472	0.606	0.909	0.525
0.959	0.301	0.664	0.341	0.500	0.750	0.585
1.029	0.323	0.710	0.270	0.444	0.667	0.632

Table A.12: Experimental results related to circular orifice B3 for θ=0°

Experiment no	h (cm)	Q_T (lt/sec)	t (sec)	V (lt)	$(Q_o)_{mea.}$ (lt/s)	D (m)	A_T =h*w (m^2)	V_T=Q_T /A_T (m/s)	A_o =(π*D^2)/4 (m^2)
1	1.40	0.482	60.22	4.000	0.066	0.020	0.004	0.115	0.00031
2	2.00	1.092	53.22	6.000	0.113	0.020	0.006	0.182	0.00031
3	2.65	1.914	43.76	6.000	0.137	0.020	0.008	0.241	0.00031
4	3.30	2.958	46.67	8.000	0.171	0.020	0.010	0.299	0.00031
5	4.00	4.398	37.95	8.000	0.211	0.020	0.012	0.367	0.00031
6	4.50	5.666	40.56	10.000	0.247	0.020	0.014	0.420	0.00031

V_o =(2g(h+V_T^2/2g))^{0,5} (m/s)	$(Q_o)_{the.}$=A_0*V_0 (lt/s)	C_D=$(Q_o)_{mea.}$/$(Q_o)_{the.}$	K=$(Q_o)_{mea.}$/(V_T*h^2)	D/h	x/h	Fr=V_T/(g*h)^{0,5}
0.537	0.169	0.394	2.953	1.429	6.429	0.310
0.652	0.205	0.550	1.549	1.000	4.500	0.411
0.760	0.239	0.574	0.811	0.755	3.396	0.472
0.858	0.270	0.636	0.527	0.606	2.727	0.525
0.959	0.301	0.700	0.359	0.500	2.250	0.585
1.029	0.323	0.763	0.290	0.444	2.000	0.632

Table A.13: Experimental results related to circular orifice C3 for θ=0°

Experiment no	h (cm)	Q_T (lt/sec)	t (sec)	V (lt)	$(Q_o)_{mea.}$ (lt/s)	D (m)	A_T =h*w (m^2)	V_T=Q_T /A_T (m/s)	A_o =(π*D^2)/4 (m^2)
1	1.40	0.482	52.85	4.000	0.076	0.020	0.004	0.115	0.00031
2	1.95	1.037	49.98	6.000	0.120	0.020	0.006	0.177	0.00031
3	2.65	1.914	40.59	6.000	0.148	0.020	0.008	0.241	0.00031
4	3.20	2.781	45.20	8.000	0.177	0.020	0.010	0.290	0.00031
5	4.00	4.398	36.81	8.000	0.217	0.020	0.012	0.367	0.00031
6	4.50	5.666	39.90	10.000	0.251	0.020	0.014	0.420	0.00031

V_o =(2g(h+V_T^2/2g))^{0,5} (m/s)	$(Q_o)_{the.}$=A_0*V_0 (lt/s)	C_D=$(Q_o)_{mea.}$/$(Q_o)_{the.}$	K=$(Q_o)_{mea.}$/(V_T*h^2)	D/h	x/h	Fr=V_T/(g*h)^{0,5}
0.537	0.169	0.449	3.365	1.429	10.714	0.310
0.643	0.202	0.594	1.781	1.026	7.692	0.405
0.760	0.239	0.619	0.874	0.755	5.660	0.472
0.844	0.265	0.668	0.597	0.625	4.688	0.517
0.959	0.301	0.722	0.371	0.500	3.750	0.585
1.029	0.323	0.775	0.295	0.444	3.333	0.632

Table A.14: Experimental results related to circular orifice D3 for θ=0°

Experiment no	h (cm)	Q_T (lt/sec)	t (sec)	V (lt)	$(Q_o)_{mea.}$ (lt/s)	D (m)	A_T =h*w (m^2)	V_T=Q_T /A_T (m/s)	A_o =(π*D^2)/4 (m^2)
1	1.35	0.436	48.28	4.000	0.083	0.020	0.004	0.108	0.00031
2	1.95	1.037	47.53	6.000	0.126	0.020	0.006	0.177	0.00031
3	2.65	1.914	38.49	6.000	0.156	0.020	0.008	0.241	0.00031
4	3.20	2.781	41.44	8.000	0.193	0.020	0.010	0.290	0.00031
5	4.00	4.398	35.75	8.000	0.224	0.020	0.012	0.367	0.00031
6	4.50	5.666	38.80	10.000	0.258	0.020	0.014	0.420	0.00031

V_o =(2g(h+V_T^2/2g))^{0,5} (m/s)	$(Q_o)_{the.}$=A_0*V_0 (lt/s)	C_D=$(Q_o)_{mea.}$/$(Q_o)_{the.}$	K=$(Q_o)_{mea.}$/(V_T*h^2)	D/h	x/h	Fr=V_T/(g*h)^{0,5}
0.526	0.165	0.502	4.223	1.481	15.556	0.296
0.643	0.202	0.624	1.873	1.026	10.769	0.405
0.760	0.239	0.653	0.922	0.755	7.925	0.472
0.844	0.265	0.728	0.651	0.625	6.563	0.517
0.959	0.301	0.743	0.382	0.500	5.250	0.585
1.029	0.323	0.797	0.303	0.444	4.667	0.632

Table A.15: Experimental results related to circular orifice E3 for θ=0°

Experiment no	h (cm)	Q_T (lt/sec)	t (sec)	V (lt)	$(Q_o)_{mea.}$ (lt/s)	D (m)	A_T =h*w (m^2)	V_T=Q_T /A_T (m/s)	A_o =(π*D^2)/4 (m^2)
1	1.35	0.436	44.93	4.000	0.089	0.020	0.004	0.108	0.00031
2	1.95	1.037	44.95	6.000	0.133	0.020	0.006	0.177	0.00031
3	2.65	1.914	38.32	6.000	0.157	0.020	0.008	0.241	0.00031
4	3.20	2.781	40.63	8.000	0.197	0.020	0.010	0.290	0.00031
5	4.00	4.398	34.83	8.000	0.230	0.020	0.012	0.367	0.00031
6	4.50	5.666	37.72	10.000	0.265	0.020	0.014	0.420	0.00031

V_o =(2g(h+V_T^2/2g))^{0,5} (m/s)	$(Q_o)_{the.}$=A_0*V_0 (lt/s)	C_D=$(Q_o)_{mea.}$/$(Q_o)_{the.}$	K=$(Q_o)_{mea.}$/(V_T*h^2)	D/h	x/h	Fr=V_T/(g*h)^{0,5}
0.526	0.165	0.539	4.538	1.481	20.000	0.296
0.643	0.202	0.660	1.980	1.026	13.846	0.405
0.760	0.239	0.656	0.926	0.755	10.189	0.472
0.844	0.265	0.743	0.664	0.625	8.438	0.517
0.959	0.301	0.763	0.392	0.500	6.750	0.585
1.029	0.323	0.820	0.312	0.444	6.000	0.632

Table A.16: Experimental results related to circular orifice A2 for θ=0°

Experiment no	h (cm)	Q_T (lt/sec)	t (sec)	V (lt)	$(Q_o)_{mea.}$ (lt/s)	D (m)	A_T =h*w (m^2)	V_T=Q_T /A_T (m/s)	A_o =(π*D^2)/4 (m^2)
1	1.40	0.482	80.30	4.000	0.050	0.015	0.004	0.115	0.00018
2	2.00	1.092	53.97	4.000	0.074	0.015	0.006	0.182	0.00018
3	2.75	2.059	46.48	4.000	0.086	0.015	0.008	0.250	0.00018
4	3.25	2.869	46.58	6.000	0.129	0.015	0.010	0.294	0.00018
5	4.00	4.398	41.70	6.000	0.144	0.015	0.012	0.367	0.00018
6	4.50	5.666	49.55	8.000	0.161	0.015	0.014	0.420	0.00018

V_o =(2g(h+V_T^2/2g))^{0,5} (m/s)	$(Q_o)_{the.}$=A_0*V_0 (lt/s)	C_D=$(Q_o)_{mea.}$/$(Q_o)_{the.}$	K=$(Q_o)_{mea.}$/(V_T*h^2)	D/h	x/h	Fr=V_T/(g*h)^{0,5}
0.537	0.095	0.525	2.215	1.071	2.143	0.310
0.652	0.115	0.643	1.018	0.750	1.500	0.411
0.776	0.137	0.628	0.456	0.545	1.091	0.481
0.851	0.150	0.857	0.414	0.462	0.923	0.521
0.959	0.169	0.849	0.245	0.375	0.750	0.585
1.029	0.182	0.888	0.190	0.333	0.667	0.632

Table A.17: Experimental results related to circular orifice B2 for θ=0°

Experiment no	h (cm)	Q_T (lt/sec)	t (sec)	V (lt)	$(Q_o)_{mea.}$ (lt/s)	D (m)	A_T =h*w (m^2)	V_T=Q_T /A_T (m/s)	A_o =(π*D^2)/4 (m^2)
1	1.40	0.482	72.80	4.000	0.055	0.015	0.004	0.115	0.00018
2	2.00	1.092	53.35	4.000	0.075	0.015	0.006	0.182	0.00018
3	2.70	1.986	44.62	4.000	0.090	0.015	0.008	0.245	0.00018
4	3.25	2.869	44.80	6.000	0.134	0.015	0.010	0.294	0.00018
5	4.00	4.398	39.97	6.000	0.150	0.015	0.012	0.367	0.00018
6	4.50	5.666	45.76	8.000	0.175	0.015	0.014	0.420	0.00018

V_o =(2g(h+V_T^2/2g))^{0,5} (m/s)	$(Q_o)_{the.}$=A_0*V_0 (lt/s)	C_D=$(Q_o)_{mea.}$/$(Q_o)_{the.}$	K=$(Q_o)_{mea.}$/(V_T*h^2)	D/h	x/h	Fr=V_T/(g*h)^{0,5}
0.537	0.095	0.580	2.443	1.071	6.429	0.310
0.652	0.115	0.650	1.030	0.750	4.500	0.411
0.768	0.136	0.661	0.502	0.556	3.333	0.476
0.851	0.150	0.891	0.431	0.462	2.769	0.521
0.959	0.169	0.886	0.256	0.375	2.250	0.585
1.029	0.182	0.961	0.206	0.333	2.000	0.632

Table A.18: Experimental results related to circular orifice C2 for θ=0°

Experiment no	h (cm)	Q_T (lt/sec)	t (sec)	V (lt)	$(Q_o)_{mea.}$ (lt/s)	D (m)	A_T =h*w (m^2)	V_T=Q_T /A_T (m/s)	A_o =(π*D^2)/4 (m^2)
1	1.35	0.436	64.47	4.000	0.062	0.015	0.004	0.108	0.00018
2	2.00	1.092	48.82	4.000	0.082	0.015	0.006	0.182	0.00018
3	2.70	1.986	41.30	4.000	0.097	0.015	0.008	0.245	0.00018
4	3.25	2.869	43.45	6.000	0.138	0.015	0.010	0.294	0.00018
5	4.00	4.398	39.51	6.000	0.152	0.015	0.012	0.367	0.00018
6	4.50	5.666	44.28	8.000	0.181	0.015	0.014	0.420	0.00018

V_o =(2g(h+V_T^2/2g))^{0,5} (m/s)	$(Q_o)_{the.}$=A_0*V_0 (lt/s)	C_D=$(Q_o)_{mea.}$/$(Q_o)_{the.}$	K=$(Q_o)_{mea.}$/(V_T*h^2)	D/h	x/h	Fr=V_T/(g*h)^{0,5}
0.526	0.093	0.668	3.162	1.111	11.111	0.296
0.652	0.115	0.711	1.125	0.750	7.500	0.411
0.768	0.136	0.714	0.542	0.556	5.556	0.476
0.851	0.150	0.918	0.444	0.462	4.615	0.521
0.959	0.169	0.896	0.259	0.375	3.750	0.585
1.029	0.182	0.993	0.213	0.333	3.333	0.632

Table A.19: Experimental results related to circular orifice D2 for θ=0°

Experiment no	h (cm)	Q_T (lt/sec)	t (sec)	V (lt)	$(Q_o)_{mea.}$ (lt/s)	D (m)	$A_T = h*w$ (m^2)	$V_T = Q_T / A_T$ (m/s)	$A_o = (\pi * D^2)/4$ (m^2)
1	1.35	0.436	60.01	4.000	0.067	0.015	0.004	0.108	0.00018
2	1.95	1.037	46.22	4.000	0.087	0.015	0.006	0.177	0.00018
3	2.70	1.986	41.01	4.000	0.098	0.015	0.008	0.245	0.00018
4	3.25	2.869	41.52	6.000	0.145	0.015	0.010	0.294	0.00018
5	4.00	4.398	38.15	6.000	0.157	0.015	0.012	0.367	0.00018
6	4.50	5.666	43.51	8.000	0.184	0.015	0.014	0.420	0.00018

$V_o = (2g(h+V_T^2/2g))^{0,5}$ (m/s)	$(Q_o)_{the.} = A_0 * V_0$ (lt/s)	$C_D = (Q_o)_{mea.}/(Q_o)_{the.}$	$K = (Q_o)_{mea.}/(V_T * h^2)$	D/h	x/h	$Fr = V_T/(g*h)^{0,5}$
0.526	0.093	0.717	3.397	1.111	15.556	0.296
0.643	0.114	0.761	1.284	0.769	10.769	0.405
0.768	0.136	0.719	0.546	0.556	7.778	0.476
0.851	0.150	0.961	0.465	0.462	6.462	0.521
0.959	0.169	0.928	0.268	0.375	5.250	0.585
1.029	0.182	1.011	0.216	0.333	4.667	0.632

Table A.20: Experimental results related to circular orifice E2 for θ=0°

Experiment no	h (cm)	Q_T (lt/sec)	t (sec)	V (lt)	$(Q_o)_{mea.}$ (lt/s)	D (m)	$A_T = h*w$ (m^2)	$V_T = Q_T / A_T$ (m/s)	$A_o = (\pi * D^2)/4$ (m^2)
1	1.35	0.436	57.12	4.000	0.070	0.015	0.004	0.108	0.00018
2	1.95	1.037	45.94	4.000	0.087	0.015	0.006	0.177	0.00018
3	2.65	1.914	39.58	4.000	0.101	0.015	0.008	0.241	0.00018
4	3.20	2.781	40.05	6.000	0.150	0.015	0.010	0.290	0.00018
5	4.00	4.398	37.40	6.000	0.160	0.015	0.012	0.367	0.00018
6	4.50	5.666	42.37	8.000	0.189	0.015	0.014	0.420	0.00018

$V_o = (2g(h+V_T^2/2g))^{0,5}$ (m/s)	$(Q_o)_{the.} = A_0 * V_0$ (lt/s)	$C_D = (Q_o)_{mea.}/(Q_o)_{the.}$	$K = (Q_o)_{mea.}/(V_T * h^2)$	D/h	x/h	$Fr = V_T/(g*h)^{0,5}$
0.526	0.093	0.754	3.569	1.111	20.000	0.296
0.643	0.114	0.766	1.292	0.769	13.846	0.405
0.760	0.134	0.752	0.598	0.566	10.189	0.472
0.844	0.149	1.005	0.505	0.469	8.438	0.517
0.959	0.169	0.947	0.274	0.375	6.750	0.585
1.029	0.182	1.038	0.222	0.333	6.000	0.632

Table A.21: Experimental results related to circular orifice A1 for θ=0°

Experiment no	h (cm)	Q_T (lt/sec)	t (sec)	V (lt)	$(Q_o)_{mea.}$ (lt/s)	D (m)	A_T =h*w (m^2)	$V_T=Q_T/A_T$ (m/s)	$A_o=(\pi*D^2)/4$ (m^2)
1	1.40	0.482	86.56	3.000	0.035	0.010	0.004	0.115	0.00008
2	2.05	1.149	63.01	3.000	0.048	0.010	0.006	0.187	0.00008
3	2.75	2.059	58.16	3.000	0.052	0.010	0.008	0.250	0.00008
4	3.30	2.958	54.21	4.000	0.074	0.010	0.010	0.299	0.00008
5	4.05	4.516	40.62	4.000	0.098	0.010	0.012	0.372	0.00008
6	4.50	5.666	50.87	6.000	0.118	0.010	0.014	0.420	0.00008

$V_o=(2g(h+V_T^2/2g))^{0,5}$ (m/s)	$(Q_o)_{the.}=A_0*V_0$ (lt/s)	$C_D=(Q_o)_{mea.}/(Q_o)_{the.}$	$K=(Q_o)_{mea.}/(V_T*h^2)$	D/h	x/h	$Fr=V_T/(g*h)^{0,5}$
0.537	0.042	0.822	1.541	0.714	2.143	0.310
0.661	0.052	0.917	0.606	0.488	1.463	0.417
0.776	0.061	0.847	0.273	0.364	1.091	0.481
0.858	0.067	1.095	0.227	0.303	0.909	0.525
0.966	0.076	1.298	0.162	0.247	0.741	0.590
1.029	0.081	1.459	0.139	0.222	0.667	0.632

Table A.22: Experimental results related to circular orifice B1 for θ=0°

Experiment no	h (cm)	Q_T (lt/sec)	t (sec)	V (lt)	$(Q_o)_{mea.}$ (lt/s)	D (m)	A_T =h*w (m^2)	$V_T=Q_T/A_T$ (m/s)	$A_o=(\pi*D^2)/4$ (m^2)
1	1.40	0.482	83.27	3.000	0.036	0.010	0.004	0.115	0.00008
2	2.00	1.092	60.62	3.000	0.049	0.010	0.006	0.182	0.00008
3	2.70	1.986	54.47	3.000	0.055	0.010	0.008	0.245	0.00008
4	3.30	2.958	53.01	4.000	0.075	0.010	0.010	0.299	0.00008
5	4.05	4.516	38.65	4.000	0.103	0.010	0.012	0.372	0.00008
6	4.50	5.666	47.50	6.000	0.126	0.010	0.014	0.420	0.00008

$V_o=(2g(h+V_T^2/2g))^{0,5}$ (m/s)	$(Q_o)_{the.}=A_0*V_0$ (lt/s)	$C_D=(Q_o)_{mea.}/(Q_o)_{the.}$	$K=(Q_o)_{mea.}/(V_T*h^2)$	D/h	x/h	$Fr=V_T/(g*h)^{0,5}$
0.537	0.042	0.855	1.602	0.714	6.429	0.310
0.652	0.051	0.966	0.680	0.500	4.500	0.411
0.768	0.060	0.913	0.308	0.370	3.333	0.476
0.858	0.067	1.119	0.232	0.303	2.727	0.525
0.966	0.076	1.364	0.170	0.247	2.222	0.590
1.029	0.081	1.563	0.149	0.222	2.000	0.632

Table A.23: Experimental results related to circular orifice C1 for θ=0°

Experiment no	h (cm)	Q_T (lt/sec)	t (sec)	V (lt)	$(Q_o)_{mea.}$ (lt/s)	D (m)	$A_T = h*w$ (m^2)	$V_T = Q_T / A_T$ (m/s)	$A_o = (\pi*D^2)/4$ (m^2)
1	1.40	0.482	80.53	3.000	0.037	0.010	0.004	0.115	0.00008
2	2.00	1.092	59.66	3.000	0.050	0.010	0.006	0.182	0.00008
3	2.70	1.986	51.53	3.000	0.058	0.010	0.008	0.245	0.00008
4	3.30	2.958	52.11	4.000	0.077	0.010	0.010	0.299	0.00008
5	4.05	4.516	37.97	4.000	0.105	0.010	0.012	0.372	0.00008
6	4.50	5.666	46.57	6.000	0.129	0.010	0.014	0.420	0.00008

$V_o = (2g(h+V_T^2/2g))^{0,5}$ (m/s)	$(Q_o)_{the.} = A_0*V_0$ (lt/s)	$C_D = (Q_o)_{mea.}/(Q_o)_{the.}$	$K = (Q_o)_{mea.}/(V_T*h^2)$	D/h	x/h	$Fr = V_T/(g*h)^{0,5}$
0.537	0.042	0.884	1.656	0.714	10.714	0.310
0.652	0.051	0.981	0.691	0.500	7.500	0.411
0.768	0.060	0.965	0.326	0.370	5.556	0.476
0.858	0.067	1.139	0.236	0.303	4.545	0.525
0.966	0.076	1.389	0.173	0.247	3.704	0.590
1.029	0.081	1.594	0.152	0.222	3.333	0.632

Table A.24: Experimental results related to circular orifice D1 for θ=0°

Experiment no	h (cm)	Q_T (lt/sec)	t (sec)	V (lt)	$(Q_o)_{mea.}$ (lt/s)	D (m)	$A_T = h*w$ (m^2)	$V_T = Q_T / A_T$ (m/s)	$A_o = (\pi*D^2)/4$ (m^2)
1	1.40	0.482	75.03	3.000	0.040	0.010	0.004	0.115	0.00008
2	2.00	1.092	57.37	3.000	0.052	0.010	0.006	0.182	0.00008
3	2.70	1.986	50.12	3.000	0.060	0.010	0.008	0.245	0.00008
4	3.30	2.958	50.96	4.000	0.078	0.010	0.010	0.299	0.00008
5	4.05	4.516	37.51	4.000	0.107	0.010	0.012	0.372	0.00008
6	4.50	5.666	46.28	6.000	0.130	0.010	0.014	0.420	0.00008

$V_o = (2g(h+V_T^2/2g))^{0,5}$ (m/s)	$(Q_o)_{the.} = A_0*V_0$ (lt/s)	$C_D = (Q_o)_{mea.}/(Q_o)_{the.}$	$K = (Q_o)_{mea.}/(V_T*h^2)$	D/h	x/h	$Fr = V_T/(g*h)^{0,5}$
0.537	0.042	0.949	1.778	0.714	15.000	0.310
0.652	0.051	1.021	0.718	0.500	10.500	0.411
0.768	0.060	0.992	0.335	0.370	7.778	0.476
0.858	0.067	1.164	0.241	0.303	6.364	0.525
0.966	0.076	1.406	0.175	0.247	5.185	0.590
1.029	0.081	1.604	0.153	0.222	4.667	0.632

Table A.25: Experimental results related to circular orifice E1 for θ=0°

Experiment no	h (cm)	Q_T (lt/sec)	t (sec)	V (lt)	$(Q_o)_{mea.}$ (lt/s)	D (m)	A_T =h*w (m^2)	V_T=Q_T /A_T (m/s)	A_o =(π*D^2)/4 (m^2)
1	1.40	0.482	73.85	3.000	0.041	0.010	0.004	0.115	0.00008
2	2.00	1.092	55.69	3.000	0.054	0.010	0.006	0.182	0.00008
3	2.70	1.986	49.69	3.000	0.060	0.010	0.008	0.245	0.00008
4	3.25	2.869	48.49	4.000	0.082	0.010	0.010	0.294	0.00008
5	4.05	4.516	36.97	4.000	0.108	0.010	0.012	0.372	0.00008
6	4.50	5.666	45.56	6.000	0.132	0.010	0.014	0.420	0.00008

V_o =(2g(h+V_T^2/2g))^{0,5} (m/s)	$(Q_o)_{the.}$=A_0*V_0 (lt/s)	C_D=$(Q_o)_{mea.}$/$(Q_o)_{the.}$	K=$(Q_o)_{mea.}$/(V_T*h^2)	D/h	x/h	Fr=V_T/(g*h)^{0,5}
0.537	0.042	0.964	1.806	0.714	19.286	0.310
0.652	0.051	1.051	0.740	0.500	13.500	0.411
0.768	0.060	1.001	0.338	0.370	10.000	0.476
0.851	0.067	1.234	0.265	0.308	8.308	0.521
0.966	0.076	1.426	0.177	0.247	6.667	0.590
1.029	0.081	1.629	0.155	0.222	6.000	0.632

Table A.26: Experimental results related to circular orifice A5 for θ=10°

Experiment no	h (cm)	Q_T (lt/sec)	t (sec)	V (lt)	$(Q_o)_{mea.}$ (lt/s)	D (m)	A_T =h*w (m^2)	V_T=Q_T /A_T (m/s)	A_o =(π*D^2)/4 (m^2)
1	1.30	0.391	32.53	4.000	0.123	0.040	0.004	0.100	0.00126
2	2.00	1.092	26.25	6.000	0.229	0.040	0.006	0.182	0.00126
3	2.70	1.986	27.16	8.000	0.295	0.040	0.008	0.245	0.00126
4	3.40	3.142	23.84	8.000	0.336	0.040	0.010	0.308	0.00126
5	3.90	4.170	28.50	10.000	0.351	0.040	0.012	0.356	0.00126
6	4.40	5.395	54.16	20.250	0.374	0.040	0.013	0.409	0.00126

V_o =(2g(h+V_T^2/2g))^{0,5} (m/s)	$(Q_o)_{the.}$=A_0*V_0 (lt/s)	C_D=$(Q_o)_{mea.}$/$(Q_o)_{the.}$	K=$(Q_o)_{mea.}$/(V_T*h^2)	D/h	x/h	Fr=V_T/(g*h)^{0,5}
0.515	0.647	0.190	7.257	3.077	2.308	0.281
0.652	0.820	0.279	3.140	2.000	1.500	0.411
0.768	0.965	0.305	1.648	1.481	1.111	0.476
0.873	1.097	0.306	0.942	1.176	0.882	0.533
0.945	1.187	0.296	0.647	1.026	0.769	0.576
1.015	1.276	0.293	0.473	0.909	0.682	0.622

Table A.27: Experimental results related to circular orifice B5 for θ=10°

Experiment no	h (cm)	Q_T (lt/sec)	t (sec)	V (lt)	$(Q_o)_{mea.}$ (lt/s)	D (m)	A_T =h*w (m^2)	V_T=Q_T /A_T (m/s)	A_o =(π*D^2)/4 (m^2)
1	1.30	0.391	31.66	4.000	0.126	0.040	0.004	0.100	0.00126
2	2.00	1.092	25.09	6.000	0.239	0.040	0.006	0.182	0.00126
3	2.70	1.986	25.65	8.000	0.312	0.040	0.008	0.245	0.00126
4	3.40	3.142	22.04	8.000	0.363	0.040	0.010	0.308	0.00126
5	3.90	4.170	26.35	10.000	0.380	0.040	0.012	0.356	0.00126
6	4.40	5.395	50.47	20.250	0.401	0.040	0.013	0.409	0.00126

V_o =(2g(h+V_T^2/2g))^{0,5} (m/s)	$(Q_o)_{the.}$=A_0*V_0 (lt/s)	C_D=$(Q_o)_{mea.}$/$(Q_o)_{the.}$	K=$(Q_o)_{mea.}$/(V_T*h^2)	D/h	x/h	Fr=V_T/(g*h)^{0,5}
0.515	0.647	0.195	7.457	3.077	6.923	0.281
0.652	0.820	0.292	3.285	2.000	4.500	0.411
0.768	0.965	0.323	1.745	1.481	3.333	0.476
0.873	1.097	0.331	1.019	1.176	2.647	0.533
0.945	1.187	0.320	0.700	1.026	2.308	0.576
1.015	1.276	0.315	0.507	0.909	2.045	0.622

Table A.28: Experimental results related to circular orifice C5 for θ=10°

Experiment no	h (cm)	Q_T (lt/sec)	t (sec)	V (lt)	$(Q_o)_{mea.}$ (lt/s)	D (m)	A_T =h*w (m^2)	V_T=Q_T /A_T (m/s)	A_o =(π*D^2)/4 (m^2)
1	1.30	0.391	29.08	4.000	0.138	0.040	0.004	0.100	0.00126
2	2.00	1.092	24.23	6.000	0.248	0.040	0.006	0.182	0.00126
3	2.70	1.986	24.84	8.000	0.322	0.040	0.008	0.245	0.00126
4	3.40	3.142	21.53	8.000	0.372	0.040	0.010	0.308	0.00126
5	3.90	4.170	25.44	10.000	0.393	0.040	0.012	0.356	0.00126
6	4.40	5.395	48.34	20.250	0.419	0.040	0.013	0.409	0.00126

V_o =(2g(h+V_T^2/2g))^{0,5} (m/s)	$(Q_o)_{the.}$=A_0*V_0 (lt/s)	C_D=$(Q_o)_{mea.}$/$(Q_o)_{the.}$	K=$(Q_o)_{mea.}$/(V_T*h^2)	D/h	x/h	Fr=V_T/(g*h)^{0,5}
0.515	0.647	0.213	8.118	3.077	11.538	0.281
0.652	0.820	0.302	3.401	2.000	7.500	0.411
0.768	0.965	0.334	1.802	1.481	5.556	0.476
0.873	1.097	0.339	1.043	1.176	4.412	0.533
0.945	1.187	0.331	0.725	1.026	3.846	0.576
1.015	1.276	0.328	0.529	0.909	3.409	0.622

Table A.29: Experimental results related to circular orifice D5 for θ=10°

Experiment no	h (cm)	Q_T (lt/sec)	t (sec)	V (lt)	$(Q_o)_{mea.}$ (lt/s)	D (m)	A_T =h*w (m^2)	V_T=Q_T /A_T (m/s)	A_o =(π*D^2)/4 (m^2)
1	1.30	0.391	28.87	4.000	0.139	0.040	0.004	0.100	0.00126
2	2.00	1.092	22.10	6.000	0.271	0.040	0.006	0.182	0.00126
3	2.70	1.986	23.00	8.000	0.348	0.040	0.008	0.245	0.00126
4	3.40	3.142	19.37	8.000	0.413	0.040	0.010	0.308	0.00126
5	3.90	4.170	22.96	10.000	0.436	0.040	0.012	0.356	0.00126
6	4.40	5.395	43.76	20.250	0.463	0.040	0.013	0.409	0.00126

V_o =(2g(h+V_T^2/2g))^{0,5} (m/s)	$(Q_o)_{the.}$=A_0*V_0 (lt/s)	C_D=$(Q_o)_{mea.}$/$(Q_o)_{the.}$	K=$(Q_o)_{mea.}$/(V_T*h^2)	D/h	x/h	Fr=V_T/(g*h)^{0,5}
0.515	0.647	0.214	8.177	3.077	16.154	0.281
0.652	0.820	0.331	3.729	2.000	10.500	0.411
0.768	0.965	0.360	1.946	1.481	7.778	0.476
0.873	1.097	0.377	1.160	1.176	6.176	0.533
0.945	1.187	0.367	0.803	1.026	5.385	0.576
1.015	1.276	0.363	0.585	0.909	4.773	0.622

Table A.30: Experimental results related to circular orifice E5 for θ=10°

Experiment no	h (cm)	Q_T (lt/sec)	t (sec)	V (lt)	$(Q_o)_{mea.}$ (lt/s)	D (m)	A_T =h*w (m^2)	V_T=Q_T /A_T (m/s)	A_o =(π*D^2)/4 (m^2)
1	1.30	0.391	27.38	4.000	0.146	0.040	0.004	0.100	0.00126
2	2.00	1.092	20.84	6.000	0.288	0.040	0.006	0.182	0.00126
3	2.70	1.986	20.28	8.000	0.394	0.040	0.008	0.245	0.00126
4	3.40	3.142	17.83	8.000	0.449	0.040	0.010	0.308	0.00126
5	3.90	4.170	20.65	10.000	0.484	0.040	0.012	0.356	0.00126
6	4.40	5.395	38.89	20.250	0.521	0.040	0.013	0.409	0.00126

V_o =(2g(h+V_T^2/2g))^{0,5} (m/s)	$(Q_o)_{the.}$=A_0*V_0 (lt/s)	C_D=$(Q_o)_{mea.}$/$(Q_o)_{the.}$	K=$(Q_o)_{mea.}$/(V_T*h^2)	D/h	x/h	Fr=V_T/(g*h)^{0,5}
0.515	0.647	0.226	8.622	3.077	20.769	0.281
0.652	0.820	0.351	3.955	2.000	13.500	0.411
0.768	0.965	0.409	2.207	1.481	10.000	0.476
0.873	1.097	0.409	1.260	1.176	7.941	0.533
0.945	1.187	0.408	0.893	1.026	6.923	0.576
1.015	1.276	0.408	0.658	0.909	6.136	0.622

Table A.31: Experimental results related to circular orifice A4 for θ=10°

Experiment no	h (cm)	Q_T (lt/sec)	t (sec)	V (lt)	$(Q_o)_{mea.}$ (lt/s)	D (m)	$A_T = h*w$ (m^2)	$V_T = Q_T / A_T$ (m/s)	$A_o = (\pi*D^2)/4$ (m^2)
1	1.30	0.391	38.20	4.000	0.105	0.030	0.004	0.100	0.00071
2	2.00	1.092	36.01	6.000	0.167	0.030	0.006	0.182	0.00071
3	2.70	1.986	41.25	8.000	0.194	0.030	0.008	0.245	0.00071
4	3.40	3.142	37.43	8.000	0.214	0.030	0.010	0.308	0.00071
5	3.90	4.170	43.34	10.000	0.231	0.030	0.012	0.356	0.00071
6	4.40	5.395	41.03	10.000	0.244	0.030	0.013	0.409	0.00071

$V_o = (2g(h+V_T^2/2g))^{0,5}$ (m/s)	$(Q_o)_{the.} = A_0*V_0$ (lt/s)	$C_D = (Q_o)_{mea.}/(Q_o)_{the.}$	$K = (Q_o)_{mea.}/(V_T*h^2)$	D/h	x/h	$Fr = V_T/(g*h)^{0,5}$
0.515	0.364	0.288	6.180	2.308	2.308	0.281
0.652	0.461	0.361	2.289	1.500	1.500	0.411
0.768	0.543	0.357	1.085	1.111	1.111	0.476
0.873	0.617	0.346	0.600	0.882	0.882	0.533
0.945	0.668	0.346	0.426	0.769	0.769	0.576
1.015	0.717	0.340	0.308	0.682	0.682	0.622

Table A.32: Experimental results related to circular orifice B4 for θ=10°

Experiment no	h (cm)	Q_T (lt/sec)	t (sec)	V (lt)	$(Q_o)_{mea.}$ (lt/s)	D (m)	$A_T = h*w$ (m^2)	$V_T = Q_T / A_T$ (m/s)	$A_o = (\pi*D^2)/4$ (m^2)
1	1.30	0.391	35.91	4.000	0.111	0.030	0.004	0.100	0.00071
2	2.00	1.092	35.41	6.000	0.169	0.030	0.006	0.182	0.00071
3	2.70	1.986	38.66	8.000	0.207	0.030	0.008	0.245	0.00071
4	3.40	3.142	35.61	8.000	0.225	0.030	0.010	0.308	0.00071
5	3.90	4.170	41.18	10.000	0.243	0.030	0.012	0.356	0.00071
6	4.40	5.395	37.42	10.000	0.267	0.030	0.013	0.409	0.00071

$V_o = (2g(h+V_T^2/2g))^{0,5}$ (m/s)	$(Q_o)_{the.} = A_0*V_0$ (lt/s)	$C_D = (Q_o)_{mea.}/(Q_o)_{the.}$	$K = (Q_o)_{mea.}/(V_T*h^2)$	D/h	x/h	$Fr = V_T/(g*h)^{0,5}$
0.515	0.364	0.306	6.574	2.308	6.923	0.281
0.652	0.461	0.367	2.328	1.500	4.500	0.411
0.768	0.543	0.381	1.158	1.111	3.333	0.476
0.873	0.617	0.364	0.631	0.882	2.647	0.533
0.945	0.668	0.364	0.448	0.769	2.308	0.576
1.015	0.717	0.372	0.338	0.682	2.045	0.622

Table A.33: Experimental results related to circular orifice C4 for θ=10°

Experiment no	h (cm)	Q_T (lt/sec)	t (sec)	V (lt)	$(Q_o)_{mea.}$ (lt/s)	D (m)	A_T =h*w (m^2)	V_T=Q_T /A_T (m/s)	A_o =(π*D^2)/4 (m^2)
1	1.30	0.391	34.92	4.000	0.115	0.030	0.004	0.100	0.00071
2	2.00	1.092	33.15	6.000	0.181	0.030	0.006	0.182	0.00071
3	2.70	1.986	37.42	8.000	0.214	0.030	0.008	0.245	0.00071
4	3.40	3.142	33.20	8.000	0.241	0.030	0.010	0.308	0.00071
5	3.90	4.170	39.20	10.000	0.255	0.030	0.012	0.356	0.00071
6	4.40	5.395	37.01	10.000	0.270	0.030	0.013	0.409	0.00071

V_o =(2g(h+V_T^2/2g))^{0,5} (m/s)	$(Q_o)_{the.}$=A_0*V_0 (lt/s)	C_D=$(Q_o)_{mea.}$/$(Q_o)_{the.}$	K=$(Q_o)_{mea.}$/(V_T*h^2)	D/h	x/h	Fr=V_T/(g*h)^{0,5}
0.515	0.364	0.315	6.761	2.308	11.538	0.281
0.652	0.461	0.393	2.486	1.500	7.500	0.411
0.768	0.543	0.394	1.196	1.111	5.556	0.476
0.873	0.617	0.391	0.677	0.882	4.412	0.533
0.945	0.668	0.382	0.471	0.769	3.846	0.576
1.015	0.717	0.377	0.341	0.682	3.409	0.622

Table A.34: Experimental results related to circular orifice D4 for θ=10°

Experiment no	h (cm)	Q_T (lt/sec)	t (sec)	V (lt)	$(Q_o)_{mea.}$ (lt/s)	D (m)	A_T =h*w (m^2)	V_T=Q_T /A_T (m/s)	A_o =(π*D^2)/4 (m^2)
1	1.30	0.391	34.22	4.000	0.117	0.030	0.004	0.100	0.00071
2	2.00	1.092	30.72	6.000	0.195	0.030	0.006	0.182	0.00071
3	2.70	1.986	34.91	8.000	0.229	0.030	0.008	0.245	0.00071
4	3.40	3.142	30.69	8.000	0.261	0.030	0.010	0.308	0.00071
5	3.90	4.170	36.12	10.000	0.277	0.030	0.012	0.356	0.00071
6	4.40	5.395	34.00	10.000	0.294	0.030	0.013	0.409	0.00071

V_o =(2g(h+V_T^2/2g))^{0,5} (m/s)	$(Q_o)_{the.}$=A_0*V_0 (lt/s)	C_D=$(Q_o)_{mea.}$/$(Q_o)_{the.}$	K=$(Q_o)_{mea.}$/(V_T*h^2)	D/h	x/h	Fr=V_T/(g*h)^{0,5}
0.515	0.364	0.321	6.899	2.308	16.154	0.281
0.652	0.461	0.424	2.683	1.500	10.500	0.411
0.768	0.543	0.422	1.282	1.111	7.778	0.476
0.873	0.617	0.422	0.732	0.882	6.176	0.533
0.945	0.668	0.415	0.511	0.769	5.385	0.576
1.015	0.717	0.410	0.372	0.682	4.773	0.622

Table A.35: Experimental results related to circular orifice E4 for θ=10°

Experiment no	h (cm)	Q_T (lt/sec)	t (sec)	V (lt)	$(Q_o)_{mea.}$ (lt/s)	D (m)	A_T =h*w (m^2)	V_T=Q_T /A_T (m/s)	A_o =(π*D^2)/4 (m^2)
1	1.30	0.391	33.21	4.000	0.120	0.030	0.004	0.100	0.00071
2	2.00	1.092	28.12	6.000	0.213	0.030	0.006	0.182	0.00071
3	2.70	1.986	32.03	8.000	0.250	0.030	0.008	0.245	0.00071
4	3.40	3.142	27.85	8.000	0.287	0.030	0.010	0.308	0.00071
5	3.90	4.170	33.00	10.000	0.303	0.030	0.012	0.356	0.00071
6	4.40	5.395	30.85	10.000	0.324	0.030	0.013	0.409	0.00071

V_o =(2g(h+V_T^2/2g))^{0,5} (m/s)	$(Q_o)_{the.}$=A_0*V_0 (lt/s)	C_D=$(Q_o)_{mea.}$/$(Q_o)_{the.}$	K=$(Q_o)_{mea.}$/(V_T*h^2)	D/h	x/h	Fr=V_T/(g*h)^{0,5}
0.515	0.364	0.331	7.109	2.308	20.769	0.281
0.652	0.461	0.463	2.931	1.500	13.500	0.411
0.768	0.543	0.460	1.397	1.111	10.000	0.476
0.873	0.617	0.466	0.807	0.882	7.941	0.533
0.945	0.668	0.454	0.559	0.769	6.923	0.576
1.015	0.717	0.452	0.410	0.682	6.136	0.622

Table A.36: Experimental results related to circular orifice A3 for θ=10°

Experiment no	h (cm)	Q_T (lt/sec)	t (sec)	V (lt)	$(Q_o)_{mea.}$ (lt/s)	D (m)	A_T =h*w (m^2)	V_T=Q_T /A_T (m/s)	A_o =(π*D^2)/4 (m^2)
1	1.30	0.391	35.30	3.000	0.085	0.020	0.004	0.100	0.00031
2	2.00	1.092	39.50	4.000	0.101	0.020	0.006	0.182	0.00031
3	2.70	1.986	49.45	6.000	0.121	0.020	0.008	0.245	0.00031
4	3.40	3.142	43.13	6.000	0.139	0.020	0.010	0.308	0.00031
5	3.90	4.170	54.22	8.000	0.148	0.020	0.012	0.356	0.00031
6	4.40	5.395	66.25	10.000	0.151	0.020	0.013	0.409	0.00031

V_o =(2g(h+V_T^2/2g))^{0,5} (m/s)	$(Q_o)_{the.}$=A_0*V_0 (lt/s)	C_D=$(Q_o)_{mea.}$/$(Q_o)_{the.}$	K=$(Q_o)_{mea.}$/(V_T*h^2)	D/h	x/h	Fr=V_T/(g*h)^{0,5}
0.515	0.162	0.525	5.016	1.538	2.308	0.281
0.652	0.205	0.494	1.391	1.000	1.500	0.411
0.768	0.241	0.503	0.679	0.741	1.111	0.476
0.873	0.274	0.507	0.391	0.588	0.882	0.533
0.945	0.297	0.497	0.272	0.513	0.769	0.576
1.015	0.319	0.473	0.191	0.455	0.682	0.622

Table A.37: Experimental results related to circular orifice B3 for θ=10°

Experiment no	h (cm)	Q_T (lt/sec)	t (sec)	V (lt)	$(Q_o)_{mea.}$ (lt/s)	D (m)	A_T =h*w (m^2)	V_T=Q_T /A_T (m/s)	A_o =(π*D^2)/4 (m^2)
1	1.30	0.391	35.22	3.000	0.085	0.020	0.004	0.100	0.00031
2	2.00	1.092	38.47	4.000	0.104	0.020	0.006	0.182	0.00031
3	2.70	1.986	46.65	6.000	0.129	0.020	0.008	0.245	0.00031
4	3.40	3.142	41.38	6.000	0.145	0.020	0.010	0.308	0.00031
5	3.90	4.170	51.10	8.000	0.157	0.020	0.012	0.356	0.00031
6	4.40	5.395	61.81	10.000	0.162	0.020	0.013	0.409	0.00031

V_o =(2g(h+V_T^2/2g))^{0,5} (m/s)	$(Q_o)_{the.}$=A_0*V_0 (lt/s)	C_D=$(Q_o)_{mea.}$/$(Q_o)_{the.}$	K=$(Q_o)_{mea.}$/(V_T*h^2)	D/h	x/h	Fr=V_T/(g*h)^{0,5}
0.515	0.162	0.527	5.027	1.538	6.923	0.281
0.652	0.205	0.507	1.428	1.000	4.500	0.411
0.768	0.241	0.533	0.720	0.741	3.333	0.476
0.873	0.274	0.529	0.407	0.588	2.647	0.533
0.945	0.297	0.528	0.289	0.513	2.308	0.576
1.015	0.319	0.507	0.204	0.455	2.045	0.622

Table A.38: Experimental results related to circular orifice C3 for θ=10°

Experiment no	h (cm)	Q_T (lt/sec)	t (sec)	V (lt)	$(Q_o)_{mea.}$ (lt/s)	D (m)	A_T =h*w (m^2)	V_T=Q_T /A_T (m/s)	A_o =(π*D^2)/4 (m^2)
1	1.30	0.391	33.45	3.000	0.090	0.020	0.004	0.100	0.00031
2	2.00	1.092	37.47	4.000	0.107	0.020	0.006	0.182	0.00031
3	2.70	1.986	43.72	6.000	0.137	0.020	0.008	0.245	0.00031
4	3.40	3.142	39.25	6.000	0.153	0.020	0.010	0.308	0.00031
5	3.90	4.170	48.58	8.000	0.165	0.020	0.012	0.356	0.00031
6	4.40	5.395	59.48	10.000	0.168	0.020	0.013	0.409	0.00031

V_o =(2g(h+V_T^2/2g))^{0,5} (m/s)	$(Q_o)_{the.}$=A_0*V_0 (lt/s)	C_D=$(Q_o)_{mea.}$/$(Q_o)_{the.}$	K=$(Q_o)_{mea.}$/(V_T*h^2)	D/h	x/h	Fr=V_T/(g*h)^{0,5}
0.515	0.162	0.554	5.293	1.538	11.538	0.281
0.652	0.205	0.521	1.466	1.000	7.500	0.411
0.768	0.241	0.569	0.768	0.741	5.556	0.476
0.873	0.274	0.557	0.429	0.588	4.412	0.533
0.945	0.297	0.555	0.304	0.513	3.846	0.576
1.015	0.319	0.527	0.212	0.455	3.409	0.622

Table A.39: Experimental results related to circular orifice D3 for θ=10°

Experiment no	h (cm)	Q_T (lt/sec)	t (sec)	V (lt)	$(Q_o)_{mea.}$ (lt/s)	D (m)	A_T =h*w (m^2)	V_T=Q_T /A_T (m/s)	A_o =(π*D^2)/4 (m^2)
1	1.30	0.391	33.25	3.000	0.090	0.020	0.004	0.100	0.00031
2	2.00	1.092	34.85	4.000	0.115	0.020	0.006	0.182	0.00031
3	2.70	1.986	41.67	6.000	0.144	0.020	0.008	0.245	0.00031
4	3.40	3.142	37.81	6.000	0.159	0.020	0.010	0.308	0.00031
5	3.90	4.170	47.22	8.000	0.169	0.020	0.012	0.356	0.00031
6	4.40	5.395	56.19	10.000	0.178	0.020	0.013	0.409	0.00031

V_o =(2g(h+V_T^2/2g))^{0,5} (m/s)	$(Q_o)_{the.}$=A_0*V_0 (lt/s)	C_D=$(Q_o)_{mea.}$/$(Q_o)_{the.}$	K=$(Q_o)_{mea.}$/(V_T*h^2)	D/h	x/h	Fr=V_T/(g*h)^{0,5}
0.515	0.162	0.558	5.325	1.538	16.154	0.281
0.652	0.205	0.560	1.577	1.000	10.500	0.411
0.768	0.241	0.597	0.806	0.741	7.778	0.476
0.873	0.274	0.579	0.446	0.588	6.176	0.533
0.945	0.297	0.571	0.313	0.513	5.385	0.576
1.015	0.319	0.558	0.225	0.455	4.773	0.622

Table A.40: Experimental results related to circular orifice E3 for θ=10°

Experiment no	h (cm)	Q_T (lt/sec)	t (sec)	V (lt)	$(Q_o)_{mea.}$ (lt/s)	D (m)	A_T =h*w (m^2)	V_T=Q_T /A_T (m/s)	A_o =(π*D^2)/4 (m^2)
1	1.30	0.391	30.98	3.000	0.097	0.020	0.004	0.100	0.00031
2	2.00	1.092	32.62	4.000	0.123	0.020	0.006	0.182	0.00031
3	2.70	1.986	38.37	6.000	0.156	0.020	0.008	0.245	0.00031
4	3.40	3.142	34.85	6.000	0.172	0.020	0.010	0.308	0.00031
5	3.90	4.170	43.68	8.000	0.183	0.020	0.012	0.356	0.00031
6	4.40	5.395	51.94	10.000	0.193	0.020	0.013	0.409	0.00031

V_o =(2g(h+V_T^2/2g))^{0,5} (m/s)	$(Q_o)_{the.}$=A_0*V_0 (lt/s)	C_D=$(Q_o)_{mea.}$/$(Q_o)_{the.}$	K=$(Q_o)_{mea.}$/(V_T*h^2)	D/h	x/h	Fr=V_T/(g*h)^{0,5}
0.515	0.162	0.599	5.715	1.538	20.769	0.281
0.652	0.205	0.598	1.684	1.000	13.500	0.411
0.768	0.241	0.648	0.875	0.741	10.000	0.476
0.873	0.274	0.628	0.483	0.588	7.941	0.533
0.945	0.297	0.617	0.338	0.513	6.923	0.576
1.015	0.319	0.604	0.243	0.455	6.136	0.622

Table A.41: Experimental results related to circular orifice A2 for θ=10°

Experiment no	h (cm)	Q_T (lt/sec)	t (sec)	V (lt)	$(Q_o)_{mea.}$ (lt/s)	D (m)	A_T =h*w (m^2)	V_T=Q_T /A_T (m/s)	A_o =(π*D^2)/4 (m^2)
1	1.30	0.391	42.97	3.000	0.070	0.015	0.004	0.100	0.00018
2	2.00	1.092	48.47	4.000	0.083	0.015	0.006	0.182	0.00018
3	2.70	1.986	39.13	4.000	0.102	0.015	0.008	0.245	0.00018
4	3.40	3.142	44.87	5.000	0.111	0.015	0.010	0.308	0.00018
5	3.90	4.170	53.40	6.000	0.112	0.015	0.012	0.356	0.00018
6	4.40	5.395	52.65	6.000	0.114	0.015	0.013	0.409	0.00018

V_o =(2g(h+V_T^2/2g))^{0,5} (m/s)	$(Q_o)_{the.}$=A_0*V_0 (lt/s)	C_D=$(Q_o)_{mea.}$/$(Q_o)_{the.}$	K=$(Q_o)_{mea.}$/(V_T*h^2)	D/h	x/h	Fr=V_T/(g*h)^{0,5}
0.515	0.091	0.767	4.121	1.154	2.308	0.281
0.652	0.115	0.716	1.134	0.750	1.500	0.411
0.768	0.136	0.753	0.572	0.556	1.111	0.476
0.873	0.154	0.722	0.313	0.441	0.882	0.533
0.945	0.167	0.673	0.207	0.385	0.769	0.576
1.015	0.179	0.635	0.144	0.341	0.682	0.622

Table A.42: Experimental results related to circular orifice B2 for θ=10°

Experiment no	h (cm)	Q_T (lt/sec)	t (sec)	V (lt)	$(Q_o)_{mea.}$ (lt/s)	D (m)	A_T =h*w (m^2)	V_T=Q_T /A_T (m/s)	A_o =(π*D^2)/4 (m^2)
1	1.30	0.391	41.50	3.000	0.072	0.015	0.004	0.100	0.00018
2	2.00	1.092	47.38	4.000	0.084	0.015	0.006	0.182	0.00018
3	2.70	1.986	38.39	4.000	0.104	0.015	0.008	0.245	0.00018
4	3.40	3.142	43.75	5.000	0.114	0.015	0.010	0.308	0.00018
5	3.90	4.170	51.06	6.000	0.118	0.015	0.012	0.356	0.00018
6	4.40	5.395	49.01	6.000	0.122	0.015	0.013	0.409	0.00018

V_o =(2g(h+V_T^2/2g))^{0,5} (m/s)	$(Q_o)_{the.}$=A_0*V_0 (lt/s)	C_D=$(Q_o)_{mea.}$/$(Q_o)_{the.}$	K=$(Q_o)_{mea.}$/(V_T*h^2)	D/h	x/h	Fr=V_T/(g*h)^{0,5}
0.515	0.091	0.794	4.267	1.154	6.923	0.281
0.652	0.115	0.732	1.160	0.750	4.500	0.411
0.768	0.136	0.768	0.583	0.556	3.333	0.476
0.873	0.154	0.741	0.321	0.441	2.647	0.533
0.945	0.167	0.704	0.217	0.385	2.308	0.576
1.015	0.179	0.683	0.155	0.341	2.045	0.622

Table A.43: Experimental results related to circular orifice C2 for θ=10°

Experiment no	h (cm)	Q_T (lt/sec)	t (sec)	V (lt)	$(Q_o)_{mea.}$ (lt/s)	D (m)	A_T =h*w (m^2)	V_T=Q_T /A_T (m/s)	A_o =(π*D^2)/4 (m^2)
1	1.30	0.391	39.78	3.000	0.075	0.015	0.004	0.100	0.00018
2	2.00	1.092	46.37	4.000	0.086	0.015	0.006	0.182	0.00018
3	2.70	1.986	37.40	4.000	0.107	0.015	0.008	0.245	0.00018
4	3.40	3.142	41.19	5.000	0.121	0.015	0.010	0.308	0.00018
5	3.90	4.170	48.12	6.000	0.125	0.015	0.012	0.356	0.00018
6	4.40	5.395	47.05	6.000	0.128	0.015	0.013	0.409	0.00018

V_o =(2g(h+V_T^2/2g))^{0,5} (m/s)	$(Q_o)_{the.}$=A_0*V_0 (lt/s)	C_D=$(Q_o)_{mea.}$/$(Q_o)_{the.}$	K=$(Q_o)_{mea.}$/(V_T*h^2)	D/h	x/h	Fr=V_T/(g*h)^{0,5}
0.515	0.091	0.829	4.451	1.154	11.538	0.281
0.652	0.115	0.748	1.185	0.750	7.500	0.411
0.768	0.136	0.788	0.598	0.556	5.556	0.476
0.873	0.154	0.787	0.341	0.441	4.412	0.533
0.945	0.167	0.747	0.230	0.385	3.846	0.576
1.015	0.179	0.711	0.161	0.341	3.409	0.622

Table A.44: Experimental results related to circular orifice D2 for θ=10°

Experiment no	h (cm)	Q_T (lt/sec)	t (sec)	V (lt)	$(Q_o)_{mea.}$ (lt/s)	D (m)	A_T =h*w (m^2)	V_T=Q_T /A_T (m/s)	A_o =(π*D^2)/4 (m^2)
1	1.30	0.391	39.13	3.000	0.077	0.015	0.004	0.100	0.00018
2	2.00	1.092	43.02	4.000	0.093	0.015	0.006	0.182	0.00018
3	2.70	1.986	35.97	4.000	0.111	0.015	0.008	0.245	0.00018
4	3.40	3.142	39.69	5.000	0.126	0.015	0.010	0.308	0.00018
5	3.90	4.170	45.19	6.000	0.133	0.015	0.012	0.356	0.00018
6	4.40	5.395	43.72	6.000	0.137	0.015	0.013	0.409	0.00018

V_o =(2g(h+V_T^2/2g))^{0,5} (m/s)	$(Q_o)_{the.}$=A_0*V_0 (lt/s)	C_D=$(Q_o)_{mea.}$/$(Q_o)_{the.}$	K=$(Q_o)_{mea.}$/(V_T*h^2)	D/h	x/h	Fr=V_T/(g*h)^{0,5}
0.515	0.091	0.843	4.525	1.154	16.154	0.281
0.652	0.115	0.807	1.277	0.750	10.500	0.411
0.768	0.136	0.819	0.622	0.556	7.778	0.476
0.873	0.154	0.817	0.354	0.441	6.176	0.533
0.945	0.167	0.795	0.245	0.385	5.385	0.576
1.015	0.179	0.765	0.173	0.341	4.773	0.622

Table A.45: Experimental results related to circular orifice E2 for θ=10°

Experiment no	h (cm)	Q_T (lt/sec)	t (sec)	V (lt)	$(Q_o)_{mea.}$ (lt/s)	D (m)	A_T =h*w (m^2)	V_T=Q_T /A_T (m/s)	A_o =(π*D^2)/4 (m^2)
1	1.30	0.391	37.98	3.000	0.079	0.015	0.004	0.100	0.00018
2	2.00	1.092	42.53	4.000	0.094	0.015	0.006	0.182	0.00018
3	2.70	1.986	34.41	4.000	0.116	0.015	0.008	0.245	0.00018
4	3.40	3.142	38.56	5.000	0.130	0.015	0.010	0.308	0.00018
5	3.90	4.170	43.10	6.000	0.139	0.015	0.012	0.356	0.00018
6	4.40	5.395	42.31	6.000	0.142	0.015	0.013	0.409	0.00018

V_o =(2g(h+V_T^2/2g))^{0,5} (m/s)	$(Q_o)_{the.}$=A_0*V_0 (lt/s)	C_D=$(Q_o)_{mea.}$/$(Q_o)_{the.}$	K=$(Q_o)_{mea.}$/(V_T*h^2)	D/h	x/h	Fr=V_T/(g*h)^{0,5}
0.515	0.091	0.868	4.662	1.154	20.769	0.281
0.652	0.115	0.816	1.292	0.750	13.500	0.411
0.768	0.136	0.857	0.650	0.556	10.000	0.476
0.873	0.154	0.841	0.364	0.441	7.941	0.533
0.945	0.167	0.834	0.257	0.385	6.923	0.576
1.015	0.179	0.791	0.179	0.341	6.136	0.622

Table A.46: Experimental results related to circular orifice A1 for θ=10°

Experiment no	h (cm)	Q_T (lt/sec)	t (sec)	V (lt)	$(Q_o)_{mea.}$ (lt/s)	D (m)	A_T =h*w (m^2)	V_T=Q_T /A_T (m/s)	A_o =(π*D^2)/4 (m^2)
1	1.30	0.391	47.75	3.000	0.063	0.010	0.004	0.100	0.00008
2	2.00	1.092	42.22	3.000	0.071	0.010	0.006	0.182	0.00008
3	2.70	1.986	33.31	3.000	0.090	0.010	0.008	0.245	0.00008
4	3.40	3.142	41.04	4.000	0.097	0.010	0.010	0.308	0.00008
5	3.90	4.170	41.44	4.000	0.097	0.010	0.012	0.356	0.00008
6	4.40	5.395	53.34	5.000	0.094	0.010	0.013	0.409	0.00008

V_o =(2g(h+V_T^2/2g))^{0,5} (m/s)	$(Q_o)_{the.}$=A_0*V_0 (lt/s)	C_D=$(Q_o)_{mea.}$/$(Q_o)_{the.}$	K=$(Q_o)_{mea.}$/(V_T*h^2)	D/h	x/h	Fr=V_T/(g*h)^{0,5}
0.515	0.040	1.554	3.708	0.769	2.308	0.281
0.652	0.051	1.387	0.976	0.500	1.500	0.411
0.768	0.060	1.493	0.504	0.370	1.111	0.476
0.873	0.069	1.422	0.274	0.294	0.882	0.533
0.945	0.074	1.301	0.178	0.256	0.769	0.576
1.015	0.080	1.176	0.118	0.227	0.682	0.622

Table A.47: Experimental results related to circular orifice B1 for θ=10°

Experiment no	h (cm)	Q_T (lt/sec)	t (sec)	V (lt)	$(Q_o)_{mea.}$ (lt/s)	D (m)	$A_T = h*w$ (m^2)	$V_T = Q_T / A_T$ (m/s)	$A_o = (\pi*D^2)/4$ (m^2)
1	1.30	0.391	48.56	3.000	0.062	0.010	0.004	0.100	0.00008
2	2.00	1.092	42.47	3.000	0.071	0.010	0.006	0.182	0.00008
3	2.70	1.986	32.38	3.000	0.093	0.010	0.008	0.245	0.00008
4	3.40	3.142	41.06	4.000	0.097	0.010	0.010	0.308	0.00008
5	3.90	4.170	41.37	4.000	0.097	0.010	0.012	0.356	0.00008
6	4.40	5.395	52.44	5.000	0.095	0.010	0.013	0.409	0.00008

$V_o = (2g(h+V_T^2/2g))^{0,5}$ (m/s)	$(Q_o)_{the.} = A_0*V_0$ (lt/s)	$C_D = (Q_o)_{mea.}/(Q_o)_{the.}$	$K = (Q_o)_{mea.}/(V_T*h^2)$	D/h	x/h	$Fr = V_T/(g*h)^{0,5}$
0.515	0.040	1.528	3.646	0.769	6.923	0.281
0.652	0.051	1.379	0.970	0.500	4.500	0.411
0.768	0.060	1.536	0.518	0.370	3.333	0.476
0.873	0.069	1.421	0.274	0.294	2.647	0.533
0.945	0.074	1.303	0.178	0.256	2.308	0.576
1.015	0.080	1.196	0.120	0.227	2.045	0.622

Table A.48: Experimental results related to circular orifice C1 for θ=10°

Experiment no	h (cm)	Q_T (lt/sec)	t (sec)	V (lt)	$(Q_o)_{mea.}$ (lt/s)	D (m)	$A_T = h*w$ (m^2)	$V_T = Q_T / A_T$ (m/s)	$A_o = (\pi*D^2)/4$ (m^2)
1	1.30	0.391	47.19	3.000	0.064	0.010	0.004	0.100	0.00008
2	2.00	1.092	42.13	3.000	0.071	0.010	0.006	0.182	0.00008
3	2.70	1.986	32.15	3.000	0.093	0.010	0.008	0.245	0.00008
4	3.40	3.142	39.56	4.000	0.101	0.010	0.010	0.308	0.00008
5	3.90	4.170	40.31	4.000	0.099	0.010	0.012	0.356	0.00008
6	4.40	5.395	50.86	5.000	0.098	0.010	0.013	0.409	0.00008

$V_o = (2g(h+V_T^2/2g))^{0,5}$ (m/s)	$(Q_o)_{the.} = A_0*V_0$ (lt/s)	$C_D = (Q_o)_{mea.}/(Q_o)_{the.}$	$K = (Q_o)_{mea.}/(V_T*h^2)$	D/h	x/h	$Fr = V_T/(g*h)^{0,5}$
0.515	0.040	1.572	3.752	0.769	11.538	0.281
0.652	0.051	1.390	0.978	0.500	7.500	0.411
0.768	0.060	1.547	0.522	0.370	5.556	0.476
0.873	0.069	1.475	0.284	0.294	4.412	0.533
0.945	0.074	1.338	0.183	0.256	3.846	0.576
1.015	0.080	1.233	0.124	0.227	3.409	0.622

Table A.49: Experimental results related to circular orifice D1 for θ=10°

Experiment no	h (cm)	Q_T (lt/sec)	t (sec)	V (lt)	$(Q_o)_{mea.}$ (lt/s)	D (m)	A_T =h*w (m^2)	V_T=Q_T /A_T (m/s)	A_o =(π*D^2)/4 (m^2)
1	1.30	0.391	45.94	3.000	0.065	0.010	0.004	0.100	0.00008
2	2.00	1.092	41.75	3.000	0.072	0.010	0.006	0.182	0.00008
3	2.70	1.986	31.48	3.000	0.095	0.010	0.008	0.245	0.00008
4	3.40	3.142	38.40	4.000	0.104	0.010	0.010	0.308	0.00008
5	3.90	4.170	38.90	4.000	0.103	0.010	0.012	0.356	0.00008
6	4.40	5.395	50.25	5.000	0.100	0.010	0.013	0.409	0.00008

V_o =(2g(h+V_T^2/2g))^{0,5} (m/s)	$(Q_o)_{the.}$=A_0*V_0 (lt/s)	C_D=$(Q_o)_{mea.}$/$(Q_o)_{the.}$	K=$(Q_o)_{mea.}$/(V_T*h^2)	D/h	x/h	Fr=V_T/(g*h)^{0,5}
0.515	0.040	1.615	3.854	0.769	16.154	0.281
0.652	0.051	1.403	0.987	0.500	10.500	0.411
0.768	0.060	1.580	0.533	0.370	7.778	0.476
0.873	0.069	1.519	0.293	0.294	6.176	0.533
0.945	0.074	1.386	0.190	0.256	5.385	0.576
1.015	0.080	1.248	0.126	0.227	4.773	0.622

Table A.50: Experimental results related to circular orifice E1 for θ=10°

Experiment no	h (cm)	Q_T (lt/sec)	t (sec)	V (lt)	$(Q_o)_{mea.}$ (lt/s)	D (m)	A_T =h*w (m^2)	V_T=Q_T /A_T (m/s)	A_o =(π*D^2)/4 (m^2)
1	1.30	0.391	45.20	3.000	0.066	0.010	0.004	0.100	0.00008
2	2.00	1.092	39.30	3.000	0.076	0.010	0.006	0.182	0.00008
3	2.70	1.986	30.30	3.000	0.099	0.010	0.008	0.245	0.00008
4	3.40	3.142	37.69	4.000	0.106	0.010	0.010	0.308	0.00008
5	3.90	4.170	38.41	4.000	0.104	0.010	0.012	0.356	0.00008
6	4.40	5.395	48.25	5.000	0.104	0.010	0.013	0.409	0.00008

V_o =(2g(h+V_T^2/2g))^{0,5} (m/s)	$(Q_o)_{the.}$=A_0*V_0 (lt/s)	C_D=$(Q_o)_{mea.}$/$(Q_o)_{the.}$	K=$(Q_o)_{mea.}$/(V_T*h^2)	D/h	x/h	Fr=V_T/(g*h)^{0,5}
0.515	0.040	1.641	3.917	0.769	20.769	0.281
0.652	0.051	1.490	1.049	0.500	13.500	0.411
0.768	0.060	1.641	0.554	0.370	10.000	0.476
0.873	0.069	1.548	0.298	0.294	7.941	0.533
0.945	0.074	1.404	0.192	0.256	6.923	0.576
1.015	0.080	1.300	0.131	0.227	6.136	0.622

Table A.51: Experimental results related to circular orifice A5 for θ=20°

Experiment no	h (cm)	Q_T (lt/sec)	t (sec)	V (lt)	$(Q_o)_{mea.}$ (lt/s)	D (m)	$A_T = h*w$ (m^2)	$V_T = Q_T / A_T$ (m/s)	$A_o = (\pi*D^2)/4$ (m^2)
1	1.30	0.391	42.52	4.000	0.094	0.040	0.004	0.100	0.00126
2	2.00	1.092	38.84	6.000	0.154	0.040	0.006	0.182	0.00126
3	2.70	1.986	29.63	6.000	0.202	0.040	0.008	0.245	0.00126
4	3.40	3.142	37.30	8.000	0.214	0.040	0.010	0.308	0.00126
5	3.90	4.170	42.00	10.000	0.238	0.040	0.012	0.356	0.00126
6	4.50	5.666	40.59	10.000	0.246	0.040	0.014	0.420	0.00126

$V_o = (2g(h+V_T^2/2g))^{0,5}$ (m/s)	$(Q_o)_{the.} = A_0*V_0$ (lt/s)	$C_D = (Q_o)_{mea.}/(Q_o)_{the.}$	$K = (Q_o)_{mea.}/(V_T*h^2)$	D/h	x/h	$Fr = V_T/(g*h)^{0,5}$
0.265	0.333	0.282	5.552	3.077	2.308	0.281
0.426	0.535	0.289	2.122	2.000	1.500	0.411
0.590	0.741	0.273	1.133	1.481	1.111	0.476
0.762	0.958	0.224	0.602	1.176	0.882	0.533
0.892	1.121	0.212	0.439	1.026	0.769	0.576
1.059	1.331	0.185	0.290	0.889	0.667	0.632

Table A.52: Experimental results related to circular orifice B5 for θ=20°

Experiment no	h (cm)	Q_T (lt/sec)	t (sec)	V (lt)	$(Q_o)_{mea.}$ (lt/s)	D (m)	$A_T = h*w$ (m^2)	$V_T = Q_T / A_T$ (m/s)	$A_o = (\pi*D^2)/4$ (m^2)
1	1.30	0.391	38.05	4.000	0.105	0.040	0.004	0.100	0.00126
2	2.00	1.092	36.94	6.000	0.162	0.040	0.006	0.182	0.00126
3	2.70	1.986	28.95	6.000	0.207	0.040	0.008	0.245	0.00126
4	3.40	3.142	35.19	8.000	0.227	0.040	0.010	0.308	0.00126
5	3.90	4.170	36.53	10.000	0.274	0.040	0.012	0.356	0.00126
6	4.50	5.666	35.53	10.000	0.281	0.040	0.014	0.420	0.00126

$V_o = (2g(h+V_T^2/2g))^{0,5}$ (m/s)	$(Q_o)_{the.} = A_0*V_0$ (lt/s)	$C_D = (Q_o)_{mea.}/(Q_o)_{the.}$	$K = (Q_o)_{mea.}/(V_T*h^2)$	D/h	x/h	$Fr = V_T/(g*h)^{0,5}$
0.265	0.333	0.316	6.204	3.077	6.923	0.281
0.426	0.535	0.304	2.231	2.000	4.500	0.411
0.590	0.741	0.280	1.160	1.481	3.333	0.476
0.762	0.958	0.237	0.638	1.176	2.647	0.533
0.892	1.121	0.244	0.505	1.026	2.308	0.576
1.059	1.331	0.211	0.331	0.889	2.000	0.632

Table A.53: Experimental results related to circular orifice C5 for θ=20°

Experiment no	h (cm)	Q_T (lt/sec)	t (sec)	V (lt)	$(Q_o)_{mea.}$ (lt/s)	D (m)	A_T =h*w (m^2)	V_T=Q_T /A_T (m/s)	A_o =(π*D^2)/4 (m^2)
1	1.30	0.391	36.61	4.000	0.109	0.040	0.004	0.100	0.00126
2	2.00	1.092	35.61	6.000	0.168	0.040	0.006	0.182	0.00126
3	2.70	1.986	28.41	6.000	0.211	0.040	0.008	0.245	0.00126
4	3.40	3.142	33.47	8.000	0.239	0.040	0.010	0.308	0.00126
5	3.90	4.170	37.11	10.000	0.269	0.040	0.012	0.356	0.00126
6	4.50	5.666	33.50	10.000	0.299	0.040	0.014	0.420	0.00126

V_o =(2g(h+V_T^2/2g))^{0,5} (m/s)	$(Q_o)_{the.}$=A_0*V_0 (lt/s)	C_D=$(Q_o)_{mea.}$/$(Q_o)_{the.}$	K=$(Q_o)_{mea.}$/(V_T*h^2)	D/h	x/h	Fr=V_T/(g*h)^{0,5}
0.265	0.333	0.328	6.449	3.077	11.538	0.281
0.426	0.535	0.315	2.314	2.000	7.500	0.411
0.590	0.741	0.285	1.182	1.481	5.556	0.476
0.762	0.958	0.250	0.671	1.176	4.412	0.533
0.892	1.121	0.240	0.497	1.026	3.846	0.576
1.059	1.331	0.224	0.351	0.889	3.333	0.632

Table A.54: Experimental results related to circular orifice D5 for θ=20°

Experiment no	h (cm)	Q_T (lt/sec)	t (sec)	V (lt)	$(Q_o)_{mea.}$ (lt/s)	D (m)	A_T =h*w (m^2)	V_T=Q_T /A_T (m/s)	A_o =(π*D^2)/4 (m^2)
1	1.30	0.391	36.05	4.000	0.111	0.040	0.004	0.100	0.00126
2	2.00	1.092	29.97	6.000	0.200	0.040	0.006	0.182	0.00126
3	2.70	1.986	23.22	6.000	0.258	0.040	0.008	0.245	0.00126
4	3.40	3.142	27.51	8.000	0.291	0.040	0.010	0.308	0.00126
5	3.90	4.170	32.34	10.000	0.309	0.040	0.012	0.356	0.00126
6	4.50	5.666	28.76	10.000	0.348	0.040	0.014	0.420	0.00126

V_o =(2g(h+V_T^2/2g))^{0,5} (m/s)	$(Q_o)_{the.}$=A_0*V_0 (lt/s)	C_D=$(Q_o)_{mea.}$/$(Q_o)_{the.}$	K=$(Q_o)_{mea.}$/(V_T*h^2)	D/h	x/h	Fr=V_T/(g*h)^{0,5}
0.265	0.333	0.333	6.549	3.077	16.154	0.281
0.426	0.535	0.374	2.750	2.000	10.500	0.411
0.590	0.741	0.349	1.446	1.481	7.778	0.476
0.762	0.958	0.304	0.817	1.176	6.176	0.533
0.892	1.121	0.276	0.570	1.026	5.385	0.576
1.059	1.331	0.261	0.409	0.889	4.667	0.632

Table A.55: Experimental results related to circular orifice E5 for θ=20°

Experiment no	h (cm)	Q_T (lt/sec)	t (sec)	V (lt)	$(Q_o)_{mea.}$ (lt/s)	D (m)	A_T =h*w (m^2)	V_T=Q_T /A_T (m/s)	A_o =(π*D^2)/4 (m^2)
1	1.30	0.391	35.00	4.000	0.114	0.040	0.004	0.100	0.00126
2	2.00	1.092	26.43	6.000	0.227	0.040	0.006	0.182	0.00126
3	2.70	1.986	20.62	6.000	0.291	0.040	0.008	0.245	0.00126
4	3.40	3.142	23.78	8.000	0.336	0.040	0.010	0.308	0.00126
5	3.90	4.170	27.16	10.000	0.368	0.040	0.012	0.356	0.00126
6	4.50	5.666	24.48	10.000	0.408	0.040	0.014	0.420	0.00126

V_o =(2g(h+V_T^2/2g))^{0,5} (m/s)	$(Q_o)_{the.}$=A_0*V_0 (lt/s)	C_D=$(Q_o)_{mea.}$/$(Q_o)_{the.}$	K=$(Q_o)_{mea.}$/(V_T*h^2)	D/h	x/h	Fr=V_T/(g*h)^{0,5}
0.265	0.333	0.343	6.745	3.077	20.769	0.281
0.426	0.535	0.425	3.118	2.000	13.500	0.411
0.590	0.741	0.393	1.628	1.481	10.000	0.476
0.762	0.958	0.351	0.945	1.176	7.941	0.533
0.892	1.121	0.328	0.679	1.026	6.923	0.576
1.059	1.331	0.307	0.481	0.889	6.000	0.632

Table A.56: Experimental results related to circular orifice A4 for θ=20°

Experiment no	h (cm)	Q_T (lt/sec)	t (sec)	V (lt)	$(Q_o)_{mea.}$ (lt/s)	D (m)	A_T =h*w (m^2)	V_T=Q_T /A_T (m/s)	A_o =(π*D^2)/4 (m^2)
1	1.30	0.391	50.48	4.000	0.079	0.030	0.004	0.100	0.00071
2	2.00	1.092	61.14	6.000	0.098	0.030	0.006	0.182	0.00071
3	2.70	1.986	53.07	6.000	0.113	0.030	0.008	0.245	0.00071
4	3.40	3.142	62.00	8.000	0.129	0.030	0.010	0.308	0.00071
5	3.90	4.170	75.66	10.000	0.132	0.030	0.012	0.356	0.00071
6	4.50	5.666	66.35	10.000	0.151	0.030	0.014	0.420	0.00071

V_o =(2g(h+V_T^2/2g))^{0,5} (m/s)	$(Q_o)_{the.}$=A_0*V_0 (lt/s)	C_D=$(Q_o)_{mea.}$/$(Q_o)_{the.}$	K=$(Q_o)_{mea.}$/(V_T*h^2)	D/h	x/h	Fr=V_T/(g*h)^{0,5}
0.265	0.187	0.423	4.677	2.308	2.308	0.281
0.426	0.301	0.326	1.348	1.500	1.500	0.411
0.590	0.417	0.271	0.633	1.111	1.111	0.476
0.762	0.539	0.240	0.362	0.882	0.882	0.533
0.892	0.631	0.210	0.244	0.769	0.769	0.576
1.059	0.749	0.201	0.177	0.667	0.667	0.632

Table A.57: Experimental results related to circular orifice B4 for θ=20°

Experiment no	h (cm)	Q_T (lt/sec)	t (sec)	V (lt)	$(Q_o)_{mea.}$ (lt/s)	D (m)	A_T =h*w (m^2)	V_T=Q_T /A_T (m/s)	A_o =(π*D^2)/4 (m^2)
1	1.30	0.391	48.75	4.000	0.082	0.030	0.004	0.100	0.00071
2	2.00	1.092	59.03	6.000	0.102	0.030	0.006	0.182	0.00071
3	2.70	1.986	49.46	6.000	0.121	0.030	0.008	0.245	0.00071
4	3.40	3.142	58.33	8.000	0.137	0.030	0.010	0.308	0.00071
5	3.90	4.170	68.95	10.000	0.145	0.030	0.012	0.356	0.00071
6	4.50	5.666	59.13	10.000	0.169	0.030	0.013	0.409	0.00071

V_o =(2g(h+V_T^2/2g))^{0,5} (m/s)	$(Q_o)_{the.}$=A_0*V_0 (lt/s)	C_D=$(Q_o)_{mea.}$/$(Q_o)_{the.}$	K=$(Q_o)_{mea.}$/(V_T*h^2)	D/h	x/h	Fr=V_T/(g*h)^{0,5}
0.265	0.187	0.438	4.843	2.308	6.923	0.281
0.426	0.301	0.338	1.396	1.500	4.500	0.411
0.590	0.417	0.291	0.679	1.111	3.333	0.476
0.762	0.539	0.255	0.385	0.882	2.647	0.533
0.892	0.631	0.230	0.268	0.769	2.308	0.576
1.030	0.728	0.232	0.214	0.682	2.045	0.622

Table A.58: Experimental results related to circular orifice C4 for θ=20°

Experiment no	h (cm)	Q_T (lt/sec)	t (sec)	V (lt)	$(Q_o)_{mea.}$ (lt/s)	D (m)	A_T =h*w (m^2)	V_T=Q_T /A_T (m/s)	A_o =(π*D^2)/4 (m^2)
1	1.30	0.391	47.26	4.000	0.085	0.030	0.004	0.100	0.00071
2	2.00	1.092	54.02	6.000	0.111	0.030	0.006	0.182	0.00071
3	2.70	1.986	47.69	6.000	0.126	0.030	0.008	0.245	0.00071
4	3.40	3.142	53.42	8.000	0.150	0.030	0.010	0.308	0.00071
5	3.90	4.170	66.63	10.000	0.150	0.030	0.012	0.356	0.00071
6	4.50	5.666	55.31	10.000	0.181	0.030	0.014	0.420	0.00071

V_o =(2g(h+V_T^2/2g))^{0,5} (m/s)	$(Q_o)_{the.}$=A_0*V_0 (lt/s)	C_D=$(Q_o)_{mea.}$/$(Q_o)_{the.}$	K=$(Q_o)_{mea.}$/(V_T*h^2)	D/h	x/h	Fr=V_T/(g*h)^{0,5}
0.265	0.187	0.452	4.995	2.308	11.538	0.281
0.426	0.301	0.369	1.526	1.500	7.500	0.411
0.590	0.417	0.302	0.704	1.111	5.556	0.476
0.762	0.539	0.278	0.421	0.882	4.412	0.533
0.892	0.631	0.238	0.277	0.769	3.846	0.576
1.059	0.749	0.242	0.213	0.667	3.333	0.632

Table A.59: Experimental results related to circular orifice D4 for θ=20°

Experiment no	h (cm)	Q_T (lt/sec)	t (sec)	V (lt)	$(Q_o)_{mea.}$ (lt/s)	D (m)	A_T =h*w (m^2)	V_T=Q_T /A_T (m/s)	A_o =(π*D^2)/4 (m^2)
1	1.30	0.391	44.21	4.000	0.090	0.030	0.004	0.100	0.00071
2	2.00	1.092	47.88	6.000	0.125	0.030	0.006	0.182	0.00071
3	2.70	1.986	41.35	6.000	0.145	0.030	0.008	0.245	0.00071
4	3.40	3.142	48.59	8.000	0.165	0.030	0.010	0.308	0.00071
5	3.90	4.170	56.34	10.000	0.177	0.030	0.012	0.356	0.00071
6	4.50	5.666	49.34	10.000	0.203	0.030	0.014	0.420	0.00071

V_o =(2g(h+V_T^2/2g))^{0,5} (m/s)	$(Q_o)_{the.}$=A_0*V_0 (lt/s)	C_D=$(Q_o)_{mea.}$/$(Q_o)_{the.}$	K=$(Q_o)_{mea.}$/(V_T*h^2)	D/h	x/h	Fr=V_T/(g*h)^{0,5}
0.265	0.187	0.483	5.340	2.308	16.154	0.281
0.426	0.301	0.417	1.721	1.500	10.500	0.411
0.590	0.417	0.348	0.812	1.111	7.778	0.476
0.762	0.539	0.306	0.462	0.882	6.176	0.533
0.892	0.631	0.281	0.327	0.769	5.385	0.576
1.059	0.749	0.271	0.238	0.667	4.667	0.632

Table A.60: Experimental results related to circular orifice E4 for θ=20°

Experiment no	h (cm)	Q_T (lt/sec)	t (sec)	V (lt)	$(Q_o)_{mea.}$ (lt/s)	D (m)	A_T =h*w (m^2)	V_T=Q_T /A_T (m/s)	A_o =(π*D^2)/4 (m^2)
1	1.30	0.391	43.78	4.000	0.091	0.030	0.004	0.100	0.00071
2	2.00	1.092	40.50	6.000	0.148	0.030	0.006	0.182	0.00071
3	2.70	1.986	35.19	6.000	0.171	0.030	0.008	0.245	0.00071
4	3.40	3.142	39.85	8.000	0.201	0.030	0.010	0.308	0.00071
5	3.90	4.170	48.03	10.000	0.208	0.030	0.012	0.356	0.00071
6	4.50	5.666	40.03	10.000	0.250	0.030	0.014	0.420	0.00071

V_o =(2g(h+V_T^2/2g))^{0,5} (m/s)	$(Q_o)_{the.}$=A_0*V_0 (lt/s)	C_D=$(Q_o)_{mea.}$/$(Q_o)_{the.}$	K=$(Q_o)_{mea.}$/(V_T*h^2)	D/h	x/h	Fr=V_T/(g*h)^{0,5}
0.265	0.187	0.488	5.392	2.308	20.769	0.281
0.426	0.301	0.493	2.035	1.500	13.500	0.411
0.590	0.417	0.409	0.954	1.111	10.000	0.476
0.762	0.539	0.373	0.564	0.882	7.941	0.533
0.892	0.631	0.330	0.384	0.769	6.923	0.576
1.059	0.749	0.334	0.294	0.667	6.000	0.632

Table A.61: Experimental results related to circular orifice A3 for θ=20°

Experiment no	h (cm)	Q_T (lt/sec)	t (sec)	V (lt)	$(Q_o)_{mea.}$ (lt/s)	D (m)	A_T =h*w (m^2)	V_T=Q_T /A_T (m/s)	A_o =(π*D^2)/4 (m^2)
1	1.30	0.391	59.25	3.000	0.051	0.020	0.004	0.100	0.00031
2	2.00	1.092	72.86	4.000	0.055	0.020	0.006	0.182	0.00031
3	2.70	1.986	68.03	4.000	0.059	0.020	0.008	0.245	0.00031
4	3.40	3.142	55.49	4.000	0.072	0.020	0.010	0.308	0.00031
5	3.90	4.170	65.34	5.000	0.077	0.020	0.012	0.356	0.00031
6	4.50	5.666	56.10	5.000	0.089	0.020	0.014	0.420	0.00031

V_o =(2g(h+V_T^2/2g))^{0,5} (m/s)	$(Q_o)_{the.}$=A_0*V_0 (lt/s)	C_D=$(Q_o)_{mea.}$/$(Q_o)_{the.}$	K=$(Q_o)_{mea.}$/(V_T*h^2)	D/h	x/h	Fr=V_T/(g*h)^{0,5}
0.265	0.083	0.608	2.988	1.538	2.308	0.281
0.426	0.134	0.411	0.754	1.000	1.500	0.411
0.590	0.185	0.317	0.329	0.741	1.111	0.476
0.762	0.239	0.301	0.202	0.588	0.882	0.533
0.892	0.280	0.273	0.141	0.513	0.769	0.576
1.059	0.333	0.268	0.105	0.444	0.667	0.632

Table A.62: Experimental results related to circular orifice B3 for θ=20°

Experiment no	h (cm)	Q_T (lt/sec)	t (sec)	V (lt)	$(Q_o)_{mea.}$ (lt/s)	D (m)	A_T =h*w (m^2)	V_T=Q_T /A_T (m/s)	A_o =(π*D^2)/4 (m^2)
1	1.30	0.391	58.32	3.000	0.051	0.020	0.004	0.100	0.00031
2	2.00	1.092	70.81	4.000	0.056	0.020	0.006	0.182	0.00031
3	2.70	1.986	65.36	4.000	0.061	0.020	0.008	0.245	0.00031
4	3.40	3.142	54.75	4.000	0.073	0.020	0.010	0.308	0.00031
5	3.90	4.170	60.87	5.000	0.082	0.020	0.012	0.356	0.00031
6	4.50	5.666	54.20	5.000	0.092	0.020	0.014	0.420	0.00031

V_o =(2g(h+V_T^2/2g))^{0,5} (m/s)	$(Q_o)_{the.}$=A_0*V_0 (lt/s)	C_D=$(Q_o)_{mea.}$/$(Q_o)_{the.}$	K=$(Q_o)_{mea.}$/(V_T*h^2)	D/h	x/h	Fr=V_T/(g*h)^{0,5}
0.265	0.083	0.618	3.036	1.538	6.923	0.281
0.426	0.134	0.423	0.776	1.000	4.500	0.411
0.590	0.185	0.330	0.342	0.741	3.333	0.476
0.762	0.239	0.305	0.205	0.588	2.647	0.533
0.892	0.280	0.293	0.152	0.513	2.308	0.576
1.059	0.333	0.277	0.109	0.444	2.000	0.632

Table A.63: Experimental results related to circular orifice C3 for θ=20°

Experiment no	h (cm)	Q_T (lt/sec)	t (sec)	V (lt)	$(Q_o)_{mea.}$ (lt/s)	D (m)	A_T =h*w (m^2)	V_T=Q_T /A_T (m/s)	A_o =(π*D^2)/4 (m^2)
1	1.30	0.391	56.10	3.000	0.053	0.020	0.004	0.100	0.00031
2	2.00	1.092	66.90	4.000	0.060	0.020	0.006	0.182	0.00031
3	2.70	1.986	58.81	4.000	0.068	0.020	0.008	0.245	0.00031
4	3.40	3.142	51.64	4.000	0.077	0.020	0.010	0.308	0.00031
5	3.90	4.170	56.85	5.000	0.088	0.020	0.012	0.356	0.00031
6	4.50	5.666	51.41	5.000	0.097	0.020	0.014	0.420	0.00031

V_o =(2g(h+V_T^2/2g))^{0,5} (m/s)	$(Q_o)_{the.}$=A_0*V_0 (lt/s)	C_D=$(Q_o)_{mea.}$/$(Q_o)_{the.}$	K=$(Q_o)_{mea.}$/(V_T*h^2)	D/h	x/h	Fr=V_T/(g*h)^{0,5}
0.265	0.083	0.642	3.156	1.538	11.538	0.281
0.426	0.134	0.447	0.821	1.000	7.500	0.411
0.590	0.185	0.367	0.381	0.741	5.556	0.476
0.762	0.239	0.324	0.218	0.588	4.412	0.533
0.892	0.280	0.314	0.162	0.513	3.846	0.576
1.059	0.333	0.292	0.114	0.444	3.333	0.632

Table A.64: Experimental results related to circular orifice D3 for θ=20°

Experiment no	h (cm)	Q_T (lt/sec)	t (sec)	V (lt)	$(Q_o)_{mea.}$ (lt/s)	D (m)	A_T =h*w (m^2)	V_T=Q_T /A_T (m/s)	A_o =(π*D^2)/4 (m^2)
1	1.30	0.391	53.50	3.000	0.056	0.020	0.004	0.100	0.00031
2	2.00	1.092	63.94	4.000	0.063	0.020	0.006	0.182	0.00031
3	2.70	1.986	52.28	4.000	0.077	0.020	0.008	0.245	0.00031
4	3.40	3.142	48.82	4.000	0.082	0.020	0.010	0.308	0.00031
5	3.90	4.170	52.56	5.000	0.095	0.020	0.012	0.356	0.00031
6	4.50	5.666	47.00	5.000	0.106	0.020	0.014	0.420	0.00031

V_o =(2g(h+V_T^2/2g))^{0,5} (m/s)	$(Q_o)_{the.}$=A_0*V_0 (lt/s)	C_D=$(Q_o)_{mea.}$/$(Q_o)_{the.}$	K=$(Q_o)_{mea.}$/(V_T*h^2)	D/h	x/h	Fr=V_T/(g*h)^{0,5}
0.265	0.083	0.673	3.310	1.538	16.154	0.281
0.426	0.134	0.468	0.859	1.000	10.500	0.411
0.590	0.185	0.413	0.428	0.741	7.778	0.476
0.762	0.239	0.342	0.230	0.588	6.176	0.533
0.892	0.280	0.339	0.175	0.513	5.385	0.576
1.059	0.333	0.320	0.125	0.444	4.667	0.632

Table A.65: Experimental results related to circular orifice E3 for θ=20°

Experiment no	h (cm)	Q_T (lt/sec)	t (sec)	V (lt)	$(Q_o)_{mea.}$ (lt/s)	D (m)	A_T =h*w (m^2)	V_T=Q_T /A_T (m/s)	A_o =(π*D^2)/4 (m^2)
1	1.30	0.391	49.85	3.000	0.060	0.020	0.004	0.100	0.00031
2	2.00	1.092	56.63	4.000	0.071	0.020	0.006	0.182	0.00031
3	2.70	1.986	47.31	4.000	0.085	0.020	0.008	0.245	0.00031
4	3.40	3.142	41.00	4.000	0.098	0.020	0.010	0.308	0.00031
5	3.90	4.170	46.01	5.000	0.109	0.020	0.012	0.356	0.00031
6	4.50	5.666	40.84	5.000	0.122	0.020	0.014	0.420	0.00031

V_o =(2g(h+V_T^2/2g))^{0,5} (m/s)	$(Q_o)_{the.}$=A_0*V_0 (lt/s)	C_D=$(Q_o)_{mea.}$/$(Q_o)_{the.}$	K=$(Q_o)_{mea.}$/(V_T*h^2)	D/h	x/h	Fr=V_T/(g*h)^{0,5}
0.265	0.083	0.723	3.552	1.538	20.769	0.281
0.426	0.134	0.528	0.970	1.000	13.500	0.411
0.590	0.185	0.456	0.473	0.741	10.000	0.476
0.762	0.239	0.408	0.274	0.588	7.941	0.533
0.892	0.280	0.388	0.200	0.513	6.923	0.576
1.059	0.333	0.368	0.144	0.444	6.000	0.632

Table A.66: Experimental results related to circular orifice A2 for θ=20°

Experiment no	h (cm)	Q_T (lt/sec)	t (sec)	V (lt)	$(Q_o)_{mea.}$ (lt/s)	D (m)	A_T =h*w (m^2)	V_T=Q_T /A_T (m/s)	A_o =(π*D^2)/4 (m^2)
1	1.30	0.391	74.44	3.000	0.040	0.015	0.004	0.100	0.00018
2	2.00	1.092	69.50	3.000	0.043	0.015	0.006	0.182	0.00018
3	2.70	1.986	63.59	3.000	0.047	0.015	0.008	0.245	0.00018
4	3.40	3.142	75.13	4.000	0.053	0.015	0.010	0.308	0.00018
5	3.90	4.170	84.50	5.000	0.059	0.015	0.012	0.356	0.00018
6	4.50	5.666	74.78	5.000	0.067	0.015	0.014	0.420	0.00018

V_o =(2g(h+V_T^2/2g))^{0,5} (m/s)	$(Q_o)_{the.}$=A_0*V_0 (lt/s)	C_D=$(Q_o)_{mea.}$/$(Q_o)_{the.}$	K=$(Q_o)_{mea.}$/(V_T*h^2)	D/h	x/h	Fr=V_T/(g*h)^{0,5}
0.265	0.047	0.860	2.379	1.154	2.308	0.281
0.426	0.075	0.574	0.593	0.750	1.500	0.411
0.590	0.104	0.453	0.264	0.556	1.111	0.476
0.762	0.135	0.395	0.150	0.441	0.882	0.533
0.892	0.158	0.375	0.109	0.385	0.769	0.576
1.059	0.187	0.357	0.079	0.333	0.667	0.632

Table A.67: Experimental results related to circular orifice B2 for θ=20°

Experiment no	h (cm)	Q_T (lt/sec)	t (sec)	V (lt)	$(Q_o)_{mea.}$ (lt/s)	D (m)	A_T =h*w (m^2)	V_T=Q_T /A_T (m/s)	A_o =(π*D^2)/4 (m^2)
1	1.30	0.391	73.00	3.000	0.041	0.015	0.004	0.100	0.00018
2	2.00	1.092	65.92	3.000	0.046	0.015	0.006	0.182	0.00018
3	2.70	1.986	60.50	3.000	0.050	0.015	0.008	0.245	0.00018
4	3.40	3.142	73.88	4.000	0.054	0.015	0.010	0.308	0.00018
5	3.90	4.170	81.21	5.000	0.062	0.015	0.012	0.356	0.00018
6	4.50	5.666	72.31	5.000	0.069	0.015	0.014	0.420	0.00018

V_o =(2g(h+V_T^2/2g))^{0,5} (m/s)	$(Q_o)_{the.}$=A_0*V_0 (lt/s)	C_D=$(Q_o)_{mea.}$/$(Q_o)_{the.}$	K=$(Q_o)_{mea.}$/(V_T*h^2)	D/h	x/h	Fr=V_T/(g*h)^{0,5}
0.265	0.047	0.877	2.425	1.154	6.923	0.281
0.426	0.075	0.605	0.625	0.750	4.500	0.411
0.590	0.104	0.476	0.277	0.556	3.333	0.476
0.762	0.135	0.402	0.152	0.441	2.647	0.533
0.892	0.158	0.391	0.114	0.385	2.308	0.576
1.059	0.187	0.369	0.081	0.333	2.000	0.632

Table A.68: Experimental results related to circular orifice C2 for θ=20°

Experiment no	h (cm)	Q_T (lt/sec)	t (sec)	V (lt)	$(Q_o)_{mea.}$ (lt/s)	D (m)	A_T =h*w (m^2)	V_T=Q_T /A_T (m/s)	A_o =(π*D^2)/4 (m^2)
1	1.30	0.391	70.38	3.000	0.043	0.015	0.004	0.100	0.00018
2	2.00	1.092	63.97	3.000	0.047	0.015	0.006	0.182	0.00018
3	2.70	1.986	60.00	3.000	0.050	0.015	0.008	0.245	0.00018
4	3.40	3.142	65.19	4.000	0.061	0.015	0.010	0.308	0.00018
5	3.90	4.170	74.78	5.000	0.067	0.015	0.012	0.356	0.00018
6	4.50	5.666	69.88	5.000	0.072	0.015	0.014	0.420	0.00018

V_o =(2g(h+V_T^2/2g))^{0,5} (m/s)	$(Q_o)_{the.}$=A_0*V_0 (lt/s)	C_D=$(Q_o)_{mea.}$/$(Q_o)_{the.}$	K=$(Q_o)_{mea.}$/(V_T*h^2)	D/h	x/h	Fr=V_T/(g*h)^{0,5}
0.265	0.047	0.910	2.516	1.154	11.538	0.281
0.426	0.075	0.624	0.644	0.750	7.500	0.411
0.590	0.104	0.480	0.280	0.556	5.556	0.476
0.762	0.135	0.456	0.172	0.441	4.412	0.533
0.892	0.158	0.424	0.123	0.385	3.846	0.576
1.059	0.187	0.382	0.084	0.333	3.333	0.632

Table A.69: Experimental results related to circular orifice D2 for θ=20°

Experiment no	h (cm)	Q_T (lt/sec)	t (sec)	V (lt)	$(Q_o)_{mea.}$ (lt/s)	D (m)	A_T =h*w (m^2)	V_T=Q_T /A_T (m/s)	A_o =(π*D^2)/4 (m^2)
1	1.30	0.391	69.56	3.000	0.043	0.015	0.004	0.100	0.00018
2	2.00	1.092	61.40	3.000	0.049	0.015	0.006	0.182	0.00018
3	2.70	1.986	53.25	3.000	0.056	0.015	0.008	0.245	0.00018
4	3.40	3.142	63.66	4.000	0.063	0.015	0.010	0.308	0.00018
5	3.90	4.170	70.53	5.000	0.071	0.015	0.012	0.356	0.00018
6	4.50	5.666	62.50	5.000	0.080	0.015	0.014	0.420	0.00018

V_o =(2g(h+V_T^2/2g))^{0,5} (m/s)	$(Q_o)_{the.}$=A_0*V_0 (lt/s)	C_D=$(Q_o)_{mea.}$/$(Q_o)_{the.}$	K=$(Q_o)_{mea.}$/(V_T*h^2)	D/h	x/h	Fr=V_T/(g*h)^{0,5}
0.265	0.047	0.921	2.545	1.154	16.154	0.281
0.426	0.075	0.650	0.671	0.750	10.500	0.411
0.590	0.104	0.540	0.315	0.556	7.778	0.476
0.762	0.135	0.467	0.176	0.441	6.176	0.533
0.892	0.158	0.450	0.131	0.385	5.385	0.576
1.059	0.187	0.427	0.094	0.333	4.667	0.632

Table A.70: Experimental results related to circular orifice E2 for θ=20°

Experiment no	h (cm)	Q_T (lt/sec)	t (sec)	V (lt)	$(Q_o)_{mea.}$ (lt/s)	D (m)	A_T =h*w (m^2)	V_T=Q_T /A_T (m/s)	A_o =(π*D^2)/4 (m^2)
1	1.30	0.391	65.15	3.000	0.046	0.015	0.004	0.100	0.00018
2	2.00	1.092	57.78	3.000	0.052	0.015	0.006	0.182	0.00018
3	2.70	1.986	51.09	3.000	0.059	0.015	0.008	0.245	0.00018
4	3.40	3.142	58.64	4.000	0.068	0.015	0.010	0.308	0.00018
5	3.90	4.170	65.12	5.000	0.077	0.015	0.012	0.356	0.00018
6	4.50	5.666	57.57	5.000	0.087	0.015	0.014	0.420	0.00018

V_o =(2g(h+V_T^2/2g))^{0,5} (m/s)	$(Q_o)_{the.}$=A_0*V_0 (lt/s)	C_D=$(Q_o)_{mea.}$/$(Q_o)_{the.}$	K=$(Q_o)_{mea.}$/(V_T*h^2)	D/h	x/h	Fr=V_T/(g*h)^{0,5}
0.265	0.047	0.983	2.718	1.154	20.769	0.281
0.426	0.075	0.690	0.713	0.750	13.500	0.411
0.590	0.104	0.563	0.329	0.556	10.000	0.476
0.762	0.135	0.507	0.192	0.441	7.941	0.533
0.892	0.158	0.487	0.142	0.385	6.923	0.576
1.059	0.187	0.464	0.102	0.333	6.000	0.632

Table A.71: Experimental results related to circular orifice A1 for θ=20°

Experiment no	h (cm)	Q_T (lt/sec)	t (sec)	V (lt)	$(Q_o)_{mea.}$ (lt/s)	D (m)	A_T =h*w (m^2)	V_T=Q_T /A_T (m/s)	A_o =(π*D^2)/4 (m^2)
1	1.30	0.391	95.81	3.000	0.031	0.010	0.004	0.100	0.00008
2	2.00	1.092	88.94	3.000	0.034	0.010	0.006	0.182	0.00008
3	2.70	1.986	80.19	3.000	0.037	0.010	0.008	0.245	0.00008
4	3.40	3.142	70.62	3.000	0.042	0.010	0.010	0.308	0.00008
5	3.90	4.170	65.00	3.000	0.046	0.010	0.012	0.356	0.00008
6	4.50	5.666	59.85	3.000	0.050	0.010	0.014	0.420	0.00008

V_o =(2g(h+V_T^2/2g))^{0,5} (m/s)	$(Q_o)_{the.}$=A_0*V_0 (lt/s)	C_D=$(Q_o)_{mea.}$/$(Q_o)_{the.}$	K=$(Q_o)_{mea.}$/(V_T*h^2)	D/h	x/h	Fr=V_T/(g*h)^{0,5}
0.265	0.021	1.504	1.848	0.769	2.308	0.281
0.426	0.033	1.009	0.463	0.500	1.500	0.411
0.590	0.046	0.808	0.209	0.370	1.111	0.476
0.762	0.060	0.710	0.119	0.294	0.882	0.533
0.892	0.070	0.659	0.085	0.256	0.769	0.576
1.059	0.083	0.603	0.059	0.222	0.667	0.632

Table A.72: Experimental results related to circular orifice B1 for θ=20°

Experiment no	h (cm)	Q_T (lt/sec)	t (sec)	V (lt)	$(Q_o)_{mea.}$ (lt/s)	D (m)	A_T =h*w (m^2)	V_T=Q_T /A_T (m/s)	A_o =(π*D^2)/4 (m^2)
1	1.30	0.391	94.16	3.000	0.032	0.010	0.004	0.100	0.00008
2	2.00	1.092	87.65	3.000	0.034	0.010	0.006	0.182	0.00008
3	2.70	1.986	77.41	3.000	0.039	0.010	0.008	0.245	0.00008
4	3.40	3.142	68.68	3.000	0.044	0.010	0.010	0.308	0.00008
5	3.90	4.170	64.22	3.000	0.047	0.010	0.012	0.356	0.00008
6	4.50	5.666	58.47	3.000	0.051	0.010	0.014	0.420	0.00008

V_o =(2g(h+V_T^2/2g))^{0,5} (m/s)	$(Q_o)_{the.}$=A_0*V_0 (lt/s)	C_D=$(Q_o)_{mea.}$/$(Q_o)_{the.}$	K=$(Q_o)_{mea.}$/(V_T*h^2)	D/h	x/h	Fr=V_T/(g*h)^{0,5}
0.265	0.021	1.530	1.880	0.769	6.923	0.281
0.426	0.033	1.024	0.470	0.500	4.500	0.411
0.590	0.046	0.837	0.217	0.370	3.333	0.476
0.762	0.060	0.730	0.123	0.294	2.647	0.533
0.892	0.070	0.667	0.086	0.256	2.308	0.576
1.059	0.083	0.617	0.060	0.222	2.000	0.632

Table A.73: Experimental results related to circular orifice C1 for θ=20°

Experiment no	h (cm)	Q_T (lt/sec)	t (sec)	V (lt)	$(Q_o)_{mea.}$ (lt/s)	D (m)	A_T =h*w (m^2)	V_T=Q_T /A_T (m/s)	A_o =(π*D^2)/4 (m^2)
1	1.30	0.391	92.86	3.000	0.032	0.010	0.004	0.100	0.00008
2	2.00	1.092	86.96	3.000	0.034	0.010	0.006	0.182	0.00008
3	2.70	1.986	76.97	3.000	0.039	0.010	0.008	0.245	0.00008
4	3.40	3.142	66.81	3.000	0.045	0.010	0.010	0.308	0.00008
5	3.90	4.170	63.25	3.000	0.047	0.010	0.012	0.356	0.00008
6	4.50	5.666	56.72	3.000	0.053	0.010	0.014	0.420	0.00008

V_o =(2g(h+V_T^2/2g))^{0,5} (m/s)	$(Q_o)_{the.}$=A_0*V_0 (lt/s)	C_D=$(Q_o)_{mea.}$/$(Q_o)_{the.}$	K=$(Q_o)_{mea.}$/(V_T*h^2)	D/h	x/h	Fr=V_T/(g*h)^{0,5}
0.265	0.021	1.552	1.907	0.769	11.538	0.281
0.426	0.033	1.032	0.474	0.500	7.500	0.411
0.590	0.046	0.841	0.218	0.370	5.556	0.476
0.762	0.060	0.750	0.126	0.294	4.412	0.533
0.892	0.070	0.677	0.087	0.256	3.846	0.576
1.059	0.083	0.636	0.062	0.222	3.333	0.632

Table A.74: Experimental results related to circular orifice D1 for θ=20°

Experiment no	h (cm)	Q_T (lt/sec)	t (sec)	V (lt)	$(Q_o)_{mea.}$ (lt/s)	D (m)	A_T =h*w (m^2)	V_T=Q_T /A_T (m/s)	A_o =(π*D^2)/4 (m^2)
1	1.30	0.391	91.79	3.000	0.033	0.010	0.004	0.100	0.00008
2	2.00	1.092	85.87	3.000	0.035	0.010	0.006	0.182	0.00008
3	2.70	1.986	75.22	3.000	0.040	0.010	0.008	0.245	0.00008
4	3.40	3.142	62.68	3.000	0.048	0.010	0.010	0.308	0.00008
5	3.90	4.170	59.15	3.000	0.051	0.010	0.012	0.356	0.00008
6	4.50	5.666	53.65	3.000	0.056	0.010	0.014	0.420	0.00008

V_o =(2g(h+V_T^2/2g))^{0,5} (m/s)	$(Q_o)_{the.}$=A_0*V_0 (lt/s)	C_D=$(Q_o)_{mea.}$/$(Q_o)_{the.}$	K=$(Q_o)_{mea.}$/(V_T*h^2)	D/h	x/h	Fr=V_T/(g*h)^{0,5}
0.265	0.021	1.570	1.929	0.769	16.154	0.281
0.426	0.033	1.045	0.480	0.500	10.500	0.411
0.590	0.046	0.861	0.223	0.370	7.778	0.476
0.762	0.060	0.800	0.134	0.294	6.176	0.533
0.892	0.070	0.724	0.094	0.256	5.385	0.576
1.059	0.083	0.672	0.066	0.222	4.667	0.632

Table A.75: Experimental results related to circular orifice E1 for θ=20°

Experiment no	**h (cm)**	**Q_T (lt/sec)**	**t (sec)**	**V (lt)**	**$(Q_o)_{mea.}$ (lt/s)**	**D (m)**	**A_T =h*w (m^2)**	**$V_T=Q_T/A_T$ (m/s)**	**$A_o=(\pi*D^2)/4$ (m^2)**
1	1.30	0.391	89.47	3.000	0.034	0.010	0.004	0.100	0.00008
2	2.00	1.092	83.68	3.000	0.036	0.010	0.006	0.182	0.00008
3	2.70	1.986	69.88	3.000	0.043	0.010	0.008	0.245	0.00008
4	3.40	3.142	59.34	3.000	0.051	0.010	0.010	0.308	0.00008
5	3.90	4.170	56.25	3.000	0.053	0.010	0.012	0.356	0.00008
6	4.50	5.666	50.62	3.000	0.059	0.010	0.014	0.420	0.00008

$V_o=(2g(h+V_T^2/2g))^{0,5}$ (m/s)	**$(Q_o)_{the.}=A_0*V_0$ (lt/s)**	**$C_D=(Q_o)_{mea.}/(Q_o)_{the.}$**	**$K=(Q_o)_{mea.}/(V_T*h^2)$**	**D/h**	**x/h**	**$Fr=V_T/(g*h)^{0,5}$**
0.265	0.021	1.610	1.979	0.769	20.769	0.281
0.426	0.033	1.073	0.492	0.500	13.500	0.411
0.590	0.046	0.927	0.240	0.370	10.000	0.476
0.762	0.060	0.845	0.142	0.294	7.941	0.533
0.892	0.070	0.761	0.098	0.256	6.923	0.576
1.059	0.083	0.713	0.070	0.222	6.000	0.632

APPENDIX B

MEASURED AND CALCULATED PARAMETERS FOR THE EXPERIMENTS PERFORMED WITH THE MULTIPLE CIRCULAR BOTTOM INTAKE ORIFICES

Table B.1: Experimental results related to circular orifice s A1-E1 for θ=0°

Experiment no	h (cm)	Q_T (lt/sec)	t (sec)	V (lt)	$(Q_o)_{mea.}$ (lt/s)	D (m)	A_T =h*w (m^2)	V_T=Q_T /A_T (m/s)	A_o =(π*D^2)/4 (m^2)
1	1.30	0.391	39.87	6.000	0.150	0.010	0.004	0.100	0.00008
2	2.05	1.149	30.71	6.000	0.195	0.010	0.006	0.187	0.00008
3	2.75	2.059	35.09	8.000	0.228	0.010	0.008	0.250	0.00008
4	3.35	3.049	31.69	8.000	0.252	0.010	0.010	0.303	0.00008
5	3.85	4.059	38.30	10.000	0.261	0.010	0.012	0.351	0.00008
6	4.50	5.666	35.81	10.000	0.279	0.010	0.014	0.420	0.00008

V_o =(2g(h+V_T^2/2g))^{0,5} (m/s)	$(Q_o)_{the.}$=A_0*V_0 (lt/s)	C_D=$(Q_o)_{mea.}$/$(Q_o)_{the.}$	K=$(Q_o)_{mea.}$/(V_T*h^2)	D/h	Fr=V_T/(g*h)^{0,5}
0.515	0.202	0.744	8.882	0.769	0.281
0.661	0.260	0.753	2.488	0.488	0.417
0.776	0.305	0.748	1.208	0.364	0.481
0.866	0.340	0.743	0.741	0.299	0.529
0.937	0.368	0.709	0.501	0.260	0.572
1.029	0.404	0.691	0.329	0.222	0.632

Table B.2: Experimental results related to circular orifice s A2-E2 for θ=0°

Experiment no	h (cm)	Q_T (lt/sec)	t (sec)	V (lt)	$(Q_o)_{mea.}$ (lt/s)	D (m)	A_T =h*w (m^2)	V_T=Q_T /A_T (m/s)	A_o =(π*D^2)/4 (m^2)
1	1.30	0.391	26.65	6.000	0.225	0.015	0.004	0.100	0.00018
2	2.05	1.149	17.86	6.000	0.336	0.015	0.006	0.187	0.00018
3	2.75	2.059	20.23	8.000	0.395	0.015	0.008	0.250	0.00018
4	3.35	3.049	23.13	10.000	0.432	0.015	0.010	0.303	0.00018
5	3.85	4.059	41.01	20.250	0.494	0.015	0.012	0.351	0.00018
6	4.50	5.666	39.10	20.250	0.518	0.015	0.014	0.420	0.00018

V_o =(2g(h+V_T^2/2g))^{0,5} (m/s)	$(Q_o)_{the.}$=A_0*V_0 (lt/s)	C_D=$(Q_o)_{mea.}$/$(Q_o)_{the.}$	K=$(Q_o)_{mea.}$/(V_T*h^2)	D/h	Fr=V_T/(g*h)^{0,5}
0.515	0.455	0.495	13.288	1.154	0.281
0.661	0.584	0.575	4.279	0.732	0.417
0.776	0.685	0.577	2.095	0.545	0.481
0.866	0.765	0.565	1.270	0.448	0.529
0.937	0.828	0.596	0.948	0.390	0.572
1.029	0.909	0.570	0.609	0.333	0.632

Table B.3: Experimental results related to circular orifice s A3-E3 for θ=0°

Experiment no	h (cm)	Q_T (lt/sec)	t (sec)	V (lt)	$(Q_o)_{mea.}$ (lt/s)	D (m)	A_T =h*w (m^2)	V_T=Q_T /A_T (m/s)	A_o =(π*D^2)/4 (m^2)
1	1.30	0.391	29.86	8.000	0.268	0.020	0.004	0.100	0.00031
2	2.05	1.149	18.62	8.000	0.430	0.020	0.006	0.187	0.00031
3	2.75	2.059	17.01	10.000	0.588	0.020	0.008	0.250	0.00031
4	3.35	3.049	15.30	10.000	0.654	0.020	0.010	0.303	0.00031
5	3.85	4.059	27.71	20.250	0.731	0.020	0.012	0.351	0.00031
6	4.50	5.666	25.75	20.250	0.786	0.020	0.014	0.420	0.00031

V_o =(2g(h+V_T^2/2g))^{0,5} (m/s)	$(Q_o)_{the.}$=A_0*V_0 (lt/s)	C_D=$(Q_o)_{mea.}$/$(Q_o)_{the.}$	K=$(Q_o)_{mea.}$/(V_T*h^2)	D/h	Fr=V_T/(g*h)^{0,5}
0.515	0.809	0.331	15.813	1.538	0.281
0.661	1.039	0.414	5.472	0.976	0.417
0.776	1.219	0.482	3.115	0.727	0.481
0.866	1.360	0.481	1.920	0.597	0.529
0.937	1.473	0.496	1.403	0.519	0.572
1.029	1.617	0.486	0.925	0.444	0.632

Table B.4: Experimental results related to circular orifice s A1-E1 for θ=10°

Experiment no	h (cm)	Q_T (lt/sec)	t (sec)	V (lt)	$(Q_o)_{mea.}$ (lt/s)	D (m)	A_T =h*w (m^2)	V_T=Q_T /A_T (m/s)	A_o =(π*D^2)/4 (m^2)
1	1.30	0.391	37.97	4.000	0.105	0.010	0.004	0.100	0.00008
2	2.00	1.092	49.78	6.000	0.121	0.010	0.006	0.182	0.00008
3	2.70	1.986	51.28	8.000	0.156	0.010	0.008	0.245	0.00008
4	3.40	3.142	57.10	10.000	0.175	0.010	0.010	0.308	0.00008
5	3.90	4.170	56.42	10.000	0.177	0.010	0.012	0.356	0.00008
6	4.40	5.395	52.94	10.000	0.189	0.010	0.013	0.409	0.00008

V_o =(2g(h+V_T^2/2g))^{0,5} (m/s)	$(Q_o)_{the.}$=A_0*V_0 (lt/s)	C_D=$(Q_o)_{mea.}$/$(Q_o)_{the.}$	K=$(Q_o)_{mea.}$/(V_T*h^2)	D/h	Fr=V_T/(g*h)^{0,5}
0.515	0.202	0.521	6.218	0.769	0.281
0.652	0.256	0.471	1.656	0.500	0.411
0.768	0.302	0.517	0.873	0.370	0.476
0.873	0.343	0.511	0.492	0.294	0.533
0.945	0.371	0.478	0.327	0.256	0.576
1.015	0.399	0.474	0.239	0.227	0.622

Table B.5: Experimental results related to circular orifice s A2-E2 for θ=10°

Experiment no	h (cm)	Q_T (lt/sec)	t (sec)	V (lt)	$(Q_o)_{mea.}$ (lt/s)	D (m)	A_T =h*w (m^2)	V_T=Q_T /A_T (m/s)	A_o =(π*D^2)/4 (m^2)
1	1.30	0.391	29.53	4.000	0.135	0.015	0.004	0.100	0.00018
2	2.00	1.092	30.62	6.000	0.196	0.015	0.006	0.182	0.00018
3	2.70	1.986	34.04	8.000	0.235	0.015	0.008	0.245	0.00018
4	3.40	3.142	35.47	10.000	0.282	0.015	0.010	0.308	0.00018
5	3.90	4.170	34.15	10.000	0.293	0.015	0.012	0.356	0.00018
6	4.40	5.395	63.43	20.250	0.319	0.015	0.013	0.409	0.00018

V_o =(2g(h+V_T^2/2g))^{0,5} (m/s)	$(Q_o)_{the.}$=A_0*V_0 (lt/s)	C_D=$(Q_o)_{mea.}$/$(Q_o)_{the.}$	K=$(Q_o)_{mea.}$/(V_T*h^2)	D/h	Fr=V_T/(g*h)^{0,5}
0.515	0.455	0.298	7.995	1.154	0.281
0.652	0.576	0.340	2.692	0.750	0.411
0.768	0.679	0.346	1.315	0.556	0.476
0.873	0.771	0.366	0.792	0.441	0.533
0.945	0.835	0.351	0.540	0.385	0.576
1.015	0.897	0.356	0.403	0.341	0.622

Table B.6: Experimental results related to circular orifice s A3-E3 for θ=10°

Experiment no	h (cm)	Q_T (lt/sec)	t (sec)	V (lt)	$(Q_o)_{mea.}$ (lt/s)	D (m)	A_T =h*w (m^2)	V_T=Q_T /A_T (m/s)	A_o =(π*D^2)/4 (m^2)
1	1.30	0.391	28.34	4.000	0.141	0.020	0.004	0.100	0.00031
2	2.00	1.092	20.59	6.000	0.291	0.020	0.006	0.182	0.00031
3	2.70	1.986	22.41	8.000	0.357	0.020	0.008	0.245	0.00031
4	3.40	3.142	24.47	10.000	0.409	0.020	0.010	0.308	0.00031
5	3.90	4.170	22.95	10.000	0.436	0.020	0.012	0.356	0.00031
6	4.40	5.395	42.50	20.250	0.476	0.020	0.013	0.409	0.00031

V_o =(2g(h+V_T^2/2g))^{0,5} (m/s)	$(Q_o)_{the.}$=A_0*V_0 (lt/s)	C_D=$(Q_o)_{mea.}$/$(Q_o)_{the.}$	K=$(Q_o)_{mea.}$/(V_T*h^2)	D/h	Fr=V_T/(g*h)^{0,5}
0.515	0.809	0.175	8.330	1.538	0.281
0.652	1.025	0.284	4.003	1.000	0.411
0.768	1.206	0.296	1.997	0.741	0.476
0.873	1.371	0.298	1.148	0.588	0.533
0.945	1.484	0.294	0.804	0.513	0.576
1.015	1.594	0.299	0.602	0.455	0.622

Table B.7: Experimental results related to circular orifices A1-E1 for θ=20°

Experiment no	h (cm)	Q_T (lt/sec)	t (sec)	V (lt)	$(Q_o)_{mea}$ (lt/s)	D (m)	A_T =h*w (m^2)	V_T=Q_T /A_T (m/s)	A_o =(π*D^2)/4 (m^2)
1	1.30	0.391	45.75	3.000	0.066	0.010	0.004	0.100	0.00008
2	2.00	1.092	54.01	4.000	0.074	0.010	0.006	0.182	0.00008
3	2.70	1.986	71.93	6.000	0.083	0.010	0.008	0.245	0.00008
4	3.40	3.142	61.15	6.000	0.098	0.010	0.010	0.308	0.00008
5	3.90	4.170	63.92	7.000	0.110	0.010	0.012	0.356	0.00008
6	4.50	5.666	57.72	7.000	0.121	0.010	0.014	0.420	0.00008

V_o =(2g(h+V_T^2/2g))^{0,5} (m/s)	$(Q_o)_{the}$=A_0*V_0 (lt/s)	C_D=$(Q_o)_{mea}$/$(Q_o)_{the}$	K=$(Q_o)_{mea}$/(V_T*h^2)	D/h	Fr=V_T/(g*h)^{0,5}
0.265	0.104	0.630	3.870	0.769	0.281
0.426	0.167	0.443	1.017	0.500	0.411
0.590	0.232	0.360	0.467	0.370	0.476
0.762	0.299	0.328	0.276	0.294	0.533
0.892	0.350	0.313	0.202	0.256	0.576
1.059	0.416	0.292	0.143	0.222	0.632

Table B.8: Experimental results related to circular orifice s A2-E2 for θ=20°

Experiment no	h (cm)	Q_T (lt/sec)	t (sec)	V (lt)	$(Q_o)_{mea}$ (lt/s)	D (m)	A_T =h*w (m^2)	V_T=Q_T /A_T (m/s)	A_o =(π*D^2)/4 (m^2)
1	1.30	0.391	38.37	3.000	0.078	0.015	0.004	0.100	0.00018
2	2.00	1.092	38.31	5.000	0.131	0.015	0.006	0.182	0.00018
3	2.70	1.986	46.15	7.000	0.152	0.015	0.008	0.245	0.00018
4	3.40	3.142	44.25	8.000	0.181	0.015	0.010	0.308	0.00018
5	3.90	4.170	52.47	10.000	0.191	0.015	0.012	0.356	0.00018
6	4.50	5.666	44.48	10.000	0.225	0.015	0.014	0.420	0.00018

V_o =(2g(h+V_T^2/2g))^{0,5} (m/s)	$(Q_o)_{the}$=A_0*V_0 (lt/s)	C_D=$(Q_o)_{mea}$/$(Q_o)_{the}$	K=$(Q_o)_{mea}$/(V_T*h^2)	D/h	Fr=V_T/(g*h)^{0,5}
0.265	0.234	0.334	4.615	1.154	0.281
0.426	0.376	0.347	1.793	0.750	0.411
0.590	0.521	0.291	0.849	0.556	0.476
0.762	0.673	0.269	0.508	0.441	0.533
0.892	0.788	0.242	0.352	0.385	0.576
1.059	0.936	0.240	0.265	0.333	0.632

Table B.9: Experimental results related to circular orifices A3-E3 for θ=20°

Experiment no	h (cm)	Q_T (lt/sec)	t (sec)	V (lt)	$(Q_o)_{mea}$ (lt/s)	D (m)	A_T =h*w (m^2)	V_T=Q_T /A_T (m/s)	A_o =(π*D^2)/4 (m^2)
1	1.30	0.391	45.25	4.000	0.088	0.020	0.004	0.100	0.00031
2	2.00	1.092	29.41	6.000	0.204	0.020	0.006	0.182	0.00031
3	2.70	1.986	33.25	8.000	0.241	0.020	0.008	0.245	0.00031
4	3.40	3.142	28.85	8.000	0.277	0.020	0.010	0.308	0.00031
5	3.90	4.170	33.06	10.000	0.302	0.020	0.012	0.356	0.00031
6	4.50	5.666	28.35	10.000	0.353	0.020	0.014	0.420	0.00031

V_o =(2g(h+V_T^2/2g))^{0,5} (m/s)	$(Q_o)_{the}$=A_0*V_0 (lt/s)	C_D=$(Q_o)_{mea}$/$(Q_o)_{the}$	K=$(Q_o)_{mea}$/(V_T*h^2)	D/h	Fr=V_T/(g*h)^{0,5}
0.265	0.416	0.212	5.217	1.538	0.281
0.426	0.668	0.305	2.802	1.000	0.411
0.590	0.927	0.260	1.346	0.741	0.476
0.762	1.197	0.232	0.779	0.588	0.533
0.892	1.401	0.216	0.558	0.513	0.576
1.059	1.664	0.212	0.415	0.444	0.632